

# STUDIES TOWARDS THE TOTAL SYNTHESIS OF **MADEIROLIDE A**

A dissertation submitted in partial fulfilment  
of the requirements for the degree of  
Doctor of Philosophy at the  
University of Cambridge

Adam Christopher Loy Yip

August 2018



UNIVERSITY OF  
CAMBRIDGE







# DECLARATION

This dissertation is submitted for the degree of Doctor of Philosophy. Unless otherwise indicated in the text, the research described is my own and not the product of collaboration. No substantial part of this dissertation, or the research described, is the same as any that I have submitted or will submit for another qualification at the University of Cambridge or any other institution. It does not exceed the limit of 60,000 words (excluding footnotes, references, captions and experimental data).

Adam Christopher Loy Yip

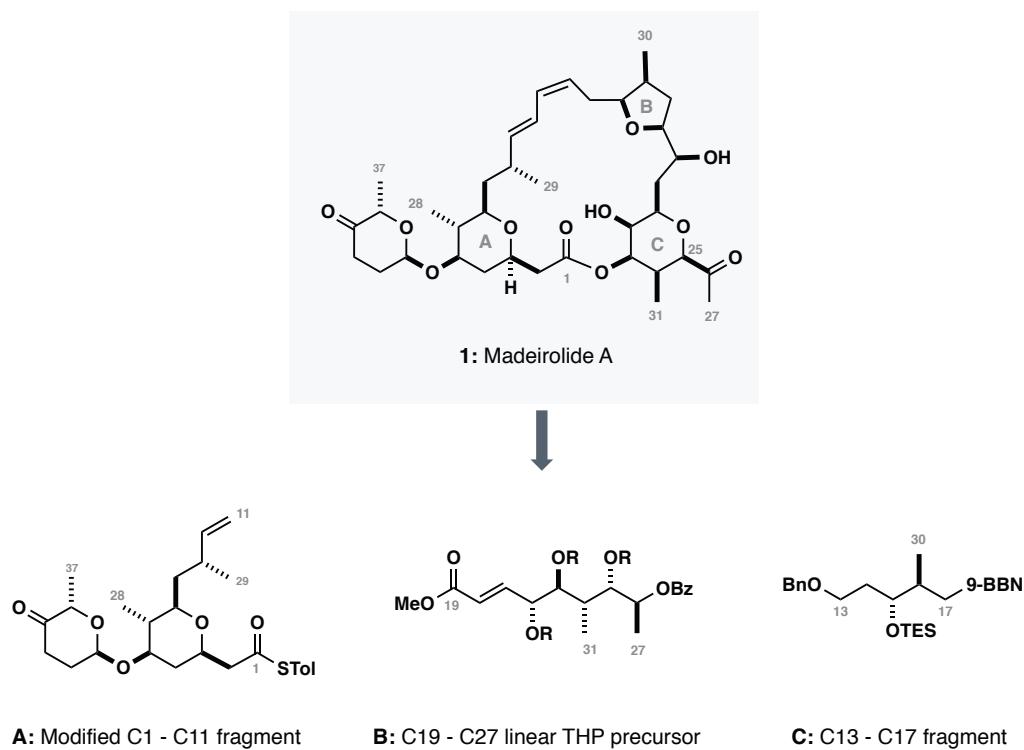
2018



# SUMMARY

Madeirolide A (**1**) is a structurally novel polyketide natural product first isolated from the deep-sea sponge *Leiodermatium* sp. by Wright in 2009. Initial biological investigations of madeirolide A revealed potent inhibition of the fungal pathogen *Candida albicans* but failed to determine any appreciable cytotoxicity when tested against a limited range of cancer cell lines.

The unusual bioactivity of madeirolide A coupled with uncertainty over the true stereostructure of the natural product makes it a compelling target for synthesis. This thesis discloses synthetic efforts towards the total synthesis of madeirolide A with an emphasis on the construction of the all-*cis* C21 – C27 eastern tetrahydropyran.



Chapters 1 and 2 provide an introduction to the importance of natural products in drug discovery and outline the context of this project with details of the isolation and biological activity of madeirolide A (**1**). Previous synthetic efforts are also reviewed including those from within the group which formed the basis of the present studies.

Chapter 3 describes the synthesis of a fully elaborated C1 - C11 fragment (**A**), building upon previously published work in the group. Specifically, it details the successful completion of a

modified approach designed to avoid some of the major challenges previously encountered such as undesired migration of protecting groups and challenges in selectively installing an (*E*)-vinyl iodide.

Chapter 4 discusses ongoing efforts towards the challenging C12 - C27 fragment of madeirolide A. The stereocontrolled synthesis of several linear C19 – C27 precursors (**B**) is outlined, followed by details of screening reactions conducted to affect the desired oxy-Michael cyclisation. Additionally, extensive computational studies have been undertaken in an attempt to rationalise the frustrating lack of reactivity observed with the goal of developing a substrate suitably elaborated to cyclise. Finally, the asymmetric synthesis of the C13 – C17 subfragment (**C**) is outlined, which will provide eventual access to the eastern tetrahydrofuran.

Chapter 5 summarises the synthetic work carried out thus far and explores potential strategies for the future completion of the natural product with a focus on alternative disconnections of the eastern tetrahydropyran.

Finally, the appendices contain full experimental details and copies of NMR spectra for key compounds, and specifics of the computational work conducted.

# ACKNOWLEDGEMENTS

The work described in this thesis would not have been possible without the support and guidance of many friends and colleagues. I would like to thank the following:

- Ian Paterson for the opportunity to carry out this PhD, working on a challenging target. I thank him not only for his guidance and support in moving the project forward, but also for his commitment to keeping his research group a friendly and pleasant place to work.
- Jonathan Goodman for his endless optimism, especially in the final months of this project when nothing appeared to be going to plan. I also thank him for encouragement to carry out the computational studies described in this thesis, and, by extension Kristaps Ermanis for taking the time to show me how to run the calculations.
- The many technical staff in the department of chemistry, who make our research possible. Particularly to Naomi Hobbs and Nic Davies for their amazing support in keeping the lab functioning.
- Andrew Phillips and Matthew Anketell for proof-reading this document, often at short notice.
- The members of the Paterson and Goodman groups who I've been fortunate to overlap with. Lab 122 has been an enjoyable place to work, and I'm deeply grateful to all of those who've taken the time to share their knowledge, run spectra, and generally keep the lab running smoothly. Simon Williams deserves a special mention for his patience and guidance in the early stages of my PhD when total synthesis was an unfamiliar area. Also, I thank Andrew Phillips, Talia Pettigrew, Matthew Anketell, Rachel Porter, Nelson Lam, Bing Yuan (Leroy) Han, and Nika Anzikec for the cheesy music, coffee breaks and extended pub lunches.
- The EPSRC for generous funding of this project along with Magdalene College, Cambridge for additional financial support.
- Finally, I thank my parents and Chris for their love and support over the past four years.



# TABLE OF CONTENTS

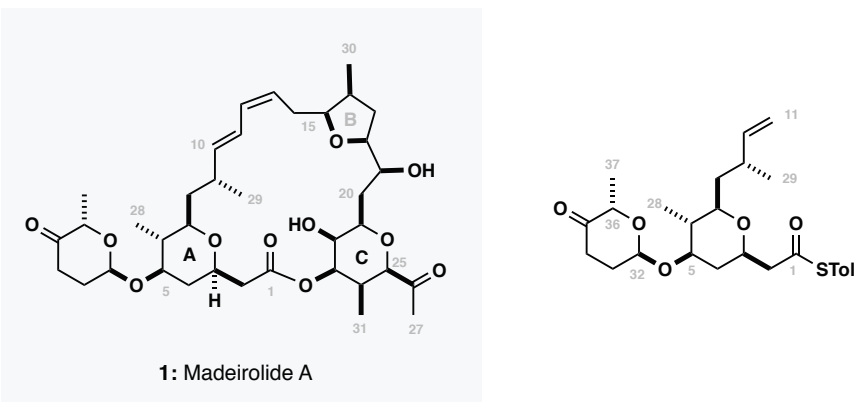
DECLARATION.....	i
SUMMARY .....	iii
ACKNOWLEDGEMENTS .....	v
TABLE OF CONTENTS .....	vii
NOMENCLATURE.....	ix
COMPOUND NUMBERING.....	ix
RELATIVE STEREOCHEMICAL RELATIONSHIPS.....	ix
ENOLATE GEOMETRY .....	x
TETRAHYDROPYRANS.....	x
ABBREVIATIONS.....	xi
1. INTRODUCTION: NATURAL PRODUCTS & ORGANIC SYNTHESIS .....	1
1.1 BIOACTIVE NATURAL PRODUCTS.....	1
1.1.1 NATURAL PRODUCTS OF MARINE ORIGIN.....	2
1.1.2 NATURAL PRODUCTS AS DRUG DISCOVERY LEADS .....	2
1.2 THE ROLE OF ORGANIC SYNTHESIS IN NATURAL PRODUCT CHEMISTRY .....	3
1.2.1 SYNTHESIS AS A SOURCE OF MATERIAL.....	3
1.2.2 SYNTHESIS AS A METHOD FOR STRUCTURE DETERMINATION .....	5
1.3 SUMMARY & ANALYSIS.....	8
2. INTRODUCTION PART II: MADEIROLIDE A .....	9
2.1 MADEIROLIDE A.....	9
2.1.1 ISOLATION & STRUCTURE ELUCIDATION .....	9
2.1.2 STRUCTURE REASSIGNMENT .....	12
2.1.3 STRUCTURE VERIFICATION USING THE DP4 PARAMETER.....	14
2.1.4 BIOLOGICAL ACTIVITY .....	18
2.1.5 CYTOTOXICITY.....	18
2.1.6 FUNGISTATIC/FUNGICIDAL PROPERTIES.....	18
2.2 RELATED NATURAL PRODUCTS – THE MANDELA LIDES .....	19
2.2.1 STRUCTURAL REASSIGNMENT .....	19
2.2.2 BIOLOGICAL ACTIVITY .....	20
2.3 PREVIOUS SYNTHETIC STUDIES TOWARDS MADEIROLIDE A .....	23
2.3.1 PREVIOUS SYNTHETIC STUDIES WITHIN THE PATERSON GROUP.....	24
2.3.1.1 PREVIOUS STUDIES TOWARDS THE C12 - C27 EASTERN FRAGMENT.....	26
2.3.2 OTHER SYNTHETIC STUDIES TOWARDS MADEIROLIDE A .....	28
2.3.2.1 CARTER.....	28
2.3.2.2 LEE.....	32
2.4 SUMMARY & ANALYSIS.....	35
3. RESULTS & DISCUSSION I: SYNTHESIS OF A MODIFIED WESTERN FRAGMENT ...	37
3.1 AIMS AND RATIONALE FOR MODIFICATION OF THE STRATEGY .....	37
3.1.1 RETROSYNTHESIS .....	41
3.2 SYNTHESIS OF THE C3 - C10 ACETONIDE.....	43
3.2.1 SYNTHESIS OF THE C6 - C10 ETHYL KETONE .....	43
3.2.2 INSTALLATION OF THE C5 - C7 STEREOTRIAD .....	44
3.2.2.1 BORON ALDOL REACTION.....	44
3.2.2.2 ELABORATION TO THE C3 - C10 ACETONIDE.....	50
3.3 ELABORATION TO THE MODIFIED C1 - C11 WESTERN FRAGMENT.....	52
3.3.1 PREPARATION OF THE LINEAR C1 - C11 PRECURSOR.....	52
3.3.2 INTRAMOLECULAR OXY-CONJUGATE CYCLISATION .....	54

3.3.2.1	SYNTHETIC STUDIES.....	58
3.3.2.2	MECHANISTIC AND COMPUTATIONAL STUDIES.....	60
3.3.3	COMPLETION OF THE FRAGMENT.....	70
3.3.3.1	SYNTHESIS OF THE CINERULOSE DONOR.....	71
3.3.3.2	GLYCOSYLATION .....	74
3.3.4	SUMMARY AND ANALYSIS.....	75
<b>4.</b>	<b>RESULTS &amp; DISCUSSION II: INVESTIGATIONS INTO THE EASTERN TETRAHYDROFURAN.....</b>	<b>79</b>
<b>4.1</b>	<b>SYNTHETIC STRATEGY FOR THE EASTERN FRAGMENT .....</b>	<b>79</b>
<b>4.2</b>	<b>SYNTHESIS OF THE C13 – C17 FRAGMENT .....</b>	<b>81</b>
4.2.1	RETROSYNTHESIS .....	81
4.2.2	RACEMIC MODEL STUDIES .....	82
4.2.3	ENANTIOSELECTIVE SYNTHESIS THE C13 – C17 ALCOHOL .....	85
4.2.4	SUMMARY AND ANALYSIS.....	90
<b>5.</b>	<b>RESULTS &amp; DISCUSSION III: SYNTHESIS OF THE EASTERN TETRAHYDROPYRAN...91</b>	
<b>5.1</b>	<b>GENERAL SYNTHETIC STRATEGY.....</b>	<b>91</b>
<b>5.2</b>	<b>THE TARTRATE APPROACH.....</b>	<b>92</b>
5.2.1	PREPARATION OF THE LACTATE ETHYL KETONE .....	94
5.2.2	SYNTHESIS OF THE ALDEHYDE .....	95
5.2.3	LACTATE ALDOL COUPLING.....	99
<b>5.3</b>	<b>THE NHK COUPLING APPROACH .....</b>	<b>100</b>
5.3.1.1	LACTATE ALDOL AND PREPARATION OF THE C21 – C27 ALLYLIC ALCOHOL 101	
5.3.1.2	PREPARATION OF THE VINYL IODIDE COUPLING PARTNER.....	105
5.3.1.3	NOZAKI-HIYAMA-KISHI (NHK) COUPLING .....	106
5.3.1.4	CYCLISATION.....	110
5.3.2	COMPUTATIONAL INVESTIGATIONS.....	114
5.3.3	CONSTRAINED CYCLISATION .....	122
	PALLADIUM-CATALYSED CARBONYLATIVE CYCLISATION .....	127
<b>5.4</b>	<b>SUMMARY &amp; ANALYSIS.....</b>	<b>131</b>
<b>6.</b>	<b>SUMMARY &amp; FUTURE DIRECTIONS FOR THE TOTAL SYNTHESIS OF MADEIROLIDE A 133</b>	
<b>6.1</b>	<b>SUMMARY .....</b>	<b>133</b>
<b>6.2</b>	<b>FUTURE WORK .....</b>	<b>135</b>
6.2.1	COMPLETION OF THE C12 - C27 EASTERN FRAGMENT .....	135
6.2.1.1	CONSTRUCTION OF THE THP .....	135
6.2.1.2	FRAGMENT UNION AND ELABORATION INTO THE COMPLETE C12 - C27 FRAGMENT.....	137
6.2.2	END-GAME AND COMPLETION OF MADEIROLIDE A.....	140
<b>6.3</b>	<b>CONCLUSIONS .....</b>	<b>141</b>
<b>APPENDIX A: EXPERIMENTAL.....</b>	<b>145</b>	
GENERAL EXPERIMENTAL DETAILS.....	145	
PREPARATION OF REAGENTS.....	147	
GENERAL PROCEDURES.....	150	
EXPERIMENTAL PROCEDURES FOR THE WESTERN FRAGMENT OF MADEIROLIDE A151		
EXPERIMENTAL PROCEDURES FOR THE EASTERN FRAGMENT OF MADEIROLIDE A168		
COMPOUNDS TOWARDS THE THF.....	168	
COMPOUNDS TOWARDS THE THP.....	170	
<b>APPENDIX B: SELECTED NMR SPECTRA.....</b>	<b>187</b>	
<b>APPENDIX C: DETAILS OF COMPUTATIONAL PROCEDURES.....</b>	<b>217</b>	
GENERAL DETAILS .....	217	
<b>REFERENCES .....</b>	<b>221</b>	

# NOMENCLATURE

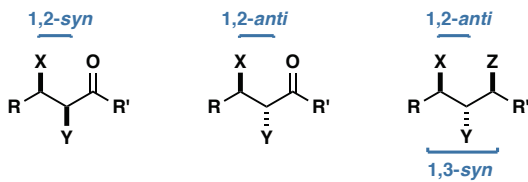
## COMPOUND NUMBERING

The naming and numbering of compounds follows priorities laid out by IUPAC. For the purposes of clarity, madeirolide A **1** and fragments derived from it are numbered in accordance with the system proposed by the isolation group. To avoid ambiguity, this numbering is used for assignment of resonances in NMR spectra. Additional numbers (32 – 37) have been used for the cinerulose sugar to avoid confusion with the assignment of diastereotopic protons.



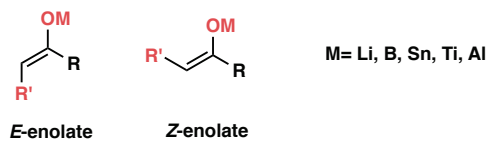
## RELATIVE STEREOCHEMICAL RELATIONSHIPS

As defined by Masamune, *syn*- and *anti*- nomenclature is used in this thesis to define the relative stereochemistry of two substituent groups along a carbon chain. Groups are considered *syn* if they point in the same direction out of the plane of the paper, conversely, they are considered *anti* if they point in different directions out of the plane of the paper.



## ENOLATE GEOMETRY

Metal enolates are described as *E*- and *Z*-enolates on the basis of IUPAC recommendations. The metal-oxygen bond is taken to have the highest priority in all cases, irrespective of the R-substituent adjacent to it.



## TETRAHYDROPYRANS

The relative stereochemistry of THP rings is described as either *2,6-cis* or *2,6-trans* based upon the relative configuration at the carbons adjacent to oxygen.



# ABBREVIATIONS

abs	absolute
Ac	acetyl
AcO	acetate
anhyd	anhydrous
APCI	atmospheric pressure chemical ionisation
aq	aqueous
Ar	aryl, generic aromartic group
asym	asymmetrical
atm	atmosphere
ATP	adeonosine triphosphate
BAIB	<i>bis</i> -acetoxyiodobenzene
Bn	benzyl
BOC	<i>tert</i> -butyloxycarbonyl
bp	boiling point
br	broad or broadened (spectra)
Bu	butyl
Bz	benzoyl
CBS	Corey-Bakishi-Shibata (reaction)
c	concentration
calcd	calculated
CI	chemical ionisation
con	conrotatory
COSY	correlation spectroscopy, $^1\text{H} - ^1\text{H}$
concd	concentrated
cryst	crystalline
CSA	camphorsulfonic acid
Cy	cyclohexyl
d	doublet (spectra)
DBU	1,8-diazabicyclo[5.4.0]undec-7-ene
DCC	<i>N,N'</i> -dicyclohexylcarbodiimide
DCM	dichloromethane

DDQ	2,3-dichloro-5,6-dicyanobenzoquinone
dec	decomposition
decomp	decompose
DFT	density functional theory
DIBAL	diisobutyl aluminium hydride
dil	dilute
DIPEA	<i>N,N'</i> -diisopropylethylamine
dis	disrotatory
DMAP	<i>N,N'</i> -dimethylaminopyridine
DMF	<i>N,N'</i> -dimethylformamide
DMP	Dess-Martin periodinane (reagent)
DMSO	dimethylsulfoxide
ee	enantiomeric excess
EI	electron impact
	electron ionisation
<i>ent</i>	enantiomer
<i>epi</i>	inversion of normal configuration
equiv	equivalent
ESI	electrospray ionisation
Et	ethyl
g	grams
gem	geminal
GIAO	gauge-invariant atomic orbitals
HF	Hartree-Fock
HMBC	heteronuclear multiple bond correlation
HMPA	hexamethylphosphoramide
HOMO	highest occupied molecular orbital
HPLC	high-performance liquid chromatography
HRMS	high-resolution mass spectrometry
HSQC	heteronuclear single quantum coherence
Hz	hertz
ipc	isopinocampheyl
IR	infrared
J	joule
<i>J</i>	coupling constant
k	kilo
K	equilibrium constant

K	kelvin
kg	kilogram
l	liquid
LCAO	linear combination of atomic orbitals
lit.	literature
LUMO	lowest unoccupied molecular orbital
Lut	lutidine
M	molar ( $\text{mol dm}^{-3}$ )
m	multiplet (spectra)
	metre
max	maximum
Me	methyl
Mes	mesityl
MHz	megahertz
min	minute
	minimum
mL	millilitre
mM	millimolar
mmHg	millimetres of mercury
mmol	millimole
MO	molecular orbital
mol	mole
MOM	methoxymethyl
mp	melting point
Ms	mesyl, methylsulfonyl
MS	mass spectrometry
	mass spectrum
<i>m/z</i>	mass-to-charge ratio
v	frequency (spectra)
NBS	<i>N</i> -bromosuccinimide
nm	nanometre
NMR	nuclear magnetic resonance
nOe	nuclear Overhauser effect
NOESY	nuclear Overhauser enhancement spectroscopy
<i>o</i>	ortho
OAc	acetate
obsd	observed

oxidn	oxidation
<i>p</i>	para
pH	negative logarithm of hydrogen ion concentration
Ph	phenyl (for C <sub>6</sub> H <sub>5</sub> only)
pKa	p <i>K</i> for association
ppb	parts per billion
ppm	parts per million
ppt	precipitate
Pr	propyl
Py	pyridine
q	quartet (spectra)
<i>rac</i>	racemic
recryst	recrystallised
rel	relative
Rf	retention factor
s	second
	singlet (spectra)
	solid
	strong (spectra)
<i>s</i>	secondary
<i>sec</i>	secondary
soln	solution
std	standard
STO	Slater-type orbital
<i>sym</i>	symmetrical
t	triplet (spectra)
<i>t</i>	time
	tertiary
<i>T</i>	temperature
TCA	trichloroacetic acid
temp	temperature
<i>tert</i>	tertiary
TFA	trifluoroacetyl
	trifluoroacetic acid
THF	tetrahydrofuran
TLC	thin-layer chromatography
TMS	tetramethylsilane

	trimethylsilyl
TOF-MS	time-of-flight mass spectrometry
Tol	tolyl
Ts	tosyl, 4-toluenesulfonyl
UV	ultraviolet
vol	volume
w	weak (spectra)
wt	weight



# 1

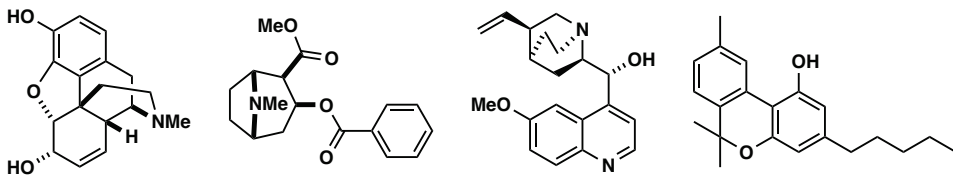
## 1. INTRODUCTION: NATURAL PRODUCTS & ORGANIC SYNTHESIS

### 1.1 BIOACTIVE NATURAL PRODUCTS

The use of natural products in traditional medicine has been extensively documented, with records of crude extracts from plant, animal and marine sources dating back as far as 2100 BC.<sup>1</sup> The development of modern synthetic and medicinal chemistry has gradually enabled the active components of these traditional remedies to be isolated in their pure forms allowing thorough evaluation of their biological properties.

While many traditional medicines have now been shown to have minimal efficacy, there are numerous examples of natural products that have progressed through clinical trials and are still widely used, either in their original form or as synthetic analogues. Morphine **1**, cocaine **2** and quinine **3** (**Figure 1.1**) are all examples of naturally occurring molecules known to humankind for hundreds of years, yet only isolated as pure compounds in recent history.

The systematic study of traditional medicines is still ongoing, a prime example being cannabinol **4** which has received significant interest in recent years owing to its potential uses for the treatment of pain, nausea, arthritis and addiction.<sup>2</sup>



**1:** Morphine

**2:** Cocaine

**3:** Quinine

**4:** Cannabinol

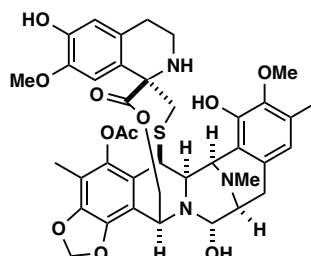
**Figure 1.1:** Structures of natural products used in traditional medicine that have subsequently been isolated and characterised as medicines in their pure forms.

### 1.1.1 NATURAL PRODUCTS OF MARINE ORIGIN

Despite accounting for more than 70% of the earth's surface,<sup>3</sup> there are remarkably few representations of marine derived natural products in traditional medicine. This can be attributed to the fact that the marine environment remained largely unexplored prior to the development of underwater breathing apparatus and deep-sea submersibles in the 20<sup>th</sup> century.

Sustained scientific interest in marine natural products has permitted the isolation of over 18000 unique chemical entities,<sup>4</sup> many of which possess novel modes of action<sup>5</sup> and structural motifs not found terrestrially.<sup>4</sup> Currently, seven marine natural products (or analogues derived from them) have been approved for use in humans by the FDA,<sup>6</sup> with around 20 at various stages of clinical trials, mostly for oncological targets. One example of a successful marine natural product now used extensively in the clinic is Yondelis® **5** (trabedectin, Pharmamar)<sup>7</sup>, first isolated from the marine tunicate *Ecteinascidia turbinata* in 1984 and approved by the FDA in 2015 for the treatment of soft tissue sarcoma.

With estimates suggesting that as little as 5% of the marine environment has been explored, the ocean represents a significant untapped potential in the discovery of new medicines. As analytical tools and deep-sea exploration techniques advance, an ever-increasing number of new chemical entities are sure to be discovered.



**5:** Yondelis (Trabedectin)

**Figure 1.2:** Structure of Yondelis® **5**, an example of a marine natural product approved by the FDA for the treatment of cancer (**Pharmamar**).

### 1.1.2 NATURAL PRODUCTS AS DRUG DISCOVERY LEADS

In recent years, there has been a resurgence of interest in natural products as lead-like compounds for drug discovery owing to the failure of ‘modern’ methods such as combinatorial synthesis and high-throughput screening (HTS) to deliver significant numbers of drug candidates. Indeed, annual FDA approvals have remained steady despite substantial increases in funding, suggesting that new medicines may be becoming harder to find. The paucity of new medicines has one key reason: specificity. To be worthwhile, a drug must bind

to its target, and only its target. This binding is difficult to achieve artificially, with most synthetic drugs occupying vastly different chemical space than natural products.<sup>8,9</sup> In contrast, evolution has meant that natural products are necessarily ‘drug-like’ – organisms would not continue to produce them as secondary metabolites if they imparted no advantage. The ability to harness this source of biological activity is of key importance for the discovery of new drugs.

The future of drug discovery likely lies at the intersection between natural products and synthetic medicines: natural product-like screening libraries offer the possibility of finding more diverse hits, diversity-oriented synthesis (DOS) offers the possibility of generating large numbers of stereochemically diverse fragments, and genomics offers the possibility of manipulating biosynthetic pathways to offer new possibilities for drug design.

## 1.2 THE ROLE OF ORGANIC SYNTHESIS IN NATURAL PRODUCT CHEMISTRY

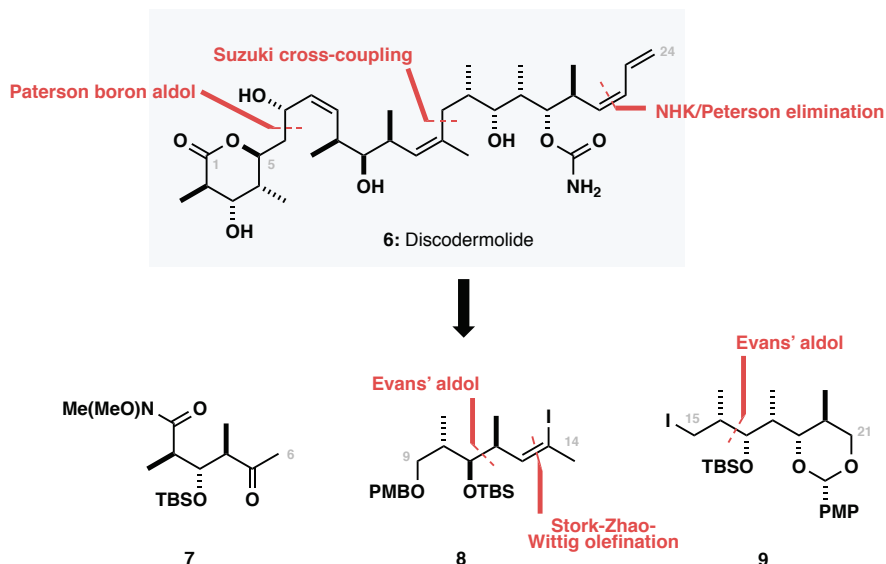
### 1.2.1 SYNTHESIS AS A SOURCE OF MATERIAL

One of the greatest challenges when considering the use of natural products and their derivatives in drug discovery is the sustainable supply of material, with multi-gram quantities required to progress a molecule through clinical trials and into the clinic. While some secondary metabolites such as opium and quinine are produced abundantly in nature, others are produced in such low concentrations that isolation from natural sources is neither economically nor environmentally sustainable. Despite the significant improvements in bioengineering that have allowed an increasing number of secondary metabolites to be produced artificially through culture, synthesis is still often the only tractable way to reliably obtain the necessary material.

The Novartis total synthesis of (+)-discodermolide **6** was a landmark achievement in process chemistry, demonstrating the viability of carrying out academic synthesis in an industrial context.<sup>10–14</sup> Reported in 2004, Mickel and co-workers at Novartis successfully synthesised 64 g of (+)-discodermolide via a route that took advantage of the best aspects of the syntheses developed independently by Paterson and Smith, including several challenging asymmetric aldol reactions. Although the clinical development of discodermolide was halted during clinical trials owing to unexpected levels of toxicity, it remains to this day one of the most complex molecules to be produced on a process scale, and validated the plausibility of using total synthesis to access significant quantities of a natural product.

A more recent example is eribulin mesylate **11** (Eisai Co.), a simplified analogue of the marine natural product halichondrin B **10** that was approved for the treatment of breast cancer in

2010.<sup>15</sup> The stereoselective synthesis of **11** takes 62 steps,<sup>16</sup> making it the most complex non-peptide drug to be obtained using organic synthesis to date.



**Scheme 1.1:** The Novartis route to (+)-discodermolide **6** demonstrating the possibility of carrying out complex asymmetric synthesis on an industrial scale (Novartis/Mickel).

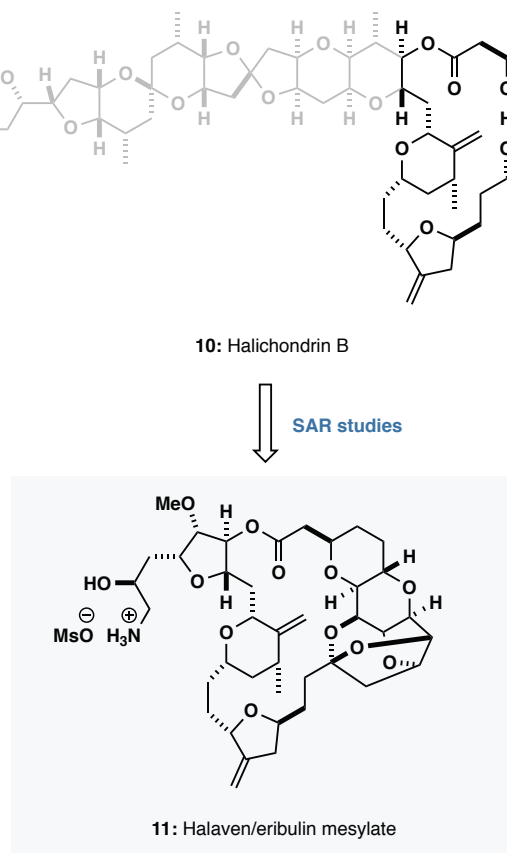


**Figure 1.3:** Structure of halichondrin B **10** and the simplified analogue eribulin mesylate **11** (Kishi/Eisai).

Semi-synthesis is also an important discipline in which abundant natural occurring molecules are chemically elaborated into more complex, higher value products. Two key examples of this are the synthesis of taxol **12** from 10-deacetylbaccatin **13**, and trabectedin **14** from cyanosafracin B **15**,<sup>17</sup> both of which are approved by the FDA as chemotherapeutic agents.

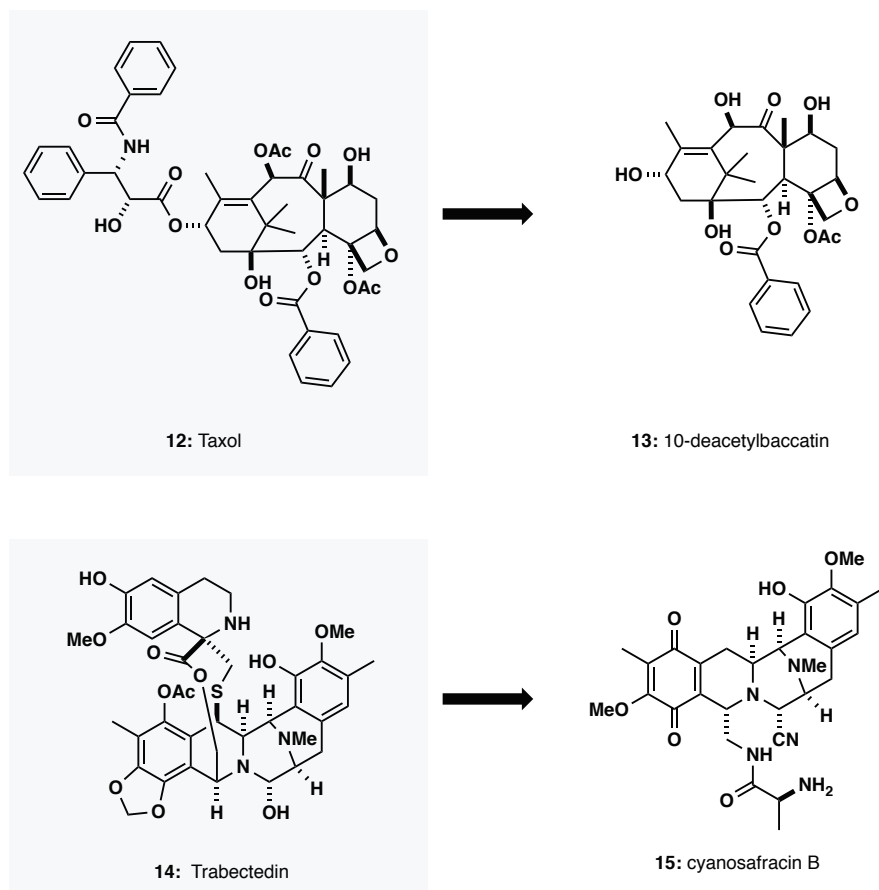


**Figure 1.4:** Semi-synthetic routes used in the process scale synthesis of taxol **12** and trabectedin **14**.

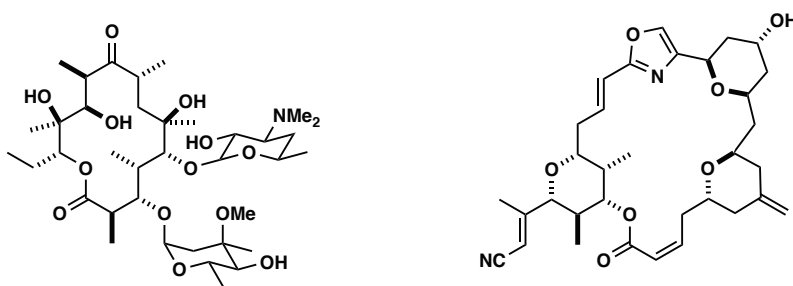
Ultimately, chemical synthesis is often the only viable way to produce natural product drugs reliably, and with new methodology constantly pushing the boundaries of what is possible, ever more complex molecules can be evaluated as potential drugs.

### 1.2.2 SYNTHESIS AS A METHOD FOR STRUCTURE DETERMINATION

The structural elucidation of new natural products facilitates interdisciplinary research across chemistry, biology and medicine. In the formative years of natural product research, structure elucidation of complex metabolites required multi-gram quantities of material to be isolated in order to enable chemical degradation and derivatisation studies which aimed to produce known fragments from which the complete structure of the molecule could be pieced together. This process was time consuming, and the unambiguous assignment of structure was often challenging and prone to error, resulting in the need for many structural revisions.

With the development of X-ray crystallography, high-resolution NMR, and advanced MS techniques, it is now common for structural elucidation to be carried out on milligram scales, significantly reducing the burden of isolation. Moreover, many of the above analytical techniques are non-destructive, allowing the material to be reused in subsequent biological assays. These techniques, coupled with advances in computational structure prediction and verification tools, make it possible to deduce the structure of even the most challenging metabolites with high-levels of confidence.

To put this in context, erythromycin A **16** was isolated in 1952 from the bacteria *Streptomyces erythreus*, but not until 1957 after exhaustive studies, was the complete structure able to be established, several years after its widespread adoption as a broad-spectrum antibiotic (**Figure 1.5**). In contrast, the structure of a similarly complex polyketide natural product, hemi-phorboxazole A **17**, isolated in trace amounts from *Phorbas sp.* was able to be elucidated fully using only 16.5 µg of material.<sup>18</sup> Both natural products have subsequently had their structures verified through total synthesis, with synthetic material correlating well to the authentic samples.<sup>19,20</sup>

**16:** erythromycin A**17:** hemi-phorboxazole

**Figure 1.5:** Structures of erythromycin **16** and hemi-phorboxazole A **17**.

While these developments in technology may suggest that any metabolite may be defined unambiguously without the requirement for structure verification (i.e. through synthesis), some challenges still exist, often due to ambiguity arising in spectroscopic data around isolated stereocentres, or in highly flexible chains where the conformation is unpredictable. In recent analyses by Nicolaou<sup>21</sup> (covering 1990 – 2005) and McPhail<sup>22</sup> (covering 2005 – 2010), over 600 natural products were identified that subsequently required structural revision.\*

These ambiguities may be resolved through the total synthesis of molecules with defined connectivity and stereochemistry, allowing for comparison between synthetic and authentic

\* The true number of incorrectly assigned structures is likely significantly higher since many reported natural products are never investigated further due to a lack of biological activity or interesting structural features.

samples of the natural product. Leiodermatolide A **21** and amphidinolide A **19** (**Figure 1.6**) were both able to be correctly identified through detailed NMR studies and synthetic efforts by Paterson<sup>23</sup> and Trost<sup>24</sup> respectively after the synthesis of several (of the many) possible diastereomers.

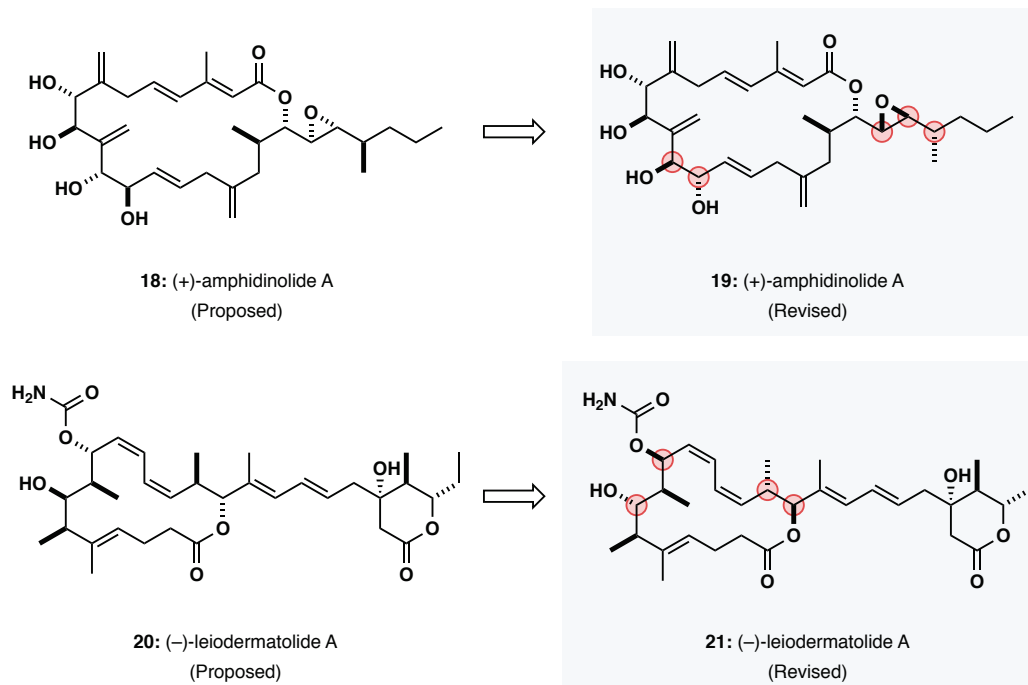


**Figure 1.6:** Representative examples of polyketide natural products reassigned using total synthesis. Stereocentres inverted relative to the initial assignment are highlighted.

Baulamycin A **23**, reported in 2014,<sup>25</sup> exemplifies the challenges associated with the complete structural elucidation of a natural product using spectroscopic methods alone (**Figure 1.7**). The natural product is highly conformationally flexible, casting doubt on the original stereochemical assignment of the natural product **22** which was established using Murata's empirical *J*-based configurational analysis known to be inaccurate for isolated stereocentres.<sup>26</sup> Recent work by Aggarwal<sup>27</sup> established that synthetic baulamycin A did not correlate with the proposed structure **22**, however the spectroscopic data did not offer any clues as to where the error may be. The true structure of baulamycin A **23** was eventually discovered after significant synthetic efforts, resulting in an impressive five stereocentres being reassigned relative to the initial report.

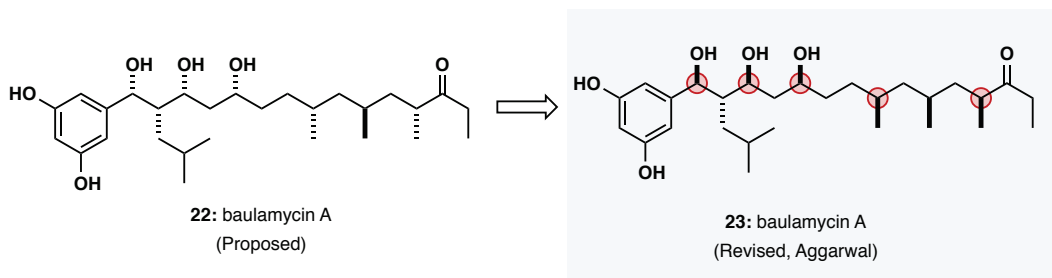


**Figure 1.7:** Structural reassignment of baulamycin A (Aggarwal).

### 1.3 SUMMARY & ANALYSIS

The discovery of new medicines is of critical importance to society. Despite significant progress, many diseases still have no effective treatment, and drug-resistance has led to many widely-used drugs rendered useless.

While nature is often able to provide inspiration for new drugs, synthesis is still deeply important in the search for novel and biologically active molecules. The above discussion aims to highlight the role of chemical synthesis as a central science to the disciplines of drug discovery and medicinal chemistry, providing examples in the contexts of structural elucidation, analogue synthesis and process chemistry.

# 2

## 2. INTRODUCTION PART II: MADEIROLIDE A

### 2.1 MADEIROLIDE A

Madeirolide A **1** (**Figure 2.1**) is a structurally unique marine polyketide isolated from the lithistid sponge *Leiodermatium sp.* At the time of discovery, only three other natural products had been isolated from a sponge of this genus: leiodermatolide A **20**,<sup>23</sup> and the leiodelides A **25** and B **26**.<sup>28</sup> Due to continued efforts, two additional congeners of leiodermatolide have recently been identified (leiodermatolide B **27** and C **28**).<sup>29</sup>

Of the known natural products isolated from *Leiodermatium* sp., only leiodermatolide A **20** has had its structure confirmed conclusively through total synthesis,<sup>30</sup> with the complete stereostructures of the leiodelides still elusive despite synthetic studies and computational investigations by several research groups.<sup>31–33</sup>

#### 2.1.1 ISOLATION & STRUCTURE ELUCIDATION

The isolation and structure elucidation of madeirolide A **1** was carried out by Winder and Wright at the Harbor Branch Oceanographic Institute (HBOI) in 2009. A 1 kg sample of *Leiodermatium* sp. was collected at a depth of 656 m off the southwest coast of Porto Santo (Madeira, Portugal). Exhaustive extraction of the sponge followed by normal and reverse phase chromatography allowed the isolation of madeirolide A **1** (1.2 mg), and a similarly complex congener, madeirolide B **24** (1.3 mg), both as amorphous white solids.

The amorphous form and resistance to crystallisation of madeirolide A **1** meant that extensive 1D- and 2D-NMR spectroscopy had to be relied upon for the purposes of structure elucidation. The 2D structure of madeirolide A was assigned to fit with the HR-ESI-MS and <sup>13</sup>C NMR data, which suggested a molecular formula of C<sub>37</sub>H<sub>56</sub>O<sub>11</sub> (*m/z* observed [M+Na]<sup>+</sup> 699.3735, calculated 699.3715) and required ten degrees of unsaturation be present within the molecule.

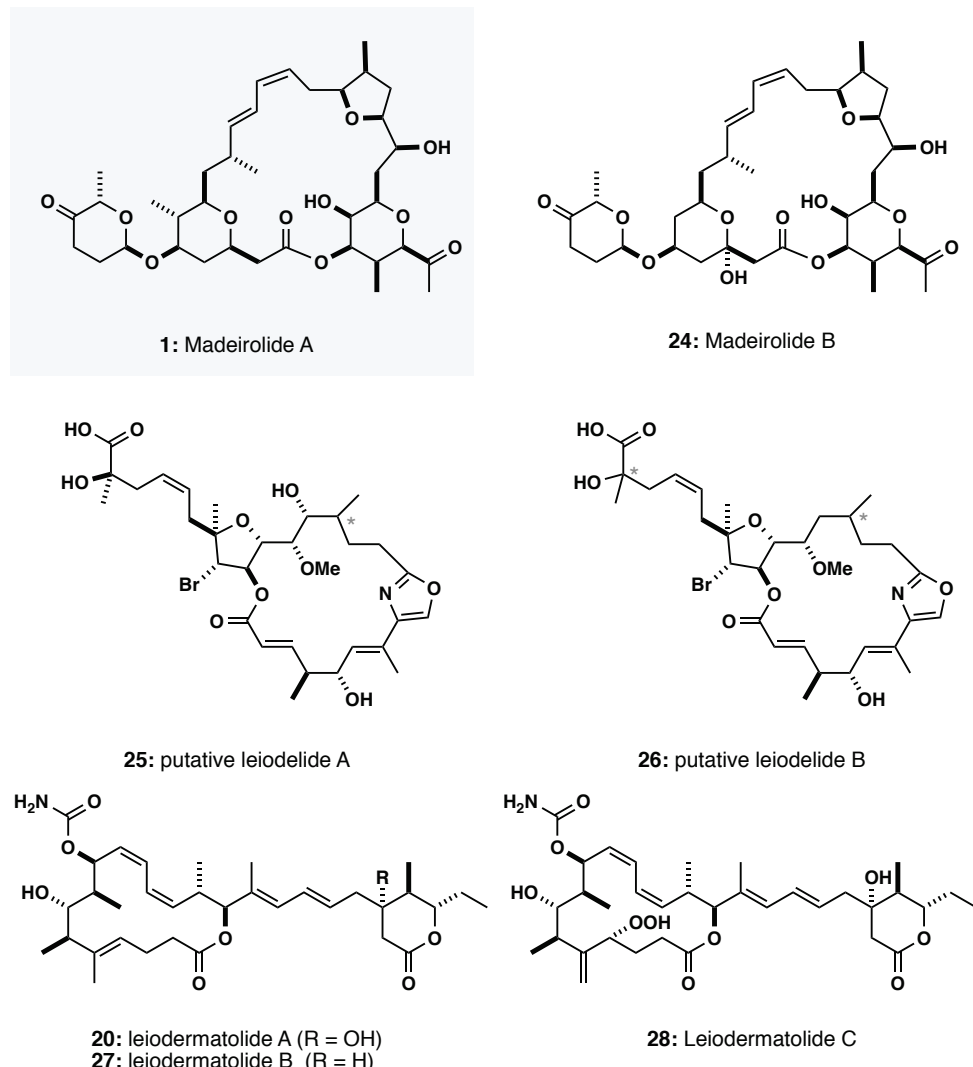


**Figure 2.1:** Structures of madeirolide A **1**, madeirolide B **24**, and other natural products isolated from *Leiodermatium sp.* Undefined stereocentres marked with (\*) represent currently unknown configuration.

Closer inspection of the  $^{13}\text{C}$  NMR shifts indicated the presence of three carbonyl groups: one ester ( $\delta_{\text{C}}$  170.9 ppm) and two ketones ( $\delta_{\text{C}}$  211.0, 208.2 ppm). Two olefins ( $\delta_{\text{C}}$  122.8, 127.5, 130.8, 142.3 ppm) were also present, accounting for five degrees of unsaturation in total. The remaining five degrees of unsaturation would later be identified as cyclic structures: two tetrahydropyrans (THP), a tetrahydrofuran (THF), a pyranose sugar, and the macrolactone itself.

The connectivity of madeirolide A **1** was established based on six isolated proton spin systems, determined using  $^1\text{H}$ - $^1\text{H}$ -COSY and  $^1\text{H}$ - $^{13}\text{C}$ -gHSQC relationships (Figure 2.2), with  $^1\text{H}$ - $^{13}\text{C}$ -HMBC correlations used to connect them into a single structure. A bis-acetate derivative was also prepared during the elucidation work to confirm the positions of the free hydroxyl groups at C19 and C22.

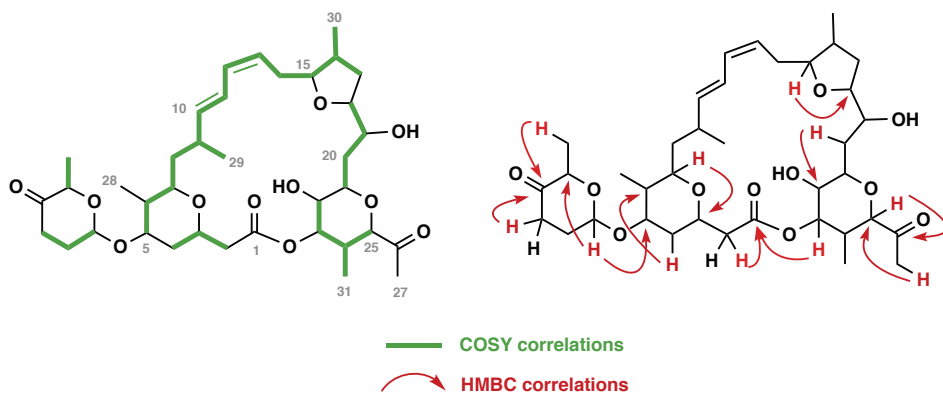


**Figure 2.2:** Planar 2D structure of madeirolide A showing relevant COSY and HMBC correlations.

The 16 stereocentres present in madeirolide A **1** are arranged in three relatively isolated clusters: **A**, containing the tetrahydrofuran and diene; **B**, containing the sugar and the western tetrahydropyran; and **C**, containing the all-*cis* eastern tetrahydropyran. The relative configuration within each stereocluster of madeirolide A was proposed on the basis of scalar  $^3J_{H-H}$  couplings and NOESY correlations. Key NOESY correlations within each stereocluster are shown in **Figure 2.3**.

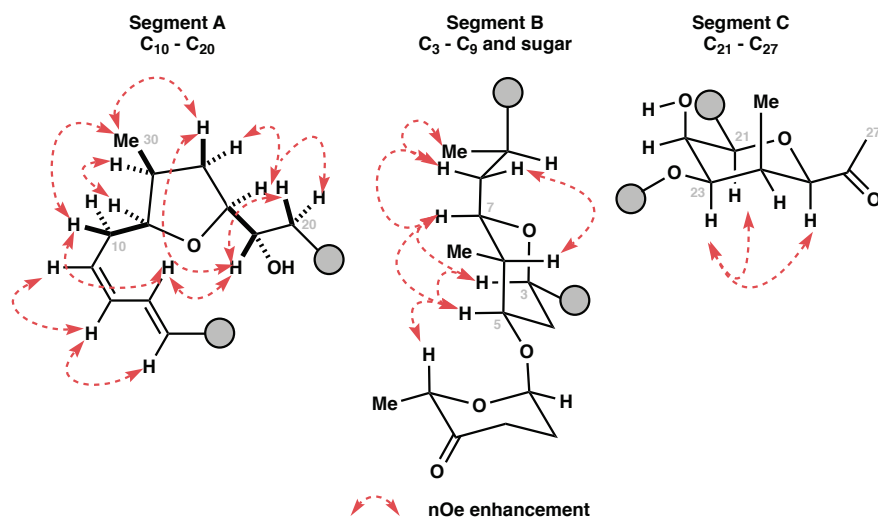
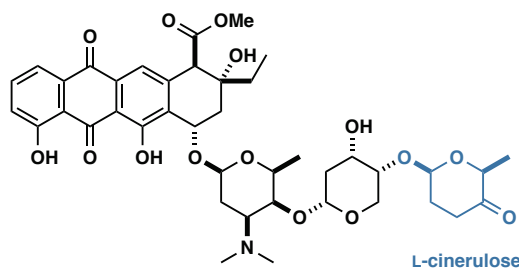


**Figure 2.3:** Key reciprocal nOe enhancements used to assign relative stereochemical relationships within the three heterocycles.

The relative stereochemistry of the six-membered rings is unambiguous; nOe analysis is highly accurate owing to the well-defined conformations adopted. For five-membered rings, nOe analysis can lead to ambiguity as the through-space *cis* and *trans* couplings often have similar magnitudes.<sup>34</sup> Additional NOESY experiments allowed for the observation of transannular correlations across the macrolactone, allowing for the relative stereochemistry between the

three stereoclusters to be determined. Crucially, the proposed assignment of relative stereochemistry was based upon a correlation between the C29-methyl group and H22/H23\*.

The absolute configuration of madeirolide A has yet to be determined conclusively, with attempts at derivatisation to generate the corresponding MTPA esters unsuccessful. As depicted, the absolute configuration of madeirolide A **1** is defined based on that of L-cinerulose, which is the naturally occurring isomer of the sugar, and found in other natural products such as aclacinomycin A **29** (**Figure 2.4**).<sup>35</sup> The completed total synthesis of mandelalide A (see §2.2.1.1) provides additional support for the proposed configuration, having the same absolute configuration as madeirolide A.



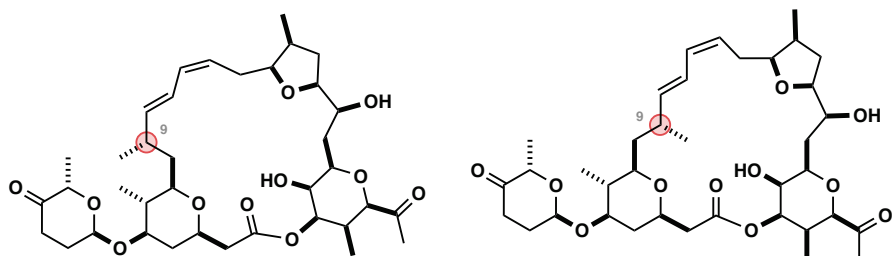
**29:** Aclacinomycin A

**Figure 2.4:** Structure of aclacinomycin A **29** showing the L-cinerulose moiety.

## 2.1.2 STRUCTURE REASSIGNMENT

Although the 2D connectivity was established unambiguously by Winder and Wright, it is now believed that an error was made in assigning the overall relative stereochemistry, due to a mix-up of a crucial transannular NOESY correlation across the macrolactone. The error is thought to have occurred when the working 3D diagrams produced during the elucidation work (**Figure 2.3**) were translated into standard 2D skeletal representations (**Figure 2.5**). Madeirolide A was initially depicted as shown in **30**, requiring that the C29-methyl group be drawn pointing downwards in order that the transannular NOESY correlations between the C29-methyl group and H22/23 were preserved. This depiction led to the C9-stereocentre ending up with an (*S*) configuration, in conflict with the (*R*) configuration of Winder's 3D diagrams.

\* While the observation of the transannular NOESY correlation was correct, the interpretation led to an incorrect assignment of the stereochemistry at C9 due to the way in which the macrolactone was represented by the isolation group. This is discussed in more detail in subsequent sections.



**30:** Winder and Wright's representation  
of putative Madeirolide A

**1:** Corrected structure of Madeirolide A

**Figure 2.5:** Comparison of madeirolide A **1** with the C9-epimer proposed by Winder and Wright in its initial representation **30**. The stereocentre inverted relative to Winder's initial assignment is highlighted.

Winder's error can be appreciated by considering the calculated lowest energy conformations of the two C9-epimers of madeirolide A in chloroform (**Figure 2.6**): **1** and **30**. In **1**, the C29 protons and H22/23 are in close proximity, allowing an nOe enhancement to be observed. This is not the case for C9-*epi*-madeirolide A **30**, where the more distant protons in question are unlikely to interact.

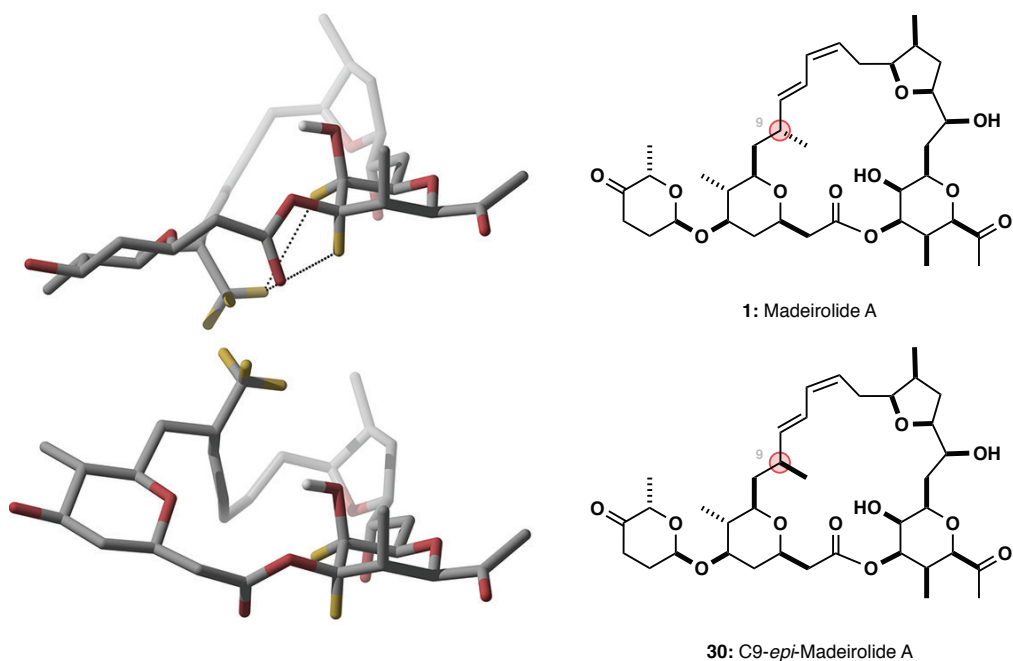


**Figure 2.6:** Lowest energy conformations of C9-*epi*-madeirolide A **30** and madeirolide A **1**. Protons involved in the observed transannular nOe enhancements are highlighted in yellow. Some hydrogens have been omitted for clarity. [DFT-B3LYP/6-31G\*\*, CHCl<sub>3</sub>].

### 2.1.3 STRUCTURE VERIFICATION USING THE DP4 PARAMETER

With remaining uncertainty over the relative stereochemistry of madeirolide A, and in order to further validate our proposed reassignment, the molecule was considered a suitable candidate for computational studies using the DP4 methodology reported by Goodman and Smith in 2010.<sup>36</sup> Initial DP4 calculations on madeirolide A were carried out by Dr Guy Naylor,<sup>37</sup> a former member of the Paterson group.

The DP4 parameter allows for the identification of the most probable relative stereochemistry of a compound by comparison of calculated NMR shifts to experimentally measured values. Given that the NMR spectrum of two enantiomers is necessarily identical, DP4 is able only to assist in assignment of *relative* stereochemistry, with other methods such as chiral derivatisation necessary to gain insight into the absolute configuration. Since its initial publication, the DP4 methodology has been widely adopted, finding extensive use in the structure determination of complex natural products. Recently, several developments have been made to the process, notably allowing for automation of the process using Python,<sup>38</sup> and improvement of accuracy when studying small molecules using DP4+.<sup>39</sup>

To utilise the DP4 parameter, a conformational search using molecular mechanics is first run on all diastereomers to be considered in the analysis\*. Low energy conformers within 10 kJ mol<sup>-1</sup> of the minimum<sup>†</sup> are then used in a calculation of NMR shielding tensors from which solvent specific chemical shifts may be derived (**Figure 2.7**). One unique feature of the DP4 methodology is that the calculated NMR shifts for each conformer are subjected to Boltzmann weighting in order to determine the averaged overall chemical shifts – in doing this, the calculation more accurately represents the distribution of conformers in solution, but also avoids computationally costly DFT optimisations of every conformer in the ensemble which is not practical for large molecules such as natural products.

\* To give an example, a molecule with 10 stereocentres would have 512 possible diastereomers, excluding enantiomers, which may be ignored during DP4 analysis as the calculated NMR shifts will necessarily be identical. This would involve 512 individual conformational searches to be conducted, with the low-energy conformers generated from each diastereomer then used in subsequent DFT calculations.

† 10 kJ mol<sup>-1</sup> was chosen as an arbitrary cut-off, providing a high enough threshold to ensure all low energy conformers are found, while minimising the computational expense. Previous studies in the Goodman group have shown that raising the cutoff to 25 kJ mol<sup>-1</sup> does not provide a significant enhancement in results.

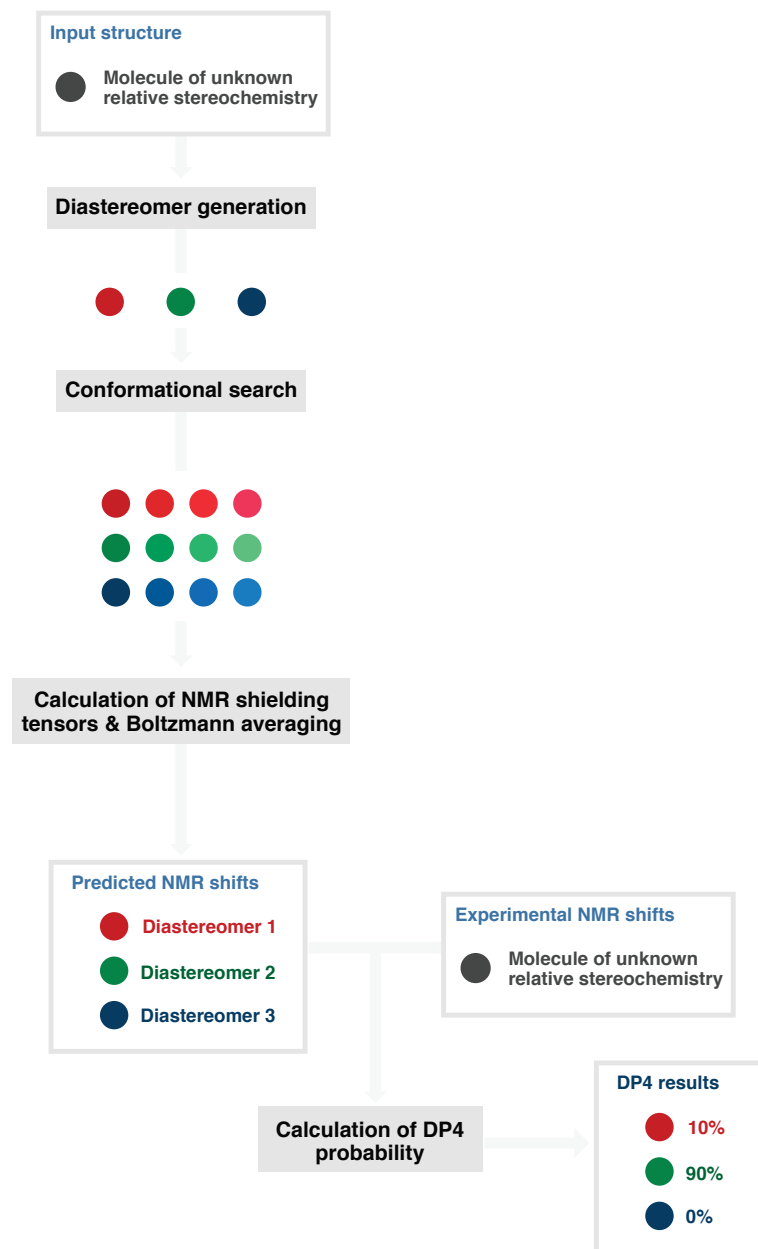
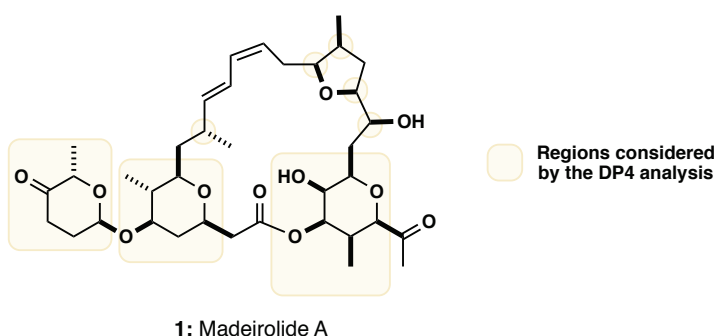


**Figure 2.7:** Computational workflow for assignment of relative stereochemistry using the DP4 methodology.

In Naylor's analysis of madeirolide A, the six-membered rings were considered as single variables with defined relative stereochemistry, while the stereocentres around the five-membered ring were considered separately along with the isolated stereocentres – this simplification was made as six-membered rings adopt predictable conformations and nOe analysis is generally considered reliable. In total, only eight variables were considered, reducing the number of diastereomers considered in the calculation from 32 768 to a more manageable 128.



1: Madeirolide A

**Figure 2.8:** Regions considered in the DP4 analysis of madeirolide A (Naylor).<sup>37</sup>

In total, the calculations on madeirolide A took six weeks to run distributed across multiple CPUs to generate 1285 low-energy conformations which were used in GIAO NMR calculations. The two diastereomers with the highest probability by DP4 based on  $^1\text{H}$ ,  $^{13}\text{C}$ , and the combined  $^1\text{H}/^{13}\text{C}$  calculations are shown in **Figure 2.9**. Diastereomer **1** (madeirolide A) was found to have the highest probability in all cases ( $^1\text{H}$ : 61.06%,  $^{13}\text{C}$ : 93.59%.  $^1\text{H}/^{13}\text{C}$ : 99.65%)\*. Notably, Winder and Wright's C9 epimer does not appear in the results, with the next most likely diastereomer being the C18 epimer **31** ( $^1\text{H}/^{13}\text{C}$ : 0.35%), inverting the relative stereochemistry across the tetrahydrofuran ring. The results of the DP4 calculations coupled with careful re-analysis of the NMR data gives strong support to **1** being the true stereostructure of madeirolide A, providing a strong basis for which a total synthesis can be carried out. Only completion of the synthesis will allow the *absolute* configuration of the molecule to be determined.

\* Empirical results from within the Goodman group suggest that a combined  $^1\text{H}/^{13}\text{C}$  weighted average provides the most reliable DP4 probabilities. During the GIAO DFT calculations, shielding tensors are calculated for all atoms, meaning calculation of  $^1\text{H}$ ,  $^{13}\text{C}$  and  $^1\text{H}/^{13}\text{C}$  probabilities does not require any additional computational resources.

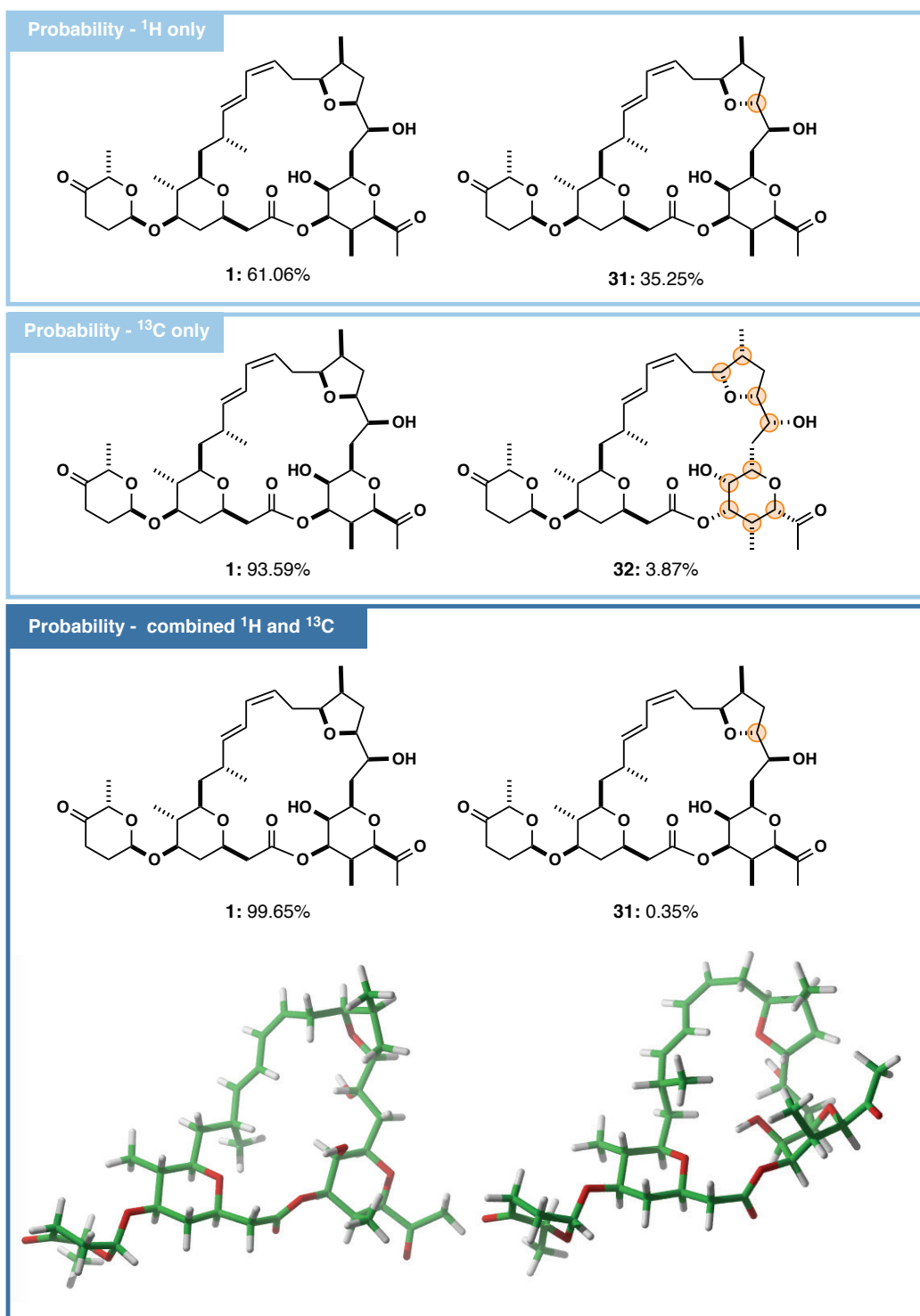


**Figure 2.9:** Results of the DP4 analysis of madeirolide A showing the two most probable diastereomers based on  $^1\text{H}$ ,  $^{13}\text{C}$  or combined  $^1\text{H}/^{13}\text{C}$  calculations. Centres inverted relative to the proposed structure of madeirolide A are highlighted. 3D structures represent the DFT optimised lowest energy conformation for each diastereomer in  $\text{CHCl}_3$  (Naylor).<sup>37</sup>

## 2.1.4 BIOLOGICAL ACTIVITY

Biological evaluation of the madeirolides was carried out by Winder at the time of isolation. Due to the low isolation yield (1.2 mg and 1.3 mg for madeirolide A and B respectively from 1 kg of wet sponge) and material lost to derivatisation attempts, only preliminary biological studies were able to be conducted, severely limiting the conclusions able to be drawn. Madeirolide A **1**, madeirolide B **24**, and the *bis*-acetyl derivative prepared during the structure elucidation work were all evaluated. The results of these studies are summarised below in **Table 2.1**:

**Table 2.1:** Summary of biological data reported for madeirolides A and B, and the *bis*-acetyl derivative of madeirolide A (**Wright**).<sup>40</sup>

	Cytotoxicity <sup>a</sup>		<i>C. albicans</i> assay		
	AsPC-1 (%inhibition)	PANC-1 (%inhibition)	ZOI (mm)	Fungistatic MIC (ug/mL)	Fungicidal MIC (ug/mL)
Madeirolide A	22	44	25	6.2	12.5
Madeirolide B	21	45	28	6.2	21
<i>bis</i> -acetyl madeirolide A	10	-4 <sup>b</sup>	-	>50 <sup>c</sup>	>50 <sup>c</sup>

<sup>a</sup>: Cytotoxicity measured at a concentration of 10 µg/mL of compound

<sup>b</sup>: Cell proliferation was greater than the drug-free control sample

<sup>c</sup>: The assay was run at concentrations of up-to 50 µg/mL, no MIC was reached below this point

## 2.1.5 CYTOTOXICITY

Madeirolides **A 1** and **B 24**, along with the *bis*-acetyl derivative prepared during the structure elucidation work were tested using standard MTT cell proliferation assays at a concentration of 10 µg/mL. The choice of cell lines used was directed by the Wright groups continued interest and funding in the discovery of novel anti-tumour agents against pancreatic cancer. Two adenocarcinoma cell lines were investigated: AsPC-1, obtained from a 62-year-old female, and PANC-1, isolated from a 56-year-old male. In both cases the cancer was found to be highly aggressive, with significant metastases to local abdominal organs.<sup>41</sup> Despite marine polyketide natural products often showing significant levels of cytotoxicity,<sup>42</sup> the above assays using the madeirolides suggests minimal inhibition of cancer cell growth, albeit against a limited range of cell-lines.

## 2.1.6 FUNGISTATIC/FUNGICIDAL PROPERTIES

In recent years, interest in small molecules active against *Candida albicans* and other fungal pathogens has increased due to the evolution of drug resistance towards currently used

pharmaceuticals, the most common class of which, the azoles, are rapidly becoming obsolete.<sup>43</sup>

The fungicidal and fungistatic properties of the madeirolides, and the *bis*-acetyl derivative were evaluated used a disk diffusion assay. As previously, the *bis*-acetyl derivative showed zero activity, however both madeirolide A and B were shown to be potent inhibitors of pathogen growth, having large zones of inhibition (ZOI) at micromolar concentrations.\*

## 2.2 RELATED NATURAL PRODUCTS – THE MANDELALIDES

Three years after the isolation and characterisation of the madeirolides, McPhail reported the discovery of mandelalide A **33** (Figure 2.10) along with three structurally related congeners.<sup>44</sup> Despite being isolated from a marine sponge of a different genus (*Lissoclinum ascidianum*) that was collected over 5000 miles away off the coast of Port Elizabeth (South Africa), the proposed structures of the mandelalides show a remarkable degree of homology to those of the madeirolides. The shared western tetrahydropyran motif (differentially glycosylated and lacking the methyl group) is evident, along with the eastern tetrahydrofuran. Given the clear structural similarities between the two polyketides, it would not be unreasonable to suggest a common biogenic origin

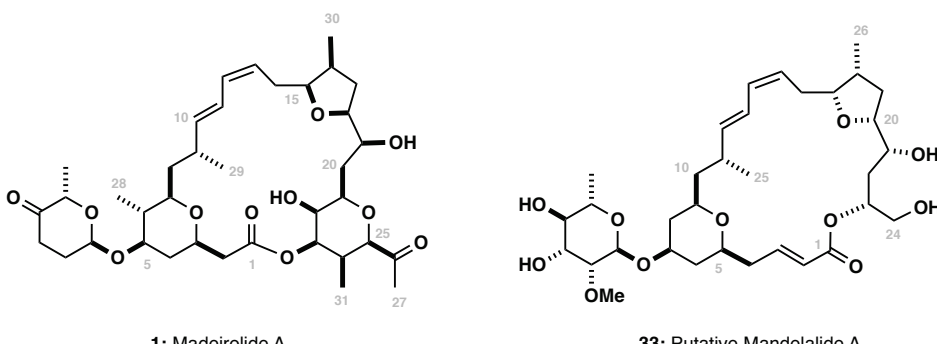


**Figure 2.10:** Comparison of madeirolide A **1** to McPhail's originally proposed structure of mandelalide A **33**.

### 2.2.1 STRUCTURAL REASSIGNMENT

The first total synthesis of putative mandelalide A **33** was completed by Fürstner and co-workers in 2014.<sup>45</sup> Disappointingly, comparison between synthetic and natural samples of the natural product revealed small but irreconcilable differences in the spectral data, suggesting either an error in the relative stereochemistry proposed by McPhail, or in the synthetic

\* Fluconazole, one of the current treatments in use for the treatment of *C. Albicans* has reported MIC values between 0.25 and 64.0 µg/mL.<sup>173</sup>

route.<sup>44</sup> An independent synthesis of the same putative structure by Ye and co-workers ruled out the possibility of a synthetic error, arriving at the same spectral discrepancies via a unique synthetic route.<sup>46</sup>

McPhail's error was initially attributed to the inversion of a single stereocentre at C11 based upon the magnitude of the errors observed in the <sup>13</sup>C NMR spectra ( $\text{C}11 \Delta\delta_{\text{C}} = +1.4 \text{ ppm}$ ;  $\text{C}25 \Delta\delta_{\text{C}} = -1.8 \text{ ppm}$ ) with Fürstner also suggesting that the same ROESY correlations could be observed from either C11 epimer.\* Unfortunately, preparation of the C11 epimer and comparison of the <sup>1</sup>H and <sup>13</sup>C NMR spectra again showed significant differences ( $\text{C}25 \Delta\delta_{\text{C}} = +3.7 \text{ ppm}$ ) suggesting that more significant errors existed in McPhail's originally proposed structure.<sup>47</sup>

Ye was the first to identify the true structure of mandelalide A **34**, completing the total synthesis and structural reassignment in 2014.<sup>46</sup> Shortly after, Fürstner published synthetic and computational studies which identified the same diastereomer as Ye,<sup>48</sup> thus allowing the stereostructure of mandelalide A **34** to be reassigned with confidence, bringing the stereochemistry into agreement with that proposed for madeirolide A.

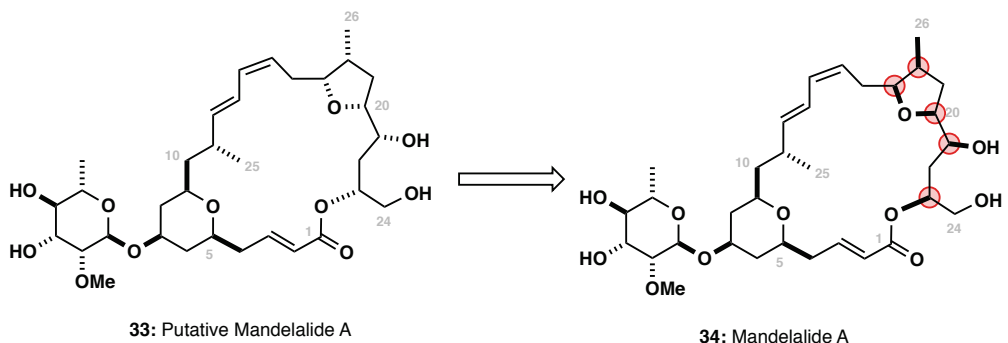


**Figure 2.11:** Structural reassignment of mandelalide A **34**. Stereocentres inverted relative to McPhail's initial assignment are highlighted.

## 2.2.2 BIOLOGICAL ACTIVITY

Biological evaluation of mandelalide A **34** and mandelalide B at the time of isolation revealed promising nanomolar cytotoxicity against two cancer cell-lines involved in small-cell lung carcinoma (NCI-H460) and mouse neuroblastoma (Neuro-2A) (**Table 2.2**).<sup>44</sup> Additional evaluation using the same samples was conducted in 2017.<sup>49</sup>

\* The suggestion that both epimers could produce the same ROESY correlations was based on a simple ball-and-stick model constructed by Fürstner and has since been shown to be invalid following computational studies.<sup>47</sup>

**Table 2.2:** Summary of biological data reported for natural mandelalide A and mandelalide B. (McPhail)<sup>44,49,50</sup>

	Cytotoxicity <sup>a</sup>		
	NCI-H460 (IC <sub>50</sub> , nM)	Neuro-2A (IC <sub>50</sub> , nM)	HeLa cervix (EC <sub>50</sub> , nM)
Mandelalide A (2012)	12	44	-
Mandelalide B (2012)	29	84	-
Mandelalide A (2017)	11	-	9.9
Mandelalide B (2017)	44	-	16

<sup>a</sup>: Cell viability determined via MTT analysis, using linear regression to compute the IC<sub>50</sub> values

Despite the initially promising biologically activity reported by McPhail, independent biological evaluation of synthetic mandelalide A has failed to replicate these results. Notably, Ye screened the synthetic material against ten cell-lines, observing only micromolar cytotoxicity in all cases.<sup>46</sup> The only direct comparison available is the Neuro-2A cell line, with McPhail reporting an IC<sub>50</sub> of 44 nM, but Ye observing no decrease in proliferation.<sup>46</sup>

A recent study by McPhail and Smith aimed to resolve the conflicting cytotoxicity data for mandelalide A, resulting in the discovery that several members of the mandelalide family (including mandelalide A) inhibit ATP synthase.<sup>49</sup> This inhibition causes cancer cell death by interruption of a key step in the aerobic glycolysis pathway used by rapidly proliferating cells to derive ATP (a source of ‘cellular energy’); this is in direct contrast to normally differentiated cells which predominantly use oxidative phosphorylation to generate ATP (**Figure 2.12**).<sup>51</sup>

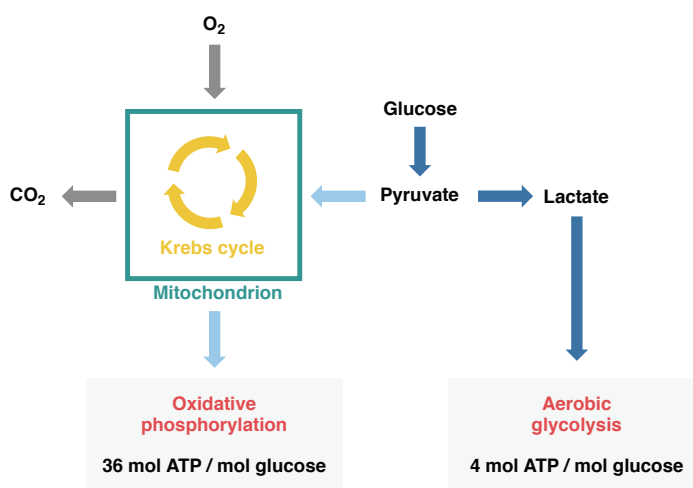


**Figure 2.12:** Glucose metabolism in cancer cells. Aerobic glycosis accounts for over 85% of the energy used by cancer cells. Figure adapted from Weinberg.<sup>51</sup>

Ostensibly, mandelalide A **34** acts through a similar mechanism to that of oligomycin A **35** and apoptolidin A, with several structural motifs conserved between the two natural products, namely the unsaturated ester and the planar diene (Figure 2.13).<sup>49</sup>

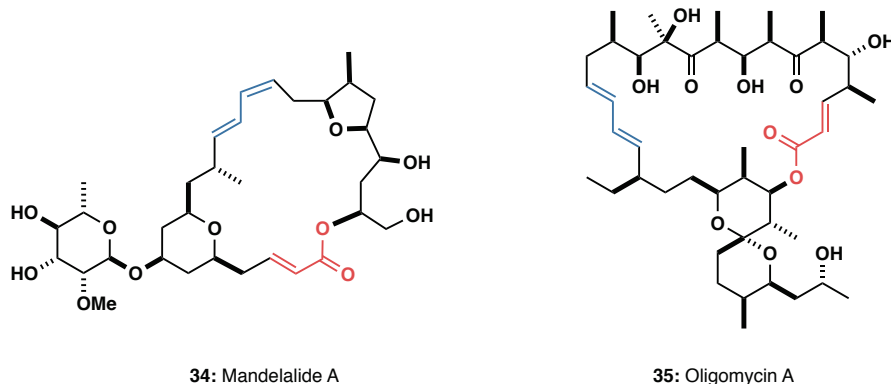


**Figure 2.13:** Mandelalide A **34** and oligomycin A **35** highlighting key structural features present in both natural products that may be responsible for the observed cytotoxicity.

The  $\alpha,\beta$ -unsaturated carbonyl moiety may be especially important in explaining the cytotoxicity of mandelalide A **34**, especially when comparing it to madeirolide A **1** which lacks this group, instead incorporating an additional THP.  $\alpha,\beta$ -Unsaturated carbonyl containing molecules are well-known to exhibit cytotoxicity owing to the ease at which sulfur containing residues such as cysteine can undergo 1,4-addition reactions.<sup>52</sup> Figure 2.14 shows several pharmaceutically relevant small-molecules incorporating the  $\alpha,\beta$ -unsaturated carbonyl motif.

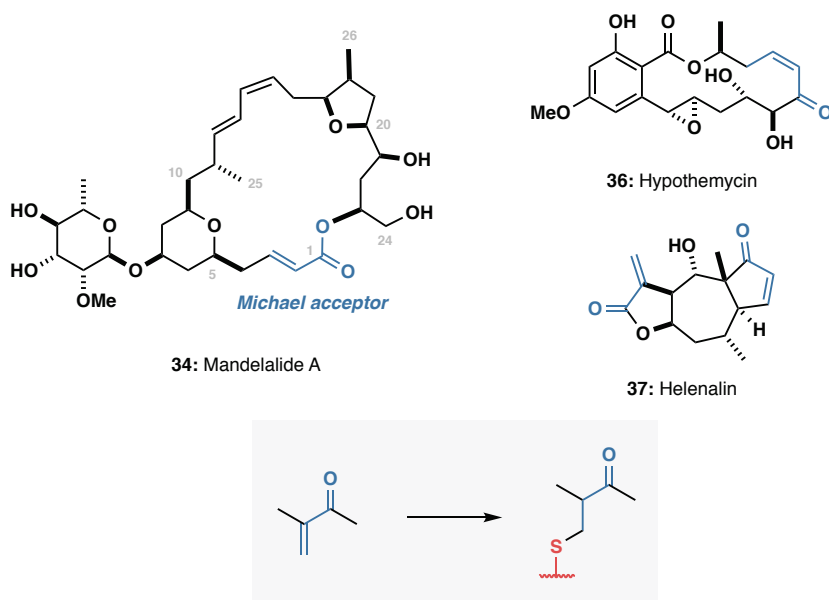
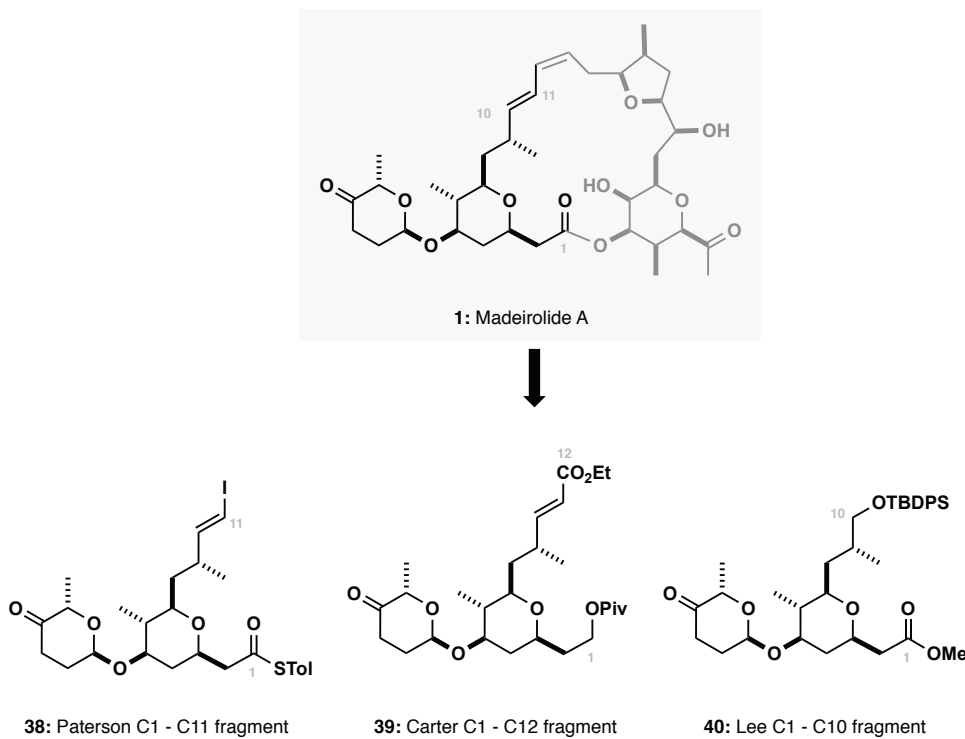


**Figure 2.14:** Cytotoxic drugs with  $\alpha,\beta$ -unsaturated carbonyl motifs.

## 2.3 PREVIOUS SYNTHETIC STUDIES TOWARDS MADEIROLIDE A

Synthetic campaigns towards madeirolide A are known to have been initiated by several groups. To date, a completed total synthesis of madeirolide A is yet to be forthcoming, however multiple fragment syntheses have been reported, initially by Paterson<sup>53</sup> with a C1 – C11 fragment synthesis **38**, and subsequently of C1 – C12 and C1 – C10 fragments by Carter<sup>54</sup> **39** and Lee<sup>55</sup> **40** respectively (**Scheme 2.1**).



**Scheme 2.1:** Fragments of madeirolide A currently reported in the literature.

Notably, the Paterson C1 - C11 fragment **38** is the only reported compound suitably functionalised to complete a total synthesis, with the Carter and Lee approaches both requiring additional redox manipulations to convert their fragments into a form amenable for fragment coupling. The step-count and yields of the three reported fragments are tabulated below in **Table 2.3**:

**Table 2.3:** Comparison of synthetic approaches to the western fragment of madeirolide A .

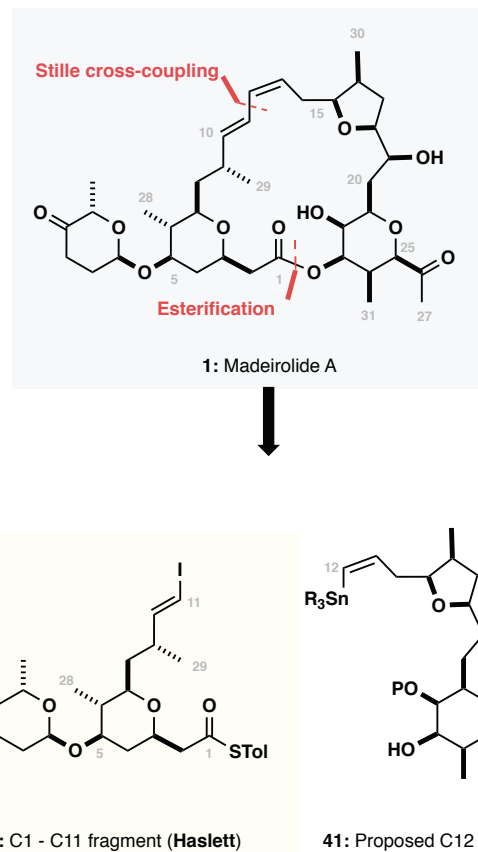
	Steps (LLS)	Yield
Paterson <sup>53,56</sup>	19 (20)	13%
Carter <sup>54</sup>	10 (16)	8%
Lee <sup>55</sup>	13 (18)	15%

Values in parentheses include the steps required to obtain the starting materials used in the synthesis.

### 2.3.1 PREVIOUS SYNTHETIC STUDIES WITHIN THE PATERSON GROUP

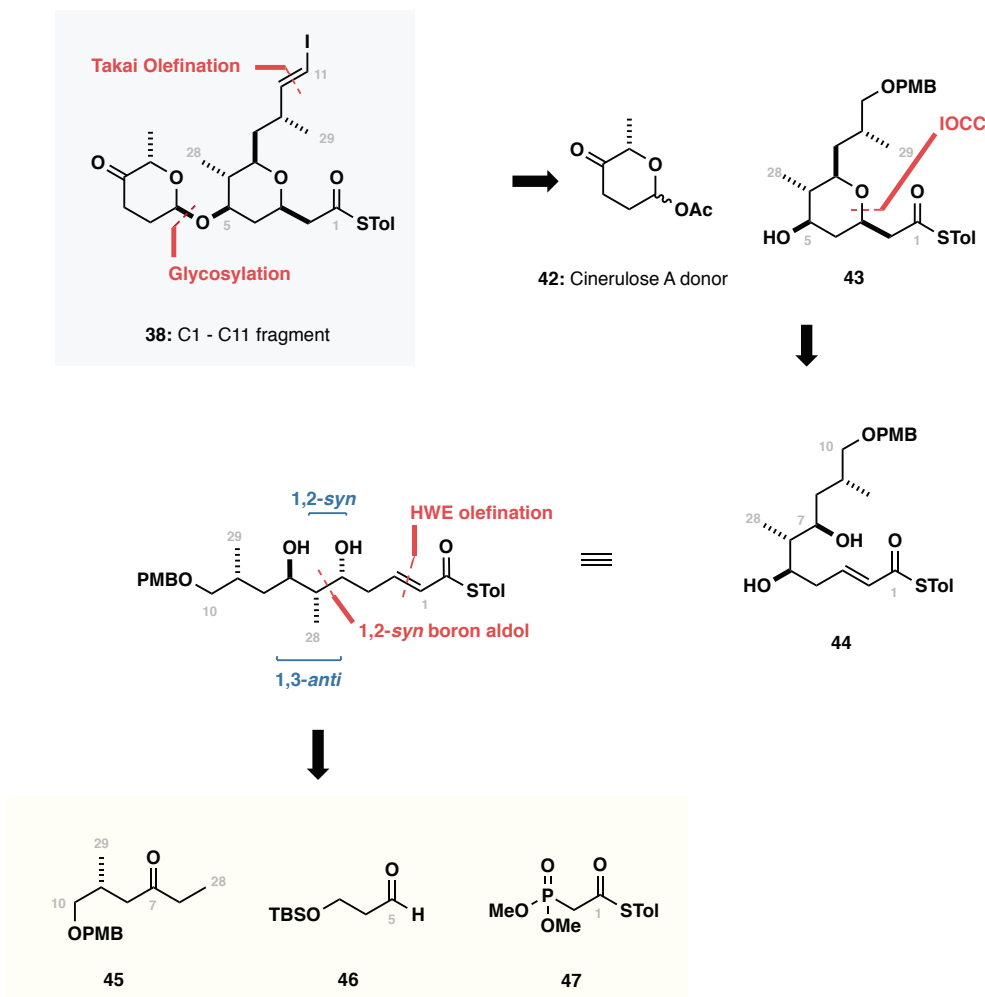
Following Wright's initial report of madeirolide A, synthetic investigations were initiated within the Paterson group with the dual aim of validating Naylor's proposed structural reassignment<sup>37</sup> and providing material for thorough biological evaluation. These studies by Haslett culminated in the synthesis of the fully elaborated C1–C11 fragment **38** and several advanced linear precursors to the C18 – C27 THP.<sup>53</sup>

The synthetic strategy was guided by the need for flexibility and convergence, given the unanswered questions about the C9 stereocentre (see §2.1.2). Directed by this, two key points of scission were identified, exploiting the C11 – C12 diene and C1 – OC23 lactone linkages as convenient points for fragment union (**Scheme 2.2**). These disconnections result in two fragments of roughly equal size: the C1 – C11 western fragment **38**, containing the cinerulose moiety and the simpler 2,6-*cis* THP; and the C12 – C27 eastern fragment **41**, containing the THF and the remaining 2,6-*cis* THP. In a forward sense, an esterification followed by Stille macrocyclisation was anticipated to join the two advanced fragments to complete the natural product.



**Scheme 2.2:** Retrosynthetic strategy for fragment union of the C1 – C11 western fragment **38** and the proposed C12 – C27 eastern fragment **41**.

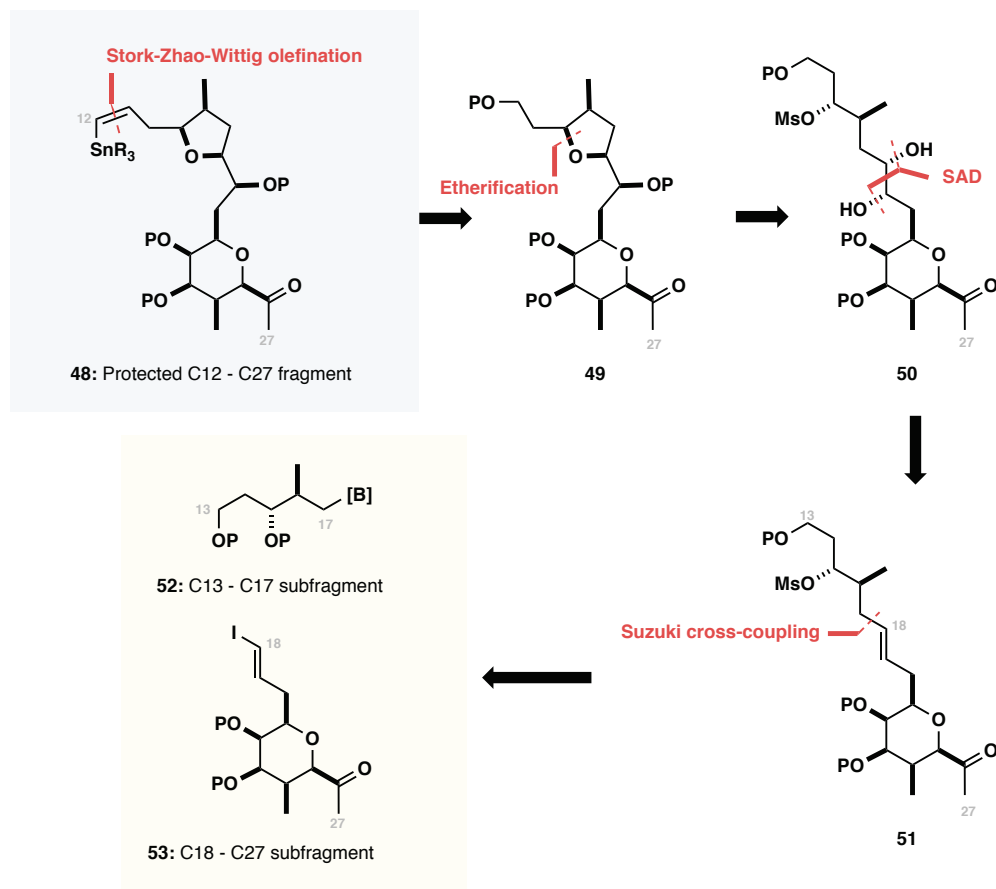
The general features of Haslett's synthesis of the C1 – C11 western fragment are illustrated in **Scheme 2.3**. Initial simplification reveals aglycone **43** which may be further disconnected to reveal linear precursor **44**; in a forward sense, treatment of **44** with catalytic *p*-TsOH would affect the desired oxy-Michael cyclisation. Analysis of the linear precursor **44** reveals a 1,2-*syn* relationship between the C5-hydroxyl and C6-methyl group and a 1,3-*anti* relationship between the C5 and C7 hydroxyl groups. This stereochemical pattern is accessible using a reagent-controlled 1,2-*syn* selective boron aldol reaction developed in the Paterson group<sup>57</sup> followed by substrate-directed 1,3-*anti* Evans-Tischenko reduction. The olefin may also be disconnected using a Horner-Wadsworth-Emmons olefination, revealing three readily accessible starting materials: Roche ester derived ethyl ketone **45**, aldehyde **46**, and phosphonate **47**. This route enabled the successful synthesis of **38** in 13% yield and 19 steps (LLS) starting from PMB protected (*S*)-Roche ester. The forward synthesis is discussed in more detail in §3.1 in the context of the development of an improved C1 – C11 fragment.



**Scheme 2.3:** Retrosynthetic analysis of the C1 – C11 fragment **38** of madeirolide A (Haslett).

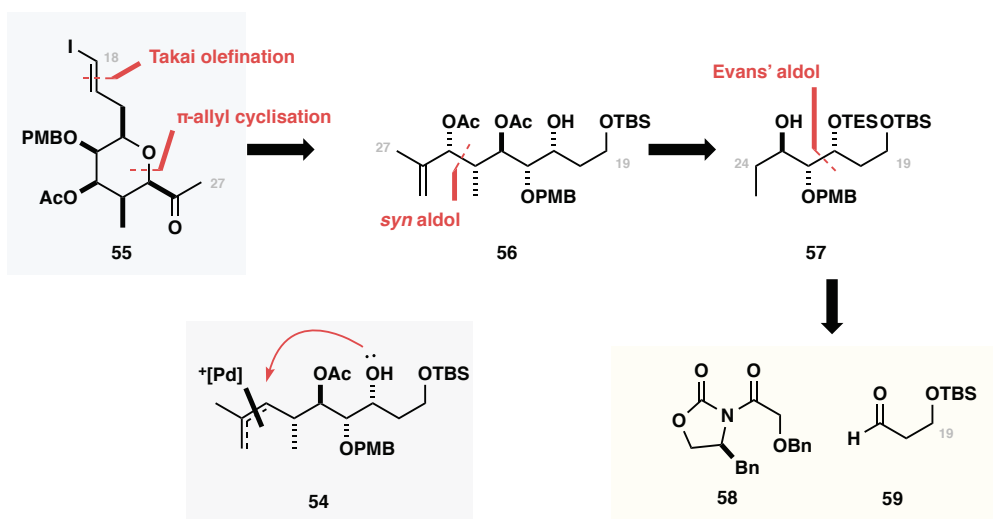
### 2.3.1.1 PREVIOUS STUDIES TOWARDS THE C12 – C27 EASTERN FRAGMENT

Concurrent with work on the western fragment **1** of madeirolide A, Haslett began investigations into the synthesis of the C12 – C27 eastern fragment **48**. The initial strategy for the construction of **48** is outlined retrosynthetically in **Scheme 2.4**. Following disconnection of the (*Z*)-vinyl stannane, the THF may be introduced using a cycloetherification of **50** using a known procedure from Ghosh in the context of mandelalide A.<sup>58</sup> Recognising that the C18 – C19 diol could be introduced using a Sharpless asymmetric dihydroxylation (SAD) reveals the key intermediate **51** which was anticipated to arise from an  $sp^2$  -  $sp^3$  Suzuki cross-coupling reaction between vinyl iodide **53** and organoborane **52**.



**Scheme 2.4:** Retrosynthetic analysis for the C12 – C27 eastern fragment **48**.

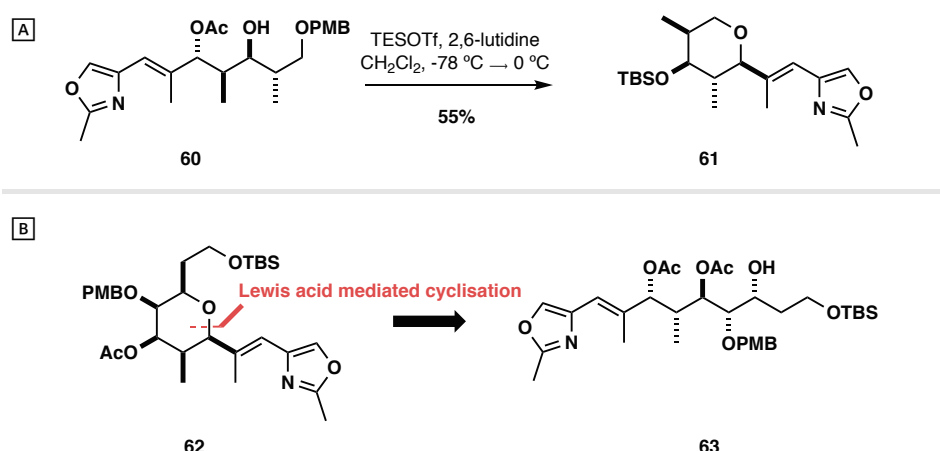
With the two heterocycles now isolated, Haslett was able to focus attention on the construction of the challenging all-*cis* THP present in **53**. It was initially anticipated that the C25-O-C21 bond could be forged via a Tsuji-Trost-type reaction of allylic acetate **56** (**Scheme 2.5**).<sup>56</sup> Mechanistically, treatment of **56** with a source of Pd(II) should generate an electrophilic  $\pi$ -allyl palladium species **54** which may be intercepted by the C21 hydroxyl group to form the THP, with the stereochemistry controlled due to double inversion of the C25 stereocentre.



**Scheme 2.5:**  $\pi$ -allyl palladium cyclisation strategy (Haslett).<sup>56</sup>

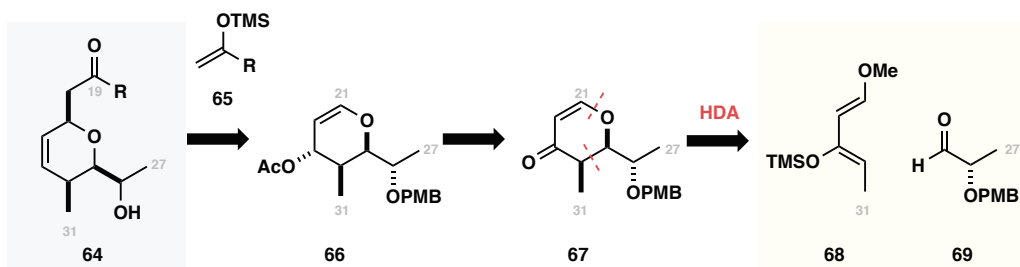
In the event, treatment of **56** with a variety of Pd(II) sources and conditions returned only starting material. The lack of reactivity is not unexpected, and may be attributed to two factors: firstly, the C21 alkoxide is a poor nucleophile for the soft  $\pi$ -allyl palladium species, and secondly, the loss of acetate to generate the  $\pi$ -allyl palladium species is reversible. Attempts at fixing these issues (formation of a softer zinc alkoxide, use of a carbonate leaving group which would irreversibly decarboxylate) were unsuccessful, prompting an alternate tactic to be explored.

Taking inspiration from the Paterson groups approach to phorboxazole A, in which oxazole **60** unexpectedly cyclised to give THP **61** (**Scheme 2.6**),<sup>59</sup> it was proposed that treatment of **63** with a suitable Lewis acid would affect cyclisation to afford **62**. Again, despite successful synthesis of the linear precursor, Haslett was unable to find conditions that enabled the desired heterocycle to be closed.



**Scheme 2.6:** **A**] Unexpected cyclisation of oxazole **60** during the Paterson synthesis of phorboxazole A.<sup>59</sup>  
**B**] Proposed THP formation based on an oxazole-mediated cyclisation of **63**.

Although the desired THP could conceivably be assembled through cyclisation of a suitably functionalised linear precursor, the on-going difficulties encountered by Haslett prompted an alternative approach to be investigated in which a simplified dihydropyran was accessed, anticipating it could be elaborated to give the fully substituted THP. This work was carried out by Fearnley, a postdoctoral researcher in the Paterson group. It was projected that the C21 – C22 *syn*-diol could be installed at a late stage using an asymmetric dihydroxylation, thus revealing dihydropyran **64** as a key intermediate which could itself be derived from a hetero-Diels Alder between diene **68** and aldehyde **69**.<sup>60</sup> While DHP **64** was able to be accessed successfully, Fearnley was unable to find a suitable set of reagents/conditions to install the diol with the required stereochemistry – substrate control dominated over reagent control, failing to procure access to the desired all-*cis* configured THP.



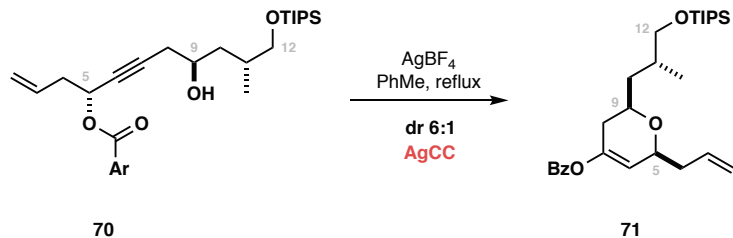
**Scheme 2.7:** Retrosynthetic analysis of dihydropyran **64**, which was anticipated to undergo elaboration to the fully substituted THP using an asymmetric dihydroxylation (**Fearnley**).<sup>61</sup>

### 2.3.2 OTHER SYNTHETIC STUDIES TOWARDS MADEIROLIDE A

#### 2.3.2.1 CARTER

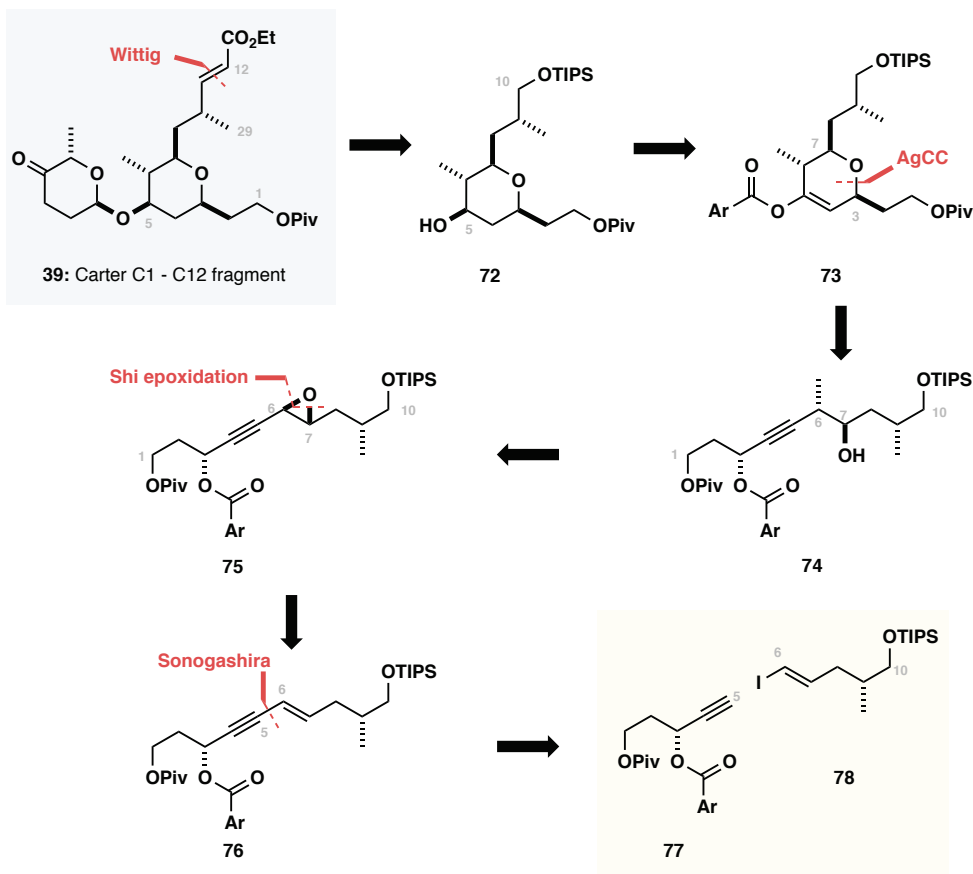
In 2016, Carter disclosed a total synthesis of mandelalide A, highlighting the power of silver catalysed cyclisation (AgCC) of a propargylic benzoate to install the requisite tetrahydropyran (**Scheme 2.8**).<sup>62</sup> Recognising the homology between the western fragments of madeirolide A **1** and mandelalide A **34**, Carter was able to exploit his group's previous synthesis to give facile access to a C1 – C12 fragment **39**, shown retrosynthetically in **Scheme 2.9**.\*

\* Note that at present, details of the proposed fragment union have not been revealed, however by analogy to their work on mandelalide A,<sup>62</sup> it could be suggested that a series of protecting group and oxidation state manipulations would enable an esterification to form the lactone functionality followed by a Wittig olefination to furnish the (*Z,E*) diene.



**Scheme 2.8:** Precedence for THP formation using Carter's AgCC methodology in the context of mandelalide A (**Carter**).<sup>62</sup>

Initial retrosynthetic scission of the cinerulose moiety and enoate reveals the pivotal dihydropyran **73**; accessed in the forward sense via AgCC of the corresponding propargylic benzoate **74**. Other salient disconnections include the introduction of the C6 - C7 *anti* relationship through opening of chiral epoxide **75**, and the scission of the C5 - C6 bond using a Sonogashira cross-coupling to reveal Carter's starting materials, **77** and **78**.

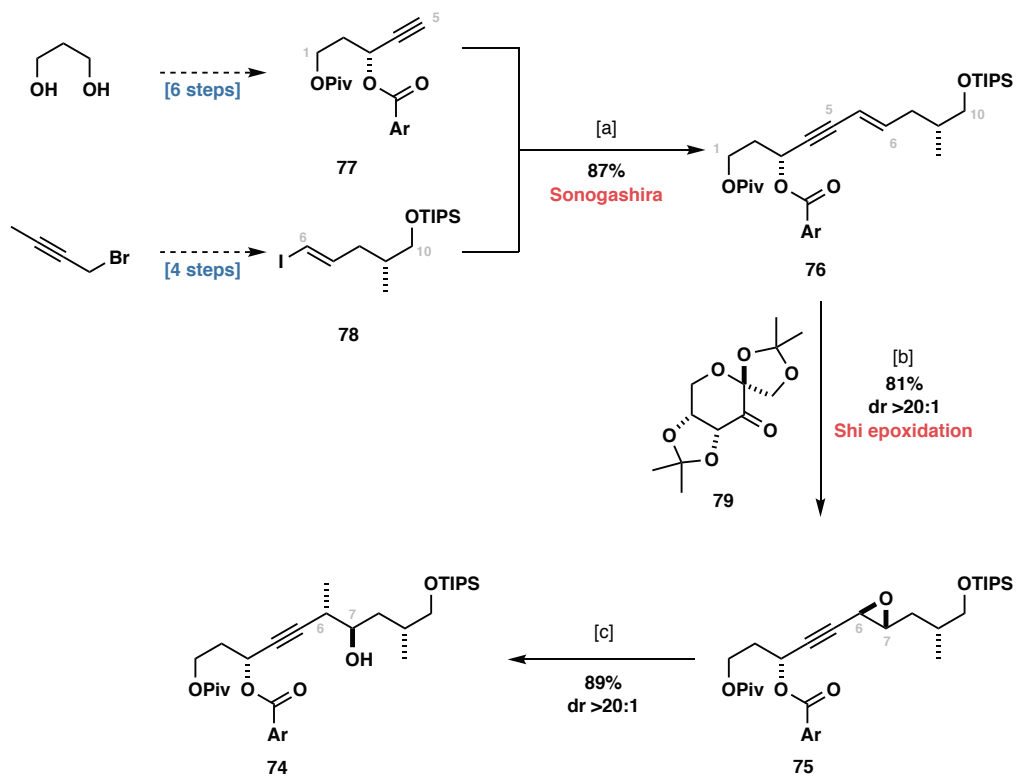


**Scheme 2.9:** Retrosynthetic analysis of a C1 – C12 fragment of madeirolide A **39** (Carter).<sup>62</sup>

Carter's synthetic efforts towards **39** commenced with the preparation of a suitably functionalised propargylic benzoate **74** which was anticipated to undergo AgCC to forge the C3–O7 bond of the THP. The core skeleton was formed through the union of **77** and **78** using a Sonogashira cross-coupling promoted by catalytic CuI and Pd(PPh<sub>3</sub>)<sub>4</sub>. Both **78** and **77** are

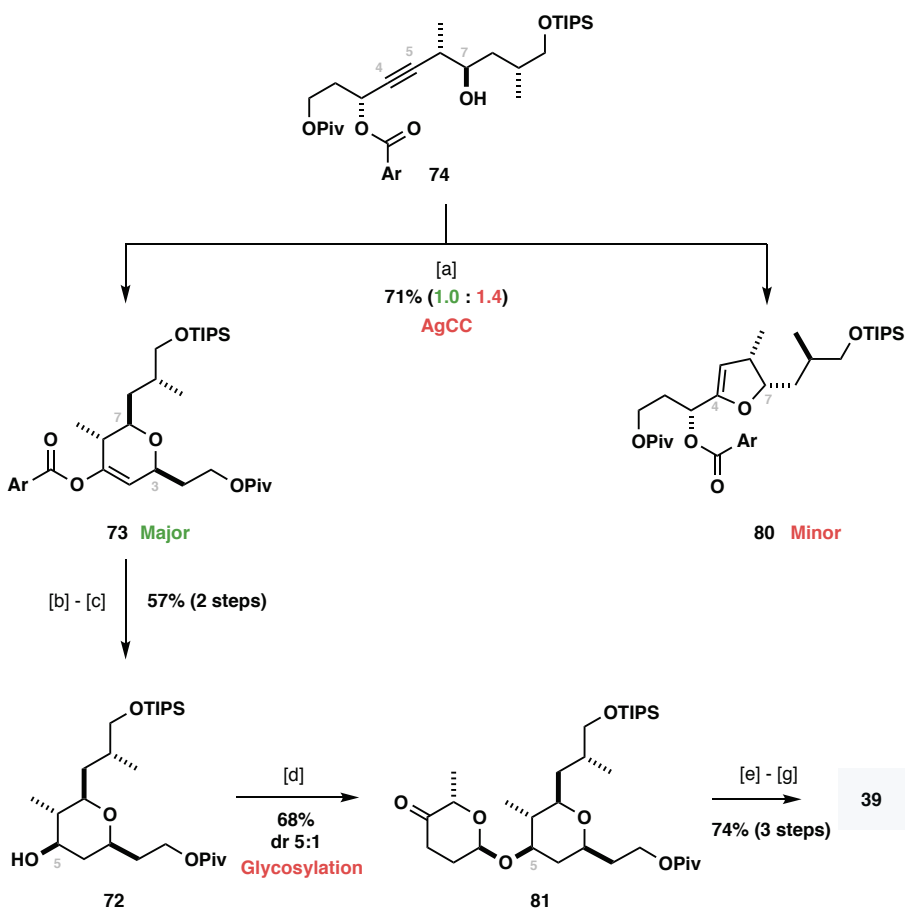
known compounds, readily accessible from commercial achiral starting materials in four and six steps respectively.<sup>63,64</sup>

With **76** in hand, attention was turned to the introduction of the required C6 and C7 stereocentres, which, given the distal nature of the existing chirality within the molecule would necessitate the use of a chiral oxidant. Accordingly, **76** was treated with fructose derived catalyst **79** using conditions developed by Shi to provide access to epoxide **75** as a single diastereomer. Subsequent treatment of **75** with LiAlMe<sub>4</sub> and BF<sub>3</sub>·Et<sub>2</sub>O established the 1,2-*anti* relationship in **74** as required, with the choice of Lewis acid and nucleophile crucial to obtaining the desired product without loss of the benzoate or pivalate esters.



**Reagents and conditions:** [a] Pd(PPh<sub>3</sub>)<sub>4</sub>, CuI, *i*-Pr<sub>2</sub>NH, rt. [b] **79**, Oxone, pH 9.3 buffer, MeCN, H<sub>2</sub>O, 0 °C. [c] LiAlMe<sub>4</sub>, BF<sub>3</sub> Et<sub>2</sub>O·CH<sub>2</sub>Cl<sub>2</sub>, -78 °C. [d] AgBF<sub>4</sub>, 100 °C.

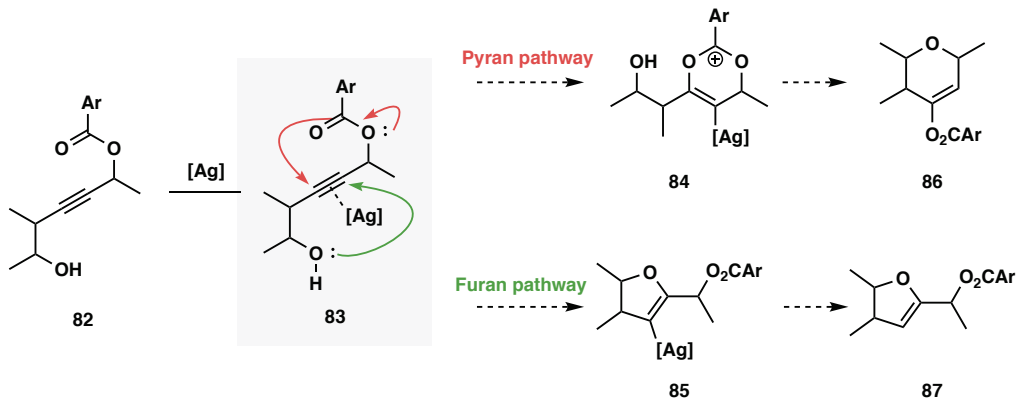
**Scheme 2.10:** Synthesis of the linear C1–C10 propargylic benzoate **74** (Carter).<sup>54</sup>



**Reagents and conditions:** [a]  $\text{AgBF}_4$  (20 mol%), PhMe, 100 °C. [b]  $\text{NaOMe}$ , MeOH, 0 °C → rt. [c]  $\text{NaBH}_4$ ,  $\text{CeCl}_3$ , MeOH, -20 °C. [d]  $\text{BF}_3 \cdot \text{Et}_2\text{O}$ ,  $\text{CH}_2\text{Cl}_2$ , 0 °C. [e]  $\text{TBAF}$ ,  $\text{HOAc}$ , THF, 0 °C. [f]  $\text{DMP}$ ,  $\text{NaHCO}_3$ ,  $\text{CH}_2\text{Cl}_2$ , rt. [g]  $\text{Ph}_3\text{P}=\text{CHCO}_2\text{Et}$ ,  $\text{CH}_2\text{Cl}_2$ , -78 °C.

**Scheme 2.11:** Cyclisation of the C1 – C10 propargylic benzoate **74** using AgCC and elaboration to the full C1 – C12 fragment **39** (**Carter**).<sup>54</sup>

The stage was now set to test the pivotal AgCC step. Disappointingly, upon treatment of **74** with catalytic  $\text{AgBF}_4$  in refluxing toluene a mixture of products was obtained, with formation of both **73** and an undesired dihydrofuran **80** in a 1.4:1.0 ratio. This result contrasts with Carter's previous work on mandelalide A in which a single product was obtained in excellent yield. Carter rationalises the outcome via competitive 6-*endo*-dig (red) and 5-*exo*-dig (green) cyclisations leading to the mixture of products, however no additional mechanistic studies have yet been reported (**Scheme 2.12**).



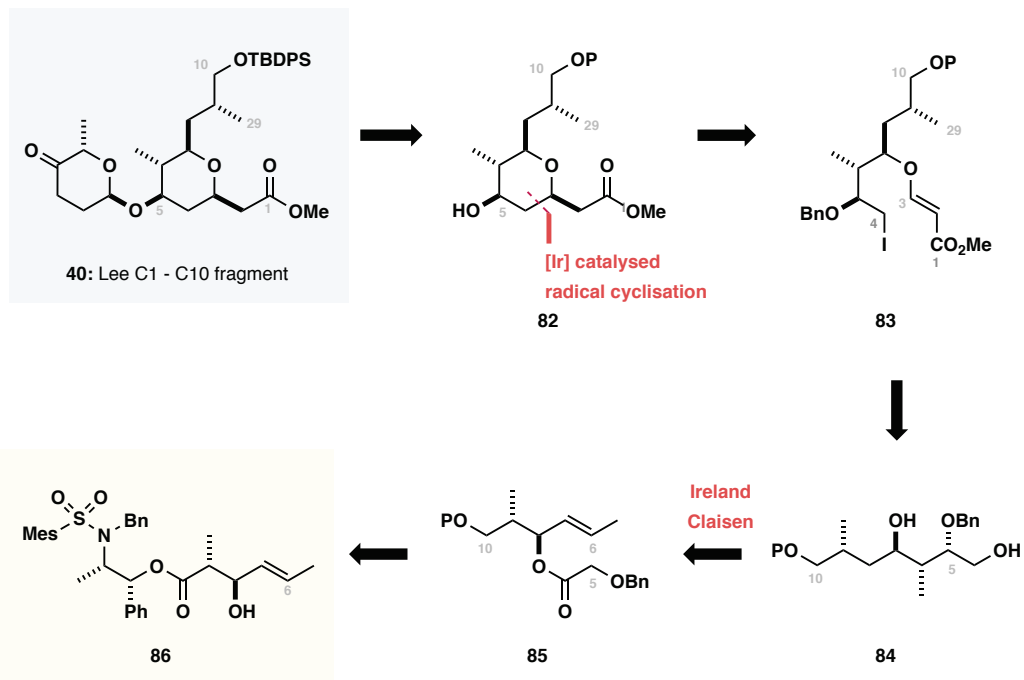
**Scheme 2.12:** Mechanistic rationale for competing dihydropyran **86** and dihydrofuran **87** formation during the AgCC of propargylic benzoates (**Carter**).<sup>54</sup>

In the event, the desired DHP **73** was in 43% yield and >20:1 dr, providing sufficient material to advance the synthesis. Subsequent cleavage of the enol benzoate under basic conditions followed by diastereoselective reduction of the ensuing ketone guided by the proximal C9-methyl group provided alcohol **72**. The remaining steps to the completion of the fragment were straightforward and followed the same synthetic route as had previously been demonstrated in the context of mandelalide A. Thus, under Lewis acid catalysis, the cinerulose moiety was installed via acetate donor **42**, with a reproducible 5:1 d.r. at the anomeric position. Elaboration of the TIPS ether via a three step deprotection, oxidation, Wittig olefination sequence furnished **39**, the completed C1 – C12 fragment, in 13% yield and 10 steps (LLS) from propargylic benzoate **77**.\*

### 2.3.2.2 LEE

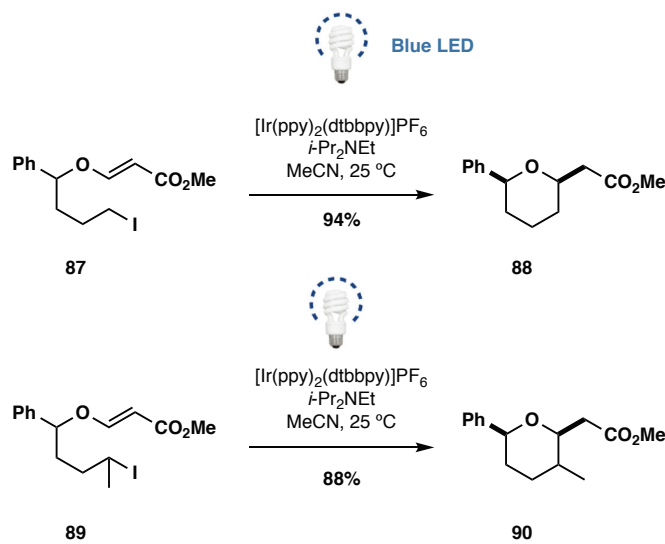
Lee and co-workers reported their synthetic endeavours towards madeirolide A in 2016 with a C1 – C10 fragment **40** synthesis, outlined retrosynthetically in **Scheme 2.13**.<sup>55</sup> Pivotal to their strategy was the use of an iridium-catalysed visible light mediated radical cyclisation to form the THP, with disconnection of the C3 – C4 bond of **82** in the manner illustrated revealing **83** as the key intermediate.

\* Carter's yield does not account for the unselective AgCC, counting the yield for that step as the mixture of the two products.



**Scheme 2.13:** Retrosynthetic analysis of a C1 – C10 fragment **40** (Lee).<sup>55</sup>

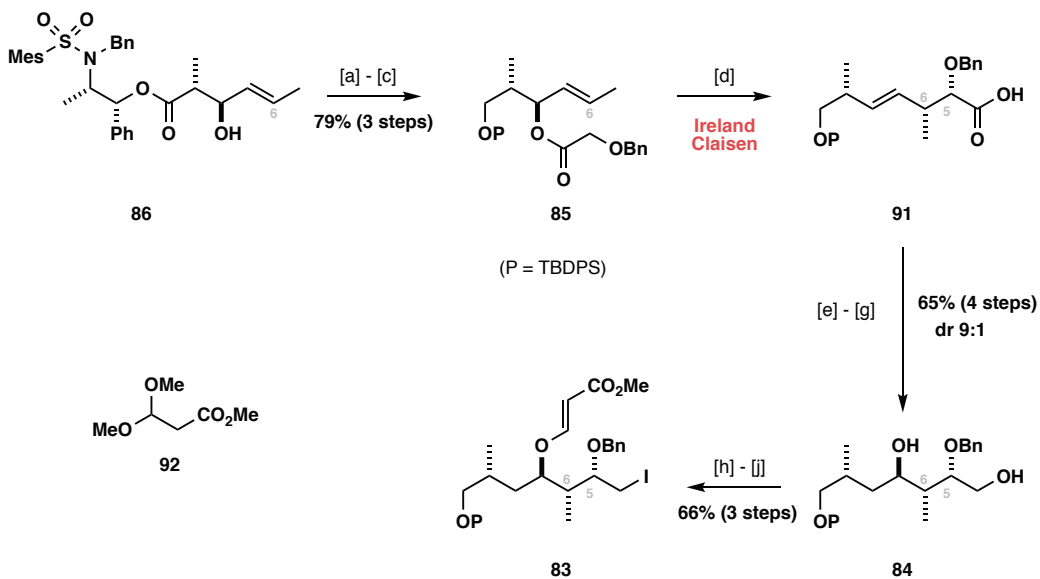
Although the Lee group had previously demonstrated the formation of saturated heterocycles using this photoredox methodology, only two examples of THP formation were reported (**Scheme 2.14**).<sup>65</sup> In both examples, the cyclisation was carried out on racemic substrates lacking any sensitive functionality and as such the application of this methodology in the context of madeirolide A was anticipated to be a significantly more demanding test of the reaction.



**Scheme 2.14:** Previous examples of THP formation using visible-light-induced photocatalytic reductive transformations of organohalides (Lee).<sup>65</sup>

Lee's route commenced from the Masamune aldol adduct **86**, accessed in five steps from crotonaldehyde (**Scheme 2.15**).<sup>66</sup> Initial cleavage of the pseudoephedrine derived auxiliary followed by regioselective TBDS protection of the C10 hydroxyl and installation of the 2-benzyloxyacetate moiety at C8 provided **85** which was suitably functionalised to undergo the proposed Ireland-Claisen rearrangement.

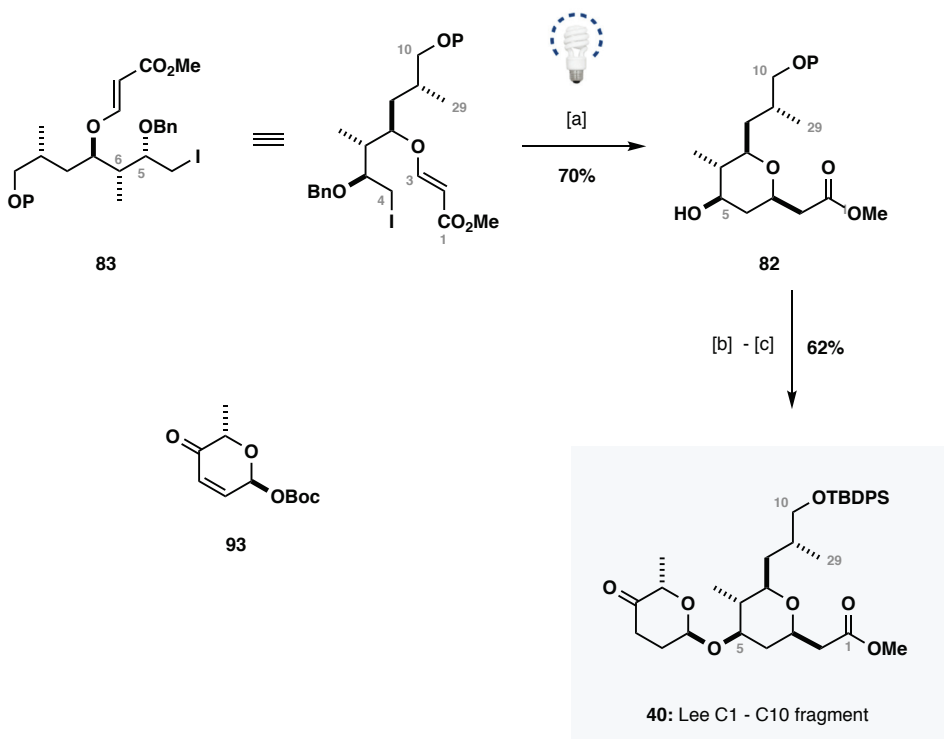
Accordingly, treatment of **85** with LiHMDS and TMSCl formed a silyl enol ether, which, upon warming to room temperature rearranged to give **91** with concomitant introduction of the C5 and C6 stereocentres. The remaining C7 oxymethine was installed in a three-step sequence, making use of an iodolactonisation reaction, affording with 9:1 dr. The C7 β-alkoxy acrylate was subsequently installed to give the key pre-cyclisation intermediate **83**.



**Reagents and conditions:** [a] LiAlH<sub>4</sub>, THF, rt. [b] TBDPSCl, imidazole, CH<sub>2</sub>Cl<sub>2</sub>, 0 °C. [c] BnOCH<sub>2</sub>CO<sub>2</sub>H, EDAC, DMAP, CH<sub>2</sub>Cl<sub>2</sub>, rt. [d] KHMDS, TMSCl, THF, -78 °C. [e] I<sub>2</sub>, NaHCO<sub>3</sub>, MeCN, -40 °C. [f] [Ir(ppy)<sub>2</sub>(dtbbpy)]PF<sub>6</sub>, i-Pr<sub>2</sub>NEt, MeCN, 2 W blue LED, rt. [g] LiBH<sub>4</sub>, THF, 50 °C. [h] **92**, PPTS, PhMe, 110 °C. [i] LiHMDS, THF, -78 °C. [j] I<sub>2</sub>, PPh<sub>3</sub>, imidazole, THF, 0 °C.

**Scheme 2.15:** Synthesis of the C1 – C10 linear precursor (Lee).<sup>55</sup>

Having successfully prepared the linear precursor **83**, the stage was set for Lee to test the ambitious cyclisation. In the event, treatment of **83** with [Ir(ppy)<sub>2</sub>(dtbbpy)]PF<sub>6</sub> and blue LED light enabled aglycone **82** to be obtained as a single diastereomer in 70% yield, exemplifying the power of Lee's methodology. Finally, the installation of the cinerulose sugar was achieved in two steps, using dehydrocinerulose donor **93** which was reduced post-glycosylation to provide Lee's C1 – C10 fragment **40** in 13% yield over 15 steps starting from Masamune aldol adduct **86**.



**Reagents and conditions:** [a]  $[\text{Ir}(\text{ppy})_2(\text{dtbbpy})]\text{PF}_6$ ,  $i\text{-Pr}_2\text{NEt}$ , MeCN, 2 W blue LED, rt. [b] **93**,  $\text{Pd}_2(\text{dba})_3 \cdot \text{CHCl}_3$ ,  $\text{PPh}_3$ ,  $\text{CH}_2\text{Cl}_2$ , 0 °C. [c]  $\text{Pd/C}$ ,  $\text{H}_2$ , EtOAc, rt.

**Scheme 2.16:** Iridium photoredox cyclisation of **83** and elaboration to the C1 – C10 fragment **40 (Lee)**.<sup>55</sup>

## 2.4 SUMMARY & ANALYSIS

Madeirolide A **1** is a novel polyketide natural product. The unique structural features coupled with unanswered questions over biological activity have made it a compelling target for total synthesis, with several research groups actively engaged in research. Despite this, the natural product has thus far proved a formidable challenge, with the eastern THP causing significant synthetic challenges. The completion of a total synthesis will facilitate thorough biological evaluation of madeirolide A, and, with a robust route to hand, may enable SAR studies to probe the differences in cytotoxicity between madeirolide A and mandelalide A.

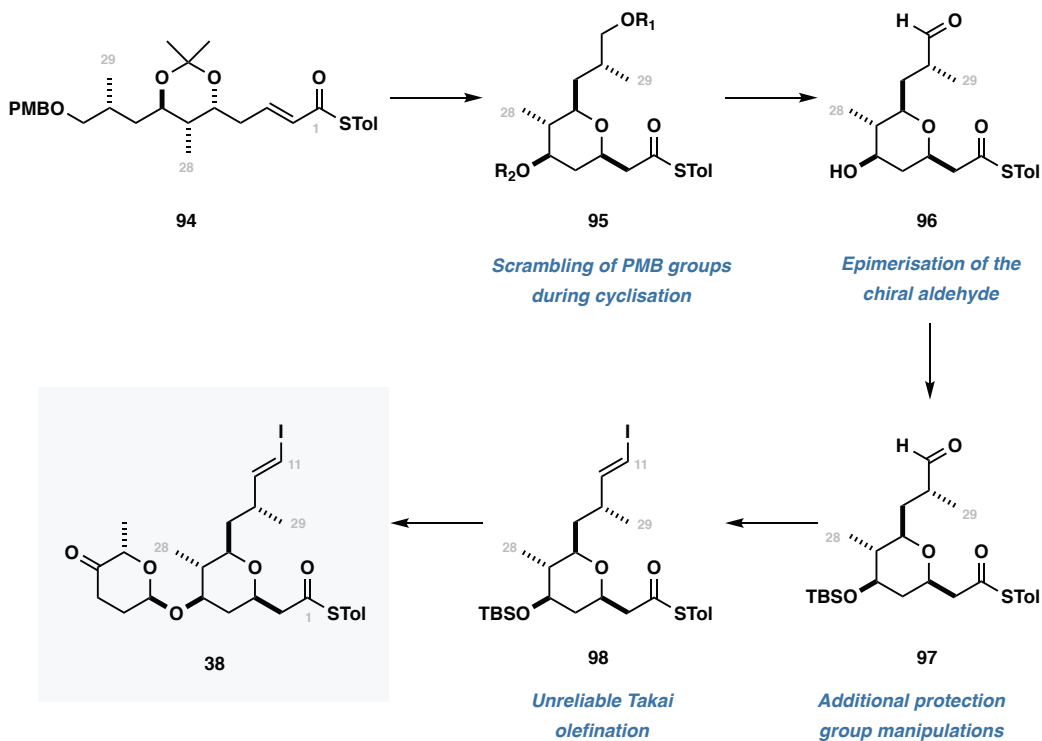


# 3

## 3. RESULTS & DISCUSSION I: SYNTHESIS OF A MODIFIED WESTERN FRAGMENT

### 3.1 AIMS AND RATIONALE FOR MODIFICATION OF THE STRATEGY

The route developed by Haslett (see §2.3.1) successfully accessed a fully elaborated C1 – C11 fragment **38** in 13% yield over 19 steps (LLS).<sup>53</sup> Despite this success, several issues persisted at the end stages of the route, namely with the cyclisation and subsequent elaboration to the (*E*)-vinyl iodide necessitated by the proposed macro-Stille fragment union (**Scheme 3.1**). These issues were not investigated further at the time as attention was focused on construction of the remaining C12 – C27 eastern fragment **48**.



**Scheme 3.1:** Final steps of Haslett's C1 – C11 fragment **38** synthesis for madeirolide A highlighting problematic steps.<sup>56</sup>

At the outset of this project, it was acknowledged that a more tractable end-game would be beneficial for material throughout as required for fragment coupling when the synthesis of the C12 – C27 fragment is completed. While considering the evolution of our strategy several lessons were learnt from the aforementioned ‘first-generation’ route:

- Protecting group strategy and chemoselectivity

The C10 PMB ether **94** is unstable under the conditions used to effect cyclisation (*p*-TsOH, CH<sub>2</sub>Cl<sub>2</sub>, rt). While treatment of the crude cyclisation mixture with DDQ side-steps the problem, a new issue of chemoselectivity is introduced: selective oxidation of a 1° alcohol in the presence of a 2° alcohol. The need for this selective oxidation limits the available options (TEMPO, BAIB), especially given the propensity for epimerisation of the C10 stereocentre observed by Haslett.

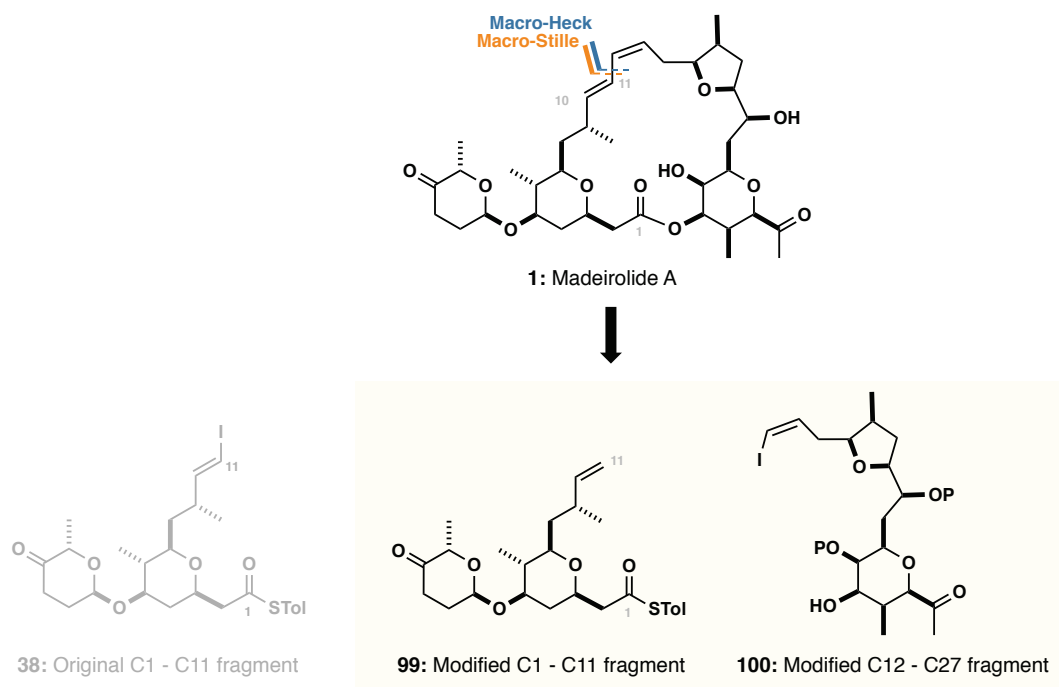
- Takai olefination

The Takai olefination of aldehyde **97** was found to be highly capricious, often failing to provide the desired (*E*)-vinyl iodide even when the same batch of reagents was used. The unpredictable nature of this reaction, coupled with the inability to recover the aldehyde without epimerisation makes this a challenging step which needs improvement.

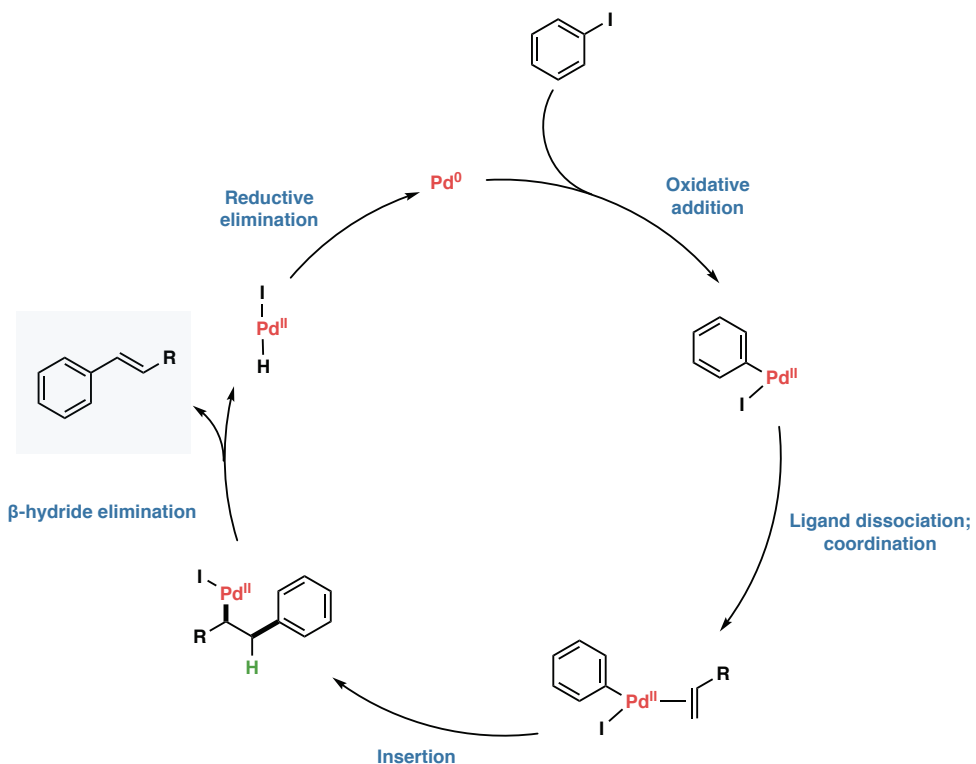
In the event, the above issues were able to be resolved through a single change in the overall strategy for fragment union: a Heck macrocyclisation reaction would be used in place of the original Stille macrocyclisation reaction (**Scheme 3.2**). This leads to a modified C1 – C11 western fragment **99** bearing a synthetically more accessible terminal olefin **99** instead of the (*E*)-vinyl iodide **38** previously used by Haslett.

Despite this, the use of a Heck reaction for macrocyclisation has the potential to introduce some additional issues of selectivity. Unlike Suzuki and Stille cross-coupling reactions, which use geometrically defined organometallic species (organoboron and organotin species respectively), the Heck reaction uses a terminal olefin as the coupling partner. This olefin has no inherent selectivity, but rather the geometry of the product is determined during the β-hydride elimination step which is mechanistically *syn* stereospecific (**Scheme 3.3**).<sup>67</sup>

Results & discussion I: synthesis of a modified western fragment



**Scheme 3.2:** Comparison of C11 – C12 bond forming strategies showing the original C1 – C11 fragment **40** (Haslett)<sup>53</sup> and the modified C1 – C11 fragment **99**. The C12 – C27 **100** fragment is also modified accordingly.



**Scheme 3.3:** Simplified catalytic cycle for the Heck coupling.<sup>67</sup>

In the context of macrocyclisation reactions, the use of a Heck reaction has the potential to cause two problems:

- Regioselectivity of insertion (ring closure)

The initial insertion (carbopalladation) step in which the organopalladium species adds across the terminal olefin may lead to either the *endo*- or *exo*- regioisomer. For large ring formation (>13 atoms), the intramolecular Heck reaction is often *endo* selective, as is required for macrocyclisation.<sup>68</sup>

- Reductive elimination (olefin formation)

When using terminal olefins as coupling partners in Heck reactions, two hydrogens are available for elimination, leading to the formation of both (*E*) and (*Z*) isomers of the resulting olefin. This is largely a thermodynamic property, and the (*E*) isomer is usually favoured through minimisation of steric clash across the C=C bond.<sup>67</sup>

Given the complexity of the cyclisation, it is difficult to predict a priori which isomer of the diene is likely to prevail. Based on a simple thermodynamic argument, the desired (*E,Z*) isomer is lower in energy by 5.9 kcal mol<sup>-1</sup>, which may limit formation of the strained (*Z,Z*) diene given the reversibility of the preceding steps (Figure 3.1).

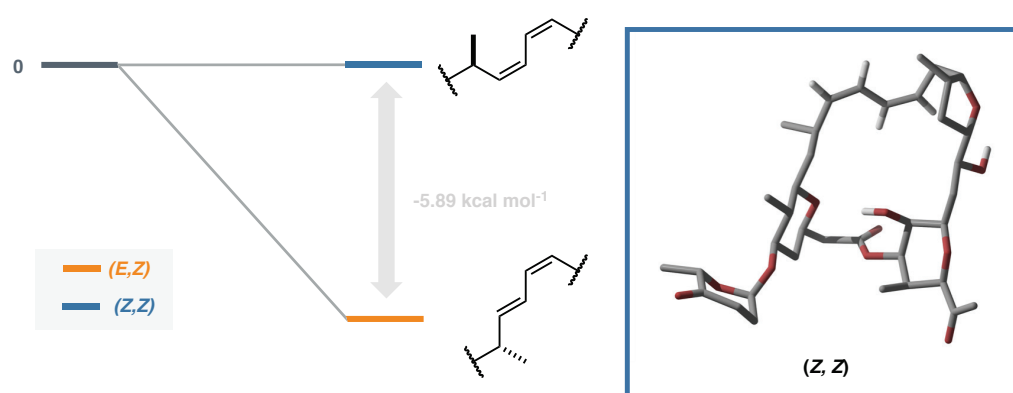
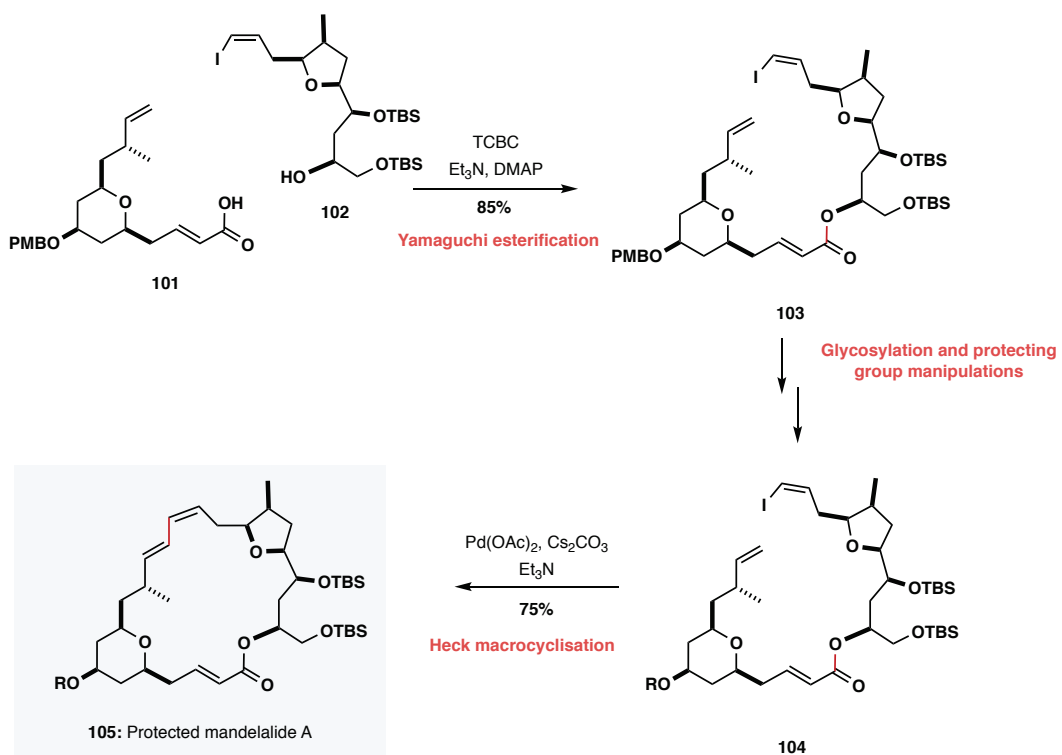


**Figure 3.1:** Relative energies of the (*E,Z*) and (*Z,Z*) isomers of madeirolide A showing the thermodynamic preference for the (*E,Z*) diene as found in the natural product. [DFT-B3LYP/6-31G\*\*, gas-phase].

Encouragingly, Smith and co-workers have recently validated a Heck macrocyclisation approach in the context of mandelalide A **34**, with cyclisation of **104** furnishing **105** with complete selectivity for the desired (*Z,E*)-diene (**Scheme 3.4**).<sup>69</sup> Although the substrate used by Smith is not directly comparable to the proposed intermediate in the madeirolide A synthesis, the two macrocyclic rings are known to adopt similar conformations.



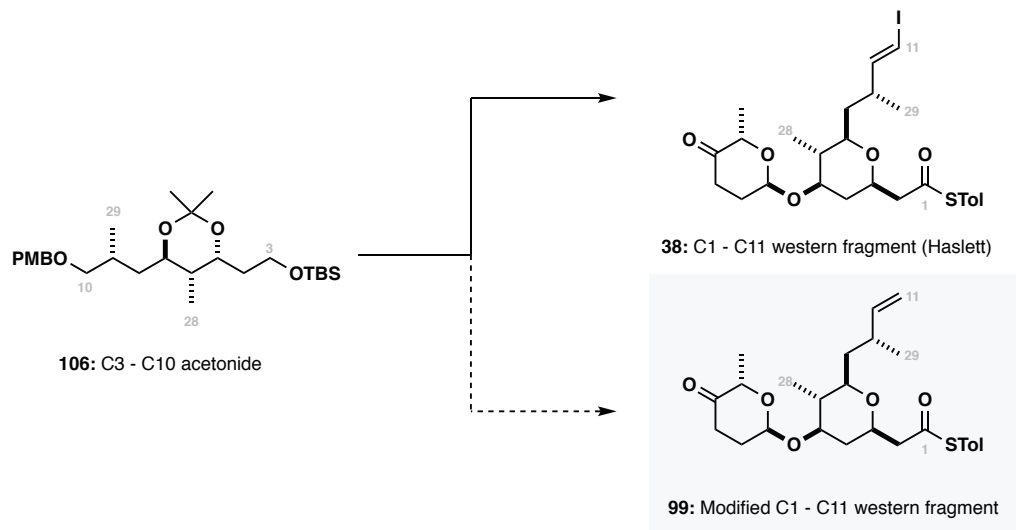
**Scheme 3.4:** Application of a ring-closing macro-Heck reaction in the context of mandelalide A leading to the desired (*E,Z*) geometry of the diene (**Smith**).<sup>69</sup>

As with the original endgame strategy, the modified Heck macrocyclisation route leaves some flexibility to the order of steps. Should the cyclisation not give the desired macrocycle, the order of steps could be reversed to first conduct an intermolecular Heck coupling followed by standard Yamaguchi macrolactonisation. More drastically, the terminal olefin provides a useful functional handle, enabling conversion to the vinyl iodide via ozonolysis and Takai olefination of the resultant aldehyde; this is somewhat circuitous and therefore undesirable.

### 3.1.1 RETROSYNTHESIS

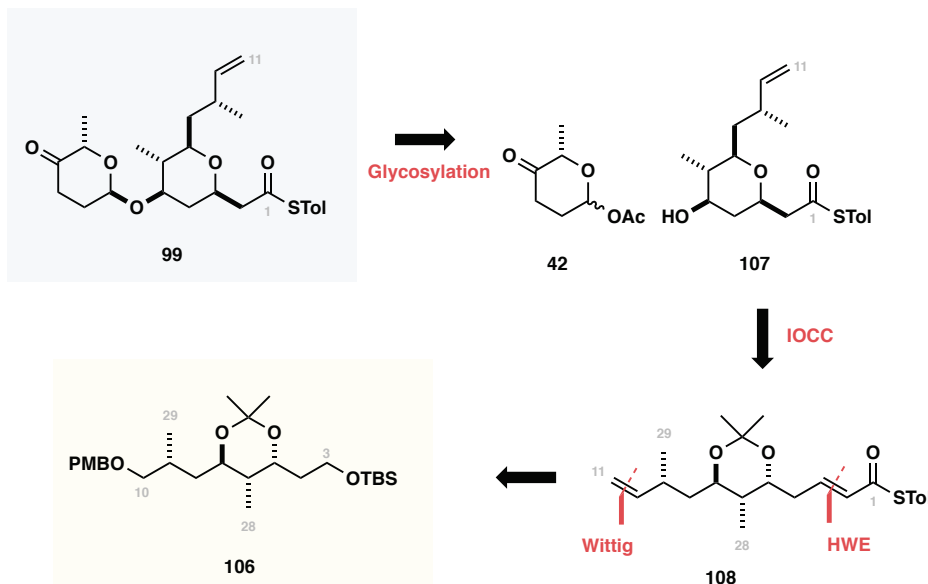
In considering the synthesis of **99**, it was desirable to retain as many of the successful elements from the original synthesis as possible in order to avoid optimisation of an entirely new route. Accordingly, the modified route was developed to diverge from acetonide **106** (**Scheme 3.5**). This intermediate was preferred as it contains all of the necessary stereochemistry (excluding the C7 oxymethine formed upon cyclisation) and is at a sufficiently late stage that it would be possible to quickly determine whether the Heck macrocyclisation approach would confer any additional benefits when compared to the original route.

Results & discussion I: synthesis of a modified western fragment



**Scheme 3.5:** Divergent synthesis from common acetonide **106** showing the original C1 – C11 fragment **38** (Haslett) and the proposed C1 – C11 fragment **99**.

The modified retrosynthetic strategy is shown in **Scheme 3.6**. Accordingly, initial scission of the cinerulose donor **42** reveals the C1-C11 aglycone **107**; envisioned to be accessible via acid-catalysed cyclisation of the corresponding linear precursor **108**. **108** may be further disconnected back to the common C3 – C10 intermediate **106** through two consecutive deprotection-oxidation-olefination sequences: a Wittig reaction to install the terminal olefin followed by a Horner-Wadsworth-Emmons reaction to install the  $\alpha,\beta$ -unsaturated thioester.

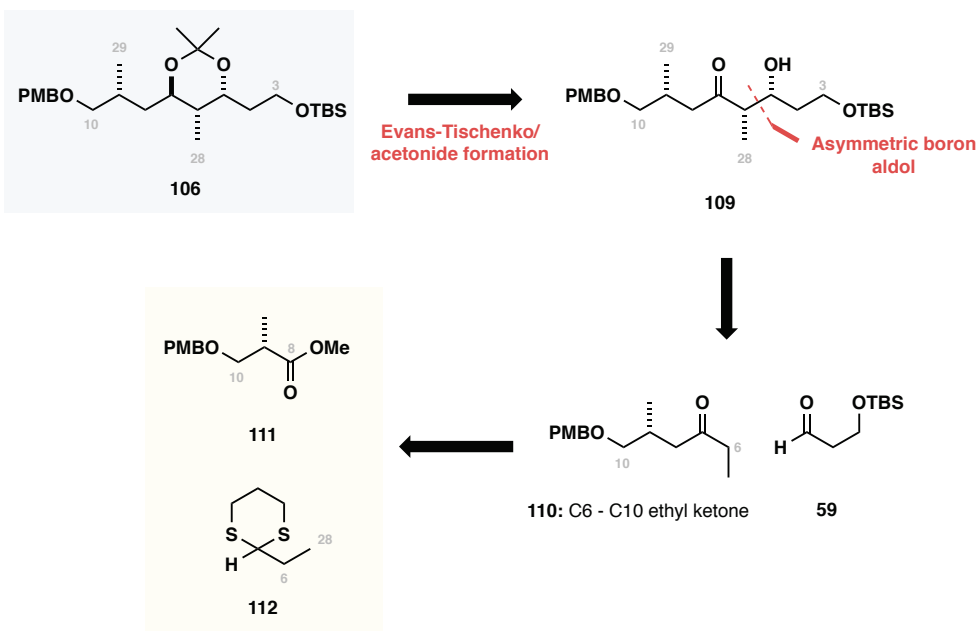


**Scheme 3.6:** Retrosynthesis for completion of the modified C1 – C11 fragment **99** from common acetonide **106**.

### 3.2 SYNTHESIS OF THE C3 - C10 ACETONIDE

*The work carried out in §3.2 builds on chemistry originally performed by Haslett.<sup>56</sup> Unless otherwise noted, all reactions/yields refer to those carried out by the author.*

Acetonide **106** can be accessed in eight steps starting from PMB-protected (*S*)-Roche ester **111**; shown retrosynthetically in **Scheme 3.7**. Key to strategy is the use of an (-)-Ipc<sub>2</sub>BOTf mediated aldol reaction between ketone **110** and aldehyde **59** to install the C5 and C6 stereocentres with control of the absolute and relative configuration. Ketone **110** may be further disconnected to PMB protected (*S*)-Roche ester **111**, using a Corey-Seebach homologation to introduce the necessary methylene (CH<sub>2</sub>) unit between the C9 stereocentre and the carbonyl.

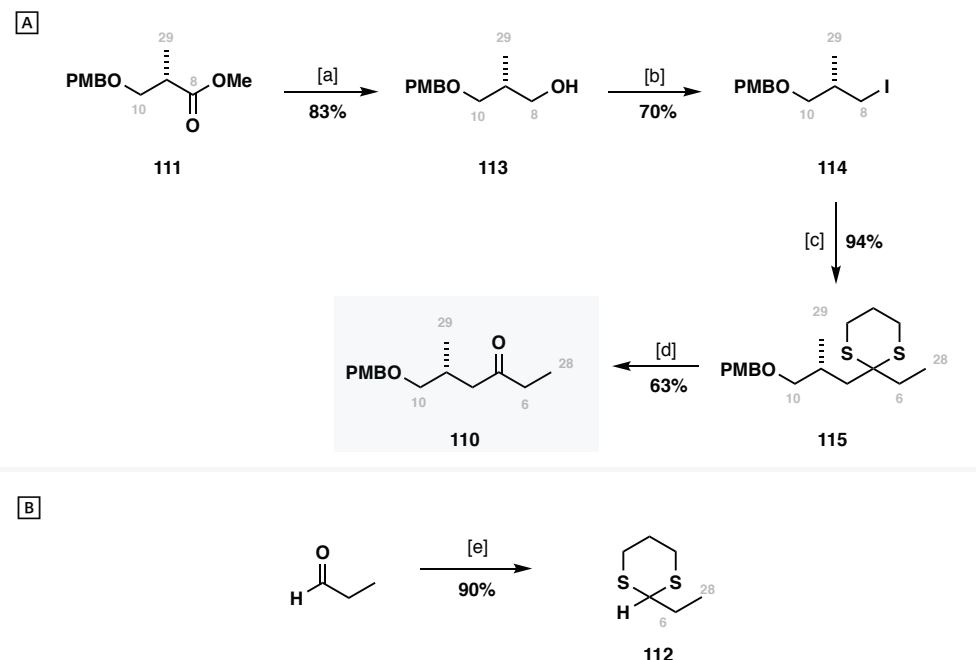


**Scheme 3.7:** Retrosynthesis for the preparation of the C3 – C10 acetonide **106**.

#### 3.2.1 SYNTHESIS OF THE C6 - C10 ETHYL KETONE

Preparation of the C6 – C10 ethyl ketone **110** began with the reduction of ester **111** to alcohol **113** (LiAlH<sub>4</sub>, 83%) followed by conversion to the analogous alkyl iodide **114** under modified Appel conditions (PPh<sub>3</sub>, I<sub>2</sub>, imidazole, 70%) to introduce a good leaving group. Subsequent displacement of the iodide with lithiated dithiane **112** (*t*-BuLi, HMPA, 94%), derived from propanal as shown in **Scheme 3.8** [8], delivered the 1,3-dithiane **115**. One of the major drawbacks to dithiane chemistry in general is the need for the toxic stoichiometric mercury (II) salts that are commonly employed to unmask the ketone; this was avoided using conditions reported by Hong (I<sub>2</sub>, NaHCO<sub>3</sub>),<sup>70</sup> which gave an acceptable 63% yield.

Overall, ethyl ketone **110** was prepared in 34% yield over 4 steps from ester **111**. Through this route, over 35 g of ketone **110** has been accessed, demonstrating the tractability of these early steps of the synthesis and providing material for future studies.



**Reagents and conditions:** [a] LiAlH<sub>4</sub>, THF, 0 °C → rt. [b] PPh<sub>3</sub>, imidazole, I<sub>2</sub>, CH<sub>2</sub>Cl<sub>2</sub>, rt. [c] t-BuLi, HMPA, **112**, THF, -78 °C; **114**. [d] I<sub>2</sub>, NaHCO<sub>3</sub>, MeCN, rt. [e] BF<sub>3</sub>·Et<sub>2</sub>O, HS-CH<sub>2</sub>-CH<sub>2</sub>-CH<sub>2</sub>-SH, THF, -78 °C

**Scheme 3.8:** **A** Preparation of ethyl ketone **110** from chiral ester **111** using a Corey-Seebach homologation. **B** Synthesis of dithiane intermediate **112**.

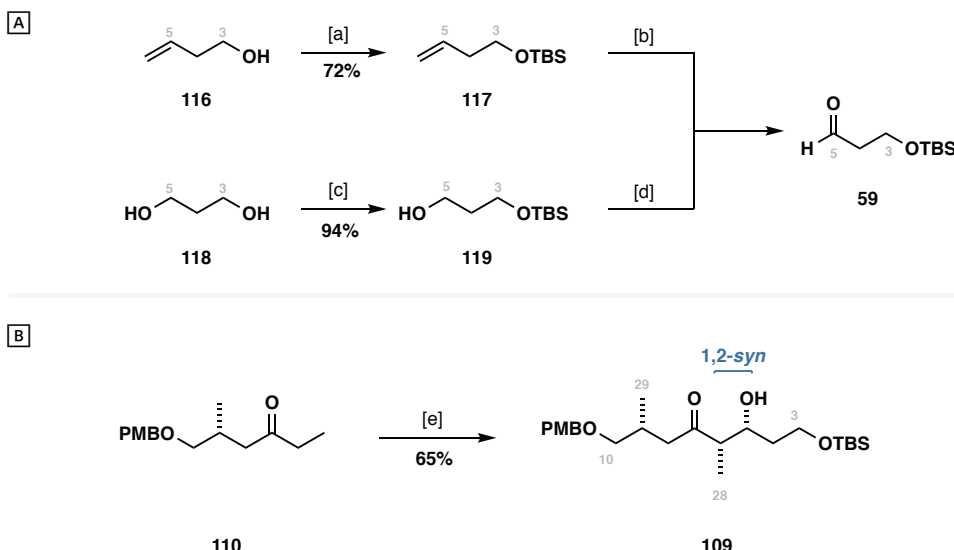
### 3.2.2 INSTALLATION OF THE C5 – C7 STEREO TRIAD

With substantial stocks of ethyl ketone **110** to hand the remaining stereocentres needed to complete the linear C1 – C11 precursor could be introduced. This was accomplished using a reagent-controlled enantio- and diastereoselective boron aldol reaction followed by a substrate-directed 1,3-*anti* reduction, the combination of which enabled all of the stereocentres in the linear C3 – C10 fragment to be introduced with exquisite selectivity.

#### 3.2.2.1 BORON ALDOL REACTION

The C3 – C5 aldehyde **59** needed for the aldol was prepared following standard literature procedures from either 3-buten-1-ol **116** or propan-1,3-diol **118**,<sup>71–73</sup> however the latter route was preferred owing to the availability of **118** and the extended time needed to effect ozonolysis of **117**. Thus, diol **118** was mono-protected as the corresponding TBS ether (NaH, TBSCl), with oxidation using Swern conditions ((COCl)<sub>2</sub>, DMSO, Et<sub>3</sub>N) providing the desired

C3 – C5 aldehyde **59**. Note that in both cases, the aldehyde **59** was sufficiently clean to be used crude in the subsequent aldol reaction, without any appreciable deterioration of yield.



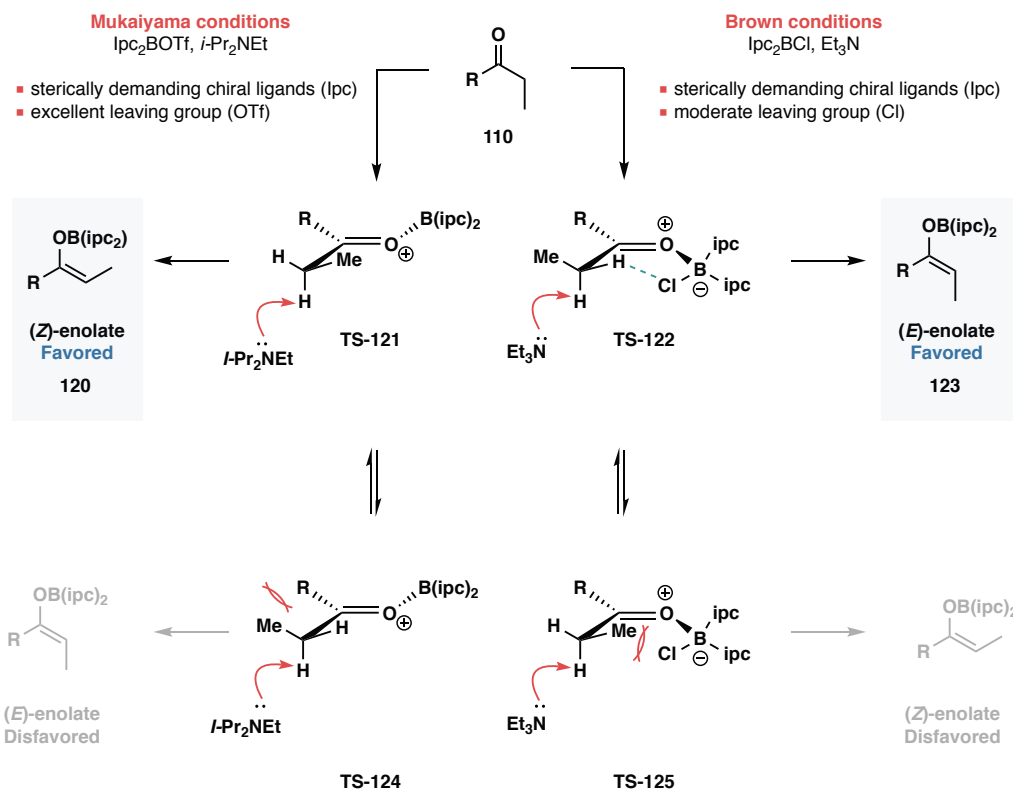
**Reagents and conditions:** [a] TBSCl, imidazole, CH<sub>2</sub>Cl<sub>2</sub>, rt. [b] O<sub>3</sub>, NaHCO<sub>3</sub>, CH<sub>2</sub>Cl<sub>2</sub>, MeOH, -78 °C. [c] NaH, THF, 0 °C; TBSCl, rt. [d] (COCl)<sub>2</sub>, DMSO, -78 °C; Et<sub>3</sub>N, -78 °C → rt. [e] (-)-Ipc<sub>2</sub>BOTf, *i*-Pr<sub>2</sub>NEt, CH<sub>2</sub>Cl<sub>2</sub>, -78 °C; **59**, CH<sub>2</sub>Cl<sub>2</sub>, -78 °C → -30 °C.

**Scheme 3.9:** **[A]** Preparation of the C3 – C5 aldehyde **59**. **[B]** Boron aldol reaction between aldehyde **59** and ethyl ketone **110**.

To carry out the aldol reaction, ketone **110** was first enolised with (-)-Ipc<sub>2</sub>BOTf and *i*-Pr<sub>2</sub>NET in CH<sub>2</sub>Cl<sub>2</sub> at -78 °C. Slow addition of aldehyde **59** at -78 °C followed by warming to -30 °C and oxidative workup (H<sub>2</sub>O<sub>2</sub>) afforded the desired 1,2-*syn* aldol adduct **109** as a single diastereomer (as determined by <sup>1</sup>H NMR spectroscopy of the crude reaction mixture) in 65% yield (**Scheme 3.9**). These results are consistent with those reported by Haslett.<sup>53</sup>

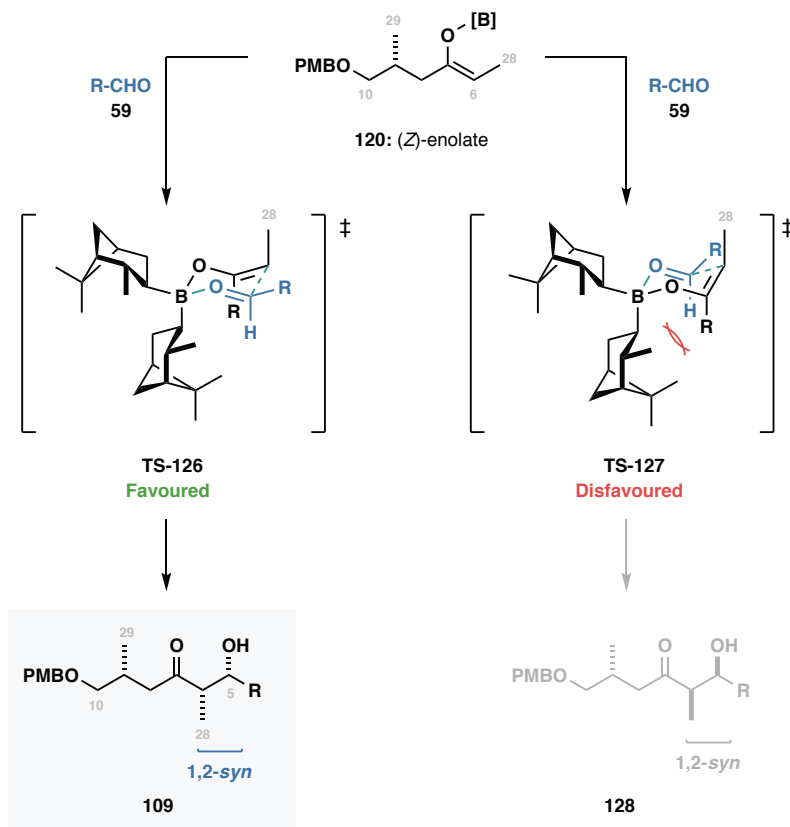
Rationalisation of the enantio- and diastereoselectivity requires consideration of both the enolate geometry and the transition state. The (*Z*)-enolate **120** is formed with high levels of selectivity using (-)-Ipc<sub>2</sub>BOTf/*i*-Pr<sub>2</sub>NET as depicted in **Scheme 3.10**. Using boron triflate reagents, the B-OTf bond is completely dissociated prior to enolisation taking place, allowing the trigonal boron group to orient itself away from the developing enolate; the use of a sterically demanding base (*i*-Pr<sub>2</sub>NET) reinforces this preference. The most favourable enolisation transition state has the methyl group eclipsing the carbonyl to minimise A<sup>1,2</sup> strain with the R group of the ketone.<sup>74</sup> Deprotonation thus takes place via **TS-121**, with the σ-C-H perpendicular to the π-C=O to allow good orbital overlap as the enolate develops. This results in the stereoselective formation of the (*Z*)-enolate **120**, leading ultimately to the required 1,2-*syn* diastereomer of the aldol adduct **109**. The diastereomeric *anti* aldol adduct is accessible via formation of the (*E*)-enolate **123**, giving a great deal of flexibility to boron aldol methodology.

Results & discussion I: synthesis of a modified western fragment



**Scheme 3.10:** Mechanistic rationale for the stereodivergent formation of (*E*)- and (*Z*)-boron enolates from ethyl ketones.<sup>75</sup>

Once formed, the (*Z*)-enolate **120** reacts with aldehyde **59** via a highly-ordered six-membered transition state (**Scheme 3.11**). By virtue of the enolate geometry, the C28-methyl group is forced into a pseudo-axial position, with the aldehyde orientating itself such that the R group is in the thermodynamically favourable equatorial position. The stereofacial discrimination is a consequence of the chiral controlling groups on boron, with the *Si* face attack via **TS-126** favoured for the (*Z*)-enolate as it minimises steric clash between the R-group of the enolate with the methyl group on the *iso*-pinocampheyl ligands on boron. This qualitative transition state model has been validated by extensive DFT studies by Goodman and Paton (**Figure 3.2**).<sup>76</sup>



**Scheme 3.11:** Mechanistic rationale for the observed facial selectivity when using (-)-ipc<sub>2</sub>BOTf.

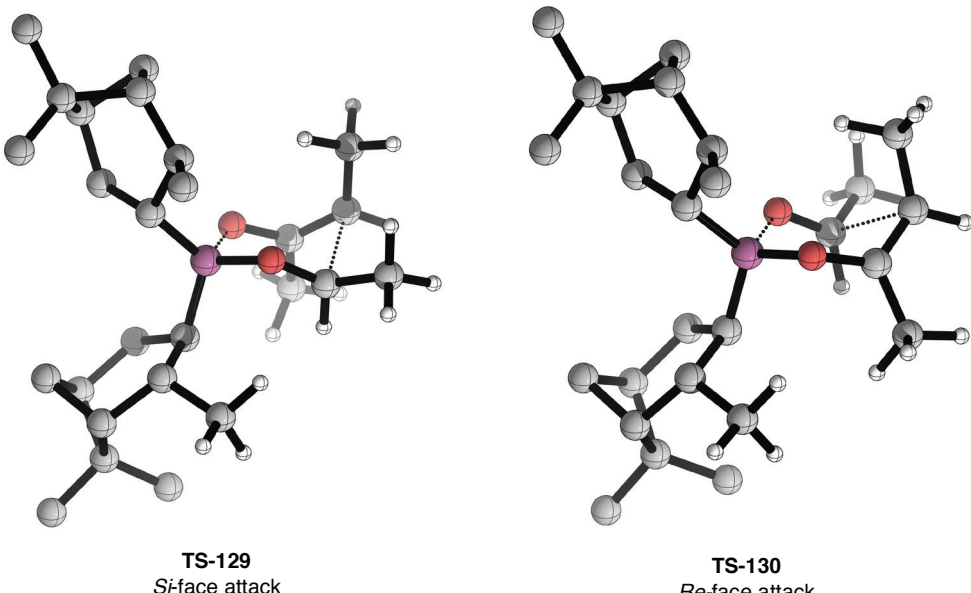


**Figure 3.2:** Calculated transition states for the Ipc aldol (Goodman/Paton).<sup>76</sup> Some hydrogens have been omitted for clarity. [DFT-B3LYP/6-31G\*\*, gas-phase]

The 1,2-*syn* stereochemistry between the C5-OH and C6-Me substituents in **109** was confirmed by inspection of the vicinal  $^3J_{\text{H}5-\text{H}6}$  coupling constant in the  $^1\text{H}$  NMR spectrum (**Figure 3.3**). This analysis works as in non-polar aprotic solvents, such as  $\text{CDCl}_3$ ,  $\beta$ -

hydroxyketones adopt chair-like conformations held together via internal hydrogen bonding. In this conformation, 1,2-*syn* aldol adducts are expected to have smaller coupling constants than 1,3-*anti* aldol adducts based on dihedral angles ( $\theta$ ) of ca.  $60^\circ$  and  $180^\circ$  respectively. The observed 4.6 Hz coupling between H5 and H6 thus suggests a *syn* relationship with a dihedral angle of ca.  $53^\circ$ , in keeping with the expected stereochemical outcome of the reaction.

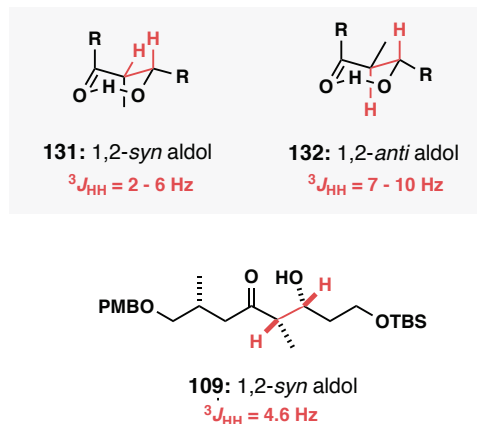
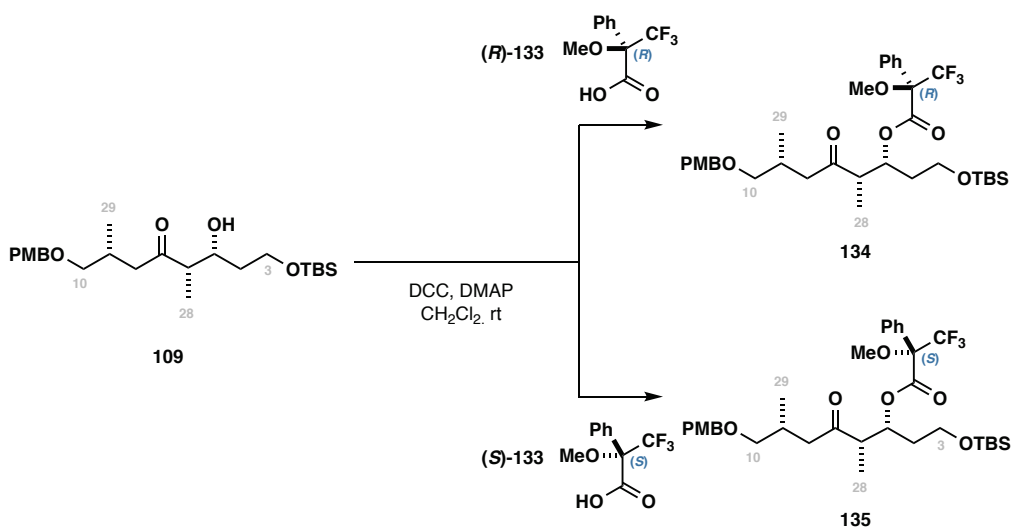


**Figure 3.3:** Confirmation of 1,2-*anti* stereochemistry via  $^1\text{H}$  NMR analysis.

To determine the absolute configuration at the newly formed C5 oxymethine stereocentre, aldol adduct **109** was derivatised as the corresponding  $\alpha$ -methoxy- $\alpha$ -trifluoromethylphenylacetic acid (MTPA) esters **134** and **135** using Steiglich conditions (DCC, DMAP) (**Scheme 3.12**).



**Scheme 3.12:** Preparation of MTPA esters for determination of absolute configuration.

Experimental and computational investigations suggest that MTPA esters adopt a conformation in which the trifluoromethyl, ester and oxymethine proton lie in the same plane (**Figure 3.4**).<sup>77,78</sup> In this conformation, the phenyl group shields one side of the molecule causing a perturbation of the chemical shift. Comparison of the proton NMR shifts between

the diastereomeric (*R*) and (*S*) MTPA esters thus allows the absolute configuration of secondary alcohols to be determined. The experimental  $^1\text{H}$  NMR data for **134** and **135** is tabulated in

**Table 3.1**, and confirms the configurational assignment of the newly formed C5 stereocentre as expected.

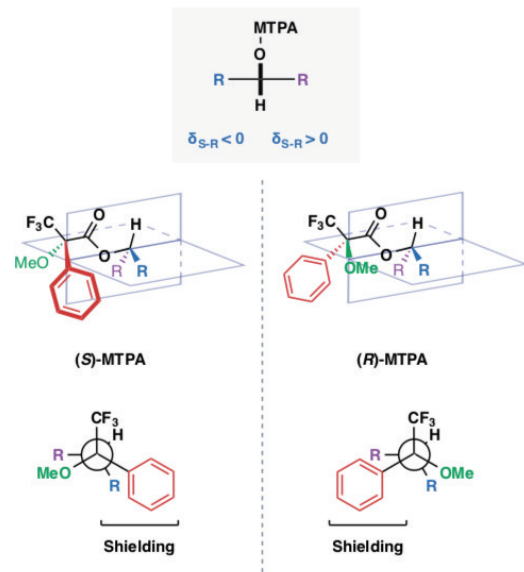


**Figure 3.4:** Assignment of absolute configuration using MTPA esters. Shielding effects in the dominant conformers of MTPA esters, and the expected  $\delta_{\text{S}-\text{R}}$  sign.

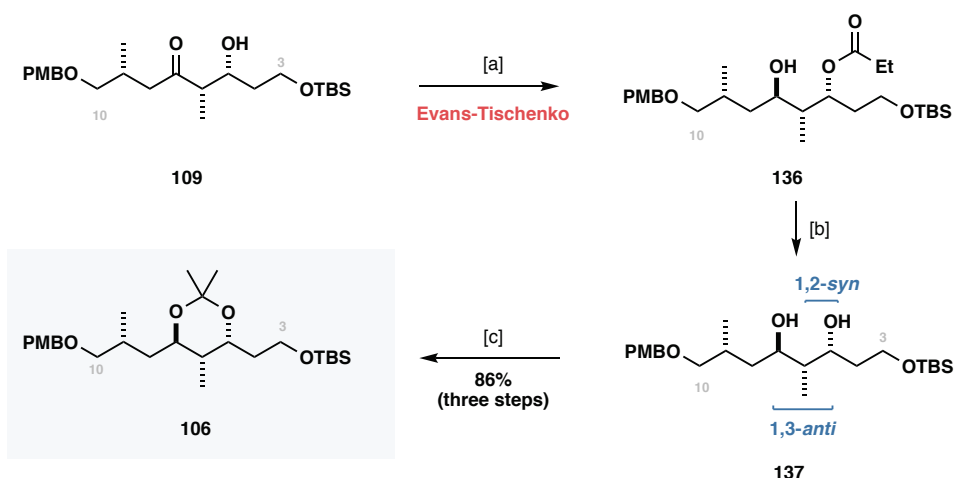
**Table 3.1:** NMR data for diastereomeric MTPA esters **134** and **135** (500 MHz,  $\text{CDCl}_3$ ).

Proton	$\delta_{\text{S}}\text{-MTPA}$	$\delta_{\text{R}}\text{-MTPA}$	$\delta_{(\text{S}-\text{R})}$
3	3.61	3.52	+0.09
4'/4"	1.83	1.79	+0.04
6	2.81	2.86	-0.05
8'	2.53	2.62	-0.09
8''	2.21	2.33	-0.12
9	2.28	2.33	-0.05
10'	3.18	3.22	-0.04
10''	2.35	2.28	-0.03
28	1.04	1.08	-0.04
29	0.86	0.91	-0.05

Chemical shifts are taken as the midpoint of multiplets for the purpose of the MTPA analysis.

### 3.2.2.2 ELABORATION TO THE C3 – C10 ACETONIDE

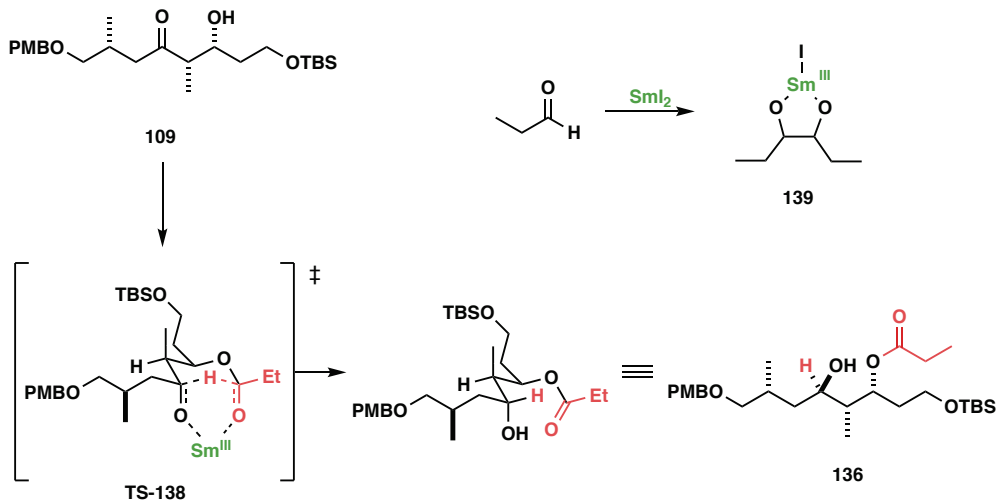
The conversion of aldol adduct **109** into the C3 – C10 acetonide **106** needed to explore the modified macro-Heck route was accomplished in three steps, using a 1,3-*anti* Evans-Tischenko reduction as a key step to introduce the remaining stereocentre at C7. Treatment of **109** with SmI<sub>2</sub> in the presence of propanal followed by solvolysis (K<sub>2</sub>CO<sub>3</sub>, MeOH) of the propionate ester and acetonide formation (Me<sub>2</sub>C(OMe)<sub>2</sub>, PPTS) provided **106** in excellent yield of 86% (**Scheme 3.13**). This three-step transformation was carried out without purification of the intermediates, which have previously been characterised by Haslett.<sup>53,56</sup>



**Reagents and conditions:** [a] SmI<sub>2</sub>, EtCHO, THF, -78 °C → 30 °C. [b] K<sub>2</sub>CO<sub>3</sub>, MeOH, rt. [c] CH<sub>3</sub>C(OMe)<sub>2</sub>, PPTS, CH<sub>2</sub>Cl<sub>2</sub>, rt.

**Scheme 3.13:** Elaboration of aldol adduct **109** to the completed C3 – C10 acetonide **106**.

Mechanistically, the Sm first promotes a pinacol-like reductive coupling between two equivalents of propanal to form a Sm (III) pinacolate species **139**—this is thought to be the active species involved in the Evans-Tischenko reduction (**Scheme 3.14**). Addition of aldol adduct **109** leads to the formation of a bicyclic transition state **TS-138** in which the ketone and aldehyde substituents are equatorially arranged to minimise unfavourable steric interactions. Intramolecular hydride transfer delivers the product **136** with the desired 1,3-*anti* configuration.



**Scheme 3.14:** Proposed mechanism for the 1,3-*anti* Evans-Tischenko reduction. Formation of the putative active species  $[(\text{EtCHO})_2\text{SmI} \cdot \text{SmI}_3]$  (inset).

The anticipated relative stereochemistry was confirmed based diagnostic chemical shifts of the acetonide carbons in the  $^{13}\text{C}$  NMR spectrum (**Figure 3.5**). The observed values at  $\delta_{\text{C}}$  ( $\text{CDCl}_3$ ) = 100.6, 24.0 and 26.1 ppm are indicative of a 1,3-*anti* acetonide adopting a twist-boat conformation **141** in which the two methyl groups are in similar environments, unlike for 1,3-*syn* acetonides **140** where the axial and equatorial methyl groups are in electronically different environments.<sup>79</sup>

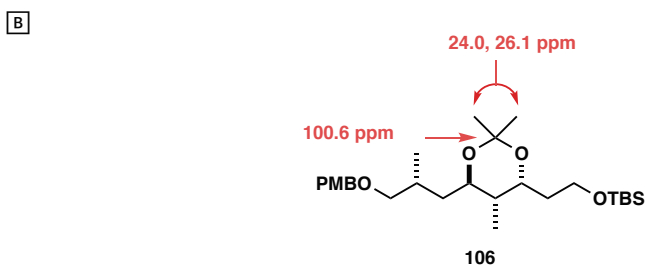
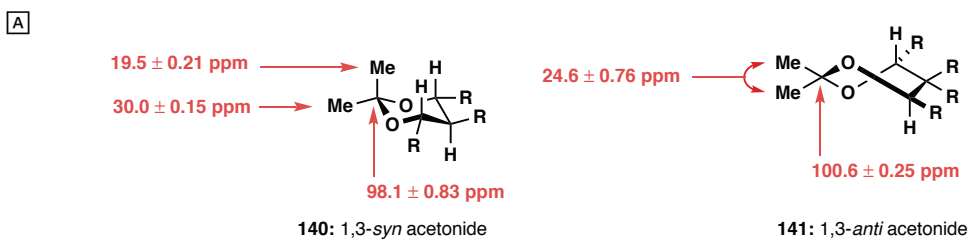


**Figure 3.5:** **[A]** Expected  $^{13}\text{C}$  NMR shifts for 1,3-*syn* **141** and 1,3-*anti* **140** acetonides (Rychnovsky/Evans)<sup>79,80</sup>. **[B]** Observed  $^{13}\text{C}$  NMR shifts for 1,3-*anti* acetonide **106**.

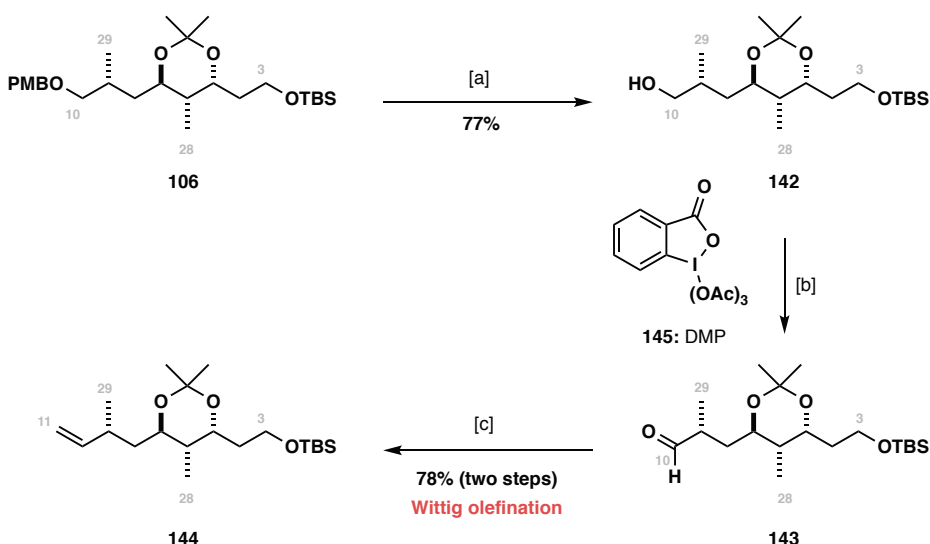
### 3.3 ELABORATION TO THE MODIFIED C1 – C11 WESTERN FRAGMENT

With adequate stocks of acetonide **106** to prepared, the divergent synthesis to the modified C1 – C11 fragment **99** could be investigated (**Scheme 3.5**). The conversion of acetonide **106** into the required linear precursor **108** requires two olefinations: conversion of the C1 PMB ether into a terminal olefin, and conversion of the C3 TBS ether into the required  $\alpha,\beta$  -unsaturated thioester.

Since conditions were already optimised for the latter transformation (the Horner-Wadsworth-Emmons olefination), attention was first focused on installation of the terminal olefin, which was envisioned to arise from a Wittig methylenation of the parent aldehyde. This would also avoid having to conduct the Wittig reaction in the presence of the thioester, which may be reactive under the necessary conditions.

#### 3.3.1 PREPARATION OF THE LINEAR C1 – C11 PRECURSOR

Accordingly, treatment of PMB ether **106** with DDQ afforded alcohol **142** (80%), which was oxidised to aldehyde **143** using the Dess-Martin periodinane (DMP). In order to circumvent the epimerisation previously observed by Haslett when conducting the C10 oxidation (TEMPO/BAIB), the potentially delicate aldehyde was used immediately without purification. Thus, treatment of **143** with  $\text{Ph}_3\text{P}=\text{CH}_2$  (generated in situ from the deprotonation of  $\text{Ph}_3\text{P}^+\text{MeBr}^-$  with *n*-BuLi) afforded terminal olefin **144** in modest yield (33%), with the mass balance accounted for by unreacted aldehyde. It was found that an excess of the ylid was needed to obtain good conversion, affording **144** in 78% yield over two steps from alcohol **142**.



**Reagents and conditions:** [a] DDQ, pH 7 buffer,  $\text{CH}_2\text{Cl}_2$ , rt. [b] DMP **145**,  $\text{NaHCO}_3$ ,  $\text{CH}_2\text{Cl}_2$ , rt. [c]  $\text{Ph}_3\text{PMeBr}$ , *n*-BuLi, THF, -78 °C.

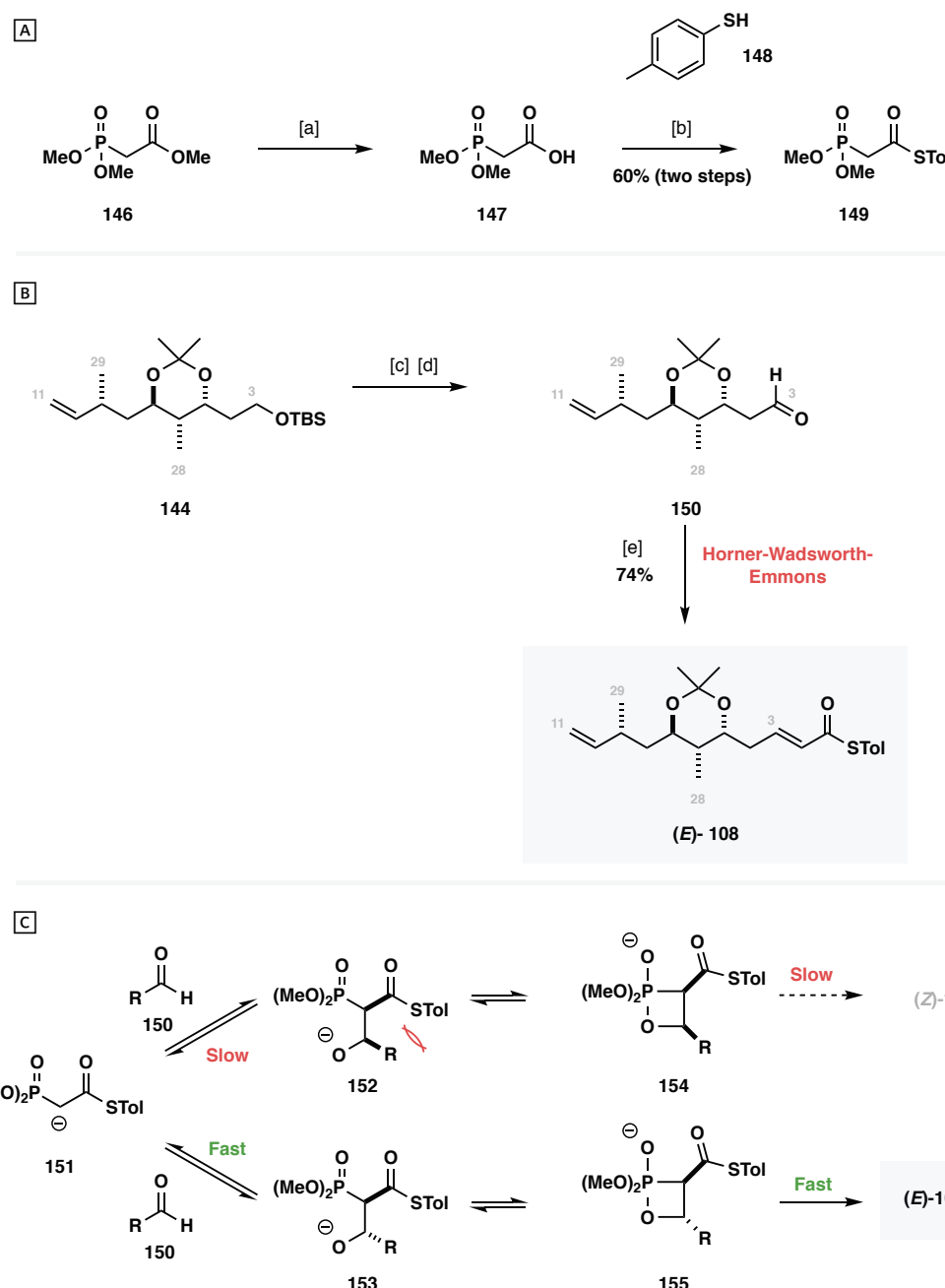
**Scheme 3.15:** Conversion of acetonide **106** into terminal olefin **144** using a Wittig methylenation.

All that remained for the completion of the C1 – C11 linear precursor **108** was the installation of the  $\alpha,\beta$ -unsaturated thioester moiety that would act as a Michael acceptor in the anticipated cyclisation step.

The phosphonate **149** needed for the Horner-Wadsworth-Emmons olefination was prepared in two steps from trimethylphosphonoacetate **146** (**Scheme 3.16 [A]**). Accordingly, sodium hydroxide mediated saponification of **146** afforded 2-phosphonoacetic acid **147** which was able to undergo thioesterification with thiol **148** under Steiglich conditions (DCC, DMAP) to provide **149** in 60% yield from **146**. This result, although not surprising, is in conflict with previous studies by Haslett, who observed significant degradation while attempting to form the thioester using the above conditions, instead installing the thioester via activation of the carboxylic acid as the corresponding acid chloride.<sup>56</sup>

At this stage, the C3 TBS ether **144** was deprotected (TBAF) and oxidised to aldehyde **150** ((COCl)<sub>2</sub>, DMSO; Et<sub>3</sub>N). The HWE olefination was conducted on **150** using modified Masamune-Roush conditions (LiCl, Et<sub>3</sub>N) as optimised by Haslett.<sup>56</sup> This proceeded uneventfully to provide **108** in good yield (74%) as a single geometric isomer. The geometry of the newly formed alkene was confirmed by <sup>1</sup>H NMR analysis, with a <sup>3</sup>J<sub>H-H</sub> coupling constant of 17.2 between H3 and H4 indicative of the predicted (*E*)-geometry. This selectivity is rationalised by the reversible addition of **151** to aldehyde **150**, with the *anti*-addition product **153** thermodynamically favoured due to minimisation of the unfavourable steric clash between the thioester and the R-group of the aldehyde (**Scheme 3.16 [C]**). The formation of oxaphosphatanes (**154** and **154'**) has been shown to be the rate-determining step of the reaction,<sup>81</sup> thus the (*E*)-olefin **108** is obtained as the major geometric isomer.

Results & discussion I: synthesis of a modified western fragment



**Reagents and conditions:** [a] NaOH, H<sub>2</sub>O, rt. [b] DCC, DMAP (cat.), CH<sub>2</sub>Cl<sub>2</sub>, rt. [c] TBAF, THF, rt. [d] DMP, NaHCO<sub>3</sub>, CH<sub>2</sub>Cl<sub>2</sub>, rt. [e] 149, LiCl, Et<sub>3</sub>N, CH<sub>2</sub>Cl<sub>2</sub>, -30 °C.

**Scheme 3.16:** **[A]** Preparation of thioester 149. **[B]** Conversion of TBS ether 144 to the complete C1 – C11 linear precursor 108. **[C]** Mechanistic rationale for the selective formation of the (*E*)-olefin using a Horner-Wadsworth-Emmons olefination.

### 3.3.2 INTRAMOLECULAR OXY-CONJUGATE CYCLISATION

The intramolecular oxy-conjugate cyclisation (IOCC) is a well-established method for the synthesis of tetrahydropyran rings.<sup>82–84</sup> While the reaction often gives excellent diastereoselectivity at the newly formed oxymethine centre, there is a general lack of

mechanistic understanding, making it challenging to predict which diastereomer is likely to dominate from a given substrate under a given set of conditions. Given the wide range of biologically active natural products containing THP motifs (see **Figure 3.6** for selected examples), the ability to form them with predictable diastereoselectivity is of critical importance.

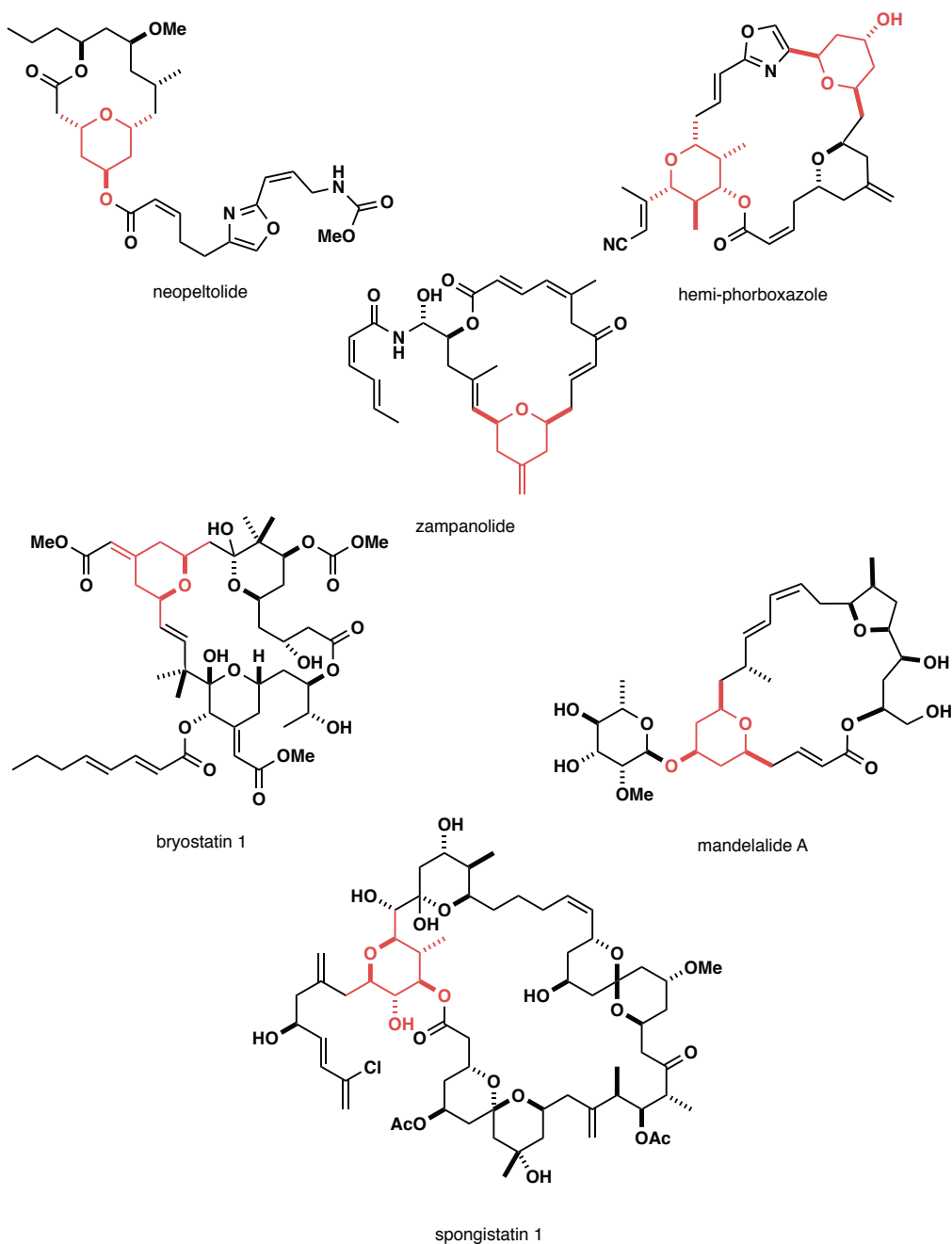
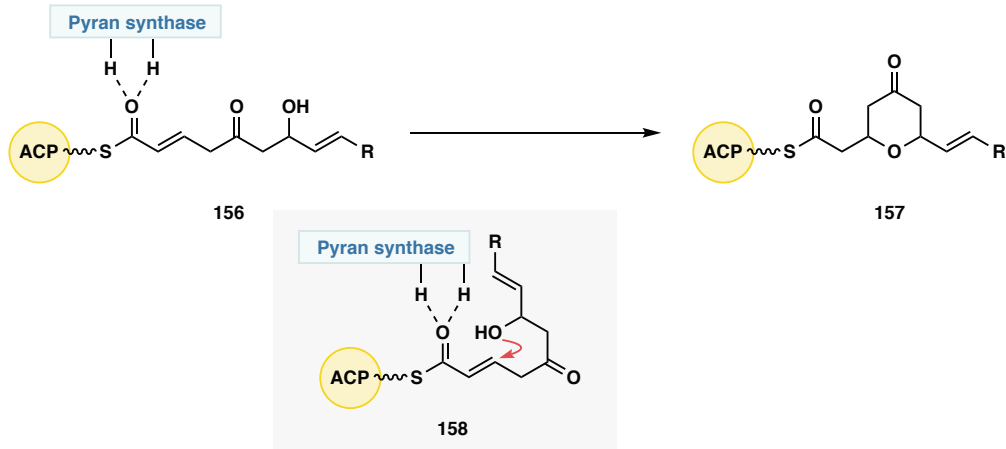


**Figure 3.6:** Examples of marine natural products containing a THP.

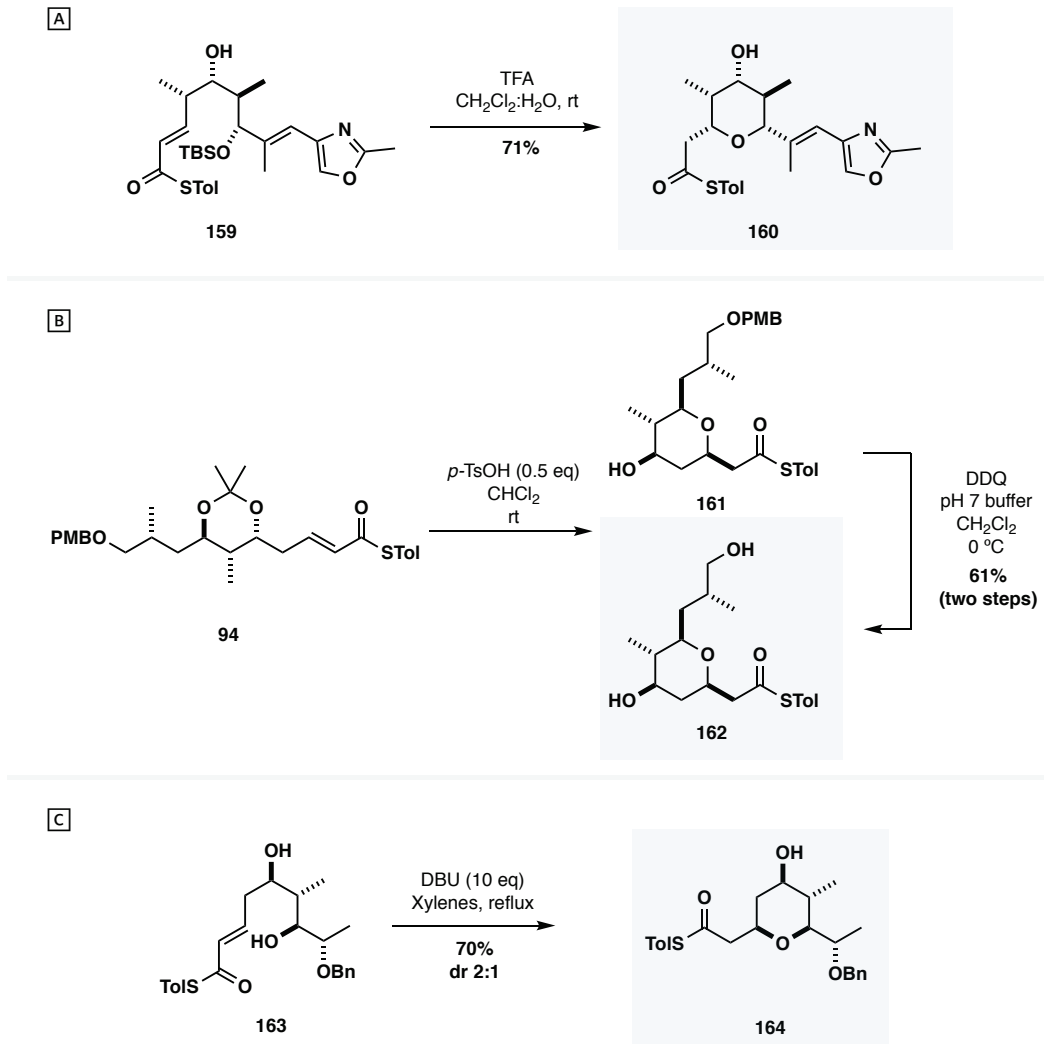
In 2011, Fuwa reported a ‘bio-inspired’ hetero-Michael cyclisation that provided reliable access to the 2,6-*cis* diastereomer using  $\alpha,\beta$ -unsaturated thioesters in place of the oxoesters that have conventionally been used in synthesis.<sup>85,86</sup> This was inspired by biosynthetic studies that determined pyrans found in polyketides are formed via enzyme mediated conjugate addition while the chain is still attached to the acyl carried protein **158** via a sulfur linkage (**Scheme 3.17**).



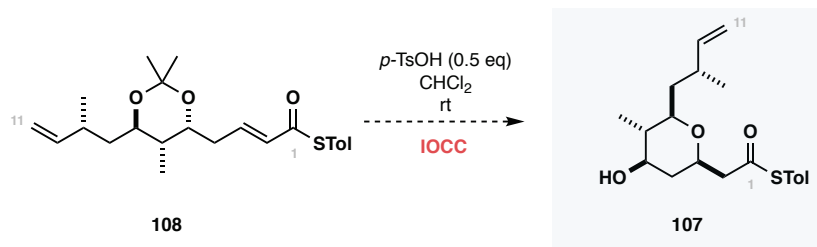
**Scheme 3.17:** Pyran formation in polyketides. The heterocycle formation is catalysed by an enzyme while the growing chain is still bound to the acyl carrier protein of the polyketide synthase.

Despite the excellent diastereoselectivity reported for the Bronsted acid mediated cyclisation of thioesters, limited examples exist of its use in the context of complex molecule synthesis: the Paterson C1 – C11 western fragment synthesis of madeirolide A **161/162**,<sup>53</sup> and the Clarke synthesis of a C20 – C32 fragment of phorboxazole A **160**<sup>87</sup> being two notable examples (**Scheme 3.18**). A further example by Romea uses stoichiometric base (DBU) to afford cyclisation of thioester **163**, however the selectivity in this case is significantly lower (2:1) than for the corresponding reactions using Bronsted acids.<sup>88</sup>

Synthetic and computational studies were carried out during investigations into the cyclisation of **108** with the aim of gaining insight into the factors governing the selectivity and reactivity of the system (**Scheme 3.19**).



**Scheme 3.18:** Examples of Fuwa's thioester cyclisation in total synthesis. **A** Application in Clarke's synthesis of a phorboxazole fragment. **B** Application in the Paterson synthesis of a C1–C11 fragment of madeirolide A. **C** Example of a base-catalysed cyclisation of thioesters in the Romea synthesis of herboxidiene.

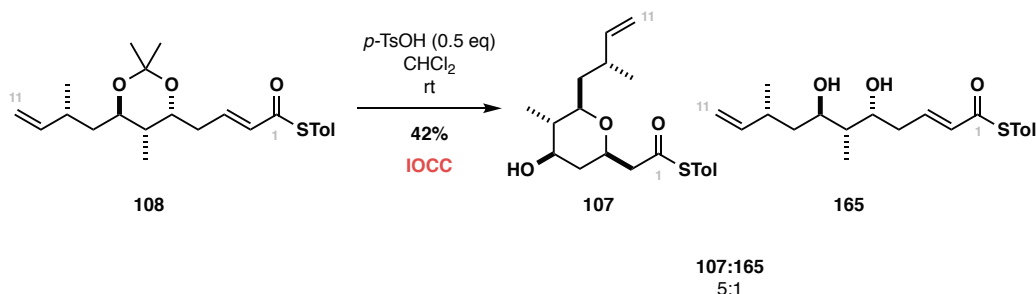


**Scheme 3.19:** Proposed oxy-Michael cyclisation to form the modified C1 – C11 macro-Heck fragment aglycone.

### 3.3.2.1 SYNTHETIC STUDIES

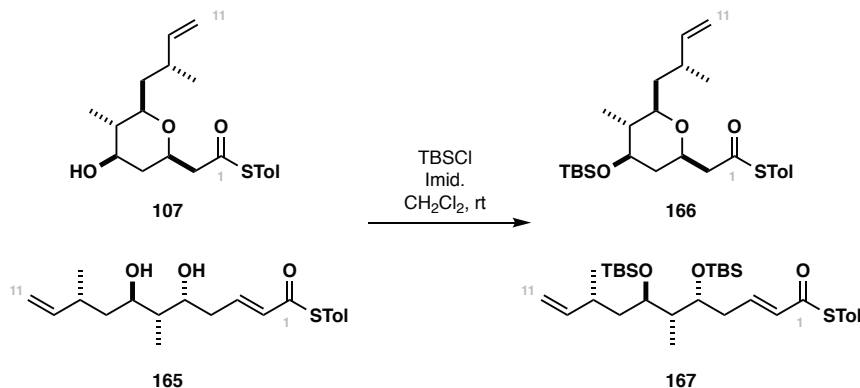
With the C1 - C11 linear precursor **108** to hand, the feasibility of the intramolecular oxy-conjugate cyclisation (IOCC) could be investigated. Given the close similarity between **108** and Haslett's C1 – C11 linear precursor **38**, bearing a PMB ether at C10, it was anticipated that the application of the IOCC conditions previously optimised would be successful.

Accordingly, **118** was treated with *p*-TsOH in CH<sub>2</sub>Cl<sub>2</sub> at ambient temperature. The reaction initially appeared to be rapid, with all the starting material consumed within 30 minutes. However, following column chromatography, <sup>1</sup>H NMR revealed that the new spot was an inseparable mixture of desired THP **107** and deprotected starting material **165** in a 5:1 ratio (based on the crude <sup>1</sup>H NMR). Attempts at re-submitting the mixture to the reaction conditions did not significantly change the ratio of **107** to **165**, plausibly indicating that the 5:1 ratio indicates a thermodynamic distribution of products.

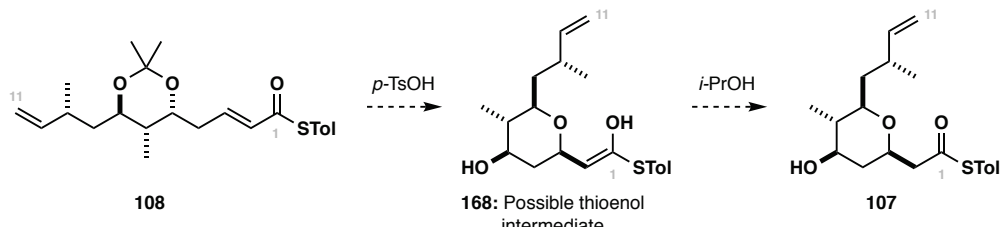


**Scheme 3.20:** Initial results for the *p*-TsOH mediated IOCC of **108**. Products **107** and **165** were isolated as an inseparable mixture.

At this juncture it became apparent that either the reaction needed to be pushed to completion, or a method for the separation of **107** from **165** needed to be found. In this instance, carrying forward the mixture was undesirable as diol **165** would likely also be reactive under the glycosylation conditions needed to complete the fragment, resulting in unnecessary attrition of material. Treatment of the crude mixture with TBSCl/imidazole did enable the separation of **107** from **165** by flash column chromatography (as the corresponding silyl ethers). This was not investigated further as it was in no way tractable, especially given that this revised route was devised to *avoid* the protecting group shuffling previously needed.

**Scheme 3.21:** Separation of **107** from **165** by conversion to the corresponding TBS ethers.

Despite repeated attempts at encouraging the reaction to completion,  $^1\text{H}$  NMR of the crude product always indicated at least 10% of **165**. The best conversion was obtained using stoichiometric *p*-TsOH (1.1 eq.), doping the  $\text{CH}_2\text{Cl}_2$  with 1% *i*-PrOH. This presumably helps by providing a proton source which facilitates protonation of the thioenol intermediate **168**, which may be rate determining when the IOCC is carried out in a non-protic solvent such as  $\text{CH}_2\text{Cl}_2$  (**Scheme 3.22**). Interestingly, heating the reaction mixture did not confer any increase in conversion.

**Scheme 3.22:** Mechanistic outline showing the proposed thioenol intermediate **168**.

With conditions now optimised to provide maximum conversion, all that remained necessary was to separate away the small quantities of diol **165**. It was found that the use of a modified eluent (TLC: 20%  $\text{Me}_2\text{CO} : \text{PhMe} + 0.1\%$  HCOOH; column chromatography: 10 - 30%  $\text{Me}_2\text{CO} : \text{PhMe} + 0.1\%$  AcOH) enabled the small amounts of **165** to be separated from **107** providing spectroscopically pure material to be taken forward. The additive was switched from formic to acetic acid for the purposes of column chromatography due to formation of the formate ester at C5.

Overall, this slight modification to the optimised conditions developed by Haslett enabled the reproducible isolation of **107** in 70% yield as a single diastereomer by NMR. The remaining mass balance of the reaction was largely accounted for by recovered diol which was able to be used in subsequent cyclisation reactions.

The stereochemistry at the newly introduced C7 oxymethine was confirmed by analysis of  $^3J_{HH}$  couplings, 1D NOESY NMR experiments, and by analogy to the THP formed by Haslett, which differs only by the presence of a PMB ether at C10 in place of the C10 – C11 olefin present in **107** (**Figure 3.7**). Specifically, irradiation of H3 showed the expected nOe enhancements to the co-axial protons at H5 and H7 – a result consistent with the ring adopting a chair conformation.

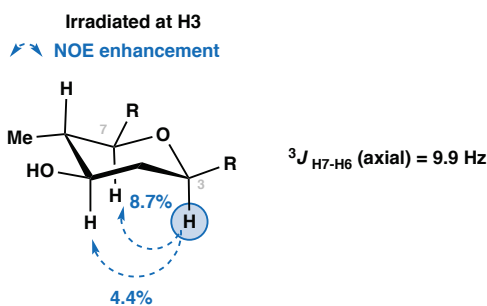
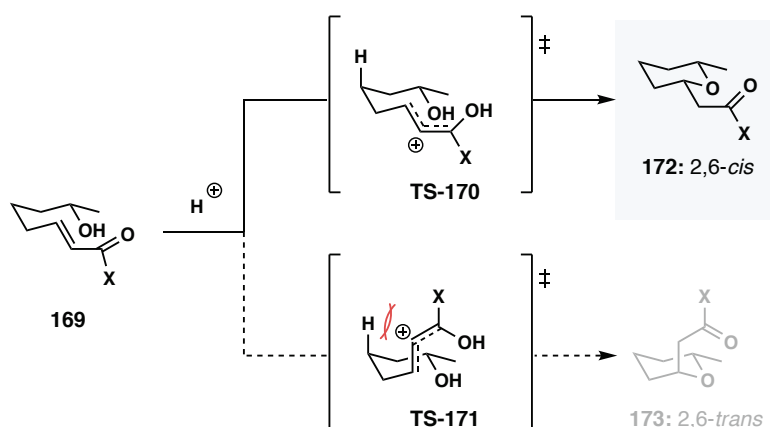


**Figure 3.7:** Reciprocal nOe enhancements across the newly formed THP ring confirming the anticipated 2,6-*cis* stereochemistry.

### 3.3.2.2 MECHANISTIC AND COMPUTATIONAL STUDIES

To rationalise the high-levels of diastereoselectivity observed, Fuwa proposed that the 2,6-*cis* diastereomer is favoured kinetically and thermodynamically for the cyclisation of  $\alpha,\beta$ -unsaturated thioesters under Bronsted acidic conditions, proposing the diastereomeric oxy-allyl cation transition states **TS-170** and **TS-171** (**Scheme 3.23**).<sup>85</sup> This mechanistic pathway rationalises the dominant formation of the 2,6-*cis* diastereomer since the transition state **TS-170** leading to it places the oxy-allyl cation in the pseudo-equatorial position, minimising A<sup>1,3</sup> strain across the ring. Conversely **TS-171** is disfavoured owing to the pseudo-axial position of the oxy-allyl cation. No additional experimental data has been provided by Fuwa to support this hypothesis, and recent computational investigations by Ermanis failed to identify either **TS-170** or **TS-171** as plausible transition states.<sup>89</sup>



**Scheme 3.23:** Proposed transition states for Brønsted-acid catalysed IOCC used to rationalise high levels of 2,6-cis selectivity (Fuwa)<sup>85</sup>

With experimental results for the cyclisation now available (§3.3.2.1), a computational studies of the reaction was initiated to better understand the factors governing the selectivity in the context of the C1 – C11 fragment of madeirolide A. These studies aimed to answer several questions:

- Is the reaction under kinetic or thermodynamic control (or both)?

While Fuwa suggests that the 2,6-cis isomer is both the kinetic *and* thermodynamic product, this is not entirely consistent with the mechanistic evidence, which shows that the 2,6-trans THP is not easily isomerised into the 2,6-cis THP suggesting a high kinetic barrier for the reverse reaction (retro-IOCC) once the THP was formed.

- What role (if any) does the thioester play in the reaction?

While the thioester moiety is certainly involved in the biosynthetic pathway during the construction of polyketides, there is no clear basis for its use in synthetic chemistry other than the claim that the reaction is ‘biomimetic’. In Haslett’s original work,<sup>56</sup> the corresponding methyl ester was found to give the same 2,6-cis diastereomer, albeit in lower yield which may suggest that the thioester is not essential. The answer to this question was particularly important, as it would greatly influence the synthetic strategy adopted for construction of the eastern tetrahydropyran, with the methyl ester significantly easier to introduce than the analogous thioester.

**Mechanistic consideration:**

In order to simplify the calculations, diol **165** was used in place of the actual acetonide as the substrate for the IOCC. This was not expected to be deleterious to the reaction, with **165** likely to be formed prior to the oxy-Michael step.

**General strategy:**

To find the energies of the stationary points (transition states, intermediates etc.) along the reaction coordinate, a starting geometry must first be obtained. This can be done manually but is often achieved using molecular mechanics – a computationally inexpensive method that allows thorough exploration of conformational space to identify the geometries of structures lying close to the global minimum.

Low-energy conformers from the conformational search are then used as input geometries in quantum mechanical optimisations using DFT. This additional step is necessary as molecular mechanics energies are known to be unreliable, especially in situations where the various transition states are likely to be close in energy. Finally, calculation of vibrational frequencies characterises the structures as minima (no imaginary frequencies) or transition states (exactly one imaginary frequency).<sup>90</sup>

**Conformational search:**

The structures subjected to the conformational search are shown in **Figure 3.8**. An additional conformational search was conducted to find starting geometries for the transition states **175** in which the C3-O7 bond was artificially constrained to 1.8 Å. For the purposes of molecular mechanics, the bonding of the various structures needed to be specified and as such the protonation state had to be inferred. No further assumptions were made about the binding between the substrate and the acid.

The conformational searches were implemented in Schrodinger MacroModel using the MMFF-94 force-field<sup>91</sup> and implicit CHCl<sub>3</sub>.<sup>\*</sup> All conformers within 50 kJ mol<sup>-1</sup> of the global minimum were recorded, with a sufficient number of steps used to ensure that all conformers

<sup>\*</sup> Chloroform was used in place of dichloromethane as a solvent model for the conformational search as gas-phase calculations vastly over-emphasised the significance of intramolecular interactions resulting in highly folded conformers for the starting material.

within  $10 \text{ kJ mol}^{-1}$  of the global minimum were found at least 10 times.\* Redundant conformer elimination was used to remove similar conformations from the ensemble.†

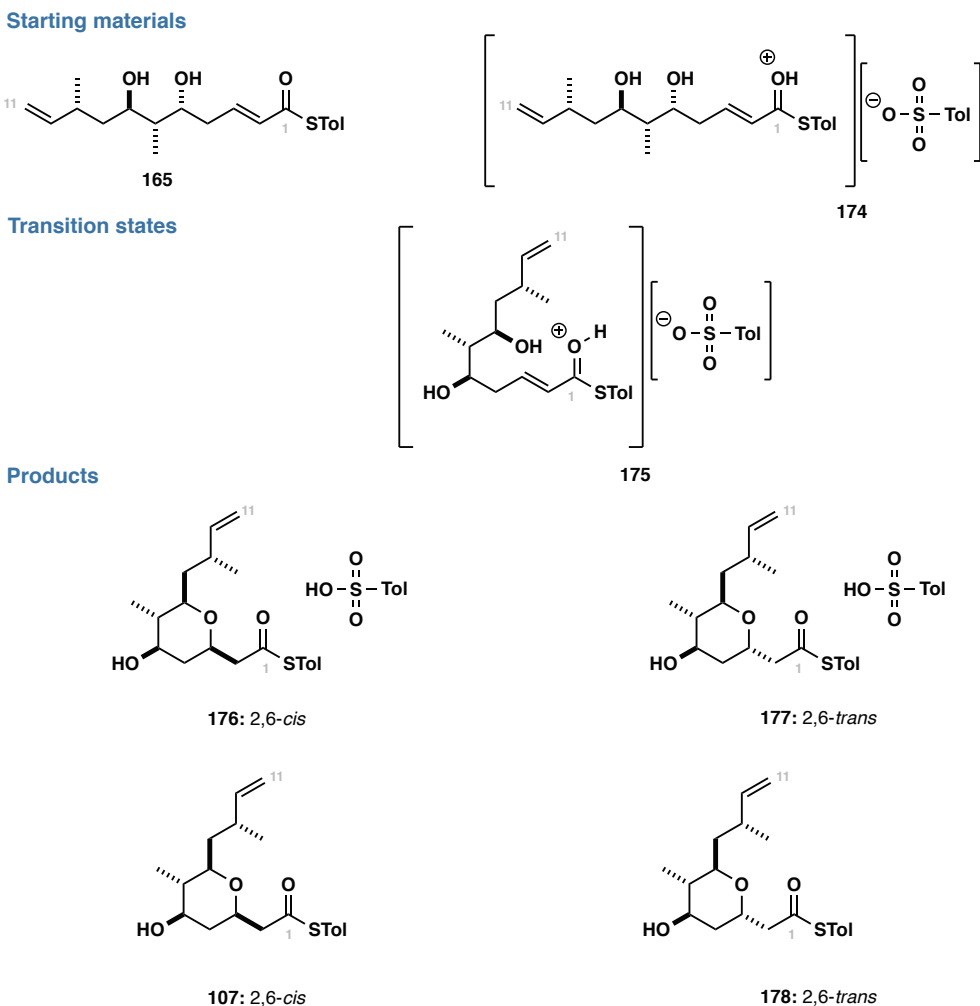


**Figure 3.8:** Structures used as inputs for the conformational search.

\* The method used for the conformational search (mixed torsional/low-mode Monte Carlo) is non-systematic, using random displacements to generate new structures for minimisation. Finding the same conformation multiple times therefore gives confidence (though not certainty) that the conformational space has been sufficiently explored. A high cut-off ( $10 \text{ kJ mol}^{-1}$ ) is used since molecular mechanics (MM) energies are known to be prone to error and as such a high-energy conformer from MM may end up significantly lower (or higher) in energy when optimised using quantum mechanical (QM) techniques such as DFT.

† Molecular mechanics often generates many similar conformers that will ultimately optimise to the same structure (e.g. Conformations that differ only by the rotation of a methyl group). Redundant conformer elimination helps to identify and remove these conformations to avoid the number of duplicate calculations being carried out, vastly reducing the computational time required.

### **Ground state optimisation:**

Optimisation is a general term for finding stationary points along a reaction pathway. In the case of ground state optimisation, the desired stationary points are minima where the first derivative of the reaction coordinate is zero (i.e. the point is stationary and not lying on a gradient). Finding local minima is relatively easy, with many algorithms available to accomplish the task – in the most straightforward implementation, it is always possible to drive a structure towards a minima by following the reaction coordinate down-hill.

DFT Optimisation was performed in Schrodinger Jaguar at the B3LYP/6-31G\*\*+ level of theory.<sup>92–94</sup> Implicit solvent ( $\text{CH}_2\text{Cl}_2$ ) was included in the calculations to represent the true reaction conditions most accurately. Since the energies from molecular mechanics are known to be inaccurate, it is not possible to optimise the lowest energy conformer. Accordingly, following redundant conformer elimination (described above), all remaining conformers within 10  $\text{kJ mol}^{-1}$  of the global minimum were subjected to optimisation with DFT and the lowest energy structure used for the construction of the energy diagrams (below).

### **Transition state optimisation:**

Unlike ground state optimisation, where the lowest energy structure can always be found given sufficient time, there is no general method that will always identify a transition state. Various methods exist to accomplish this task, the most common of which interpolates the transition state based on known structures of a starting material and a product, however there is no universal method, and the process takes significantly longer than the corresponding ground state optimisations.<sup>95</sup>

Given the increased time needed to find a transition state, the previously adopted method of optimising everything within a given window is not a viable strategy.\* To minimise the number of structures used in TS optimisation, a multi-dimensional scaling approach was used to ‘cluster’ the structures according to similarity (**Figure 3.9**).†

\* Each ‘step’ of a transition state search uses an optimisation to determine if the geometry is converged. Accordingly, if a TS search takes 20 steps to converge this is the same as running a ground-state optimisation on 20 individual structures.

† The idea for clustering conformers was demonstrated by Ermanis.<sup>89</sup> The methodology used to cluster the conformers is outlined in **Appendix C**.

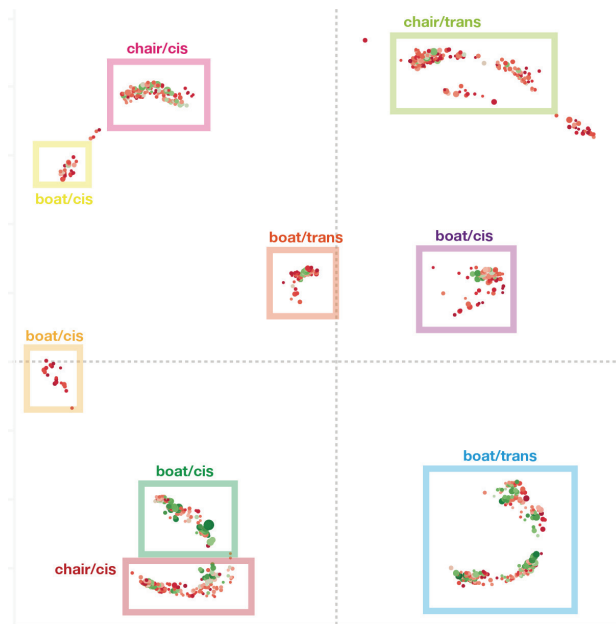


**Figure 3.9:** Clustering of conformers. [Key: points are coloured by relative MMFF-94 energy; points are sized by the number of times the conformational search identified that conformer]. Note that the axes are arbitrary, and the distance between points is not a quantitative measure of how similar/different two structures are.

Representative conformations corresponding to the expected transition states (i.e. chair and boat like conformations with sensible geometries for orbital overlap) were then subjected to a DFT coordinate scan (B3LYP/6-31G<sup>\*\*+</sup>, gas-phase), fixing the bond length at 0.2 Å intervals (1.2, 1.4, 1.6, 1.8, 2.0, 2.2 Å) in order to identify an approximate location of the transition state. These approximate geometries were subsequently refined using DFT (B3LYP/6-31G<sup>\*\*+</sup>, implicit CH<sub>2</sub>Cl<sub>2</sub>) to obtain transition states shown in **Figure 3.10** and **Figure 3.11**.

With transition states identified, minimum energy pathway (MEP) calculations were conducted.\* The MEP is used to ensure that a given transition state does indeed connect the anticipated starting material to the anticipated product (i.e. the actual reaction of interest).† A priori the computer has no understanding of the reaction being carried out, so will latch onto a transition state (single imaginary frequency) even if this is not the one being identified. By following the MEP for the four transition states above, an additional set of intermediates were obtained corresponding to the thioenol formed upon cyclisation. There is growing evidence that this intermediate may be key to the outcome of the reaction, governing whether the cyclisation occurs under kinetic or thermodynamic control.

\* The minimum energy pathway is a mass-weighted variant of the more commonly used intrinsic reaction coordinate (IRC).

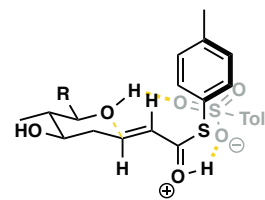
† One of the challenges with transition state searches is that the TS found will not necessarily be the one that connects two minima.

Results & discussion I: synthesis of a modified western fragment

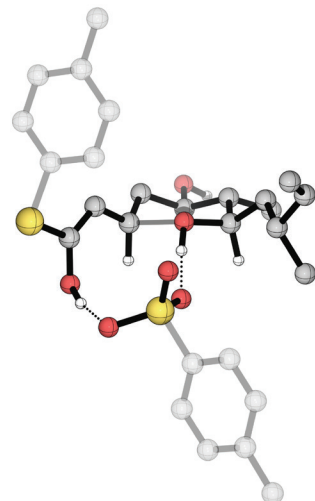
**TS-179**

TS\_chair\_cis

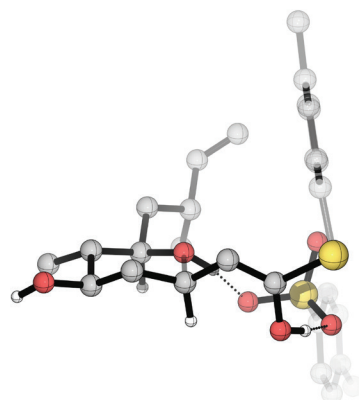
+19.4 kcal mol<sup>-1</sup>



Front:



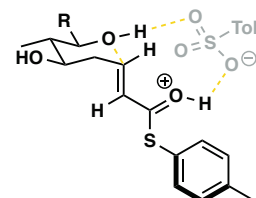
Side:



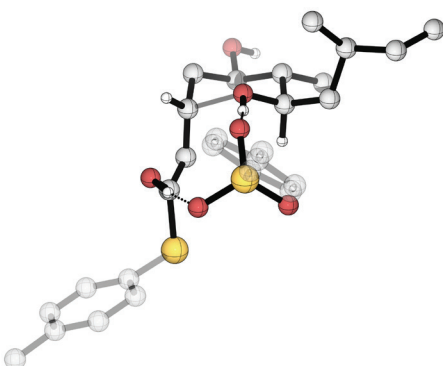
**TS-180**

TS\_chair\_trans

+20.7 kcal mol<sup>-1</sup>



Front:



Side:

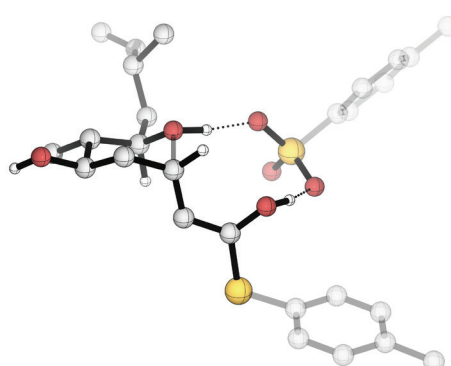


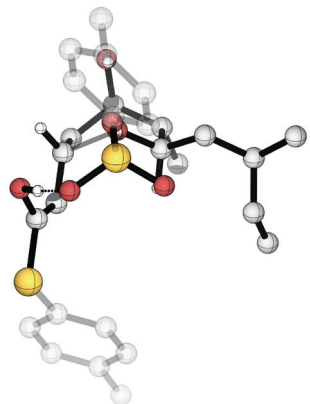
**Figure 3.10:** Chair-like transition states for the *p*-TsOH mediated IOCC. Tolyl rings have been faded and some hydrogens have been omitted for clarity. All energies calculated relative to **174** (DFT-B3LYP/6-31G\*\*+, CH<sub>2</sub>Cl<sub>2</sub>).

**TS-181**

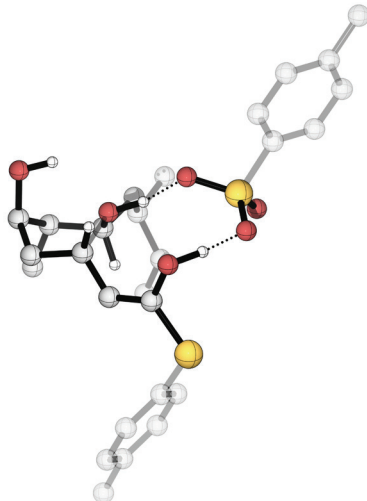
TS\_boat\_trans

+21.9 kcal mol<sup>-1</sup>

Front:



Side:

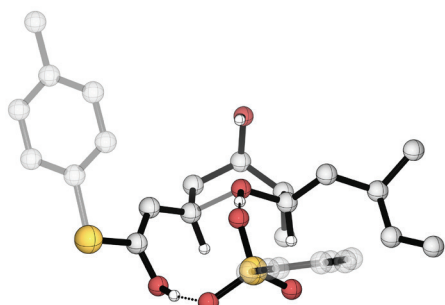


**TS-182**

TS\_boat\_cis

+21.8 kcal mol<sup>-1</sup>

Front:



Side:

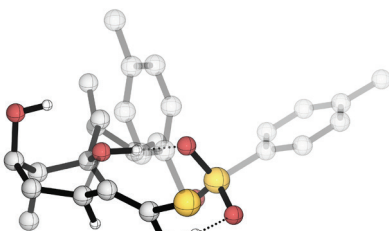
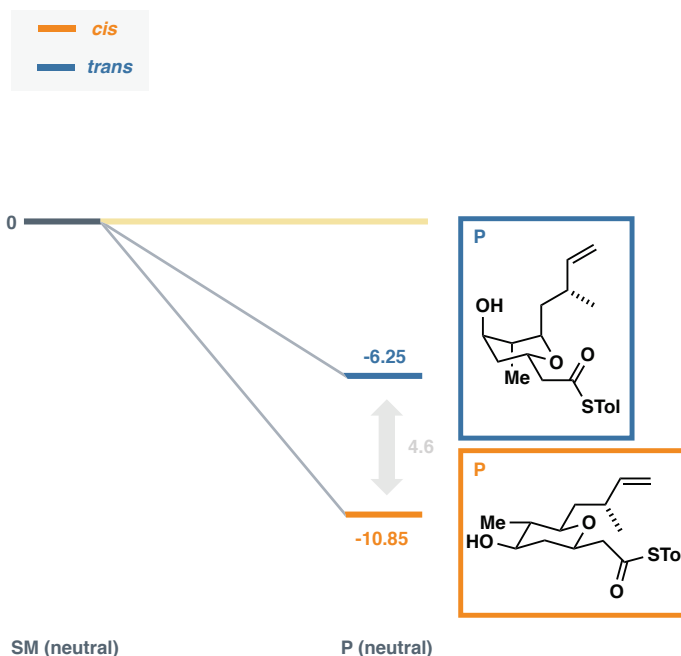


**Figure 3.11:** Boat-like transition states for the *p*-TsOH mediated IOCC. Tolyl rings have been faded and some hydrogens have been omitted for clarity. All energies calculated relative to **174** (DFT-B3LYP/6-31G\*\*+, CH<sub>2</sub>Cl<sub>2</sub>).

**Reaction pathway:**

Thermodynamically, DFT calculations suggest that the 2,6-*cis* diastereomer is 4.6 kcal mol<sup>-1</sup> lower in energy than the 2,6-*trans* diastereomer (**Scheme 3.24**), giving a Boltzmann population of >99% at 298 K. This result is consistent with experiment, in which cyclisation of **107** in the presence of *p*-TsOH affords a single diastereomer by NMR (see §3.3.2.1).\*



**Scheme 3.24:** Energy diagram for the *p*-TsOH mediated IOCC showing the lowest energy pathways to 2,6-*cis* (orange) and 2,6-*trans* (blue) products. All energies relative to the neutral starting material **165**.

This thermodynamic preference for the 2,6-*cis* diastereomer **107** is rationalised by the minimisation of 1,3-diaxial strain across the ring present in the *trans* diastereomer **178**, with three groups forced axial in order to keep the sterically demanding thioester group equatorial (**Figure 3.12**). The same thermodynamic preference is observed computationally for the corresponding methyl ester variant, with a smaller energy gap observed between the chair-like transition states leading to the *cis* and *trans* isomers respectively (3.2 kcal mol<sup>-1</sup> vs 4.6 kcal mol<sup>-1</sup>).

\* The detection limit of NMR spectroscopy is such that the predicted 1% of the *trans* diastereomer would be unable to be detected experimentally.

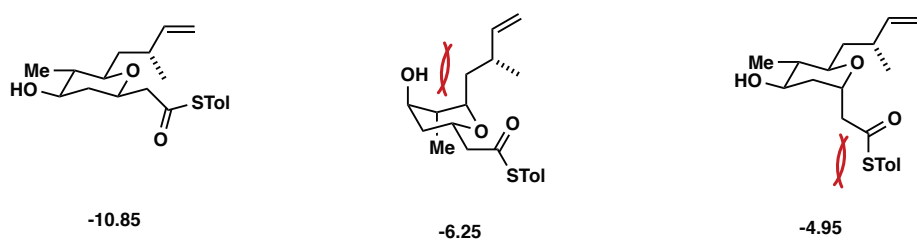


**Figure 3.12:** Ground state structures and energies for the 2,6-*cis* and 2,6-*trans* THPs.

While the 2,6-*cis* diastereomer **107** may be the thermodynamically favoured in this case, this does not explicitly determine that the reaction is under thermodynamic control — this is determined by the barrier to interconversion between the two products and requires consideration of the transition states involved in the cyclisation. Accordingly, plotting the two lowest energy transition states against the protonated starting material and product complexes gives a more complete picture of the reaction pathway (**Figure 3.13**). The reaction pathway below is still consistent with the 2,6-*cis* isomer being the thermodynamic product, however the barrier to the reverse reaction (back to the thienol) is sufficiently high that the rate will be small relative to formation of the THP.

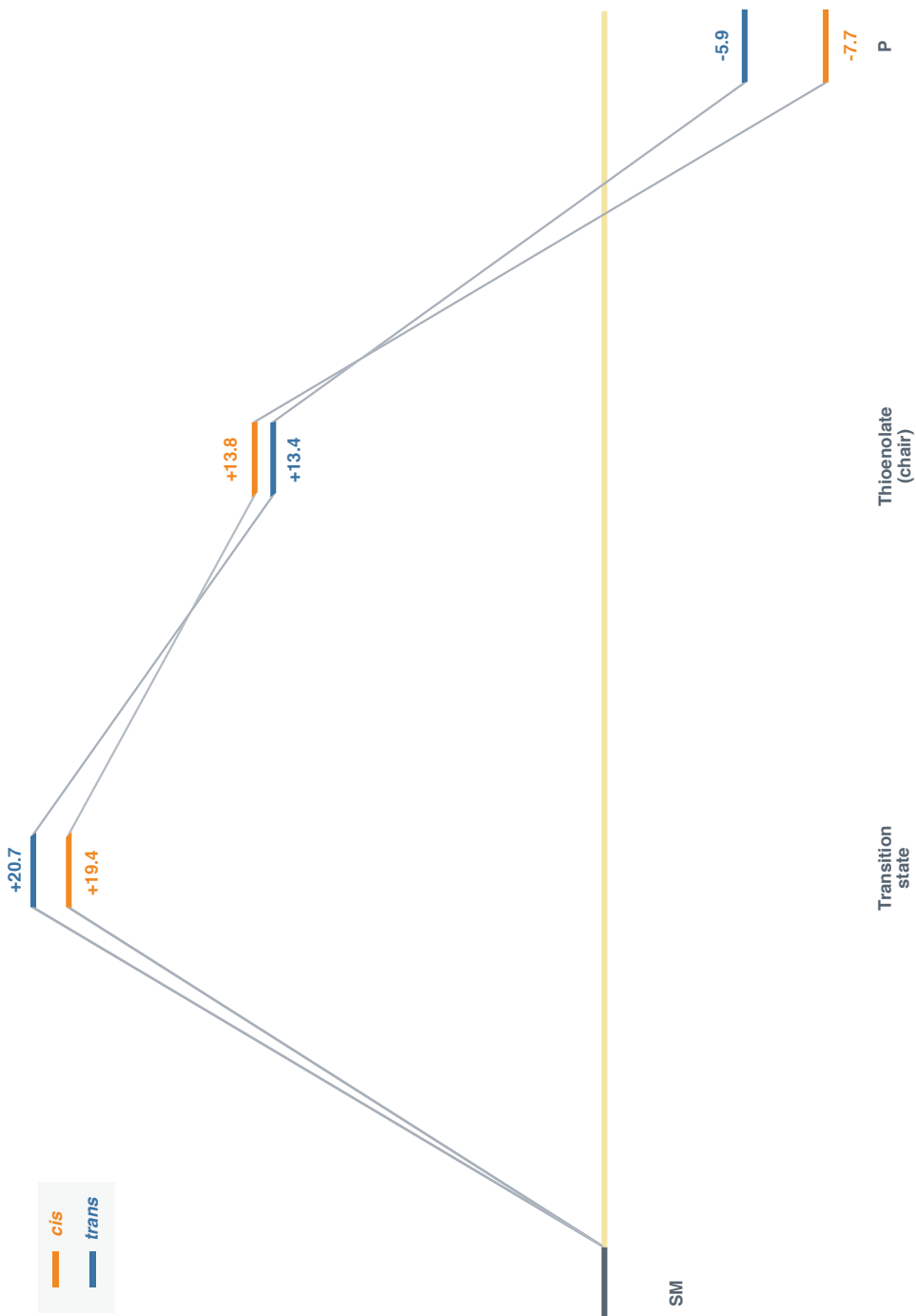


**Figure 3.13:** Energy diagram for the *p*-TsOH mediated IOCC showing the lowest energy pathways to 2,6-*cis* (orange) and 2,6-*trans* (blue) products. All energies relative to **174** (DFT-B3LYP/6-31G\*\*+,  $\text{CH}_2\text{Cl}_2$ ). Note: the transition state for the re-protonation of the thioenolate was not able to be found.

### 3.3.3 COMPLETION OF THE FRAGMENT

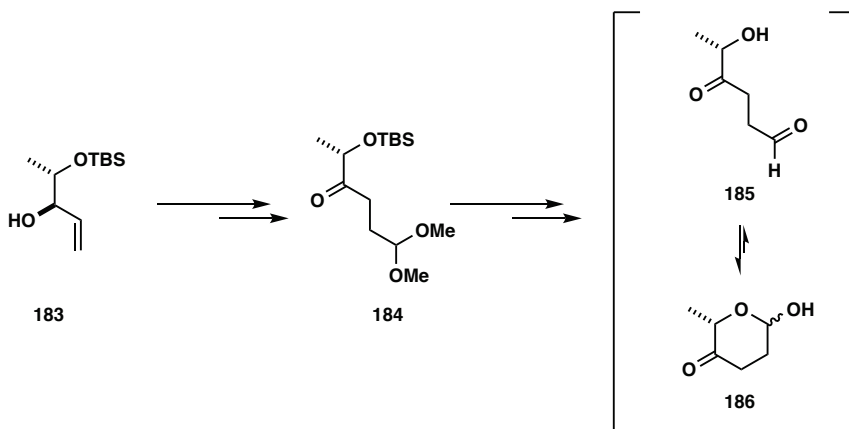
With the C1 – C11 aglycone **107** to hand, all that was required to complete the fragment was glycosylation with the cinerulose donor **42**.

### 3.3.3.1 SYNTHESIS OF THE CINERULOSE DONOR

The L-cinerulose A moiety present in madeirolide A is relatively uncommon, present only in a small number of anthracycline-type natural products such as aclacinomycin A and the ciclamycins.<sup>4</sup> Unlike other carbohydrates, deoxysugars (of which L-cinerulose is an example) are not found abundantly in nature, necessitating the use of synthesis to provide access in meaningful quantities.<sup>96,97</sup>

Previous total syntheses requiring L-cinerulose have accessed the moiety via derivatisation of L-rhamnose or another pre-existing glycoside; while successful, these approaches often require upwards of six steps to obtain a suitably functionalised donor unit, with additional post-glycosylation steps then required to remove unwanted functionality or adjust the oxidation state.<sup>98–100</sup>

A more attractive approach is the de novo synthesis of the sugar, the first asymmetric synthesis of which was reported in 2014 by Schmidt using a chiral-pool approach in which (S)-lactate was used to provide the methyl stereocentre with known absolute configuration (**Scheme 3.25**).<sup>101</sup>



**Scheme 3.25:** Asymmetric synthesis of L-cinerulose (Schmidt).<sup>101</sup>

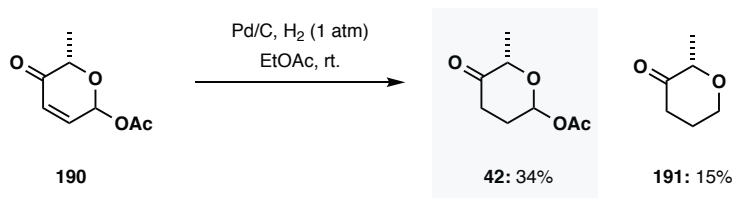
In Haslett's work, the L-cinerulose moiety in madeirolide A was previously accessed via the related 2,3-dehydrocinerulose scaffold **190**; available in three steps from 2-furyl methyl ketone<sup>102</sup> **187** via Noyori asymmetric transfer hydrogenation<sup>103,104</sup> followed by Achmatowitz rearrangement,<sup>105</sup> with subsequent acetylation providing a stable cyclic form of the molecule amenable to glycosylation (**Scheme 3.26**). The epimeric mixture at the anomeric position is inconsequential as it will later be turned into a single anomer (vide infra).



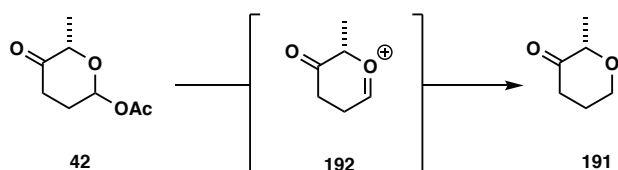
**Reagents & conditions:** [a] Ru(*p*-cymene)(*S,S*-TsDPEN), HCOOH:Et<sub>3</sub>N, rt. [b] NBS, NaHCO<sub>3</sub>, NaOAc, THF:H<sub>2</sub>O, O °C. [c] Ac<sub>2</sub>O, py., DMAP. CH<sub>2</sub>Cl<sub>2</sub>, rt.

**Scheme 3.26:** Synthesis of 2,3-dehydrocinerulose acetate as a precursor to the L-cinerulose moiety present on madeirolide A (**Haslett**).<sup>56</sup>

In the published route,<sup>53</sup> 190 was reduced using catalytic hydrogenation over Pd/C to give 42 in modest yield (34%) with small quantities (15%) of the de-acylated product 191 also isolated. The remaining mass balance was unaccounted for, presumably due to the high volatility of both 191. Although this provided sufficient material for preliminary studies, the yield was low and the reaction found to be capricious, often leading to degradation rather than the desired product. One possible explanation to this lies in the inherent acidity of the catalyst, leading to formation of an oxonium ion that subsequently gets reduced (**Scheme 3.28**).



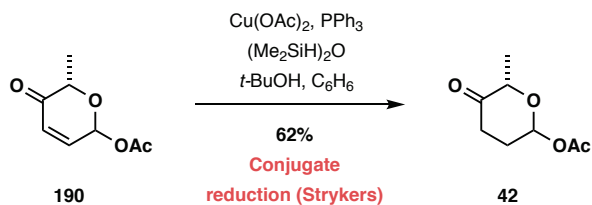
**Scheme 3.27:** Pd/C catalysed hydrogenation of 2,3-dihydrocinerulose derivative 190 (**Haslett**).



**Scheme 3.28:** Mechanistic rationale for the isolation of the deacylated product 191.

Given the poor yield of catalytic hydrogenation, an alternative tactic was explored for chemoselective reduction of the enone. The Stryker reagent, [(PPh<sub>3</sub>)CuH]<sub>6</sub>,<sup>106</sup> acts as a soft hydride source resulting in conjugate reduction of enones to the corresponding ketones with excellent chemoselectivity.<sup>107</sup> Unfortunately, the original Stryker reagent is highly air sensitive and requires storage and manipulation inside a glovebox.<sup>106,108</sup> These deficiencies, coupled with a desire to carry out the reaction catalytically, have led to the development of operationally easier copper hydride reductions.<sup>109–113</sup> Many of these alternatives allow the [Cu]-H species to be prepared *in situ* and used catalytically as a solution, avoiding the issues encountered with the original methodology.

The Yun protocol<sup>111,112</sup> generates a solution of the Stryker reagent from copper (II) acetate and triphenyl phosphine, using Ph<sub>2</sub>SiH<sub>2</sub> as the stoichiometric reductant.\* Treatment of **190** with this solution gave moderate yields (50 – 60%) of the desired saturated ketone **42**, with none of the over-reduction product **191** observed, more importantly, this reaction was highly reproducible (**Scheme 3.29**). The use of benzene (in place of the toluene used in the literature) was found to be critical as it enabled the solvent to be removed in vacuo without significant loss of **42**.

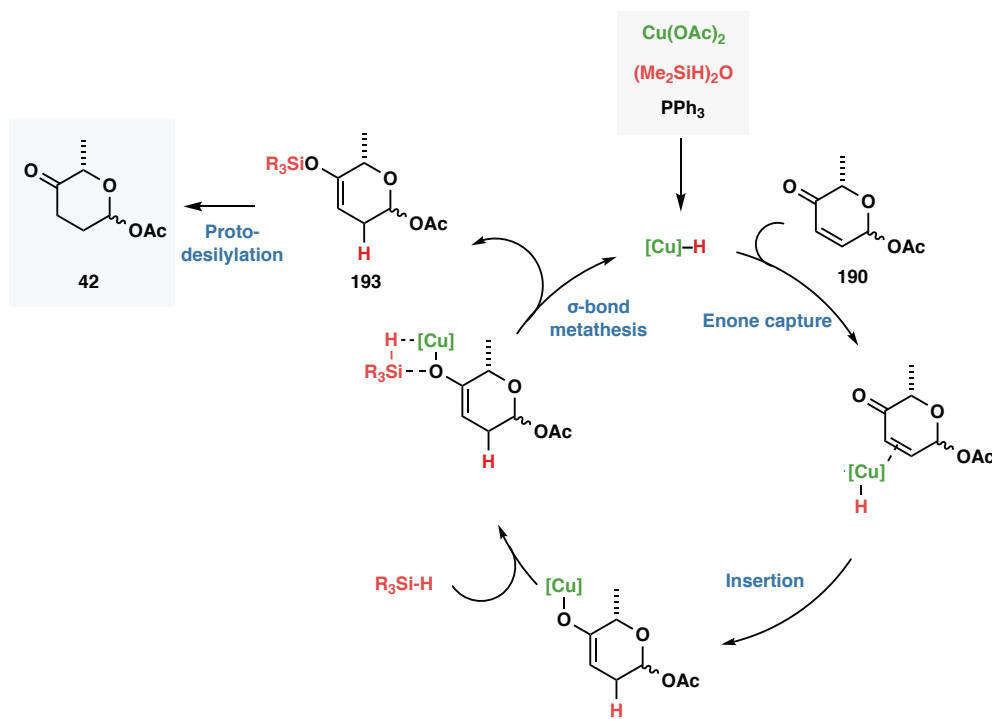


**Scheme 3.29:** Conjugate reduction of enone using a copper hydride reagent.

Detailed mechanistic studies of this copper (I) hydride reduction have not yet been reported, however several proposals have been made based on the known mechanism of the original stoichiometric Stryker reduction. Initially, coordination of [Cu]-H to the enone and hydride insertion generates a copper enolate which undergoes metathesis to the silane, converting the copper enolate into a silyl enol ether with concomitant regeneration of the [Cu]-H species, which renders the process catalytic in [Cu], with the silane acting as the stoichiometric reducing agent. In the absence of a proton source (*t*-BuOH), the silyl enol ether **193** can be isolated, which provides some mechanistic support for the proposed mechanistic pathway.

\* The solution is unable to be characterised, however evaporation in vacuo affords a red solid, the <sup>1</sup>H NMR of which matches that of the true Stryker reagent.

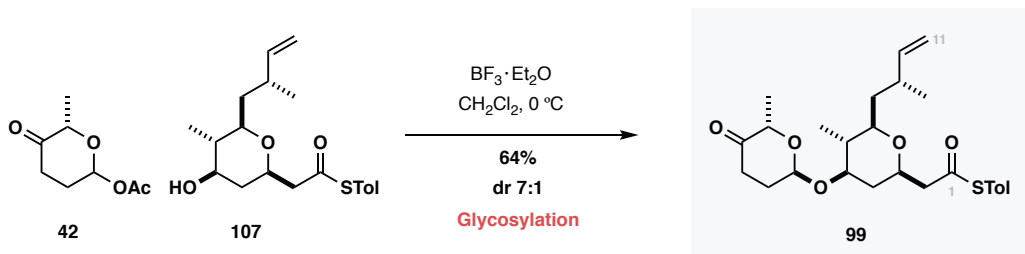
Results & discussion I: synthesis of a modified western fragment



**Scheme 3.30:** Proposed mechanistic pathway for copper hydride reduction of enones using  $(\text{Me}_2\text{SiH})_2\text{O}$  as the terminal source of hydride (**Oestreich**).<sup>113</sup>

### 3.3.3.2 GLYCOSYLATION

To complete the modified C1 – C11 western fragment **99**, all that remained was the glycosylation of **107** with cinerulose donor **42**. Thus, treatment of a mixture of **107** and **42** with  $\text{BF}_3 \cdot \text{Et}_2\text{O}$  in dry  $\text{CH}_2\text{Cl}_2$  afforded the **99** in 64% yield as a separable 7:1 mixture of anomers in favour of the axially substituted cinerulose moiety (**Scheme 3.31**).



**Scheme 3.31:** Glycosylation of aglycone **107** to provide access to the complete modified C1 – C11 fragment **99**.

Gratifyingly, detailed NMR comparison against natural madeirolide A shows excellent agreement with the synthetic fragment **99** (**Figure 3.14** and **Table 3.2**). The large errors at C10 and C11 are consistent with the terminal olefin not representing the diene present in the natural product, and consistent with those previously observed by Haslett.<sup>56</sup>

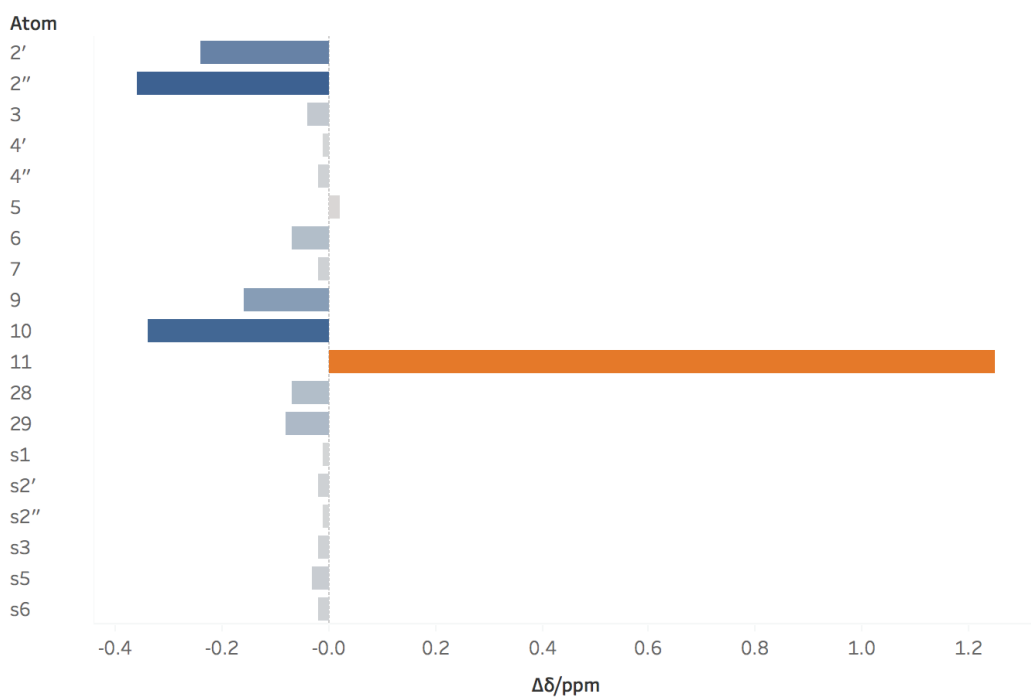


**Figure 3.14:**  $^1\text{H}$  NMR comparison of the C1 – C11 fragment **99** with natural madeirolide A.

### 3.3.4 SUMMARY AND ANALYSIS

The work described in this chapter has culminated in the synthesis of a modified C1 – C11 fragment of madeirolide A in 13 steps from PMB protected Roche ester. The key goals outlined at the beginning of this chapter have been met successfully. Namely, the issue of the protecting group shuffling and challenging vinyl iodide have been solved based on a modified fragment union strategy in which a macro-Heck cyclisation is envisioned to replace the previously anticipated macro-Stille cross-coupling. Through this modified route, around 50 mg of the C1 – C11 fragment **99** have been accessed. Additionally, the IOCC used to forge the western THP has been studied computationally. This computational study was able to successfully rationalise the formation of the observed 2,6-*cis* THP based on a chair-like transition state.

Results & discussion I: synthesis of a modified western fragment

**Table 3.2:** NMR data for madeirolide A and the C1 – C11 fragment **99**.

	Natural madeirolide A				Synthetic C1 – C11 fragment			
	<sup>13</sup> C [ppm]	<sup>1</sup> H [ppm]	mult	J [Hz]	<sup>13</sup> C [ppm]	<sup>1</sup> H [ppm]	mult	J [Hz]
1	170.9	-	-	-	195.9	-	-	-
2'	41.6	2.45	m	-	49.9	2.67	dd	14.6, 4.7
2"		2.58	m	-		2.92	dd	14.6, 8.3
3	74.2	3.80	m	-	72.4	3.82	m	-
4'	36.2	1.26	m	-	36.4	1.23	m	-
4"		2.14	m	-		2.14	ddd	12.1, 4.5, 1.9
5	75.9	3.56	td	10, 4	76.0	3.52	td	10.6, 4.6
6	42.9	1.32	m	-	42.1	1.37	ddq	9.8, 6.4, 3.4
7	77.9	3.07	td	78.9	78.9	3.08	td	9.9, 2.9
8'	40.5	1.44	m	40.0	40.0	1.52	m	-
8"						1.46	dd	10.3, 3.0
9	34.3	2.37	m	-	33.3	2.51	m	-
10	142.3	5.48	dd	15, 10	145.4	5.80	ddd	17.2, 10.4, 6.8
11'	122.8	6.24	dd	15, 11	112.0	4.97	dd	17.3, 1.6
11"						4.88	dd	10.4, 1.5
28	13.0	0.90	d	7	13.3	0.91	d	6.5
29	18.0	0.85	d	7	18.4	0.94	d	6.7
32	92.6	5.15	t	6	92.6	5.15	t	5.4
33'	28.8	1.93	m	-	28.9	1.93	ddt	14.8, 9.5, 5.6
33"		2.28	m	-		2.36	m	-
34	33.8	2.46	m	-	33.8	2.45	m	-
35	211.0	-	-	-	211.2	-	-	-
36	71.5	4.26	q	7	71.3	4.27	q	6.7
37	15.0	1.26	d	7	15.1	1.27	d	6.8

Results & discussion I: synthesis of a modified western fragment

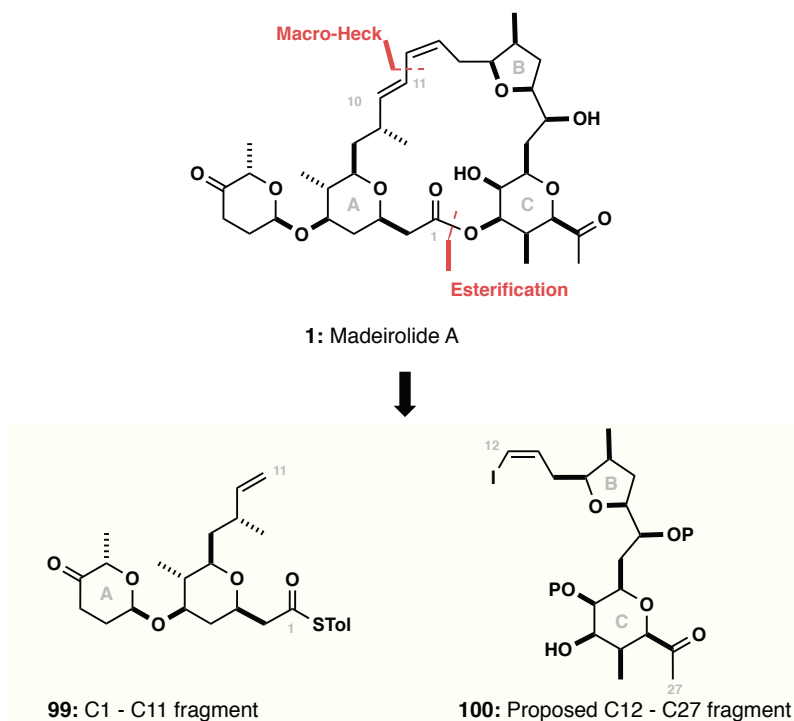


# 4

## 4. RESULTS & DISCUSSION II: INVESTIGATIONS INTO THE EASTERN TETRAHYDROFURAN

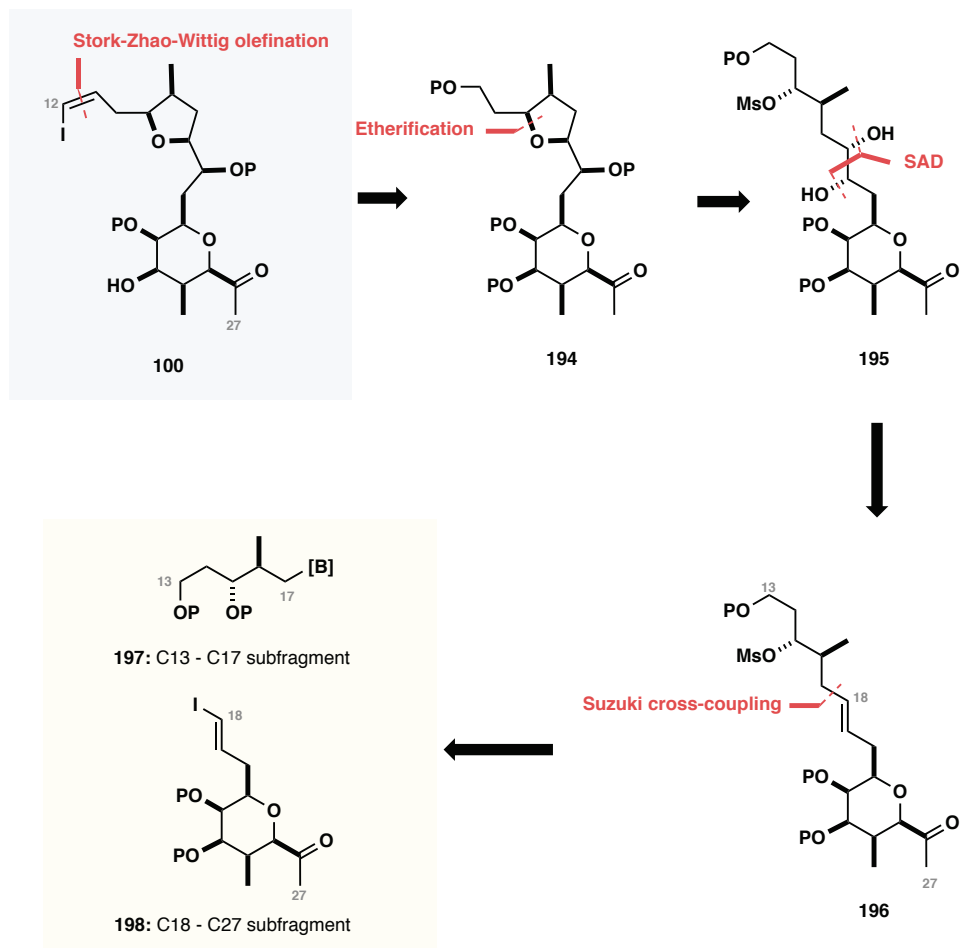
### 4.1 SYNTHETIC STRATEGY FOR THE EASTERN FRAGMENT

The proposed C12 – C27 **100** fragment of madeirolide A is highly functionalised containing nine stereocentres (five of which are contiguous), and two saturated oxygen heterocycles, including the synthetically challenging all-*cis* C21 – C25 THP. In accordance with the modified macrocyclisation strategy (see §3.1), the previously anticipated C12 (*Z*)-vinyl stannane was replaced with the corresponding (*Z*)-vinyl iodide (**Scheme 4.1**).



**Scheme 4.1:** Modified fragment union strategy showing the proposed C12 – C27 eastern fragment **100** of madeirolide A.

The overall approach to the synthesis of the modified C12 – C27 eastern fragment **100** is outlined retrosynthetically in **Scheme 4.2**. Initial simplification reveals **194**, with the THF formed through a cycloetherification of **195**. Key to this strategy was the recognition that the diol could be disconnected to alkene **196**, which provided a point of scission; thus, in a forward sense the C17 – C18 bond would be formed through an  $sp^2$  –  $sp^3$  Suzuki cross-coupling between organoborane **197** and vinyl iodide **198**. This disconnection between C17 and C18 was critical since logically, it was desirable to separate the two heterocycles; this not only provided greater convergence to the route, but also permitted synthetic work to be conducted in parallel which was necessary owing to the anticipated challenges in effecting ring closure of the THP.

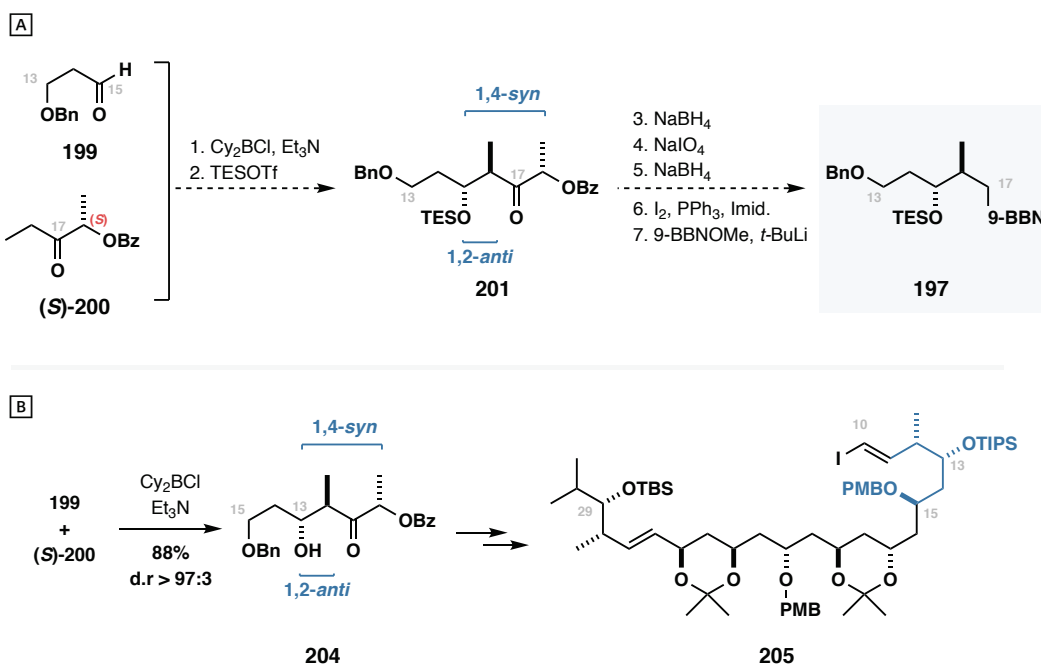


**Scheme 4.2:** Retrosynthetic strategy for construction of the C12 – C27 eastern fragment of madeirolide A.

## 4.2 SYNTHESIS OF THE C13 – C17 FRAGMENT

### 4.2.1 RETROSYNTHESIS

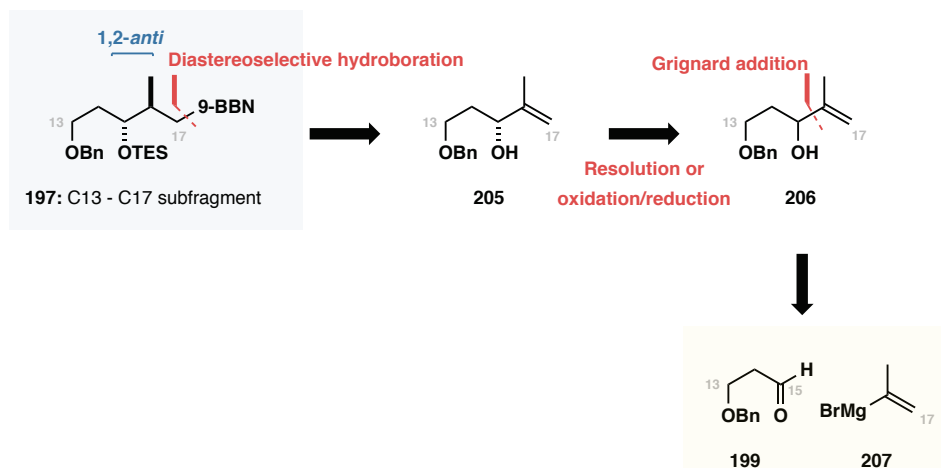
Haslett originally anticipated the C13 – C17 fragment **197** of madeirolide A to be synthesised in nine steps from (–)-ethyl-L-lactate (**Scheme 4.3**).<sup>56</sup> Central to the strategy was the use of a Cy<sub>2</sub>BCl mediated lactate aldol reaction between aldehyde **199** and ethyl ketone **(S)-200** to forge the C15 – C16 bond with concomitant installation of the required 1,2-*anti* relationship. This aldol reaction is well precedented, as illustrated in the Paterson synthesis of the C10 – C29 fragment **205** of (+)-roxaticin.<sup>114</sup> Although the lactate aldol approach would provide the desired stereochemistry, the cleavage of the auxiliary and subsequent elaboration into organoborane **197** requires a significant number of steps, the majority of which are redox manipulations. As no synthetic work had been carried out on this fragment proposed by Haslett, an alternative approach was therefore proposed, obviating the need for an auxiliary altogether.



**Scheme 4.3:** **[A]** Proposed synthesis of the C13 – C17 fragment **197** using a lactate aldol as the key step to set the necessary stereochemistry (**Haslett**). **[B]** Literature precedence for the selectivity of the proposed aldol, as used in the context of (+)-roxaticin (**Paterson**).<sup>114</sup>

The revised route to the C13 – C17 fragment **197** is shown retrosynthetically in **Scheme 4.4**. It was reasoned that the 1,2-*anti* relationship could be installed at a late stage through a diastereoselective hydroboration of alkene **206**, taking advantage of the proximal C15

stereocentre to bias formation of the desired diastereomer. Thus, retrosynthetic simplification of **205** in the manner illustrated reveals **206**, accessed via the readily available aldehyde **199** and prop-1-en-2-ylmagnesium bromide **207**, itself derived from commercially available 2-bromopropene.



**Scheme 4.4:** Retrosynthesis of the C13 – C17 fragment **197** using a diastereoselective hydroboration to set the key 1,2-*anti* relationship between C15 and C16.

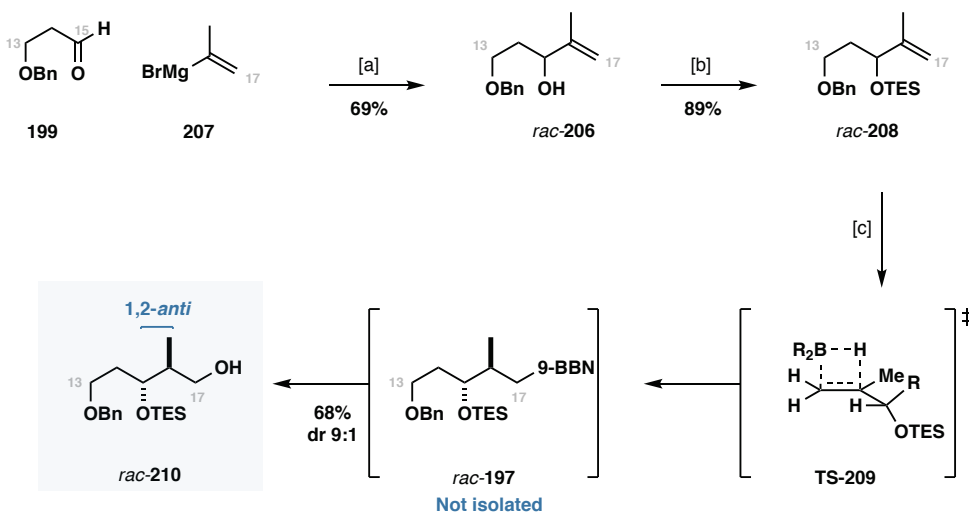
#### 4.2.2 RACEMIC MODEL STUDIES

*The racemic model studies described in this section were carried out by James Thompson, a BP funded summer student. All experiments were designed by the author, and results are provided here for completeness.*

Initial studies into the proposed hydroboration/Suzuki cross-coupling approach were carried out on a racemic model system. This allowed investigation of the hydroboration reaction and subsequent Suzuki cross-coupling reaction without the need to first prepare **205** as a single enantiomer, which was anticipated to be a straightforward task given the wide range of methods available for accessing enantiomerically pure secondary alcohols.

Accordingly, addition of prop-1-en-2-ylmagnesium bromide to **199**\* followed by protection as the corresponding TES ether (TESCl, imidazole) afforded *rac*-**208** setting the stage for the projected hydroboration (**Scheme 4.5**). In the event, treatment of **208** with 9-BBN in THF at -78 °C, followed by oxidative workup (H<sub>2</sub>O<sub>2</sub>, MeOH) gave *rac*-**210** in 68% yield as an inseparable 9:1 mixture of diastereomers in favour of the desired 1,2-*anti* product as expected from prior work by Still.<sup>115</sup>

\* A supply of aldehyde **199** was available within the Paterson group and was prepared by Ms Nadia Petersen following standard literature procedures.



**Reagents and conditions:** [a] THF, -78 °C. [b] TESOTf, 2,6-lutidine, THF, 0 °C. [c] 9-BBN, THF, -78 °C; H<sub>2</sub>O<sub>2</sub>, MeOH, pH 7 buffer.

**Scheme 4.5:** Synthesis of the *rac*-210 to test the diastereoselectivity of the proposed hydroboration (Thompson).<sup>116</sup>

The observed diastereoselectivity can be rationalised by analysis of the conformational preferences of the olefin, which bears a chiral centre in the allylic position (**Figure 4.1**). To minimise A<sup>1,3</sup> strain, the substrate is likely to adopt a reactive conformation in which the allylic proton eclipses the alkene.<sup>117</sup> In this conformation, the two diastereotopic faces of the alkene are differentiated, with hydroboration taking place on the less hindered face away from the sterically demanding TES ether. The lowest energy conformation of alkene **208** is shown in **Figure 4.1 B**, demonstrating the ability to differentiate between the two diastereotopic faces of the alkene.

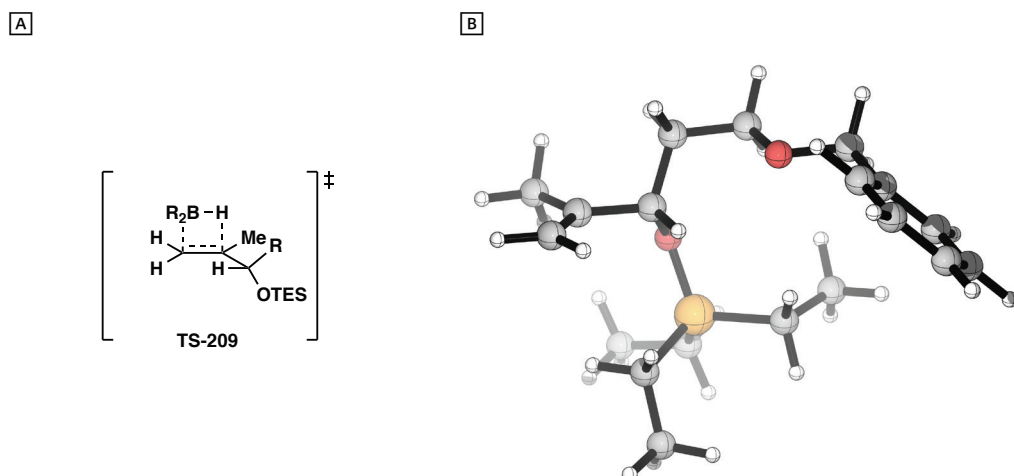
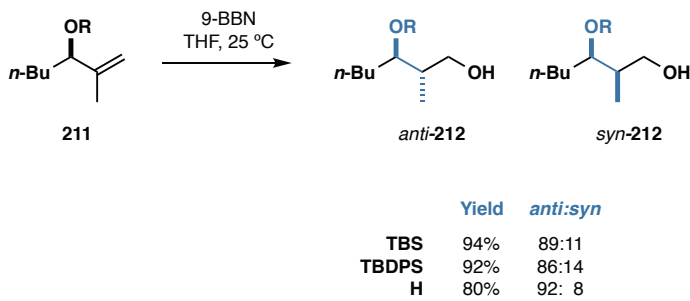


**Figure 4.1:** Rationalisation of 1,2-*anti* diastereoselectivity during hydroboration. **A**: Putative transition state for the reaction. **B**: Lowest energy conformation of **208** showing the TES ether shielding the lower face of the terminal alkene (DFT-B3LYP/6-31G\*\*, gas-phase).

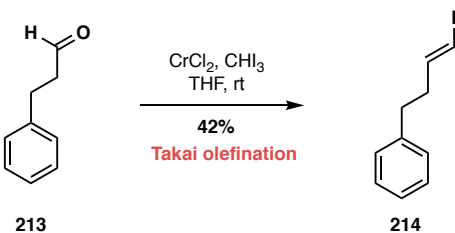
While the steric-driven ‘reactive conformer’ model described above adequately predicts the major diastereomer, it is incompatible with many experimental observations, leading to the suggestion that there is a stereoelectronic component involved in determining diastereoselectivity.<sup>118,119</sup> Evans<sup>120</sup> and Still<sup>115</sup> have independently reported significant protecting group effects when studying the hydroboration of terminal olefins using 9-BBN. When comparing the hydroboration of a terminal allylic alcohol protected with a series of silyl ethers (-TMS, -TBS, -TBDPS), selectivity was found to decrease as the protecting group got larger, contrary to the expected outcome based on minimisation of A<sup>1,3</sup> strain alone.



**Scheme 4.6:** Studies into the diastereoselectivity of uncatalysed hydroborations using 9-BBN (Evans).<sup>120</sup>

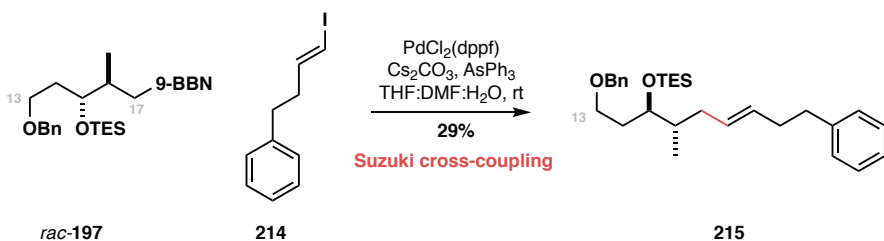
With the stereochemistry of the hydroboration confirmed, attention was turned to the proposed sp<sup>2</sup> - sp<sup>3</sup> Suzuki cross-coupling reaction that would be used to forge the C17 - C18 bond of madeirolide A (**Scheme 4.2**). While many examples of such a reaction exist in the literature, including in the synthesis of complex natural products,<sup>121</sup> the hydroboration/cross-coupling sequence was anticipated to be challenging,<sup>122</sup> as sp<sup>3</sup> alkyl boranes are known to undergo slow transmetallation, often leading to significant amounts of the protodeboronation product being formed, thus requiring super-stoichiometric amounts of the organoborane coupling partner to achieve good yields.<sup>123</sup>

Given that work was on-going into the synthesis of the C18 – C27 fragment **128**, a model vinyl iodide **214** was prepared (**Scheme 4.7**). The choice of vinyl iodide was not important since the challenging aspect of the sp<sup>2</sup> - sp<sup>3</sup> cross-coupling reaction is known to be with the sp<sup>3</sup> organoborane rather than the sp<sup>2</sup> halide. Thus, Takai olefination (CrCl<sub>2</sub>, CHI<sub>3</sub>) of hydrocinnamaldehyde **213** afforded **214** in a modest 42% yield with the desired (E)-isomer being the major product.



**Scheme 4.7:** Preparation of a model (*E*)-vinyl iodide used to investigated the proposed  $\text{sp}^2 - \text{sp}^3$  Suzuki cross-coupling reaction (**Thompson**).<sup>116</sup>

Initial attempts at effecting the convergent union of **214** and *rac*-**197** were met with disappointment, failing to return the desired product and leading to significant amounts of protodeboronation. Screening of a range of conditions eventually identified Braun's conditions ( $\text{PdCl}_2(\text{dppf})$ ,  $\text{Cs}_2\text{CO}_3$ ,  $\text{AsPh}_3$ ,  $\text{DMF}/\text{THF}/\text{H}_2\text{O}$ ) to provide modest yields of the desired coupling product **215** when using a two-equivalent excess of the organoborane (**Scheme 4.8**).



**Scheme 4.8:** Successful  $\text{sp}^2 - \text{sp}^3$  Suzuki cross coupling between vinyl iodide **214** and organoborane *rac*-**197** (**Thompson**).

Ideally, this reaction would proceed to full conversion, however the ability to recover the vinyl iodide starting material meant that there was no net loss of what would, in the real system, be the 'valuable' component. Given the known difficulties with  $\text{sp}^2 - \text{sp}^3$  cross-couplings using organoboranes, it may well be the case that in future studies it would be prudent to make use of a more stable boron derivative, such as a MIDA boronate, which allows the reactive species to be released slowly over the course of the cross-coupling reaction, preventing loss to protodeborylation. This will be investigated further in due course, with future directions discussed in Chapter 6.

#### 4.2.3 ENANTIOSELECTIVE SYNTHESIS THE C13 – C17 ALCOHOL

For the planned synthesis of madeirolide A, **197** would be required as a single enantiomer. A particularly attractive strategy for this was the kinetic resolution of allylic alcohol *rac*-**206** using a Sharpless asymmetric epoxidation.<sup>124</sup> Treatment of a racemic allylic alcohol with  $\text{Ti}(\text{O}-\text{i-Pr})_4/(+)$ -DET sets up two diastereomeric transition states (**Figure 5.3**). The presence of the chiral centre leads to a matched and a mismatched case: the transition states have differing

energies resulting in one enantiomer of the allylic alcohol undergoing rapid epoxidation, leaving behind the other enantiomer which is theoretically returned with complete enantioenrichment.

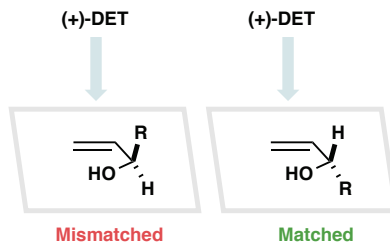
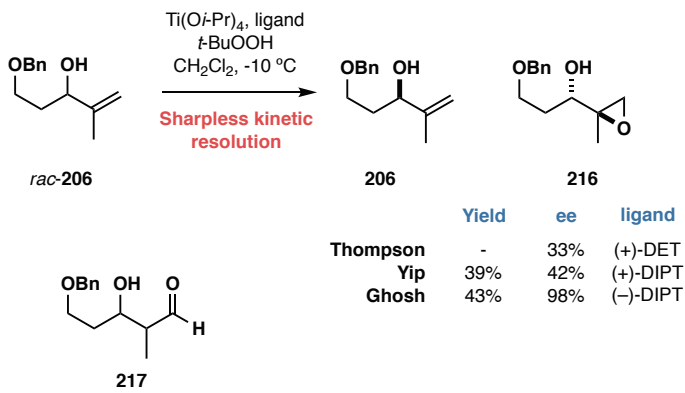


**Figure 4.2:** Schematic representation of a kinetic resolution using a Sharpless asymmetric epoxidation.

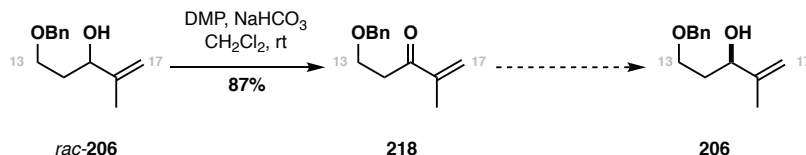
The Sharpless kinetic resolution of *rac*-**206** has been used by Ghosh and co-workers in their synthesis of (–)-lasonolide A, obtaining *ent*-**206** with excellent enantioselectivity using (–)-DIPT (**Scheme 4.9**).<sup>125</sup> Despite this precedence, significant attempts at optimisation by Thompson failed to provide access to material with an ee > 33%.<sup>\*</sup> In the authors hands, the ee was able to be increased to 42%, however this was not considered synthetically useful. Notably, Thompson also observed the formation of a by-product, proposed to be aldehyde **217** which could arise from Lewis acid catalysed opening of the epoxide and subsequent hydride shift.



**Scheme 4.9:** Kinetic resolution of racemic allylic alcohol **206** using a Sharpless asymmetric epoxidation. Note that Ghosh carried out the synthesis using (+)-DIPT and thus obtained the enantiomeric products.

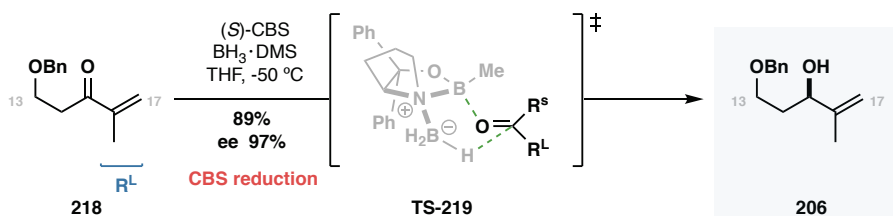
To quickly access enantioenriched alcohol **206**, the kinetic resolution attempted by Thompson was abandoned in favour of a more traditional oxidation/reduction sequence. Accordingly, *rac*-**206** was oxidised using the Dess-Martin periodinane to provide ketone **218** in 82% yield (**Scheme 4.10**).

\* Enantiomeric excess was determined by <sup>19</sup>F NMR of the corresponding MTPA esters.



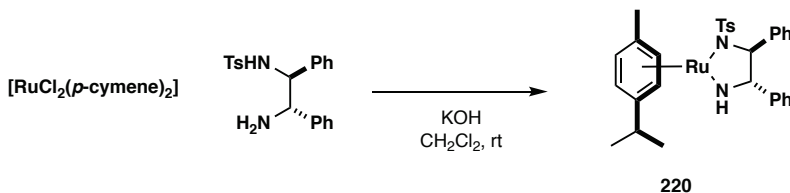
**Scheme 4.10:** Oxidation of *rac*-206 and proposed asymmetric reduction.

One of the most common asymmetric reduction methods is the Corey-Bakishi-Shibata reaction, which uses chiral B-substituted oxazaborolidines to distinguish the enantiotopic faces of a prochiral ketone.<sup>126</sup> Accordingly, treatment of ketone **218** with the (S)-CBS catalyst in the presence of  $\text{BH}_3 \cdot \text{DMS}$  as the terminal source of hydride provided allylic alcohol **206** in 89% yield and 97% ee (**Scheme 4.11**).<sup>\*</sup> The selectivity of the reaction is rationalised through cyclic transition state **TS-219** in which the large group on the ketone orients itself away from the methyl group on boron to avoid an unfavourable steric interaction.



**Scheme 4.11:** CBS reduction of ketone **218** to provide access to enantiomerically enriched allylic alcohol **206**.

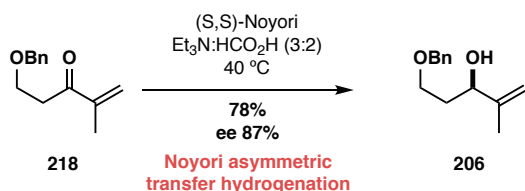
In tandem with the CBS reduction, an alternative transfer hydrogenation approach was investigated using the Noyori Ru(*p*-cymene)TsDPEN catalyst system.<sup>103,104</sup> The Noyori reduction has the advantage of not requiring low temperatures to be maintained, and the exceptionally low catalyst loadings (often <1%) allow for large quantities of ketone to be carried through the reaction. Although the catalyst is commercially available, it is most conveniently prepared from [RuCl<sub>2</sub>(*p*-cymene)<sub>2</sub>] by treatment with (1*S*, 2*S*)-TsDPEN in the presence of KOH (**Scheme 4.12**).<sup>127</sup> Once formed, the bright-purple catalyst is able to be stored at room temperature on the bench without appreciable decomposition.



**Scheme 4.12:** Preparation of (*S,S*)-Ru(*p*-cymene)TsDPEN for use in a Noyori asymmetric transfer hydrogenation.

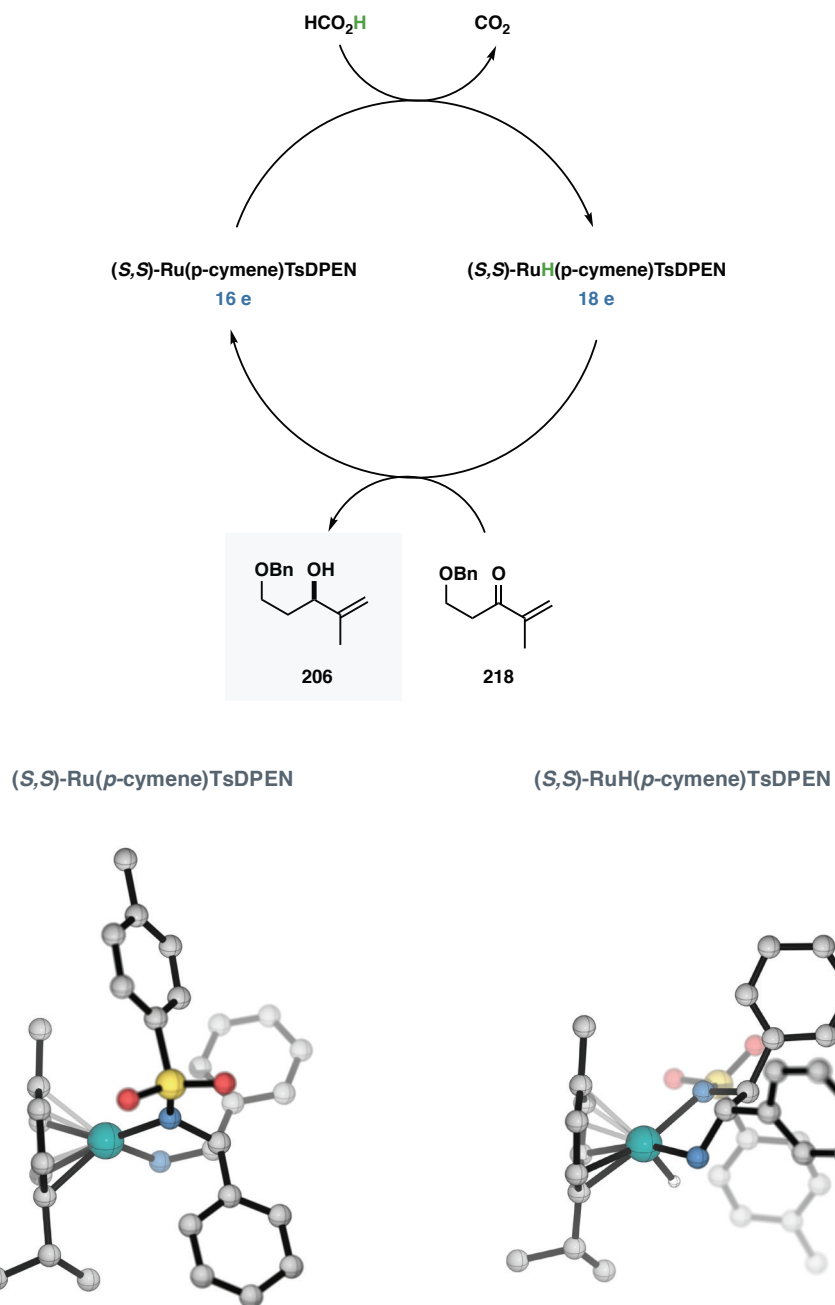
\* Enantiomeric excess was determined by chiral HPLC (Chiraldpak-IA®, 20% *i*-PrOH:*n*-hexane).

Treatment of ketone **218** with 1 mol% catalyst **220** in a mixture of triethylamine and formic acid at 40 °C provided allylic alcohol **206** in 78% yield, albeit with a reduced enantiomeric excess of 87% (**Scheme 4.13**). Attempts at optimisation (lowering temperature or catalyst loading) failed to provide any enhancements to the enantioselectivity, as such this route was abandoned in favour of the successful CBS reduction route.



**Scheme 4.13:** Noyori asymmetric transfer hydrogenation of ketone **218** to provide access to enantiomerically enriched allylic alcohol **206**.

The accepted catalytic cycle for the asymmetric transfer hydrogenation of ketones was first proposed by Noyori, and has since been validated through a combination of computational studies and the characterisation of the active ruthenium species via x-ray crystallography (**Scheme 4.14**).<sup>128,129</sup> Mechanistically, the coordinatively unsaturated 16-electron ruthenium species is first reduced by formic acid to generate the catalytically active 18-electron ruthenium hydride species. The ketone is then reduced by this species via a putative six-membered pericyclic step in which the hydride from Ru-H is delivered with simultaneous protonation of the oxygen using the protic N-H bond, thus regenerating the 16-electron ruthenium species with concomitant formation of the desired enantioenriched alcohol.



**Scheme 4.14:** Proposed catalytic cycle of the Noyori transfer hydrogenation using a  $\text{Ru}(p\text{-cymene})\text{TsDPEN}$  catalyst. Crystal structures of the proposed intermediates shown below, some hydrogens have been omitted for clarity (Noyori).<sup>130</sup>

The origin of enantioselectivity in the Noyori transfer hydrogenation is not well understood despite extensive mechanistic and computational studies. Central to the issue is the fact that the proposed model (Figure 4.3) is unable to unify the experimental evidence for the reduction of both ketones and imines, which give opposite facial selectivity when using the same catalyst. Most widely studied are aromatic ketones, where Noyori has proposed a non-

covalent interaction between the aryl group and the aromatic group bound to the ketone, as is evident from the favoured transition state **TS-221**.

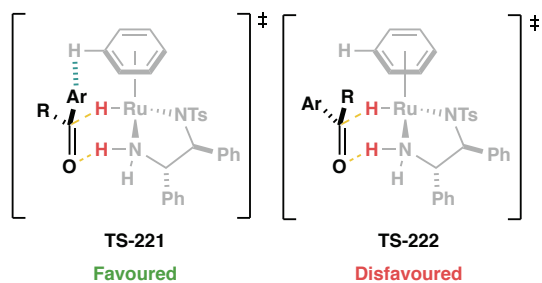


**Figure 4.3:** Proposed transition states for the Noyori transfer hydrogenation of aromatic ketones (ArCOR) using Ru(phenyl)TsDPEN catalyst (**Noyori**).

#### 4.2.4 SUMMARY AND ANALYSIS

The investigation of the C13 – C17 fragment described in this chapter achieved its intended goals. Firstly, the use of a hydroboration to generate an  $sp^3$  borane with concomitant introduction of the necessary 1,2-*anti* diastereoselectivity has been validated, precluding the need for a lactate auxiliary based approach which would require additional redox and functional group manipulations to arrive at a suitably functionalised intermediate.

The organoborane **197** was also used to affect the desired  $sp^2$  –  $sp^3$  Suzuki cross-coupling reaction using a model vinyl iodide **214**. Despite the modest 29% yield, the result acts as a ‘proof of concept’ that the coupling is possible in this context, and, given the many catalysts, ligands, and boron derivatives developed in recent years, it will undoubtedly be possible to find a suitable combination that procures access to the cross-coupling product **196** in synthetically acceptable yields.

Overall, over 5 g of homochiral allylic alcohol **206** is available for further studies, making use of a CBS reduction to install the C15 stereocentre with reliable yield and enantioselectivity. Given the highly oxygenated nature of the C12 – C27 fragment of madeirolide A, and on-going difficulties in accessing the eastern THP, alcohol **206** has not yet been elaborated to the anticipated TES ether owing to the likelihood that a change in protecting group strategy will be required.

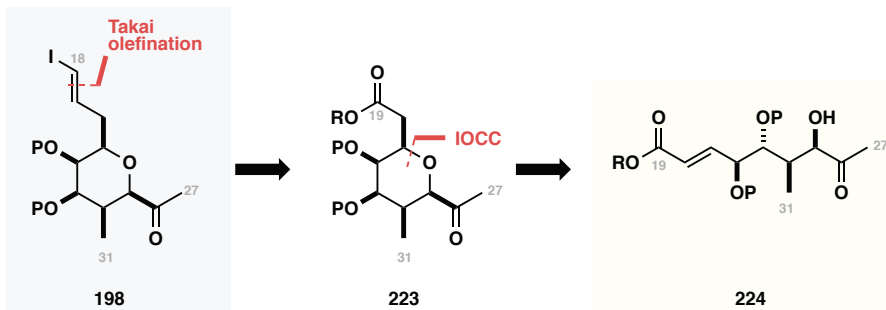
# 5

## 5.RESULTS & DISCUSSION III: SYNTHESIS OF THE EASTERN TETRAHYDROPYRAN

### 5.1 GENERAL SYNTHETIC STRATEGY

The construction of the eastern THP was anticipated to be a significant obstacle to realising a successful total synthesis of madeirolide A. Previous synthetic studies by Hasleett<sup>56</sup> and Fearnley<sup>61</sup> failed to procure access to the required heterocycle, despite the successful preparing several advanced precursors (see §2.3.1.1).

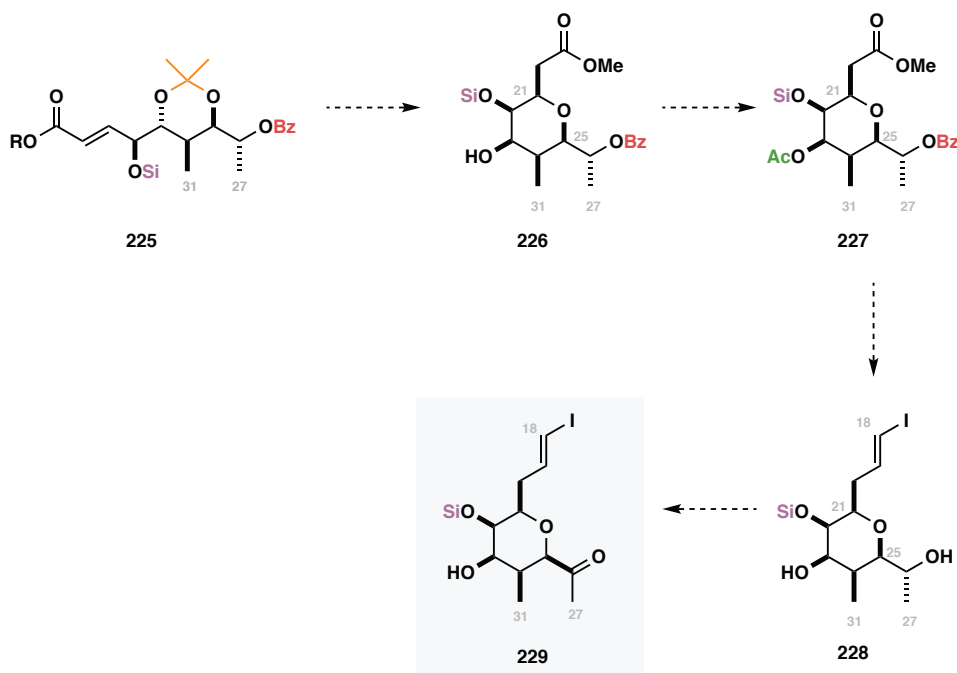
As a means of assembling highly-substituted THPs, the intramolecular oxy-conjugate cyclisation (IOCC) is unmatched in terms of versatility, with numerous examples in complex molecule synthesis making it an encouraging strategy for construction of the pentasubstituted all-*cis* eastern THP.<sup>83,131,132</sup> The proposed application of an IOCC to the synthesis of the C18 – C27 fragment **198** is shown in **Scheme 5.1**. Thus, initial retrosynthetic manipulations to remove the vinyl iodide reveals the target THP **223**, with subsequent scission of the O25 – C21 bond revealing a linear precursor **224** in which four of the five stereocentres are present.



**Scheme 5.1:** Intramolecular oxy-conjugate cyclisation strategy applied to the C18 – C27 eastern fragment **198**.

The highly-oxygenated nature of the linear C19 – C27 fragment required careful consideration of the protecting group strategy (**Scheme 5.2**). Specifically, the C22 and C23 hydroxyls need

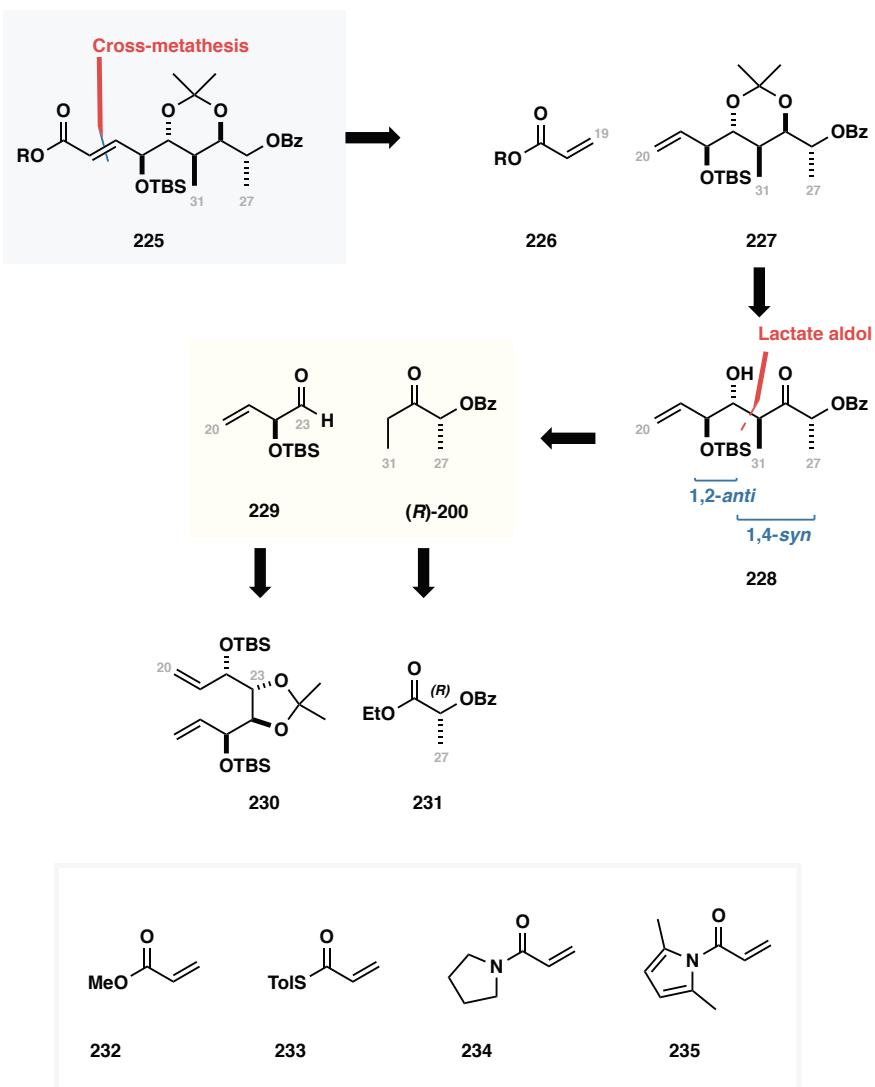
to remain differentiable throughout the synthesis to ensure that esterification between **229** and the western fragment takes place with site-selectivity. Additionally, it was decided to leave the C26 ketone as a protected alcohol prior to cyclisation to deter the possibility for formation of a hemiacetal through competitive attack of O23. To this end, **225** was identified as a suitable cyclisation precursor, bearing a silyl ether on O22 which would be easily removed at the end of the synthesis. Note that the concept of using an acetonide to constrain O23 and O25 is borrowed from the western fragment synthesis (see §2.3.1 and §3.2).



**Scheme 5.2:** Protecting group strategy and differentiation of the C22, 23, and 26 hydroxyl groups.

## 5.2 THE TARTRATE APPROACH

The C20 – C21 olefin was recognised as a strategic disconnection for simplification of the linear precursor **225** (**Scheme 5.3**). This retrosynthetic manoeuvre traces its origins to the seminal work by Fuwa who screened a variety of oxy-Michael acceptors – introduced via cross metathesis – during the development of the 2,6-*cis* selective thioester methodology (see §3.3.2).<sup>86</sup> In the context of madeirolide A, a cross-metathesis reaction could affect convergent union of **227** with a variety of acrylate derivatives **232** - **235** to probe the reactivity and diastereoselectivity of the anticipated cyclisation. The cross-metathesis is projected to give good selectivity as it takes place between a type I and type II alkene,<sup>133</sup> and the acrylate derivatives are readily accessible in one step from acroloyl chloride via the addition of a suitable nucleophile.



**Scheme 5.3:** Retrosynthetic analysis of a linear C19 – C27 precursor to the eastern THP. Michael acceptors investigated by Fuwa (inset).

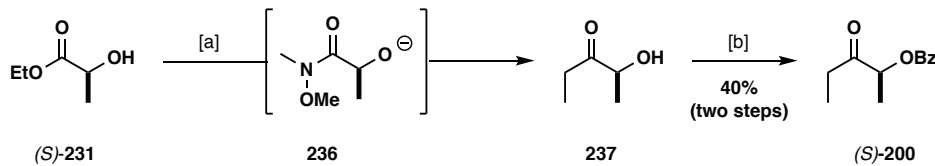
Recognising the 1,4-syn 1,2-*anti* relationship within **228**, a lactate aldol reaction could be used to forge the C23 and C24 stereocentres concomitantly.<sup>134</sup> This reveals ethyl ketone (*R*)-**200** and  $\alpha$ -siloxy- $\beta,\gamma$ -unsaturated aldehyde **229** as sub-targets, both accessible from the chiral pool using lactic and tartaric acid derivatives respectively. This lactate aldol methodology, developed within the Paterson group,<sup>134</sup> has been widely used in polyketide synthesis, giving confidence that the C22 and C23 stereocentres will be introduced with high levels of selectivity. Notably, unlike in the majority of cases, the lactate ‘auxiliary’ forms part of the natural product, providing the C27 methyl group, and thus avoiding the need for additional manipulations to cleave the C – C bond between C25 and C26.

One downside to using chiral pool materials is that one enantiomer is often naturally abundant, and hence cheaper. For the construction of madeirolide A, the unnatural enantiomer of lactate is required. Accordingly, all exploratory studies and optimisation in this

chapter, unless otherwise noted, have been carried out in the enantiomeric series using the (*S*)-lactate derived ketone (*S*)-**200**. Given that all the intended reactions are diastereoselective and under substrate control, it would be possible to procure access to the *correct* enantiomer once the route had been suitably developed. Parenthetically, at this stage it is not yet known conclusively what the absolute stereochemistry of madeirolide A **1** is, with current synthetic efforts guided by the configuration of the cinerulose sugar and by comparison to mandelalide A for which the absolute configuration is known.

### 5.2.1 PREPARATION OF THE LACTATE ETHYL KETONE

The required ketone (*S*)-**200** was accessed in two steps from natural (*S*)-(*-*)-ethyl-L-lactate (*S*)-**231** following an improved protocol from Trauner (**Scheme 5.4**).<sup>135</sup> Weinreb amide **236** was first prepared through the action of *i*-PrMgCl and Weinreb salt on (*S*)-**231**, with subsequent addition of EtMgBr *in situ* furnishing ethyl ketone **232**. While this procedure improves on the original two-step procedure developed in our group, avoiding the isolation of the Weinreb amide, the resulting unprotected alcohol is highly volatile. An overall yield of between 30 – 40% from (*S*)-**231** was obtained, in keeping with literature values.<sup>135</sup>



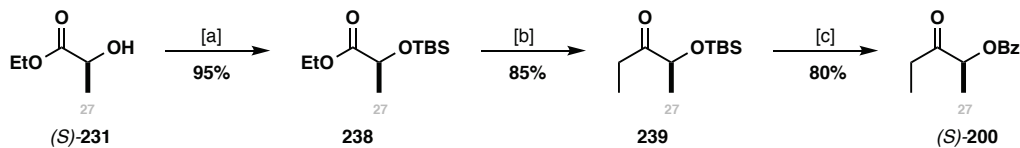
**Reagents and conditions:** [a] *i*-PrMgCl, [MeO(Me)NH·HCl], THF, 0 °C; EtMgBr, 0 °C → rt. [b] Bz<sub>2</sub>O, DMAP, Et<sub>3</sub>N, CH<sub>2</sub>Cl<sub>2</sub>, rt.

**Scheme 5.4:** Preparation of lactate derived ethyl ketone (*S*)-**200** using Trauner's 'one-pot' synthesis.

Protection of the free hydroxyl moiety at the beginning of the synthesis would increase the efficiency of the subsequent steps by preventing loss of material to evaporation. While this lacks elegance, the transformation was deemed synthetically valuable in obtaining stocks of *ent*-**200**. This would be critical when conducting the reaction on the opposite (*correct*) enantiomeric series owing to the prohibitive cost of **231**. (*S*)-(*-*)-ethyl-L-lactate *ent*-**232** was thus converted to TBS ether **238** and subjected to the Trauner conditions to afford **239** in excellent yield (60 – 85% from **231**). With the ketone to hand, the TBS group needed to be switched for the required benzoate without isolation of the intermediate unprotected secondary alcohol.\* This was achieved in one-pot by sequential treatment with TBAF and

\* The benzoate group is necessary to achieve diastereoselectivity in the lactate aldol reaction, but cannot be present from the start owing to the incompatibility of esters with Grignard reagents.<sup>134</sup>

Bz<sub>2</sub>O giving quantitative yield of (*S*)-200. Anketell has also shown this transformation to be possible using catalytic TBAF and KF as an economical stoichiometric fluoride source.<sup>136</sup>

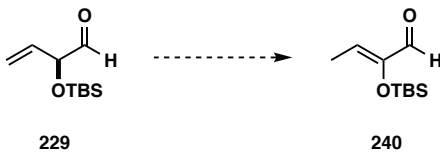


**Reagents and conditions:** [a] TBSCl, Imid., CH<sub>2</sub>Cl<sub>2</sub>, 0 °C. [b] i-PrMgCl, [MeO(Me)NH·HCl], THF, 0 °C; EtMgBr, 0 °C → rt. [c] TBAF, CH<sub>2</sub>Cl<sub>2</sub>, rt; Bz<sub>2</sub>O, Et<sub>3</sub>N, DMAP.

**Scheme 5.5:** Modified preparation of lactate derived ethyl ketone (*S*)-200.

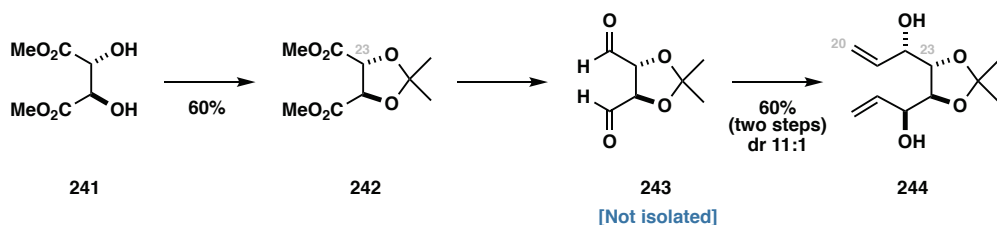
### 5.2.2 SYNTHESIS OF THE ALDEHYDE

The use of the  $\alpha$ -siloxy- $\beta,\gamma$ -unsaturated aldehyde **229** (Scheme 5.6) as the coupling partner for the lactate aldol reaction was an ambitious strategy, with the  $\beta,\gamma$ -olefin liable to migrate to form the corresponding silyl enol ether/enal **240**, which is thermodynamically favoured owing to conjugation with the carbonyl. The stability of **229** to Lewis acidic conditions has been investigated by Hayashi using the racemic compound *rac*-**229**, after 1 h at 0 °C, a 10:1 ratio of *rac*-**229** to **240** was observed, demonstrating the possibility that it may be stable enough to survive the lactate aldol reaction conditions.<sup>137</sup>



**Scheme 5.6:** Possible alkene migration to convert  $\alpha$ -siloxy- $\beta,\gamma$ -unsaturated aldehyde **229** into the corresponding enal **240**.

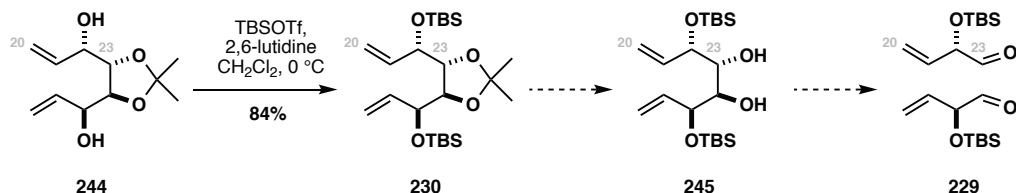
The bis-allylic diol **244** was prepared following precedent from Danishefsky.<sup>138</sup> Initial protection of **241** provided the corresponding C<sub>2</sub> symmetric acetonide (isopropylidene ketal) **242**, which was essential for good diastereoselectivity in the subsequent steps. Conversion of **242** to the bis-allylic alcohol **244** was achieved in two-steps: the esters were first reduced using DIBAL at low-temperatures, with addition of divinyl zinc to the ensuing aldehyde providing **244** in 60% yield and 11:1 dr. The use of a zinc organometallic in place of conventional magnesium or lithium reagents was necessary as the desired stereochemistry would prevail only if the addition occurred with chelation control which zinc species accomplish reliably.<sup>139</sup>



**Reagents & conditions:** [a]  $\text{Me}_2\text{C}(\text{OMe})_2$ ,  $p\text{-TsOH}$ ,  $\text{CH}_2\text{Cl}_2$ , rt. [b] DIBAL-H,  $\text{PhMe}$ ,  $-78^\circ\text{C}$ . [c]  $(\text{H}_2\text{C}=\text{CH})_2\text{Zn}$ ,  $\text{THF}$ ,  $-78^\circ\text{C}$ .

**Scheme 5.7:** Synthesis of **244** as a precursor to the  $\alpha$ -siloxy- $\beta,\gamma$ -unsaturated aldehyde **229**.

Silyl protection of the C22 hydroxyls using TBSOTf occurred uneventfully to provide **230**, setting the stage for removal of the acetonide and oxidative cleavage of the diol to the  $\alpha$ -siloxy- $\beta,\gamma$ -unsaturated aldehyde **229** (**Scheme 5.8**).



**Scheme 5.8:** TBS protection of **244** and proposed elaboration to aldehyde **229**.

Although many examples exist of chemoselective acetonide cleavage in the presence of a secondary TBS ether (or other silyl groups in general),<sup>140</sup> the methodology is not general and often requires extensive screening to find a suitable procedure. To this end, **Table 5.1** summarises the conditions investigated.

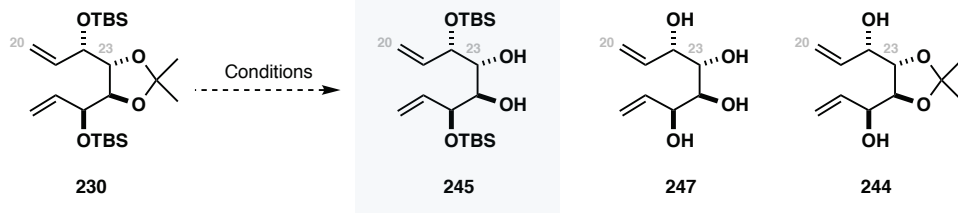
Unfortunately, despite these investigations, conditions were not able to be identified that would permit the removal of the acetonide in the presence of the TBS ethers. To overcome the above difficulties, one of two changes needed to be made: replacement of the TBS ethers with a more stable derivative, or replacement of the acetonide with a more labile derivative. The latter option was preferred as, given the already challenging cyclisation it was not desirable to further increase the steric bulk at C22, as would be necessary if the TBS was replaced with a more acid-stable derivative such as a TBDPS. Accordingly, the cyclopentylidene analogue **251** of **230** was targeted. The cyclopentylidene ketal has been shown to have roughly one-third of the half-life of the corresponding isopropylidene ketal (acetonide)<sup>141</sup> which was anticipated to provide enough of a rate difference to achieve chemoselective deprotection in the presence of the TBS ethers.

Results & discussion III: synthesis of the eastern tetrahydropyran

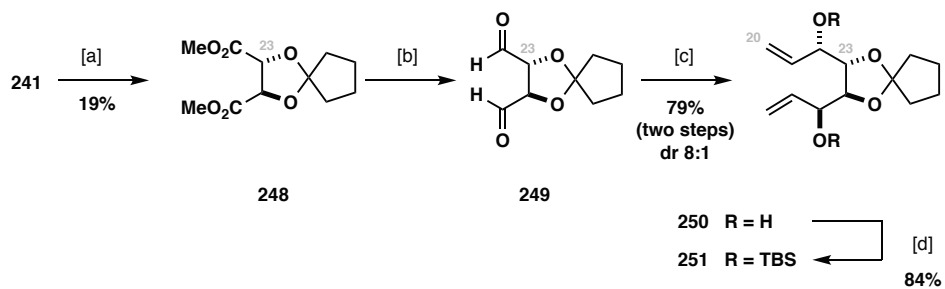
**Table 5.1:** Attempted removal of the 1,2-acetonide in the presence of the secondary TBS ether.

Reagents		Temperature	Time	Protecting groups cleaved	
				TBS	Acetonide
			24 h		No reaction
PPTS (cat), MeOH		rt	48 h		✓
			72 h		✓
		40 °C	6 h	✓	✓
			24 h	✓	✓
p-TsOH (cat), MeOH		rt	24 h	✓	✓
DOWEX-W50, MeOH		Rt	24 h	✓	✓
Amberlyst, MeOH		rt	24 h	✓	✓
FeCl <sub>3</sub> /SiO <sub>2</sub> , CHCl <sub>3</sub> <sup>142,143</sup>		rt	3 h	✓	
			3 h		No reaction
I <sub>2</sub> , MeOH <sup>144</sup>		rt	6 h		No reaction
			24 h	✓	
TFA		- 78 °C	10 min	✓	

All reactions carried out in dry CH<sub>2</sub>Cl<sub>2</sub> unless otherwise stated  
Results determined by <sup>1</sup>H NMR of reaction aliquots.



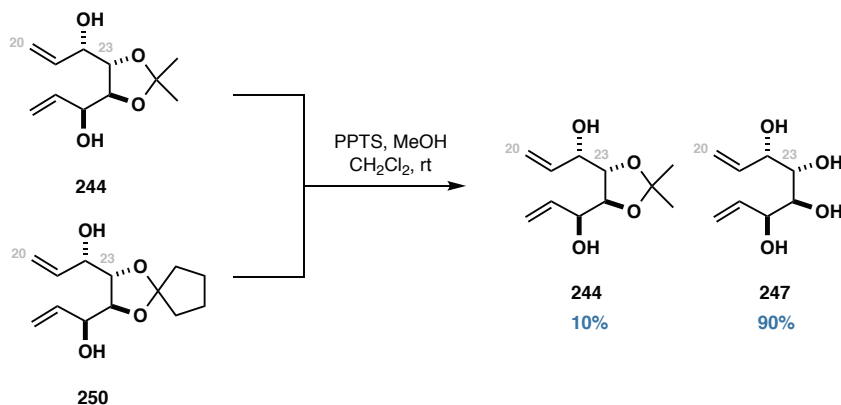
To this end, **241** was first protected as the cyclopentylidene ketal **248** by condensation with cyclopentanone under Dean-Stark conditions (**Scheme 5.9**). From **248**, the bis-TBS ether **251** could be accessed following an analogous sequence of reactions to those used for the acetonide providing access to **251** in 13% from **241**. Disappointingly, treatment of **251** with the conditions described in **Table 5.1** failed to provide the projected chemoselectivity.



**Reagents & conditions:** [a] Cyclopentanone, *p*-TsOH, PhMe, reflux. b] DIBAL-H, PhMe, -78 °C. [c]  $(\text{H}_2\text{C}=\text{CH})_2\text{Zn}$ , THF, -78 °C. [d] TBSOTf, 2,6-lutidine,  $\text{CH}_2\text{Cl}_2$ , rt.

**Scheme 5.9:** Synthesis of cyclopentylidene ketal **251**.

In an attempt to rationalise the above results, a 1:1 mixture of isopropylidene ketal **244** and cyclopentylidene ketal **250** was treated with catalytic PPTS. After 2 h, NMR analysis of the crude product showed essentially complete deprotection to the tetra-ol **247**, with around 10% of **244** remaining. This facile deprotection points to the involvement of the TBS ethers in retarding deprotection, possibly due to a steric effect in which the silyl groups are essentially shielding the molecule preventing effective nucleophilic attack. This would also explain why tetra-ol **247** was so frequently observed during screening of deprotection conditions, as, once the TBS groups were cleaved there was nothing impeding the subsequent hydrolysis of the acetonide.

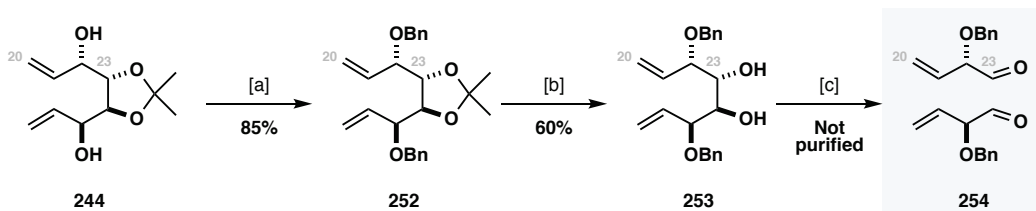


**Scheme 5.10:** Competitive hydrolysis of the isopropylidene ketal **244** and cyclopentylidene ketal **250**.

Rather than persist with the existing protecting group strategy, it appeared prudent at this juncture to replace the C22 protecting group with something that would be indefinitely stable

under the conditions required to remove the acetonide. In addition to permitting the investigation of the proposed lactate aldol, this would also avoid the same issue of chemoselectivity arising when attempting the IOCC, where a six-membered acetonide needs to be removed in the presence of a secondary TBS ether to reveal the free hydroxyl at C25 for cyclisation to occur (see **Scheme 5.3**).

A benzyl ether was selected as a suitable replacement for the TBS ether owing to its stability towards acid. The successful route to the  $\alpha$ -benzyloxy- $\beta,\gamma$ -unsaturated aldehyde **254** is shown in **Scheme 5.11**. Hence, **244** was first converted to bis-benzyl ether **252** prior to hydrolysis of the acetonide to diol **253**.\* With **253** to hand, the oxidative cleavage could finally be conducted, accordingly treatment of **253** with silica supported sodium periodate gave **254** which was used in the subsequent lactate aldol (see §5.2.3) without purification owing to the dual potential for epimerisation of the  $\alpha$ -stereocentre and migration of the  $\beta,\gamma$ -alkene.



**Reagents & conditions:** [a] NaH, BnBr, TBAI, THF, 0 °C. [b] HCl (3 M aq.), THF, rt. [c] NaIO<sub>4</sub> on SiO<sub>2</sub>, pH 4 buffer, CH<sub>2</sub>Cl<sub>2</sub>, rt.

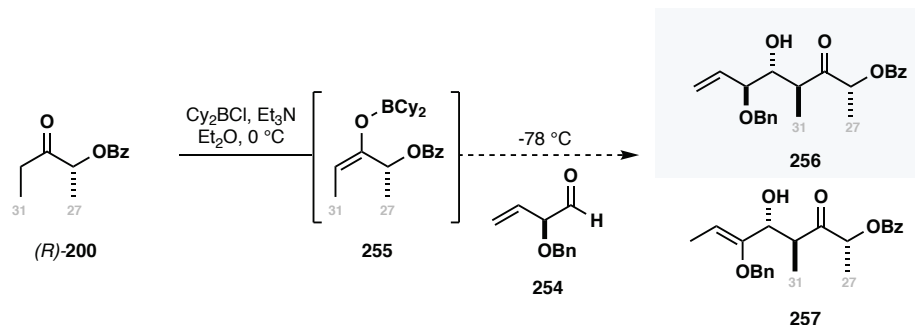
**Scheme 5.11:** Successful synthesis of the C20 – C23  $\alpha$ -benzyloxy- $\beta,\gamma$ -unsaturated aldehyde **254**.

### 5.2.3 LACTATE ALDOL COUPLING<sup>†</sup>

With a tractable route to the  $\alpha$ -benzyloxy- $\beta,\gamma$ -unsaturated aldehyde **254** developed, attention was turned to the lactate aldol reaction that was to set the C23 and C23 stereocentres. Ketone (*R*)-**200** was first enolised using Cy<sub>2</sub>BCL and Et<sub>3</sub>N at 0 °C to afford the (*E*)-enolate **255** to which a solution of aldehyde **254** was added at -78 °C (**Scheme 5.12**). The result of the aldol was a complex mixture, with <sup>1</sup>H NMR of the crude product showing two aldehyde resonances, and at least four distinct products based on the number of signals corresponding to the C31 methyl observed.

\* The conditions used for the removal of the acetonide were arbitrary, and it may well be the case that far milder methods would accomplish the same task – this was not investigated.

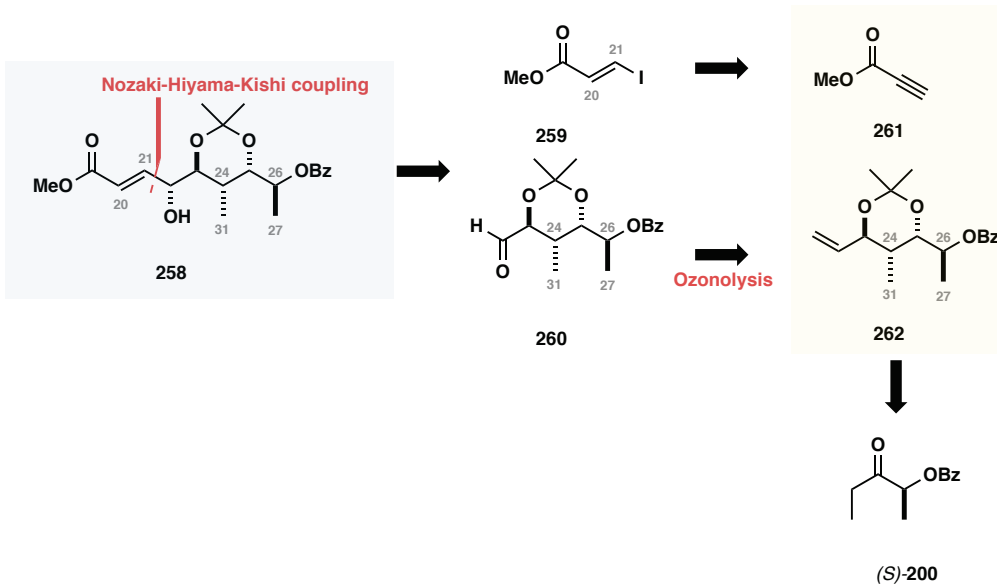
<sup>†</sup> This aldol reaction was carried out using the ethyl ketone derived from unnatural D-lactate owing to the enantiomeric series used to optimise the synthesis of aldehyde **254**.



**Scheme 5.12:** Lactate aldol coupling between ethyl ketone (*R*)-200 and  $\alpha$ -benzyloxy- $\beta,\gamma$ -unsaturated aldehyde 254.

During the protracted investigations into preparation of the tartrate-derived aldehyde, a modified synthetic strategy had been devised. This route, using an NHK reaction (see §5.3), proved successful, and accordingly the decision was taken to halt optimisation of the above lactate aldol reaction.

### 5.3 THE NHK COUPLING APPROACH



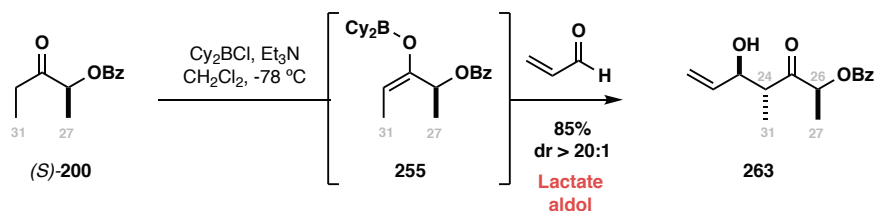
**Scheme 5.13:** Modified retrosynthesis using an NHK reaction to form the C21 – C22 bond.

The failure of the tartrate-based approach prompted a re-evaluation of the proposed strategy. Specifically, the C22-oxymethylene stereocentre and the C21 – C22 bond could conceivably be forged simultaneously using a Cr(II)/Ni(II) mediated Nozaki-Hiyama-Kishi (NHK) reaction between aldehyde 260 and a suitable vinyl iodide 259 (**Scheme 5.13**). The necessary stereochemistry at C22 would prevail if the reaction proceeded through a non-chelated Felkin-Anh transition state, which is well precedented in the literature using Cr/Ni organometallics.<sup>145</sup> Further disconnection of aldehyde 260 identifies olefin 262 as a key

intermediate; in a forward sense, ozonolysis would unmask the reactive aldehyde immediately prior to reaction to avoid the potential for epimerisation of the  $\alpha$ -stereocentre. **262** itself would then be formed through a lactate aldol reaction between ketone (*S*)-**200** and acrolein followed by a substrate-directed 1,3-*anti* Evans-Saksena reduction and subsequent protection as the acetonide. Vinyl iodide **259** is a known compound, prepared in two steps from methyl prop-2-ynoate **261** (methyl propiolate).

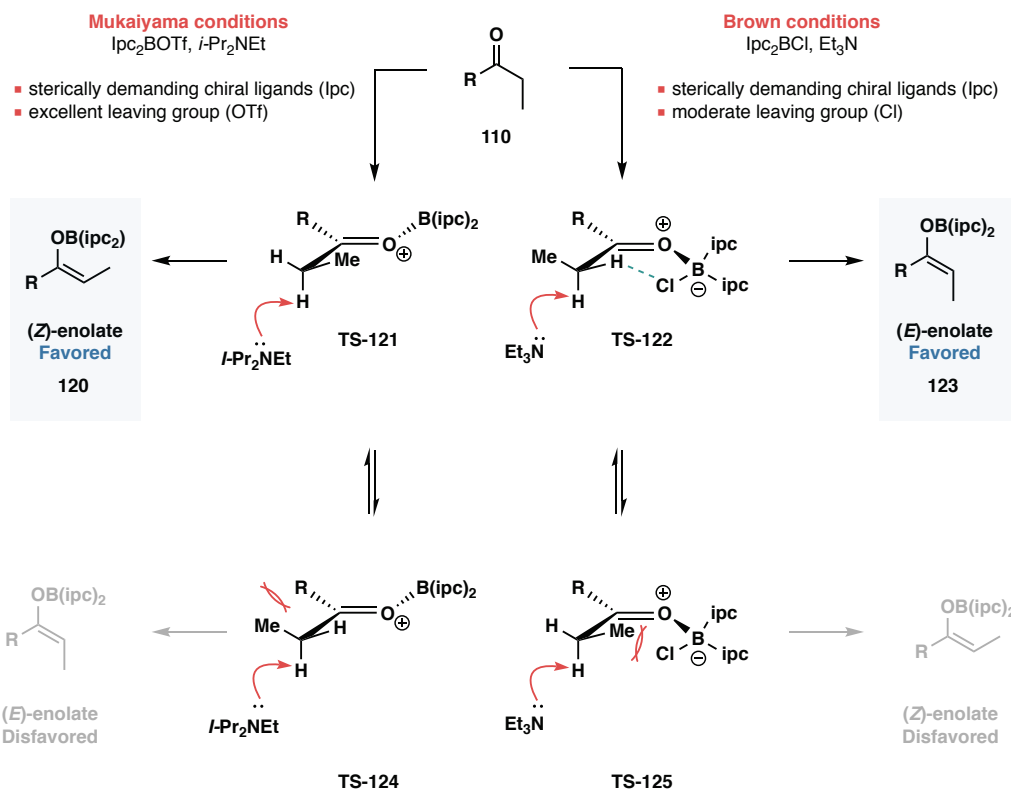
### 5.3.1.1 LACTATE ALDOL AND PREPARATION OF THE C21 – C27 ALLYLIC ALCOHOL

Synthesis of **262** commenced with a  $\text{Cy}_2\text{BCl}$  mediated lactate aldol reaction between the previously described ketone (*S*)-**200** and acrolein (**Scheme 5.14**). Following recrystallisation ( $\text{Et}_2\text{O}$  in *n*-hexane or  $\text{CH}_2\text{Cl}_2$  in benzene) the resulting aldol adduct **263** was obtained as a single diastereomer with a reproducible yield of 75 – 85 % on scales between 500 mg and 4 g. The relative stereochemistry between the C23-Me and C24-OH groups was confirmed as 1,2-*anti* by measurement of the  $^3J_{\text{HH}}$  coupling constant. Additionally, MTPA ester analysis on the crude aldol adduct **263** confirmed the expected absolute configuration at the newly formed C23 oxymethine (see Appendix A).



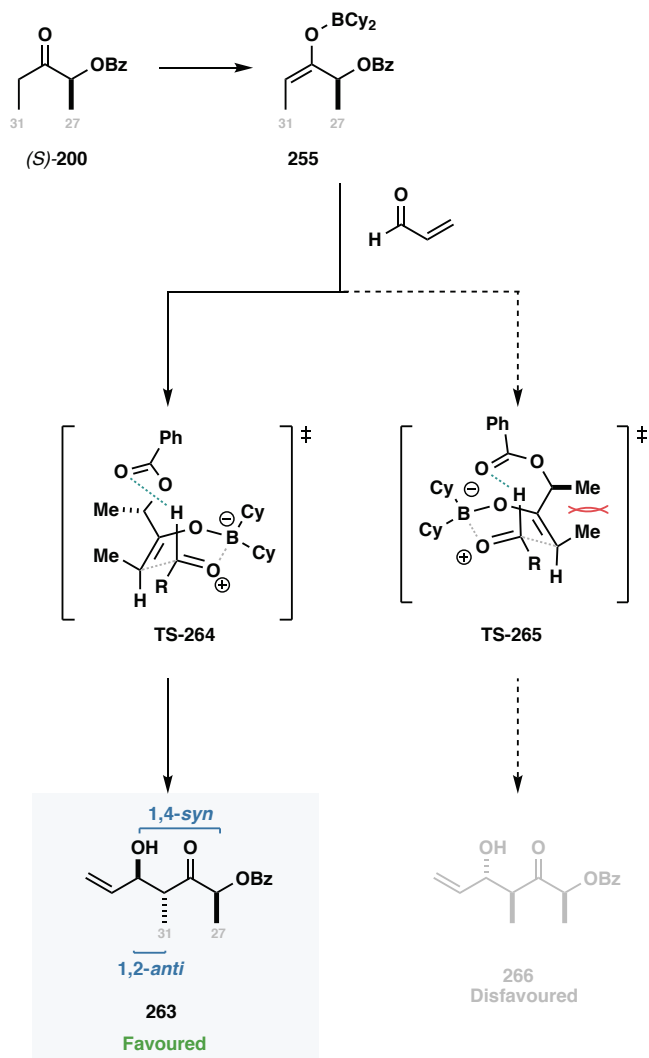
**Scheme 5.14:** Aldol reaction between ketone (*S*)-**200** and acrolein.

Rationalisation of the 1,4-*syn* 1,2-*anti* diastereoselectivity requires consideration of both the enolate formation and the aldol transition state. As previously discussed, the relative 1,2-disastereoselectivity is a consequence of the enolate geometry, with (*E*) and (*Z*) enolates providing *anti* and *syn* aldol adducts respectively. Using boron chlorides, deprotonation takes place *prior* to the departure of chloride resulting in the Lewis acid being significantly larger than that used in the Mukaiyama protocol in which the triflate counterion has completely dissociated prior to enolisation **Scheme 5.15**.<sup>134</sup> Computational studies have demonstrated a stereoelectronic preference for the B—Cl bond to lie in the same plane as the developing enolate, with a weak non-covalent interaction between the  $\alpha$ -proton and Cl facilitating deprotonation.<sup>74</sup> This results in the stereospecific formation of the desired (*E*)-enolate **255**.

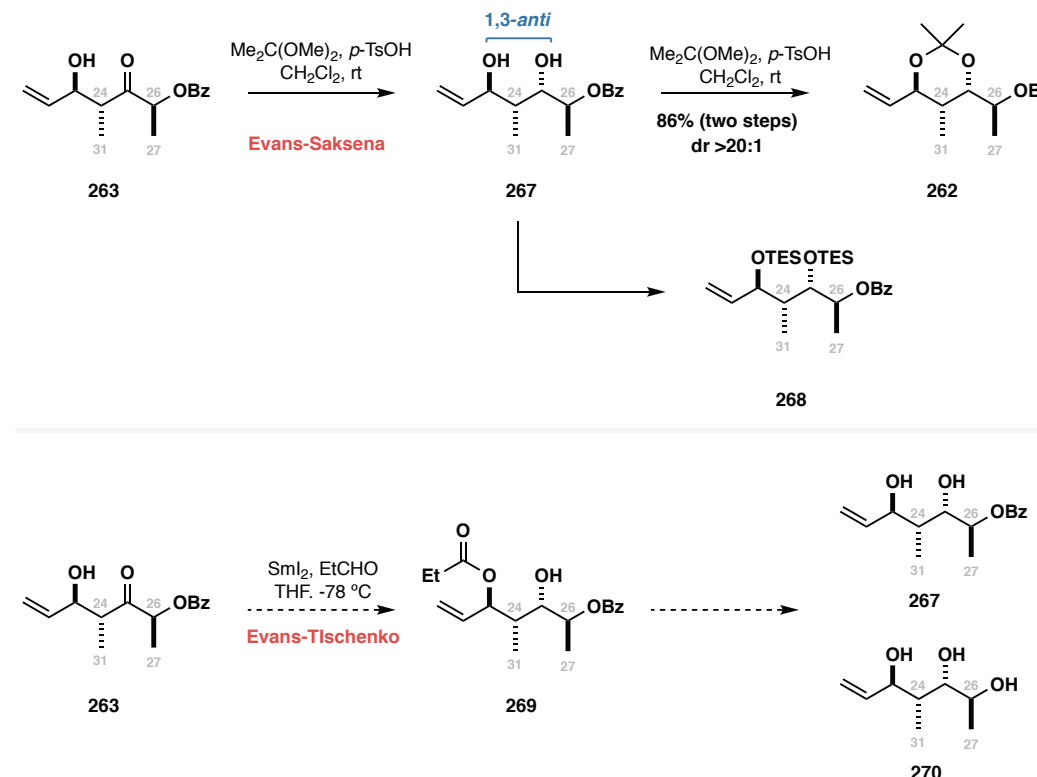


**Scheme 5.15:** Mechanistic rationale for the stereodivergent formation of (*E*)- and (*Z*)-boron enolates from ethyl ketones.<sup>75</sup>

The transition state of the lactate aldol has been the subject of several computational investigations to rationalise the high levels of diastereoselectivity observed.<sup>74</sup> Current evidence suggests the reaction takes place via the diastereomeric boat-like transition states **TS-264** and **TS-265**, with the major product arising from **TS-264** in which the benzoate forms a stabilising formyl hydrogen bonding interaction with the aldehyde and minimises the *syn*-pentane interactions, which leads to formation of the 1,4-*syn* diastereomer **263** (**Scheme 5.16**).

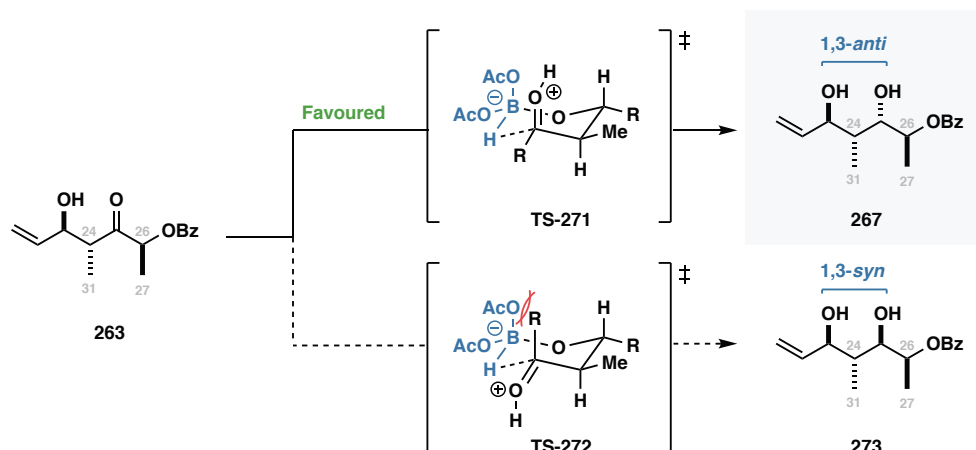
**Scheme 5.16:** Mechanistic rationale for the  $\text{Cy}_2\text{BCl}$  mediated lactate aldol.

With the aldol adduct **263** to hand, the remaining C25 stereocentre could be established by taking advantage of the proximal C23 oxygen to carry out a substrate directed *1,3-anti* reduction. Two methods are commonly used to achieve this process: the Evans-Saksena reduction using  $\text{Me}_4\text{NBH}(\text{OAc})_3$ ,<sup>146,147</sup> and the Evans-Tischenko<sup>148</sup> reduction using catalytic  $\text{SmI}_2$ . In the event, the Evans-Saksena reduction of **263** turned out to be most convenient, providing access to acetonide **262** in 86% yield over two steps without purification of the intervening 1,3-diol. The use of an Evans-Tischenko reduction was not investigated in this case as the resulting propionate ester **269** would be unable to be cleaved in the presence of the C26 benzoate.



**Scheme 5.17:** Substrate directed 1,3-*anti* reduction of **263** and protection as a 1,3-acetonide showing the successful Evans-Saksena route, and an alternative Evans-Tischenko route that was not investigated.

In agreement with the stereochemical model proposed by Evans,<sup>146</sup> **262** was obtained as a single diastereomer, confirmed as the 1,3-*anti* diastereomer using the Rychnovsky analysis ( $\delta_c = 101.42, 24.63, 24.11$  ppm). The 1,3-*anti* isomer dominates via **TS-271** due to the intramolecular delivery of hydride, with the protonated carbonyl adopting a pseudoaxial position to avoid 1,3-diaxial clash between the acetate on boron and the bulky R group (containing the benzoate protecting group) (**Scheme 5.18**).

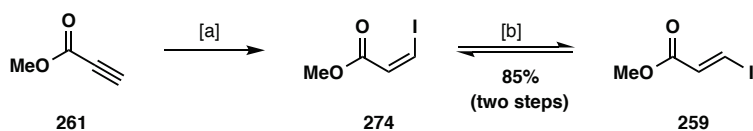


**Scheme 5.18:** Stereochemical rationale for the 1,3-*anti* Evans-Saksena reduction.

### 5.3.1.2 PREPARATION OF THE VINYL IODIDE COUPLING PARTNER

At this stage, attention was turned to the synthesis of the vinyl iodide coupling partner **259** required to carry out the NHK reaction. Unlike with the originally planned tartrate approach, it would not be possible to easily introduce a range of different Michael acceptors at a later stage, and as such the vinyl iodide used would need to be suitably functionalised prior to coupling. Given this lack of flexibility, efforts were focused on the preparation of the methyl ester, and the 4-tolyl thioester as previously used for the C1 – C11 western fragment.

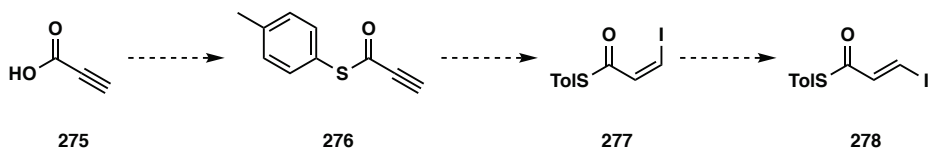
The vinyl iodide **259** was prepared in two steps from methyl propiolate following previously reported procedures. Thus, treatment of methyl propiolate **261** with NaI in AcOH/MeCN furnished the (*Z*)-vinyl iodide **274** which was thermally isomerised in refluxing benzene in the presence of catalytic HI. The isomerisation required several days of reflux, monitoring the (*Z*) → (*E*) conversion by proton NMR of a small reaction aliquot. The reaction would generally give an 8:1 mixture of geometric isomers (in favour of the desired isomer), however recrystallisation from hexane enabled geometrically pure material **259** to be isolated.



**Reagents & conditions:** [a] NaI, AcOH:MeCN (1:1), 80 °C. [b] HI (aq.), PhH, reflux.

**Scheme 5.19:** Preparation of (*E*)-vinyl iodide **259** from methyl propiolate.

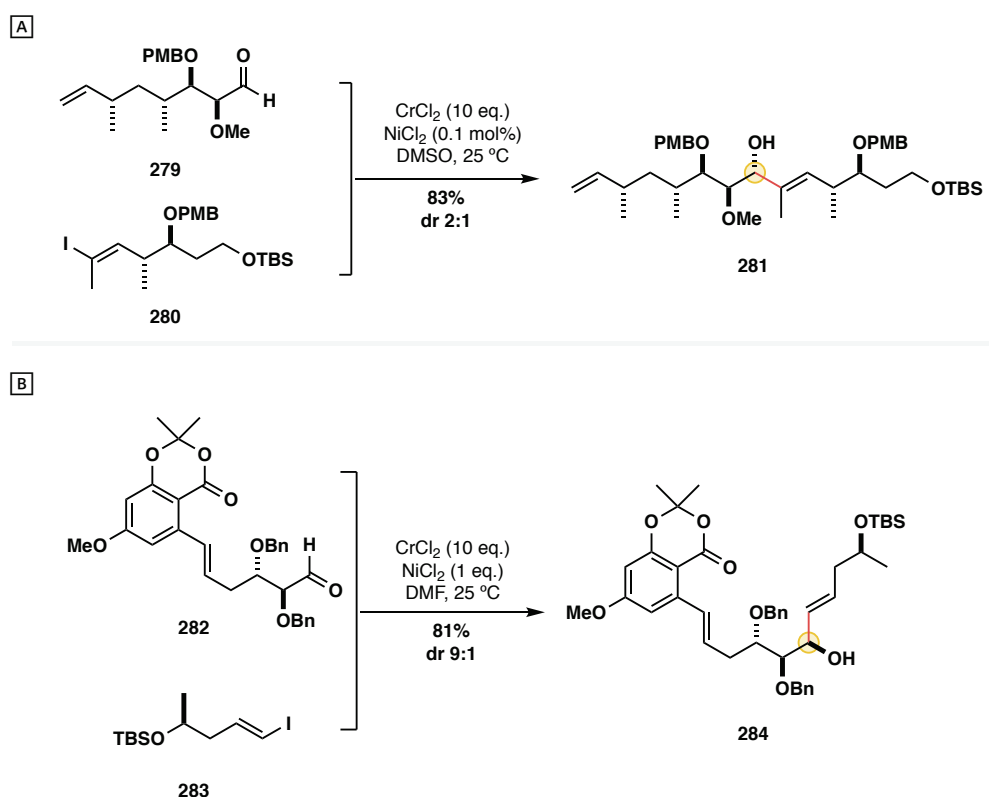
It was anticipated that the corresponding thioester **278** might be prepared in an analogous fashion starting from propiolic acid **275**, with initial thioesterification furnishing **276** which could undergo the same sequence of hydroiodination and isomerisation (**Scheme 5.20**). Attempts at forming thioester **276** under Steiglich-type conditions (DCC, DMAP) resulted in an inseparable mixture of products. Analysis of the crude <sup>1</sup>H NMR spectra and LCMS suggested the formation of the 1,4-addition product rather than the desired thioester (albeit in low yield). Thioesterification via formation of the acid chloride proved more successful, providing access to **276** in 50% yield, however **276** did not react under the hydroiodination conditions described above, leading only to hydrolysis back to the carboxylic acid **275**.



**Scheme 5.20:** Planned synthesis of the thioester analogue of **278**.

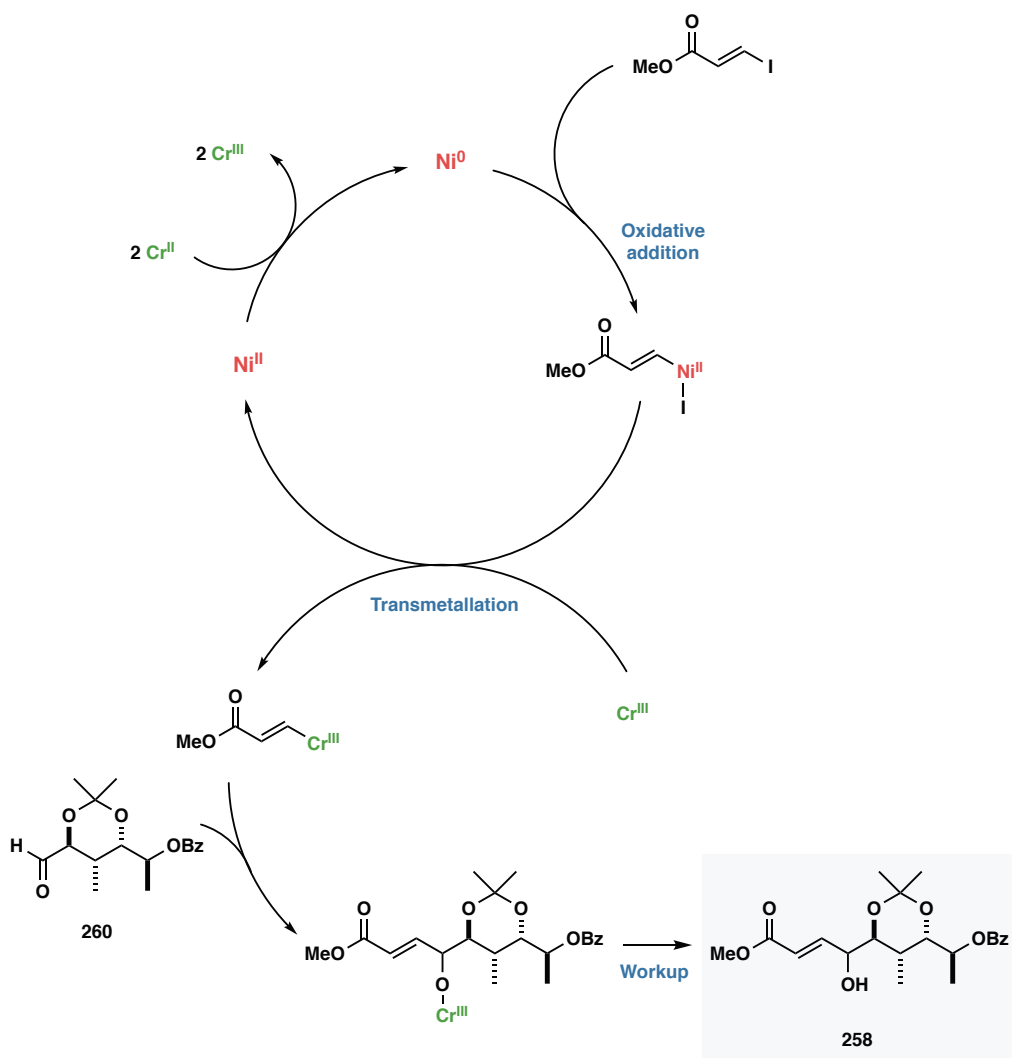
## 5.3.1.3 NOZAKI-HIYAMA-KISHI (NHK) COUPLING

The Nozaki-Hiyama-Kishi (NHK) reaction was first reported in the late 1970s. Since the initial reports, the NHK reaction has found extensive use in the synthesis of complex natural products<sup>145</sup> owing to the mild and chemoselective nature of the reaction. Two examples of this are found in Nicolaou's rapamycin synthesis<sup>149</sup> and Mohapatra's work on zeanol analogues<sup>150</sup> (**Scheme 5.21**).



**Scheme 5.21:** Selected examples of NHK couplings in complex natural product synthesis. **A** Total synthesis of Rapamycin (Nicolaou).<sup>149</sup> **B** Synthesis of 7-*epi* zeanol (Mohapatra).<sup>150</sup>

The mechanism of the NHK reaction is thought to proceed via a Grignard-like addition of an organochromium species into a carbonyl, as outlined in **Scheme 5.22**.<sup>151,152</sup> Although the exact identify of the species is not known, it is postulated that the active catalyst is obtained from Ni(II) via reduction using two equivalents of a sacrificial Cr(II) salt. The Ni(0) catalyst oxidatively inserts into the C – X bond, with X representing a halide (Br, I etc.) or psuedohalide (OTf). Subsequent transmetallation of the Ni(II) organometallic to Cr(III) provides a nucleophilic vinyl chromium species which undergoes chemoselective addition into the aldehyde.

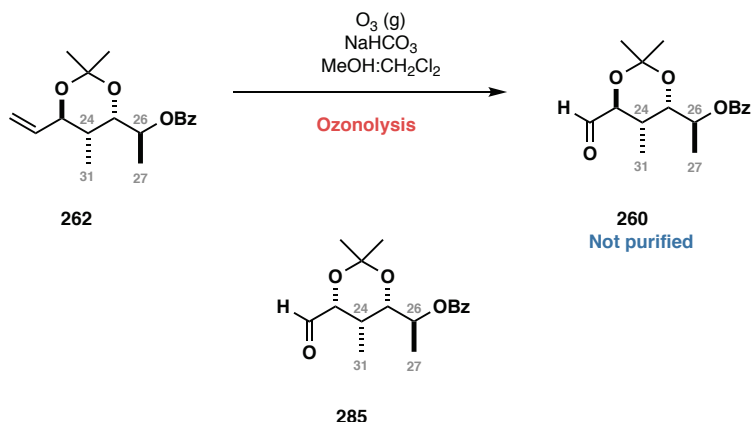


**Scheme 5.22:** Proposed mechanism for the  $\text{Ni}(\text{II})$  catalysed Nozaki-Hiyama-Kishi reaction.<sup>151</sup>

Chromium is less electropositive than lithium or magnesium, accounting for the decreased reactivity of organochromium species when compared to that of the analogous organolithium or organomagnesium reagents.<sup>153,154</sup> This reactivity allows the discrimination of various carbonyl containing functional groups, with high levels of chemoselectivity for aldehydes over ketones or esters. Additionally, unlike for lithium or magnesium, the reactivity of the chromium species can be finely tuned through the choice of ligands to control the steric and electronic properties of the metal centre.

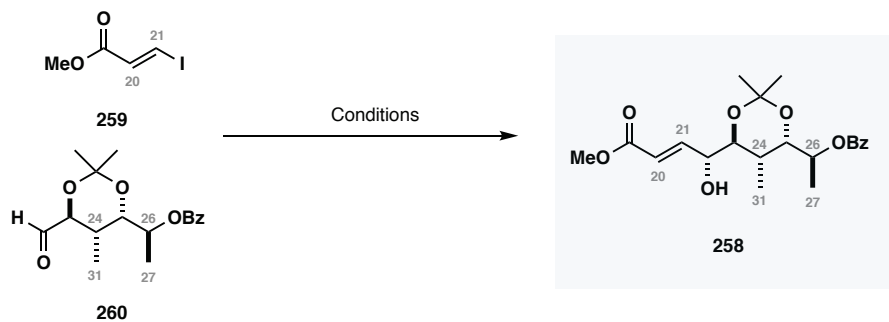
Prior to investigation of the proposed organometallic addition, the required aldehyde **260** needed to be unmasked through ozonolysis of the terminal olefin **262**. Of principle concern was the stability of aldehyde **260**, with epimerisation of the  $\alpha$ -stereocentre possible to give the undesired 1,3-syn acetonide **285**. In the event epimerisation did not prove to be a problem if the aldehyde was used immediately following preparation (**Scheme 5.19**), however upon standing, or during column chromatography the aldehyde equilibrated to a 3:2 mixture of

diastereomers, as determined by integration of the diagnostic C23 oxymethine proton. Due to this, the ozonolysis was always conducted prior to the subsequent reaction, with the crude aldehyde obtained suitably clean following filtration through a plug of cotton wool to remove insoluble  $\text{NaHCO}_3$  and azeotroping with benzene.



**Scheme 5.23:** Successful ozonolysis of the terminal alkene to unmask aldehyde **260**.

Initial attempts at forging the C22-C21 bond were met with disappointment, returning epimerised aldehyde (**260** + **285**) and methyl acrylate, presumably from quenching of the initially formed oxidative addition product. It was quickly realised that the quality of CrCl<sub>2</sub> was critical to success, as had been noted by Takai.<sup>154,155</sup> While pre-heating a mixture of CrCl<sub>2</sub>/NiCl<sub>2</sub> at 150 °C under high vacuum (0.5 mmHg) ameliorated the problem, the reaction was still found to be highly batch-dependant, with some reagents failing to return product even if dried prior to use. Optimisation of the reaction is shown in **Table 5.3**, which identified the use of 10 eq CrCl<sub>2</sub> in a 1:1 THF:DMF solvent to give optimal conversion and dr.

**Table 5.2:** Optimisation of the NHK coupling between vinyl iodide **259** and aldehyde **260**. Optimised conditions are highlighted in blue.

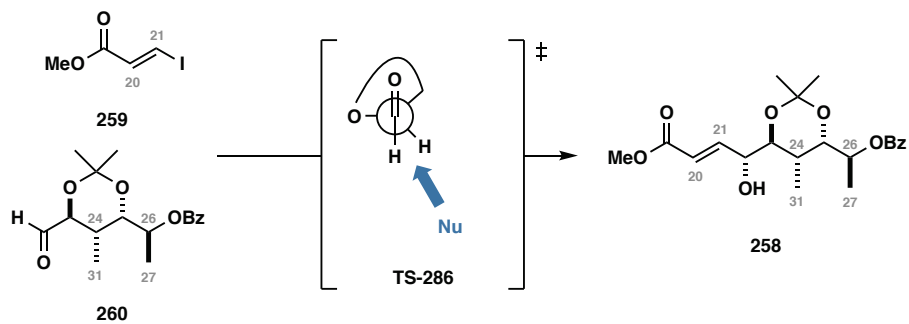
Entry	Eq. CrCl <sub>2</sub>	Eq. 259	Solvent	d.r.	Yield
1	10	3.5	DMSO	-	-
2	10	1.5	DMF	-	-
3	10	3.5	DMF	-	-
4	10	3.5	THF	-	21% (NMR)
5	10	3.5	DMF	3:1	60% (NMR)
6	10	3.5	1:1 THF:DMF	5:1	71% (NMR)
7	10	3.5	1:1 THF:DMF	5:1	87%
8	10	1.5	1:1 THF:DMF	3:1	42%

All reactions carried out at rt under argon using previously degassed solvent. NiCl<sub>2</sub> (1 mol%) used relative to the amount of CrCl<sub>2</sub> present.

Isolated yield of pure material following column chromatography  
NMR conversion.

All dr values measured from NMR spectra of crude reaction products.

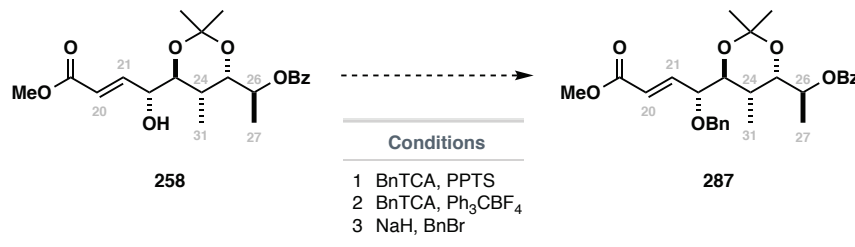
The diastereoselectivity of the NHK reaction was determined from the <sup>1</sup>H NMR spectrum of the crude reaction product **258** prior to column chromatography. Based on literature precedence, it was expected that the reaction would lead to the desired 1,2-*anti* stereochemistry based on the polar Felkin-Anh model via **TS-286**.<sup>151</sup> MTPA analysis confirmed the major product as the anticipated *anti* diastereomer (see Appendix A). As the diastereomers formed during the reaction were inseparable by column chromatography, the MTPA analysis had to be conducted on the 5:1 epimeric mixture, adding an additional level of complication when interpreting the spectra.



**Scheme 5.24:** Diastereoselectivity of the NHK reaction based on the polar Felkin-Anh model.

#### 5.3.1.4 CYCLISATION

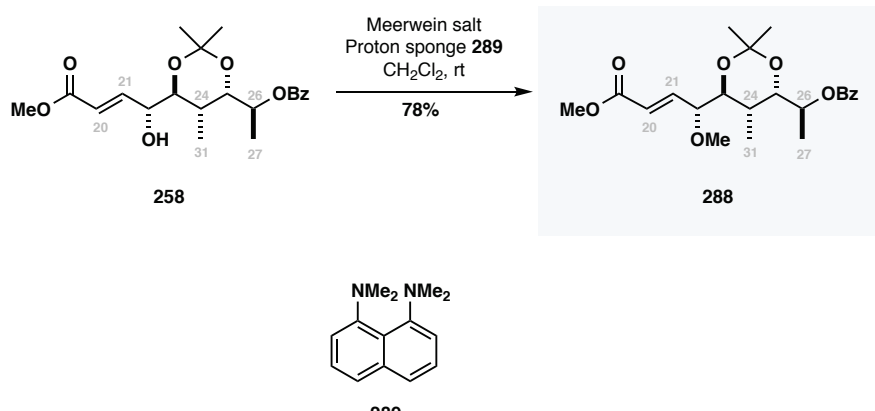
Having procured access to a linear C19 – C27 precursor **258**, the stage was now set to investigate the anticipated cyclisation. Prior to this, it was necessary to protect O22 such that it remained differentiated from O23 post-cyclisation. In keeping with the modified protecting group strategy, protection of the C22 hydroxyl as the corresponding benzyl ether was attempted but failed to provide any of the desired product (**Scheme 5.25**).<sup>\*</sup> It was reasoned that the problems encountered in protecting O22 were a result of the crowded environment, and indeed a similar issue was reported by Haslett when attempting to benzyl protect a similar intermediate in his work towards a Tsuji-Trost style cyclisation.<sup>56</sup>



**Scheme 5.25:** Attempted protection of O22 as the corresponding benzyl ether 287.

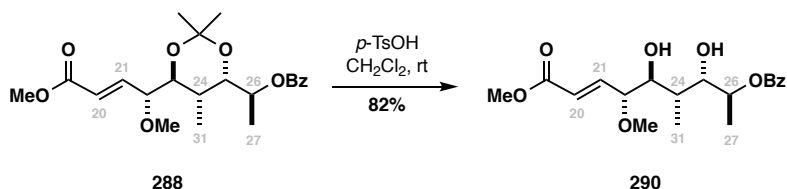
In the interest of investigating the IOCC, the issue of the O22 protecting group was put to one side temporarily, opting instead to methylate (Meerwein salt, proton sponge **289**) which took place uneventfully to give **288** in 78% yield (**Scheme 5.26**). This is not a tractable solution (there is no possibility of removing the methyl ether), and if cyclisation were successful, conditions would need to be found to procure access to a suitably protected precursor. The methyl ether should act as a suitable surrogate for the benzyl ether in terms of sterics, and as such if conditions are found for the cyclisation of **288**, they would be expected to apply to the cyclisation of **287** without complication.

\* It was later discovered that the Bn ether can be installed using BnTCA and catalytic TfOH.



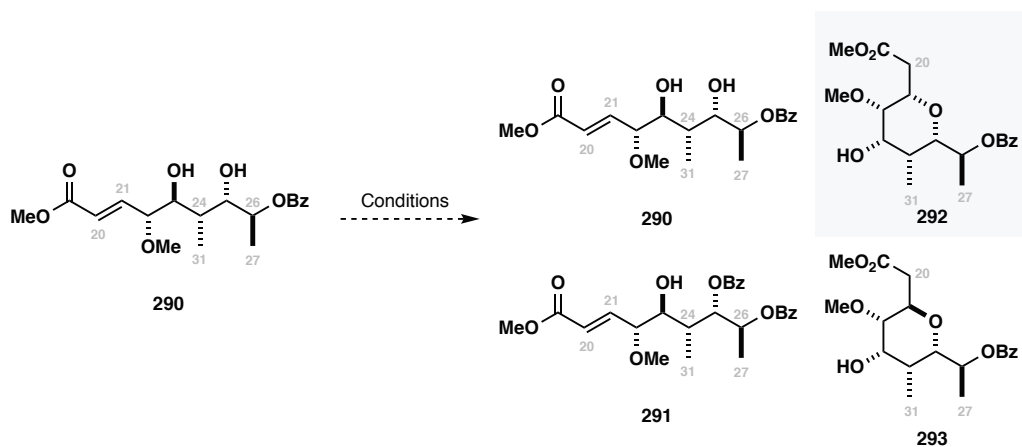
**Scheme 5.26:** Successful derivatisation of O22 as the corresponding methyl ether **288**.

With a suitable precursor **258** now to hand, the anticipated cyclisation could be attempted. Initially, **288** was subjected to the conditions that successfully affected cyclisation of **38**, the analogous precursor used to forge the western THP (see §3.3.2). Thus, treatment of **288** with *p*-TsOH in CH<sub>2</sub>Cl<sub>2</sub> at rt cleanly afforded diol **290** in 82% yield; the mass balance accounted for by recovered starting material **288** (**Scheme 5.27**). The diol was subsequently re-subjected to *p*-TsOH, this time replacing CH<sub>2</sub>Cl<sub>2</sub> for DCE to allow the reaction to be run at higher temperatures. Again, this failed to provide any cyclised product, returning only diol in almost quantitative yield. Further screening reactions using diol **290** are summarised in **Table 5.3**.



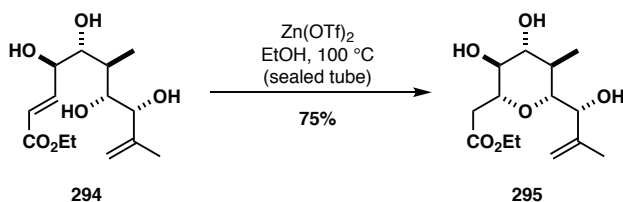
**Scheme 5.27:** Acetonide removal and attempted cyclisation of **288**.

With *p*-TsOH failing to produce any of the desired THP, a series of protic carboxylic acid derivatives were investigated (entries 8 – 10). Such conditions have been used successfully in many IOCC reactions, for instance in Clarke’s phorbazole A fragment synthesis.<sup>87,156</sup> Application of these conditions again led to complete recovery of starting material.

**Table 5.3:** Screening conditions for the attempted IOCC.

Entry	Reagent	Solvent	Temperature	Time	Result
1	p-TsOH (0.1 eq)	CH <sub>2</sub> Cl <sub>2</sub>	rt	24 h	290
2	p-TsOH (0.1 eq)	CH <sub>2</sub> Cl <sub>2</sub>	Reflux	24 h	290
3	p-TsOH (0.1 eq)	DCE	Reflux	48 h	290
4	CSA (0.1 eq)	CH <sub>2</sub> Cl <sub>2</sub>	rt	24 h	290
5	CSA (0.1 eq)	CH <sub>2</sub> Cl <sub>2</sub>	Reflux	24 h	290
6	DOWEX-w50	CH <sub>2</sub> Cl <sub>2</sub>	rt	72 h	290
7	DOWEX-w50	CH <sub>2</sub> Cl <sub>2</sub>	Reflux	72 h	290
8	AcOH (1 eq)	MeOH:THF	rt	24 h	290
9	TfOH (0.01 eq)	CH <sub>2</sub> Cl <sub>2</sub>	-78 °C to -20 °C	72 h	290
10	TFA (0.1 eq)	CH <sub>2</sub> Cl <sub>2</sub>	-78 °C to +20 °C	6 h	290
11	Zn(OTf) <sub>2</sub>	EtOH	80 °C (sealed tube)	8 h	290 + 291
12	Zn(OTf) <sub>2</sub>	MeOH	80 °C (sealed tube)	8 h	290
13	Sc(OTf) <sub>2</sub>	MeOH	80 °C (sealed tube)	8 h	Decomposition
14	KOtBu (1 eq)	THF	-78 °C	18 h	290
15	KOtBu (2 eq)	THF	-78 °C	18 h	290
16	KOtBu (1 eq)	THF	rt	5 h	290 + 291
17	KOtBu (0.1 eq)	THF	rt	5 h	290
18	DBU	Xylenes	Reflux	60 h	290
19	DBU	Xylenes	100 °C (sealed tube)	18 h	290 + 291
20	NaH (1 eq)	THF	rt	5 h	290 + 291

In Ley's synthesis of spongistatin II, similar difficulties were encountered with cyclisation of the highly substituted intermediate **294** leading to a wide range of Lewis acids being screened (**Scheme 5.28**).<sup>157</sup> Of the various metal triflates explored, Zn(OTf)<sub>2</sub> was found to give excellent conversion, providing **295** in 75% yield as a single isomer. Encouraged by this result, linear precursor **290** was subjected to similar conditions (entries 11 to 13). Zn(OTf)<sub>2</sub>/EtOH initially looked promising, with TLC showing complete consumption of the starting material after 8 h, however this was a result of transesterification to the corresponding ethyl ester. The reaction was repeated in MeOH to suppress the transesterification, leading to the clean recovery of **290** with no obvious degradation. Interestingly, Sc(OTf)<sub>2</sub> caused complete degradation of the molecule to a complex mixture of products, with LCMS suggesting fragmentation of the carbon chain based on the mass ions observed.



**Scheme 5.28:** Lewis acid mediated cyclisation of **294** en route to spongistatin II (Ley).<sup>158</sup>

Changing tact from the above acid-mediated cyclisations, a series of basic conditions were instead investigated. KOtBu was initially targeted, as the most precedent exists for its use in oxy-Michael cyclisations.<sup>82</sup> It should be noted however that unlike the acid catalysed IOCC, which predominantly gives 2,6-cis THPs, the base catalysed reaction can lead to either diastereomer, and as such a priori there was no guarantee that if the molecule did cyclise it would lead to the desired configuration at C21.

Both alkoxide bases (entries 14 to 17, 20) and organic bases (entries 18 and 19) were investigated. As previously, the cyclisation failed to occur, however an additional product was observed which was attributed to migration of the O26 benzoate onto the adjacent O25. This result was highly unusual, with benzoates generally not observed to migrate unlike the corresponding acetates.<sup>140</sup> This benzoate migration was clearly a liability, as once O25 was esterified, cyclisation would no longer be able to take place. Removal of the benzoate from **290** and subsequent treatment with the conditions used in entries 15, 18 and 20 (**Table 5.3**) did not provide access to the desired THP.

The use of an IOCC to forge the C18 – C27 THP was looking increasingly unlikely at this stage. Although the proposed cyclisation was always anticipated to be challenging, it was expected that conditions could be found that would form some of the desired product, providing a basis for further optimisation. The disappointing lack of reactivity observed here, coupled with Haslett's inability to cyclise a linear precursor using Tsuji-Trost chemistry (see §2.3.1) may

indeed point to a deeper barrier to the cyclisation in general, rather than being linked to the particular set of conditions chosen.

### 5.3.2 COMPUTATIONAL INVESTIGATIONS

Computational studies were initiated with the aim of diagnosing the observed lack of reactivity encountered above. In attempting to rationalise the lack of THP formation, two possibilities were considered:

- Kinetics (activation energies):

The most likely factor affecting cyclisation is the energy of the necessary transition states. It may be the case that the transition states leading to the THP are sufficiently high in energy that they are inaccessible, even at elevated temperatures such as those used when investigating Ley's spongistatin II conditions.

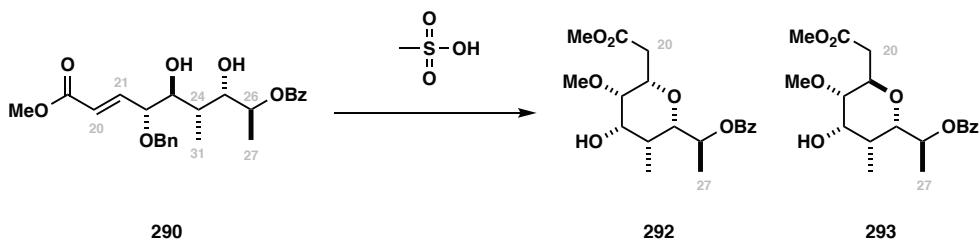
- Thermodynamics:

The lack of THP formation could also be explained if the products were higher in energy than the starting material. Thus, assuming the reaction was under thermodynamic control (which is likely in the cases using elevated temperatures / sealed tubes), the reaction would mostly give starting material. This was considered less likely, as even if this were to be the case, one would expect to isolate a mixture of starting material contaminated with the THP which would be evident from NMR analysis.

The calculations were conducted using the same methodology previously outlined for the western fragment (see §3.3.2.1), however the additional complexity of the C19 – C27 fragment coupled with limited computational resources meant that additional simplifications had to be imposed, namely that the calculations were carried out in the gas-phase without the inclusion of implicit solvent. The lack of solvent is not anticipated to change the qualitative results of the calculations; however, it should be noted that gas-phase calculations tend to over-emphasise the magnitude of non-covalent interactions, which may make some structures appear more stable than they may otherwise be if solvated.

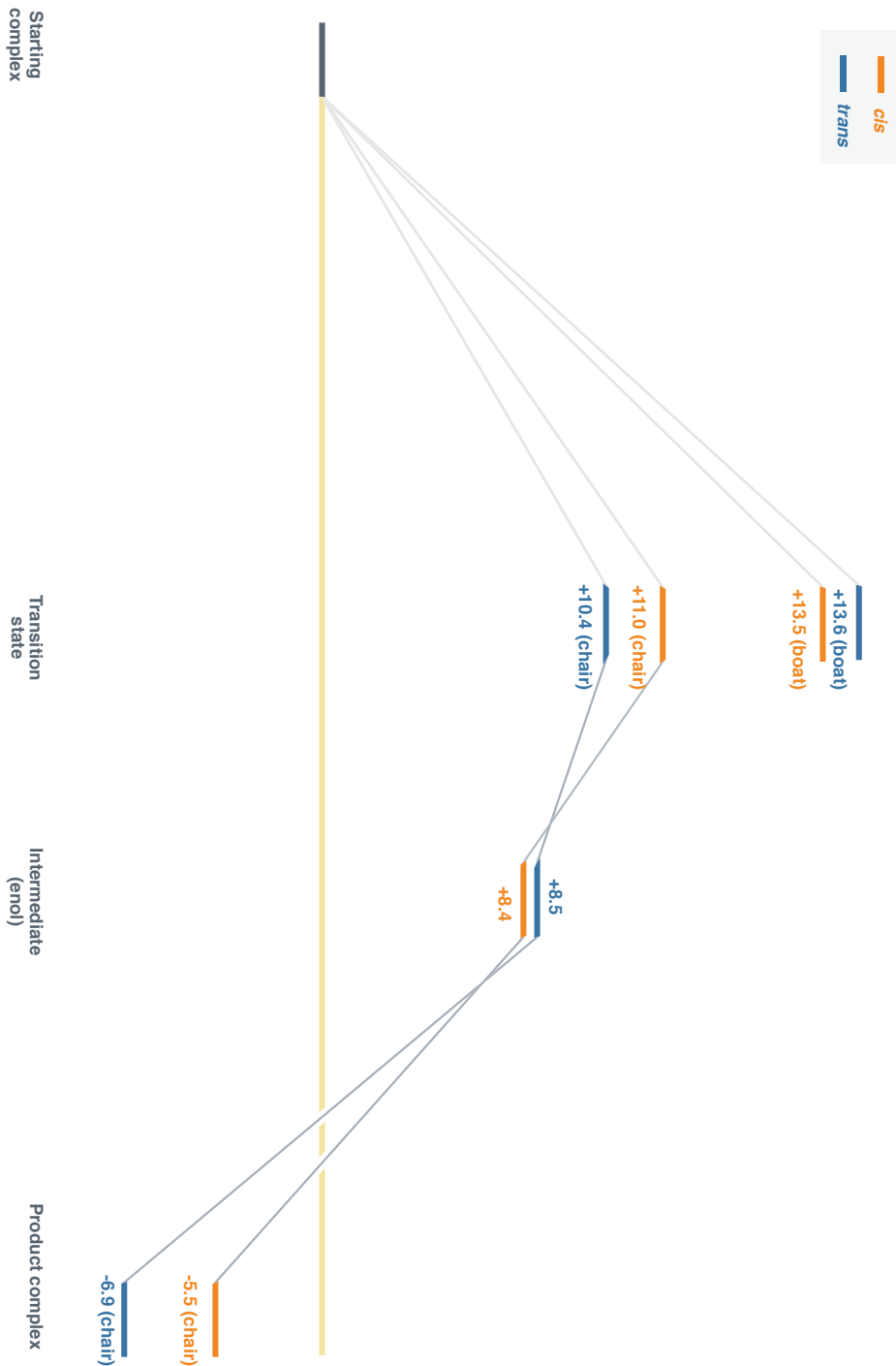
The acid mediated cyclisation was the first to be investigated as it most closely resembled the calculations carried out in the western IOCC. The exact reaction studied is shown in **Figure 5.30**. Although explicit MsOH was used in the calculations, the results should be equally valid for any of the sulfonic or carboxylic acids screened, all of which have the ability to bind in a bidentate fashion as was observed during the western fragment cyclisation. **Scheme 5.31**

shows the complete energy profile for the above reaction, with structures of the transition states provided in **Figure 5.1**.



**Scheme 5.29:** MsOH mediated cyclisation of **290** used as the basis for computational investigations.

Accordingly, the acid-mediated cyclisation of **290** is predicted to occur via the diastereomeric chair-like transition states **TS-296** and **TS-297**, with the small energy gap (0.6 kcal/mol) suggesting that the cyclisation would be unlikely to occur with high levels of diastereoselectivity. Additionally, the MsOH is predicted to act as a ‘proton shuttle’, coordinating to both O<sub>25</sub> (the nucleophilic hydroxyl) and the protonated carbonyl of the Michael acceptor.



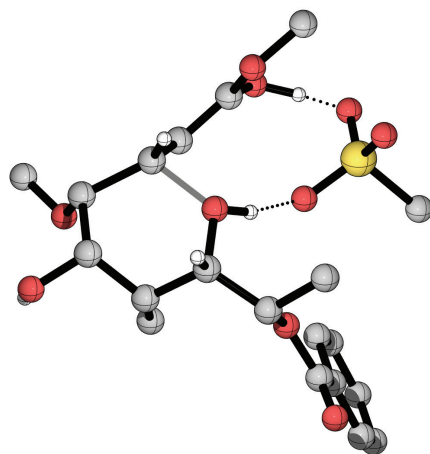
**Scheme 5.30:** Energy diagram for the MsOH mediated IOCC showing the lowest energy pathways to 2,6-*cis* (orange) and 2,6-*trans* (blue) products. All energies given in kcal/mol relative to the complex of 290 and MsOH (DFT-B3LYP/6-31G\*\*+, gas-phase).

**TS-296**

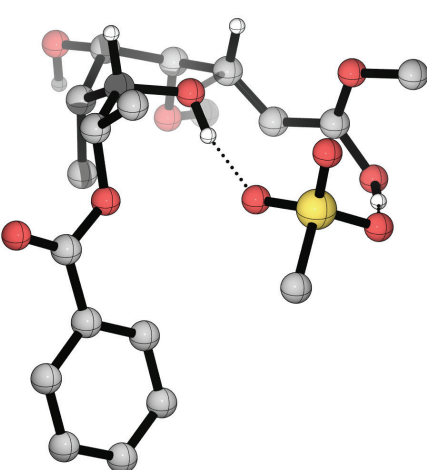
TS\_chair\_cis

+11.0 kcal/mol

Top:



Side:

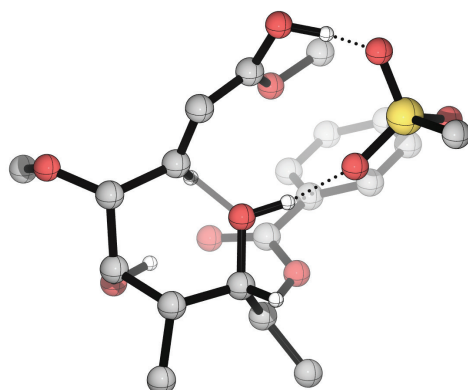


**TS-297**

TS\_chair\_trans

+10.4 kcal/mol

Top:



Side:

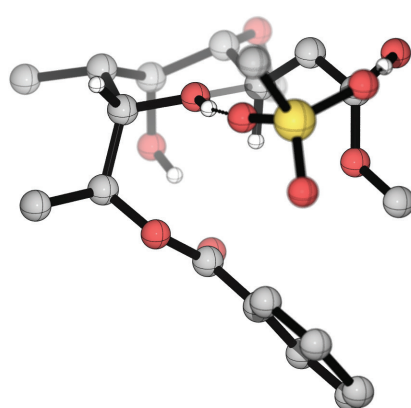
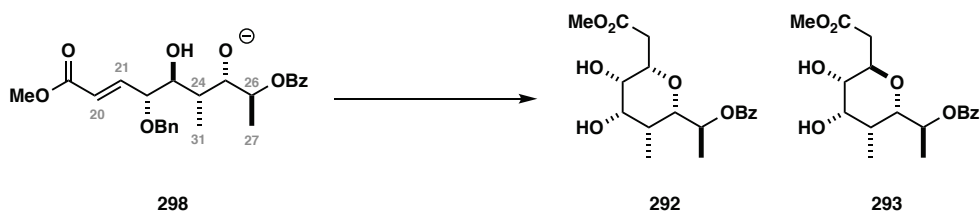


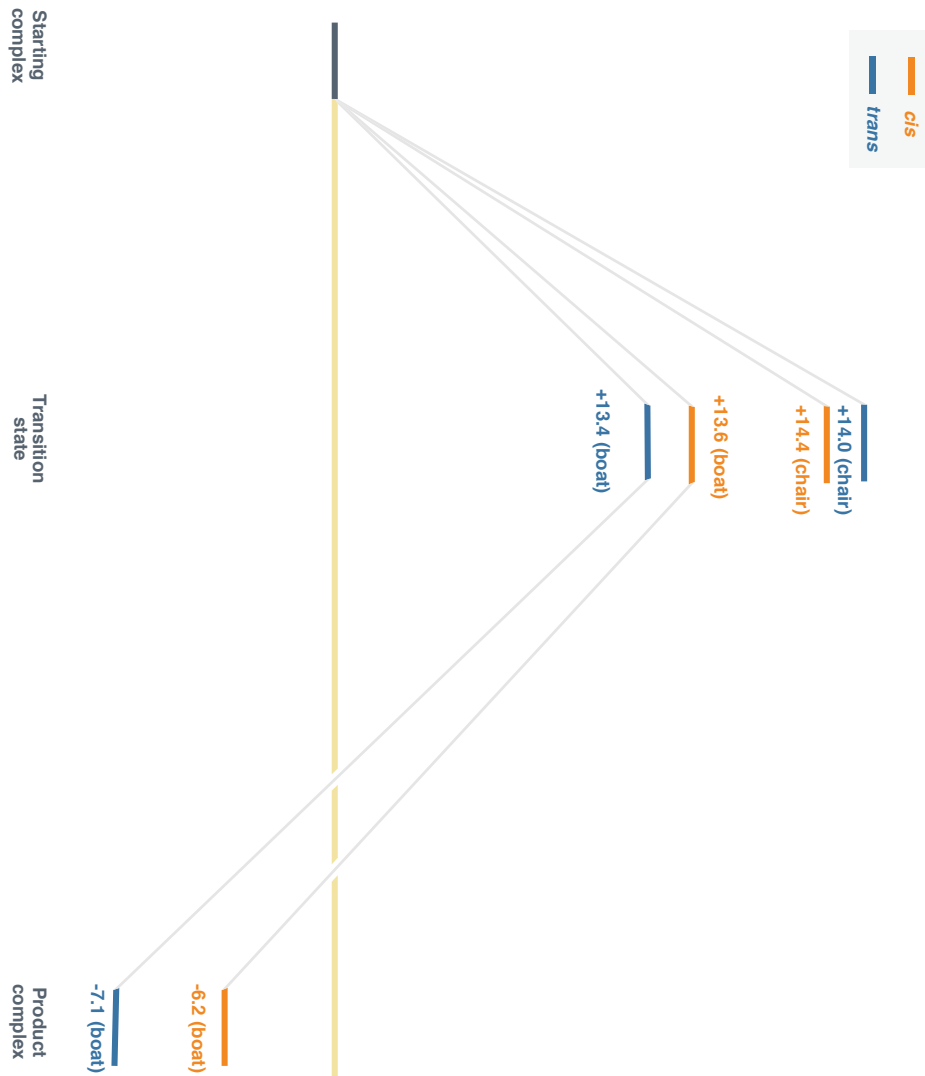
**Figure 5.1:** Chair-like transition states for the *p*-TsOH mediated IOCC. Some hydrogens have been omitted for clarity. All energies calculated relative to **174** (DFT-B3LYP/6-31G\*\*+, gas-phase).

Studying the base-mediated cyclisation computationally introduced some additional problems. Firstly, unlike the acid-mediated conditions, where MsOH, TsOH, TfOH etc can all bind via a similar motif (discussed above), the bases studied are not so similar – no comparison can be made between DBU and sodium hydride. Secondly, several of the bases screened contain metallic counterions (K and Na) which are not described well by molecular mechanics owing to the ionic nature of the bonds formed. For simplicity, the base was eschewed entirely, instead studying the cyclisation of the naked anion **298**. **Scheme 5.31** shows the complete energy profile, with structures of the transition states provided in **Figure 5.2**.



**Scheme 5.31:** base mediated cyclisation of **298**.

The base-mediated cyclisation of **298** is predicted to occur via the diastereomeric boat-like transition states **TS-299** and **TS-300**, with the small energy gap (0.2 kcal/mol) again suggesting that the cyclisation would be unlikely to occur with high levels of diastereoselectivity. As expected, the base-mediated cyclisation is predicted to occur dominantly through a boat-like transition state owing to a hydrogen bonding interaction between the C23 hydroxyl and the nucleophilic alkoxide at C25.



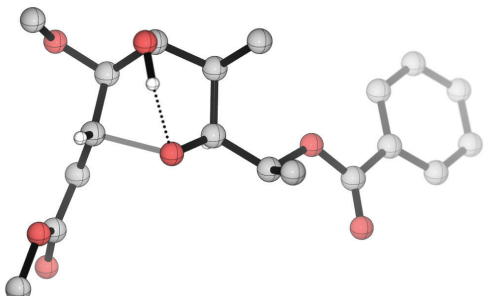
**Scheme 5.32:** Energy diagram for the base mediated IOCC showing the lowest energy pathways to 2,6-*cis* (orange) and 2,6-*trans* (blue) products. All energies given in kcal/mol relative to anion **298** (DFT-B3LYP/6-31G\*\*+, gas-phase).

**TS-299**

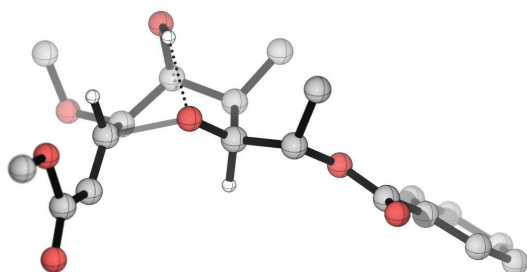
TS\_boat\_trans

**+13.4 kcal/mol**

Top:



Side:

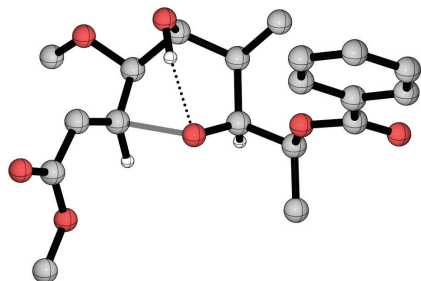


**TS-300**

TS\_boat\_cis

**+13.6 kcal/mol**

Top:



Side:

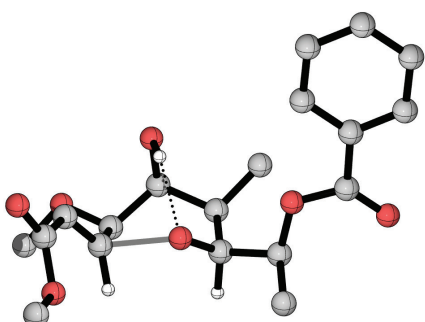


**Figure 5.2:** Chair-like transition states for the base mediated IOCC. Some hydrogens have been omitted for clarity. All energies calculated relative to **174** (DFT-B3LYP/6-31G\*\*+, gas-phase).

Comparing the reaction profiles for both the acid- and base-mediated reactions, it is not apparent where the lack of reactivity observed during the attempted IOCC arises. In both, the products are sufficiently lower in energy than the starting material (-6.9 and -7.1 kcal/mol for the 2,6-*cis* THP) to be thermodynamically preferred, although, in both cases it should be noted that the 2,6-*trans* THP is preferred over the 2,6-*cis*. Notably, the transition states for both acid- and base-mediated reactions are lower in energy (relatively) to those found in the western fragment cyclisation – a barrier of under 15 kcal/mol is accessible at room temperature, which precludes the need for the elevate temperatures attempted during screening reaction.

One major difference between the acid- and base-mediated cyclisations is the C21–O25 bond length in the transition state, corresponding to the developing bond. In the acid-mediated reaction the C–O bond is much shorter, representing a later transition state in which the bond is essentially formed (with the TS structure being closed in geometry to the thioenol intermediate observed). Conversely, the C–O bond in the base-mediated reaction is longer, with the TS closer to the starting material.

**Table 5.4:** C21–O25 bond lengths in IOCC transition states:

	Acid-mediated	Base-mediated
<i>cis</i> TS	1.85	2.01
<i>trans</i> TS	1.89	1.99

Given that the transition state energies and thermodynamic preferences of the reactions do not appear to elucidate the lack of reactivity, a different rationalisation is clearly needed. One plausible conclusion is that the lack of reactivity observed during cyclisation of linear precursor **290** may be the result of a high energy barrier preventing the molecule from adopting the required conformation for effective orbital overlap. The calculations conducted on the linear system only take into account the difference in relative energy between the starting material complex and the transition states, but do not account for the energy required to connect the two points (the energy-gap between two stationary points is independent of the path taken between them). While comprehensive analysis of the energy landscape is possible for small molecules ( $\text{H}_2\text{O}$ ,  $\text{CO}_2$ , etc), as the molecule becomes more flexible, the number of possible permutations makes the process uneconomical and difficult to visualise.\* Despite this, the point may be illustrated by considering rotation about two of the central dihedral angles required to fold the molecule into the reactive conformation, as shown in

\* This is the same reason why systematic conformational searching (which would give the desired information) was abandoned in favour of ‘random’ Monte Carlo based methods.

**Figure 5.3.** This two-dimensional coordinate scan, while not exhaustive, shows regions of high energy (red), representing barriers to conformational flexibility which may prevent the molecule from converting from the ground state conformation of the starting material to the necessary conformation for the transition state.

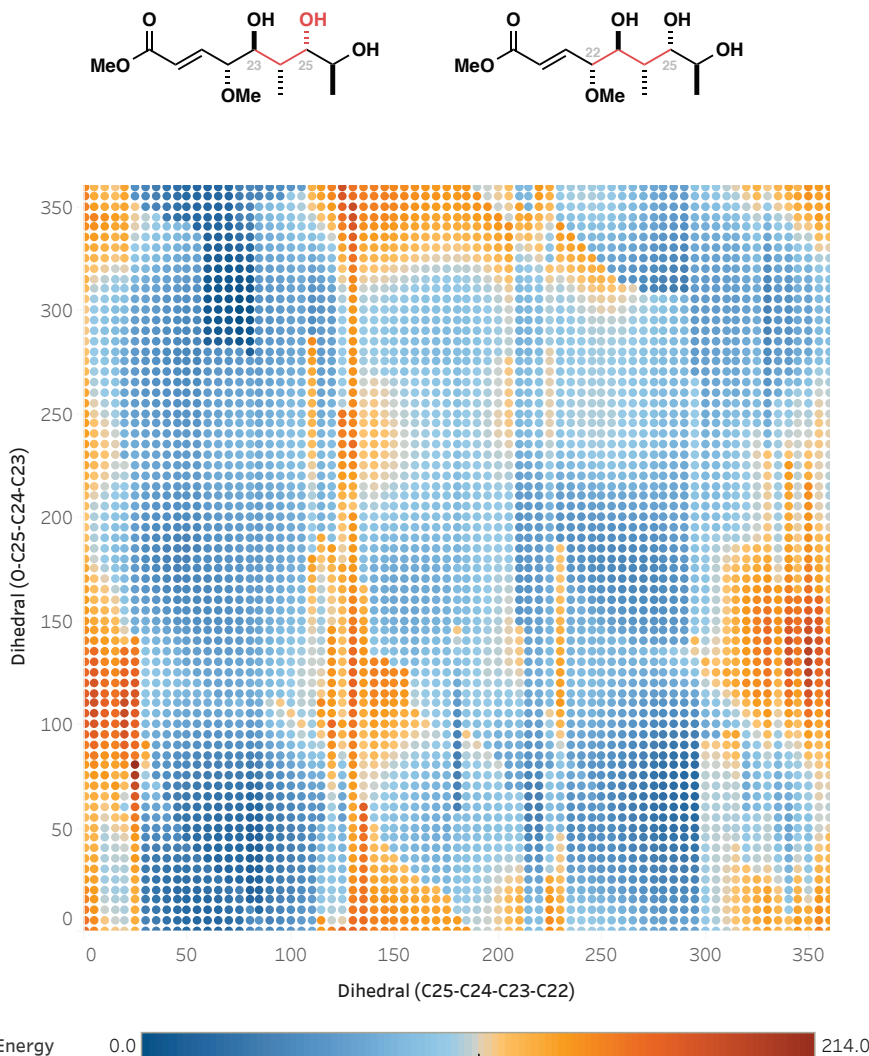


**Figure 5.3:** Contour plot showing a two-dimensional coordinate scan of linear precursor **290**. All energies in kJ/mol relative to the lowest energy conformer. Bonds in red indicate the torsional angles scanned. [MMFF-94, gas-phase].

### 5.3.3 CONSTRAINED CYCLISATION

It was hoped that by constraining the linear precursor, it would be possible to ‘lock’ the molecule into a more reactive conformation from which cyclisation could occur. For this approach to be successful, it was vital that the conformationally-controlling element did indeed hold the C25-hydroxyl in good proximity to the C21 enoate to ensure that the stereoelectronic requirement for orbital overlap be possible.

Acetonide **301** was identified as a possible substrate for the constrained cyclisation, with bis-protection of the C22/C23 diol enforcing a mutually *cis* arrangement of the two sidechains (**Figure 5.4**). The choice of the acetonide was somewhat arbitrary, and indeed if successful it may be necessary to replace the acetonide with another protecting group such as a PMP acetal or di-*t*-butylsilylene as these are able to be cleaved to give mono-protected products, avoiding the potential for regioselectivity issues upon fragment union.

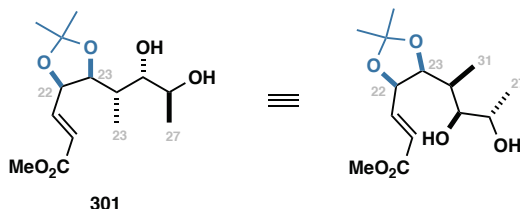


**Figure 5.4:** Proposed constrained precursor **300** to investigate whether ‘locking’ the conformation of the starting material would promote cyclisation.

Prior to commencing synthetic work, the feasibility of this approach was investigated computationally to ensure that in restricting the conformation the reactive groups weren’t held in such a geometry as to completely prevent the possibility of cyclisation. The optimised ground-state structure of **301** is consistent with the two groups being well aligned for bond-forming, as depicted in **Figure 5.5**. An analogous coordinate scan was also conducted to determine if the molecule had free rotation about the key bonds needed to perturb the geometry of the structure into a form amenable to cyclisation. Interestingly, unlike the completely linear substrate **290**, the constrained substrate appears to be more able to rotate about its key dihedral angles, allowing it to adopt a different conformation without incurring the penalty of unfavourable energetics.

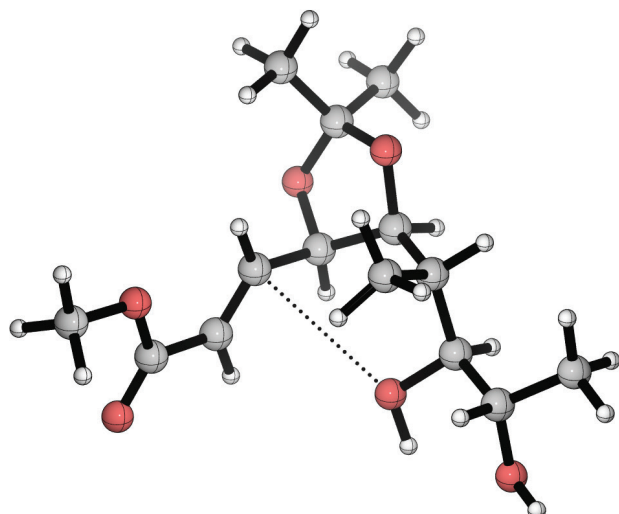


**Figure 5.5:** Lowest energy conformation of acetonide **301** showing the proximity of the C25-hydroxyl to the C21 enoate. [DFT-B3LYP/6-31G\*\*, gas-phase].

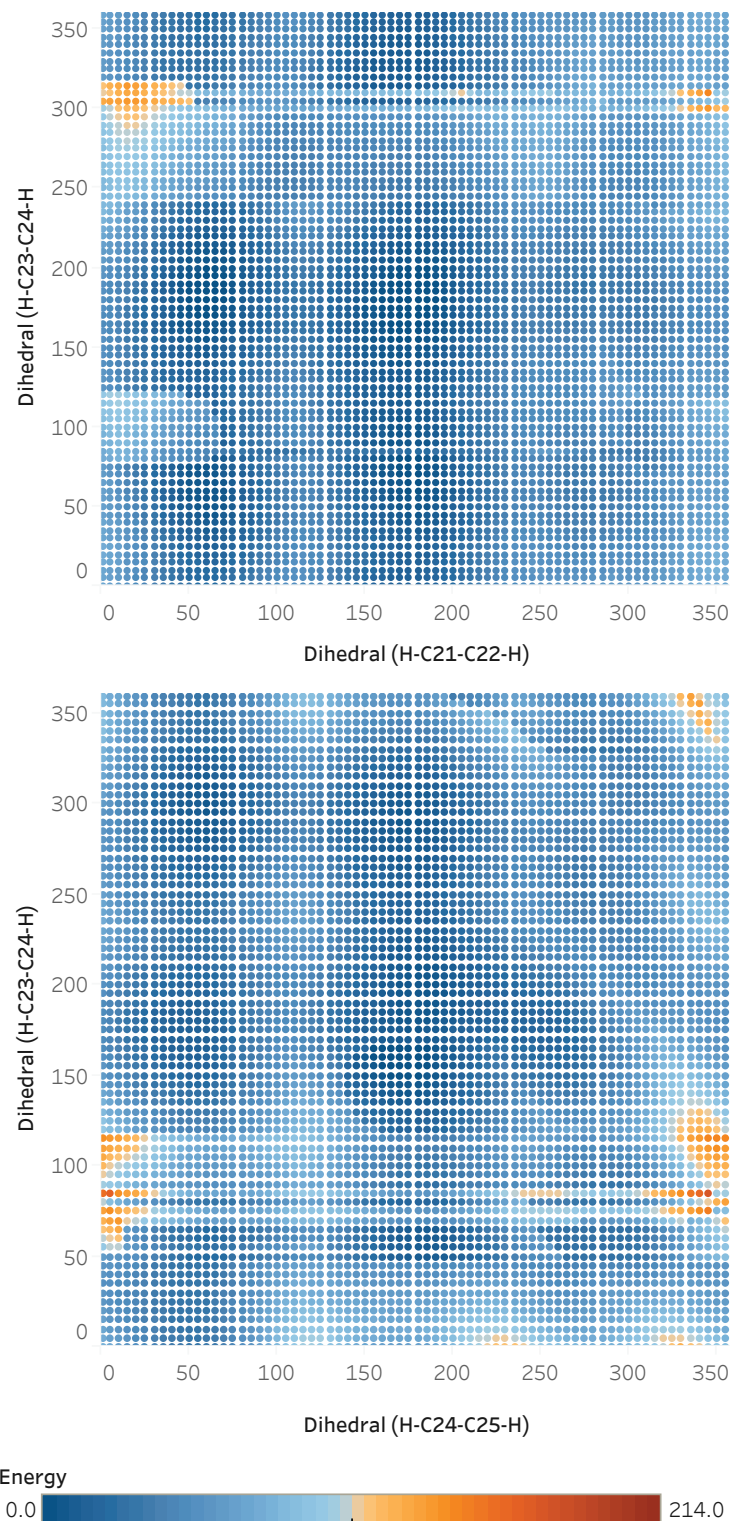
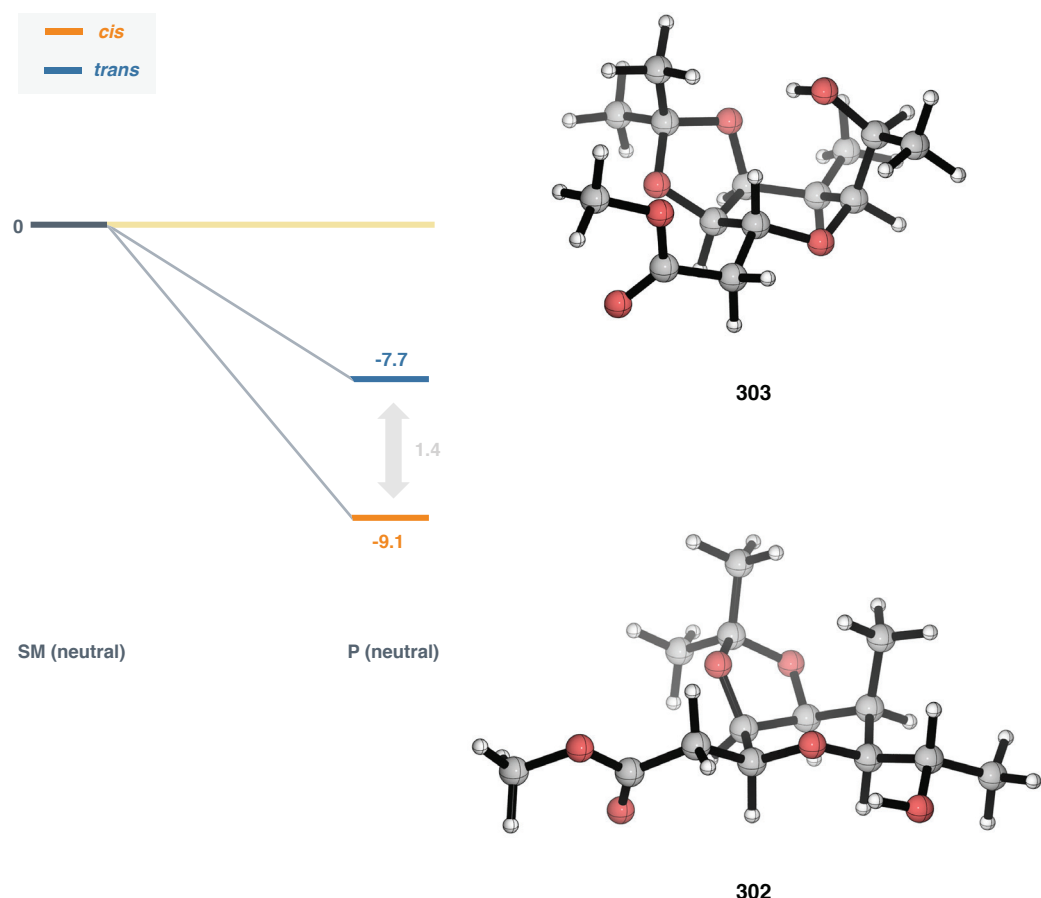


**Figure 5.6:** Contour plot showing two-dimensional coordinate scans of constrained precursor **301**. All energies in kJ/mol relative to the lowest energy conformer. [MMFF-94, gas-phase].

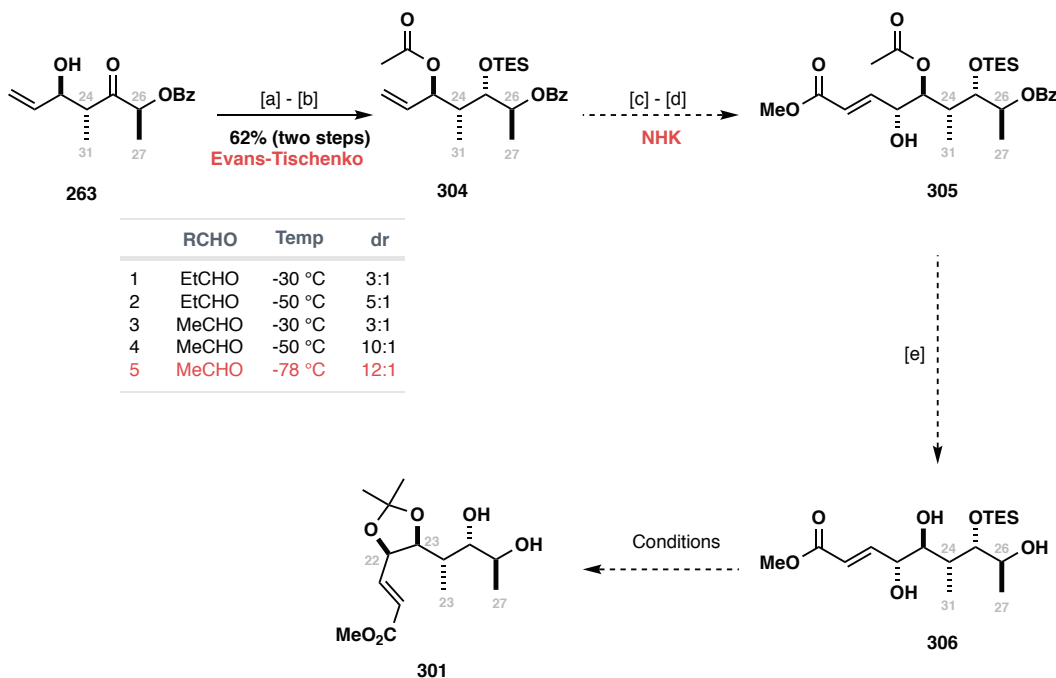
In addition to considering the conformation of the uncyclised structure, the relative energies of the resulting *2,6-cis* and *2,6-trans* THP products were computed (**Scheme 5.33**). Gratifyingly, the *2,6-cis* product **302** is ca. 1.4 kcal/mol lower in energy than the corresponding *trans* isomer **303**, with both structures adopting half-chair-like structures in order to accommodate the geometry of the acetonide.



**Scheme 5.33:** Energy diagram showing the energies of *2,6-cis* (orange) and *2,6-trans* (blue) products. All energies relative to neutral starting material **301** [DFT-B3LYP/6-31G<sup>\*\*</sup>, gas-phase].

The attempted synthesis of **301** commenced from the previously described lactate aldol adduct **263**. In order to arrive at the desired 1,2-acetonide as a single isomer, it was necessary to ensure that the O23 and O25 remained differentiated. This precluded the use of the Evans-Saksena reduction previously used to effect this transformation, however the related Evans-Tischenko reduction was ideal, selectively esterifying the pre-existing C23 hydroxyl with concomitant introduction of the 1,3-*anti* relationship between C23 and C25. Initial attempts at the Evans-Tischenko reduction of **301** led to complex mixtures, attributed to both poor diastereoselectivity and migration of the acetate/propionate ester to the adjacent oxygen. In the event, these issues were able to be fixed by lowering the temperature to -78 °C and

immediately protecting the crude product with TESOTf/2,6-lutidine prior to column chromatography.

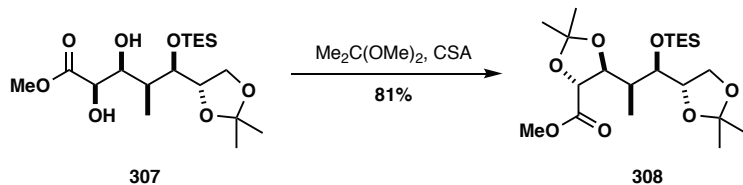


**Reagents & conditions:** [a]  $\text{SmI}_2$ , MeCHO, -78 °C, THF. [b] TESOTf, 2,6-lutidine,  $\text{CH}_2\text{Cl}_2$ . [c]  $\text{O}_3$ ,  $\text{CH}_2\text{Cl}_2$ , MeOH, -78 °C, [d]  $\text{NiCl}_2/\text{CrCl}_2$ , 259, DMF:THF, rt. [e] MeOH,  $\text{K}_2\text{CO}_3$ , rt.

**Scheme 5.34:** Attempted preparation of constrained cyclisation precursor **301**.

With access to **304** secured, attention was turned to the NHK reaction used to forge the C20 – C21 bond. Prior experience had suggested that this was likely to be a challenging reaction, with various conditions often needing to be screened to identify suitable reaction conditions. Following the previously established conditions, **304** was converted to the corresponding aldehyde via ozonolysis, which was used directly in the NHK. Unfortunately, this failed to provide access to **305** in synthetically useful quantities. Significantly, the major product from the reaction, while having the correct molecular weight by HRMS failed to show the presence of any olefinic protons. Closer inspection of 1D and 2D NMR spectra revealed two carbonyls esters: the expected benzoate, and an additional ester lacking the unsaturation that would be expected within **305**. Further evidence for the lack of the olefin was provided by the HSQC, which showed the introduction of a diastereotopic methylene group ( $\text{CH}_2$ ) with HMBC correlations to the non-benzoate ester. While it may be tempting to infer from this that a ring had been formed, C/H21 and C/H25 showed no HMBC correlation, which is indicative of the THP formation. Time constraints prevented further investigations into this strategy, with additionally work clearly warranted to determine if the use of a conformationally constraining group will enable successful synthesis of the desired THP. If the NHK can be successfully optimised. The formation of a 1,2-acetonide in the presence of a secondary TES ether should

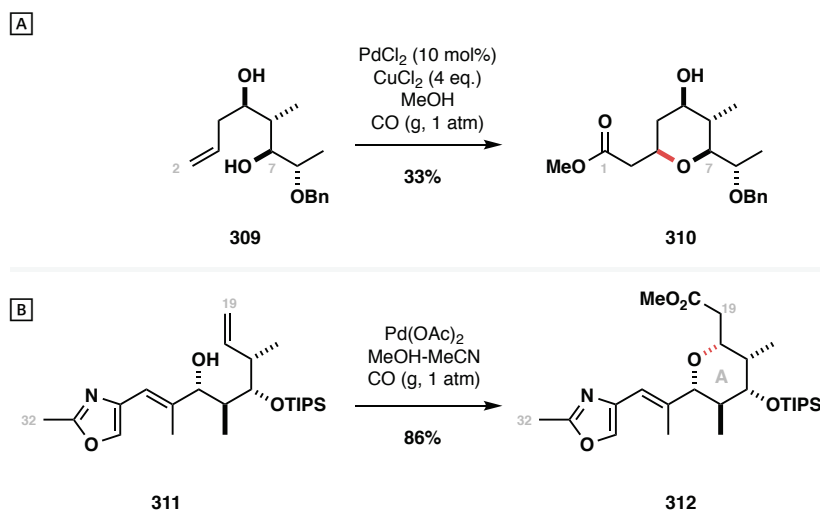
be achievable, as was recently demonstrated in the total synthesis of amphotericin B by Kalesse and co-workers (**Scheme 5.35**).



**Scheme 5.35:** Acetonide formation in the presence of a secondary TES ether in the total synthesis of amphenidolide H (Kalesse).<sup>159</sup>

PALLADIUM-CATALYSED CARBONYLATIVE CYCLISATION

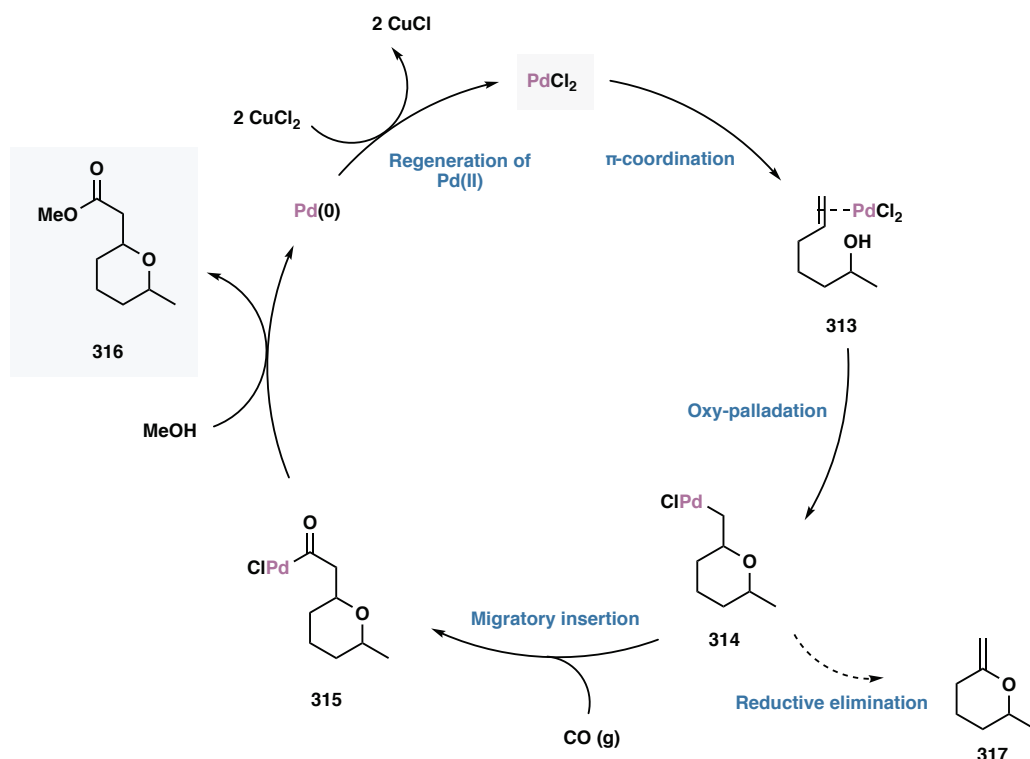
In 2017, Romea and co-workers reported a total synthesis of the marine natural product (+)-herboxidiene. During this work, a palladium (II) catalysed carbonylative cyclisation of homoallylic alcohol **309** was investigated as an alternative to an IOCC, obviating the need for installation of a Michael acceptor (**Scheme 5.36-[A]**).<sup>88</sup> Similar methodology has been applied to many complex natural products, with White's synthesis of phorboxazole A being a notable example in which a pentasubstituted 2,6-*cis* THP **312** is accessed in excellent yield (**Scheme 5.36-[A]**).<sup>160</sup> In general, these reactions are highly versatile, offering excellent substrate scope and high-levels of atom economy owing to the incorporation of CO gas and methanol to forge the desired ester.



**Scheme 5.36:** Palladium (II) catalysed carbonylative THP synthesis. **[A]** Synthesis of herboxidiene (**Romea**).<sup>88</sup> **[B]** Synthesis of the A ring of phorboxazole A (**White**).<sup>160</sup>

The general mechanism for palladium (II) mediated carbonylative THP formation is shown in **Scheme 5.37**. Following  $\pi$ -coordination, the Pd(II) complex **313** is attacked in an intramolecular sense by the tethered alcohol, closing the THP and generating an alkyl Pd(II)

species **314**. When conducted in the presence of carbon monoxide, **314** undergoes rapid migratory insertion to acyl Pd(II) species **315** which is finally trapped by MeOH (the solvent) to provide the product **316**. The acyl Pd(II) species **315** is highly versatile, allowing access to esters, aldehydes and carboxylic acids depending on the solvent system/reagents used. Finally, the reaction may be rendered catalytic in Pd by addition of stoichiometric oxidant which facilitates the re-oxidation of Pd(0) to Pd(II). The reaction reliably gives access to the 2,6-cis diastereomer owing to the preference for the Pd to adopt a pseudoequatorial position in the transition state.



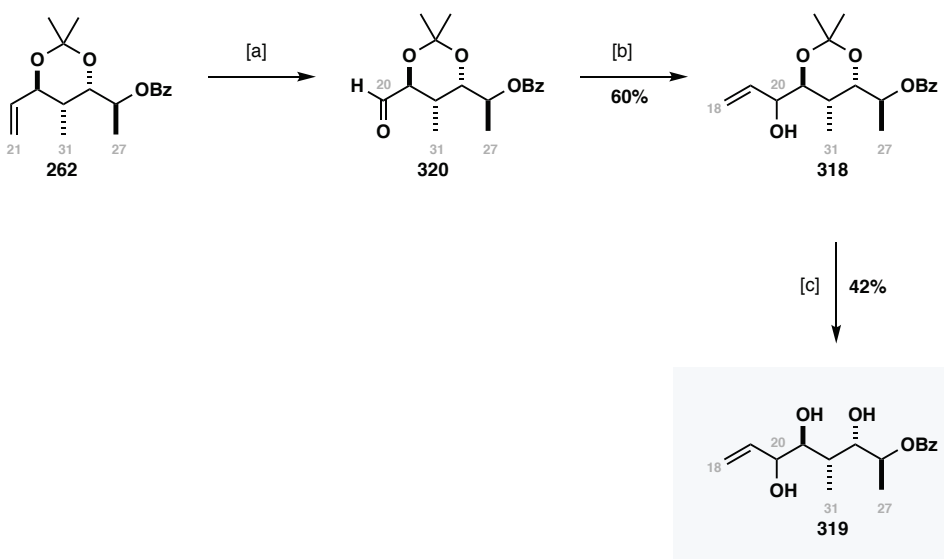
**Scheme 5.37:** Mechanism for the Pd(II)-mediated carbonylative cyclisation for the synthesis of THPs.

This Pd(II)-mediated carbonylative cyclisation offers a mechanistically distinct strategy to the IOCC strategy. As the Pd – alkene complex is formed reversibly, the molecule linear substrate should be better able to adopt the necessary conformation, with the Pd only binding equatorially. The introduction of a metal may also enable some pre-organisation of the system, with the Pd able to simultaneously interact with the olefin (via the pi-orbital) and the oxygen (via a lone pair).

Given the tentative nature of this approach and limited time available for studies, it was necessary to diverge from a previously established intermediate. A suitably functionalised substrate **318** had been prepared during early studies into the eastern THP. Allylic alcohol **318** was prepared through a two-step process from alkene **262** (**Scheme 5.38**. See §5.3 for preparation of **262**). Elaboration using ozonolysis followed by addition of either vinyl

magnesium bromide or divinyl zinc to the ensuing aldehyde **320** provided allylic alcohol **318** which was deprotected using PPTS/MeOH to give a suitable precursor **319** for the anticipated cyclisation.

This route was not investigated further at the time as the C20 stereocentre was unable to be introduced with high levels of diastereoselectivity – for the necessary stereochemistry to prevail the reaction must take place without chelation. Despite this, the available stocks of **318** provided a convenient opportunity to attempt the aforementioned Pd(II) catalysed carbonylative cyclisation to see if this approach was viable in the context of madeirolide A. If successful, it was anticipated that the resulting diastereomers may be separable,\* with future preparation of allylic alcohol **318** as a single isomer possible through an oxidation-reduction sequence or modification of the protecting group strategy to bias the organometallic addition against chelation control. Specifically, the use of a silyl ether on O21 would enforce Felkin-Anh control.



**Reagents and conditions:** [a]  $O_3$ ,  $NaHCO_3$ ,  $MeOH$ ,  $CH_2Cl_2$ ,  $-78^\circ C$ ;  $Me_2S$ . [b]  $(H_2C=CH)_2Zn$ ,  $THF$ ,  $-78^\circ C$ . [c] PPTS,  $MeOH$ , rt.

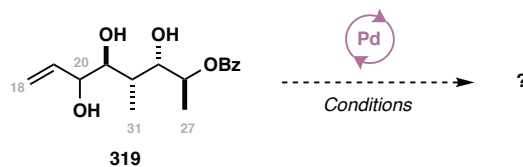
**Scheme 5.38:** Preparation of cyclisation precursor **319** from olefin **262**.

Having procured access to **319**, the cyclisation could be attempted; the results of the screening experiments are summarised in **Table 5.5**. Romea's herboxidiene conditions (**Table 5.5**, Entry 1) failed to affect the cyclisation. Increasing the catalyst loading to 50 mol% (**Table 5.5**, Entry 2) also led to the re-isolation of starting material in near-quantitative yield. The most promising result was obtained when both the catalyst and oxidant loading were increased

\* The cyclisation product may be a crystalline solid and may be amenable to recrystallization on larger scales (based on similar lactate aldol products).

(**Table 5.5.** Entry 3); after 3 h, the starting material had been completely consumed by TLC, giving rise to a complex mixture of products.

**Table 5.5:** Attempted [Pd] catalysed carbonylative cyclisation of **319**.



Entry	[Pd] source	Eq. [Pd]	Oxidant	Eq. oxidant	Comments
1	PdCl <sub>2</sub>	0.2	CuCl <sub>2</sub>	4.0	No reaction
2	PdCl <sub>2</sub>	0.5	CuCl <sub>2</sub>	4.0	No reaction
3	PdCl <sub>2</sub>	0.5	CuCl <sub>2</sub>	8.0	Complex mixture

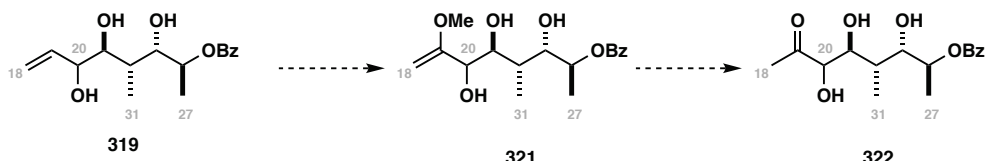
All reactions run at rt in MeOH (0.3 M in substrate) under 1 atm of CO / CO<sub>2</sub> dried through CaCl<sub>2</sub> (g)

The components of the complex mixture were unable to be cleanly separated, however a partial assignment of the major product was possible using 2D NMR. The <sup>13</sup>C shifts (obtained indirectly via HMBC and HSQC correlations) were highly diagnostic, confirming the absence of the terminal alkene, and showing the presence of two carbonyls: the pre-existing benzoate ester ( $\delta_{\text{C}} = 173$  ppm), and what is likely to be a ketone ( $\delta_{\text{C}} = 210$  ppm).\* Additionally, HRMS analysis of the major product was able to determine the unsaturation present in the molecule. The observed parent ion at 328.1751 m/z is consistent only with a molecular formula of C<sub>16</sub>H<sub>26</sub>O<sub>6</sub>N, corresponding to [M+NH<sub>4</sub>]<sup>+</sup>, and requiring six degrees of unsaturation be present within the molecule. This suggests that the product is acyclic, given that the benzoate ester already accounts for five degrees of unsaturation in addition to the putative ketone observed in the <sup>13</sup>C NMR. Additionally, the molecular formula is consistent with the introduction of an additional oxygen relative to that of the starting material **319**, however from NMR alone it is not possible to determine whether this oxygen has been incorporated from the methanol or the carbon monoxide.

One plausible side-reaction is the Wacker-type oxidation of the terminal alkene to give the putative  $\alpha$ -hydroxy ketone **322**. The oxidation of simple alkenes to the corresponding methyl ketones is known,<sup>161,162</sup> however the reactions are often slow, and require heat to drive the reaction. Romea indicates that a similar oxidation may have taken place during work on

\* Copies of relevant NMR spectra are provided in Appendix B for reference.

herboxidiene, blaming the presence of an unprotected homoallylic alcohol for the low yield of the reaction, although no by-products are identified.



**Scheme 5.39:** Plausible Wacker-type oxidation of **319** to convert terminal olefin into methyl ketone **322**.

Disappointingly, the data is not consistent with the formation of ketone **322**, and attempts at repeating the reaction to get more material for structure elucidation have been met with failure. Despite this, the reaction still represents a mechanistically novel disconnection for the THP, and given the broad substrate scope of the reaction, and plentiful Pd(II) sources available, it may be possible to find a system that provides more promising results.

#### 5.4 SUMMARY & ANALYSIS

This chapter has explored several possible approaches for construction of the C18 – C27 eastern tetrahydropyran, however the desired C21 – O25 bond formation has yet to be realised. Based on strong literature preference, an intramolecular oxy-conjugate cyclisation (IOCC) was investigated as the best option. Synthetically, this was approached from several angles, attempting both acid- and base-mediated cyclisation of various linear precursors. The lack of reactivity was not able to be rationalised by computational evaluation of the reaction pathway, however it appears likely that the molecule is unable to adopt the required conformation for productive C – O bond formation. Based on the above findings, two more speculative approaches were investigated. Firstly, attempts were made to constrain the conformational flexibility of the molecule, and secondly, a palladium (II) catalysed carbonylative cyclisation was investigated. Neither of these investigations proved successful, however time constraints prevented their complete exploration and as such they may yet prove fruitful.

At this stage, based on the above experimental and computational studies, it appears that the cyclisation of a fully elaborated linear precursor may not be a viable way to procure access to the necessary heterocycle, possibly requiring a simplified THP precursor to be elaborated post-cyclisation. Suggestions for future work are discussed in **Chapter 6**.

Results & discussion III: synthesis of the eastern tetrahydropyran

# 6

## 6. SUMMARY & FUTURE DIRECTIONS FOR THE TOTAL SYNTHESIS OF MADEIROLIDE A

### 6.1 SUMMARY

The completed synthesis of madeirolide A **1** is yet to be realised, with the synthesis of the C19 – C27 pentasubstituted all-*cis* eastern THP proving to be a particularly formidable challenge. Despite this, several fragments of the molecule have now been completed successfully, and the studies towards the remaining fragment will serve as a solid foundation for future work. The synthetic work carried out on madeirolide A in this thesis is broken up into three segments, summarised below:

- C1 – C11 western fragment **99**:

Chapter 3 described the strategy evolution for the proposed total synthesis of madeirolide A. Addressing many of the issues encountered by Haslett, a modified fragment union strategy was proposed, changing from a ring closing macro-Stille cross-coupling to a Heck macrocyclisation. This change permitted the successful synthesis of a modified C1 – C11 western fragment **99** which was completed in 13 steps (LLS) providing a tractable route for material throughput should it be required for future studies.

Additionally, in preparation for work on the C19 – C27 eastern THP, a computational model was developed using DFT calculations to rationalise the observed reactivity and selectivity of the pivotal IOCC reaction used to close the heterocycle.

- C13 – C18 eastern fragment **197**:

Chapter 4 described investigations into the C13 – C18 fragment **197** from which the eastern THF would ultimately derive. A short asymmetric synthesis was developed,

cutting the step-count significantly relative to the initial proposal (see §5). The use of an  $\text{sp}^2 - \text{sp}^3$  Suzuki cross-coupling reaction to form the C18 – C19 bond was also validated, which is pivotal to the intended strategy for the completion of madeirolide A.

- **C19 – C27 eastern fragment 198:**

Chapter 5 described the attempted synthesis of the C19 – C27 fragment, encompassing the eastern THP. The construction of the pentasubstituted all-*cis* heterocycle has proved to be an arduous challenge, with no cyclisation achieved despite the investigation of several mechanistically different approaches. The synthesis of several linear precursors has been discussed, along with computational studies to probe the disappointing lack of reactivity. At present, the reasons behind the lack of reactivity are not apparent, with further studies needed to probe the structure-reactivity relationship further.

## 6.2 FUTURE WORK

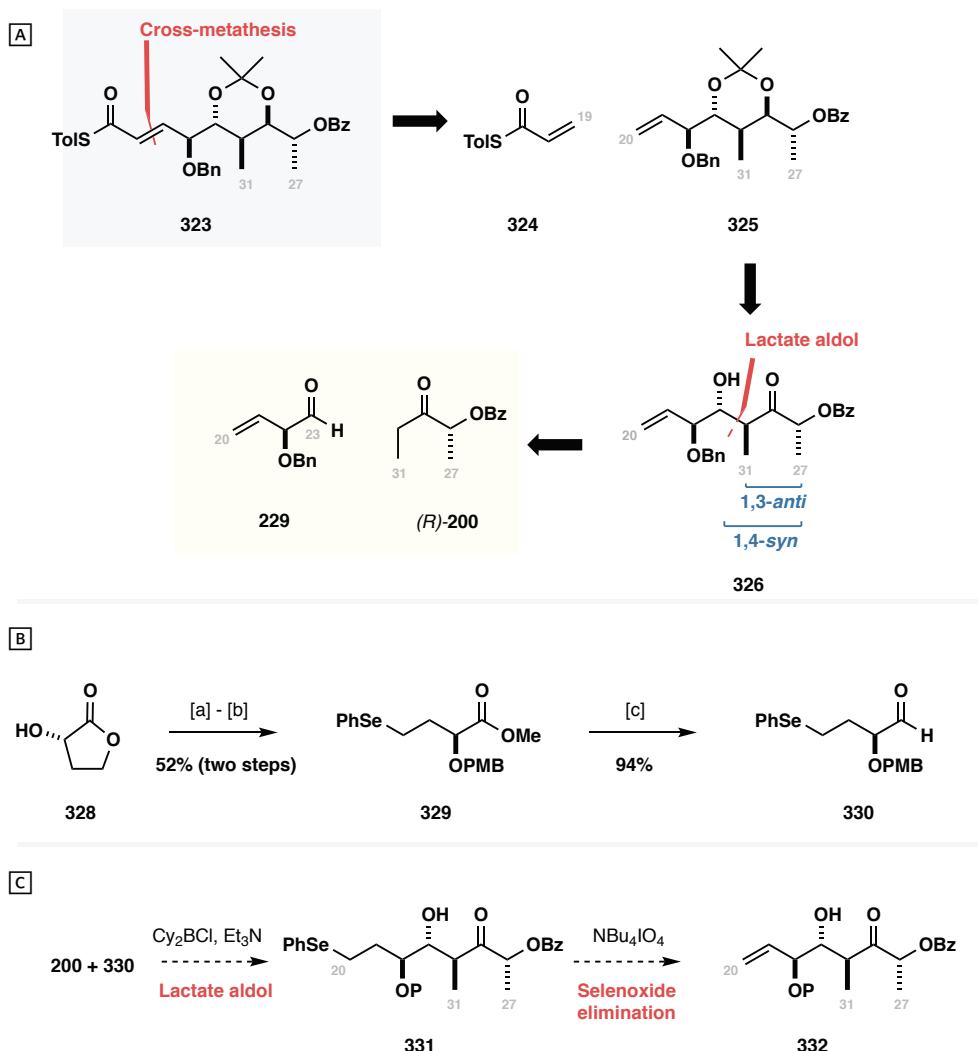
### 6.2.1 COMPLETION OF THE C12 - C27 EASTERN FRAGMENT

#### 6.2.1.1 CONSTRUCTION OF THE THP

The completion of a total synthesis of madeirolide A is contingent on the ability to procure access to the C18 – C27 fragment **100**. Although the IOCC approach has been extensively explored using a methyl ester as a Michael acceptor (see §5.3.1.4), there is still some scope for screening additional Michael acceptors as per the original plan. Specifically, thioester **323** was identified as a plausible cyclisation precursor based on the successful cyclisation carried out to forge the C21 – O25 bond of the western fragment **99** (see §3.3.2). Although computational work did not predict a marked difference in reactivity between the thioester and the methyl ester (HOMO - LUMO gap of 4.2 eV and 4.4 eV respectively), there are other examples of the thioester being significantly more electrophilic than the corresponding methyl ester.<sup>89</sup> Parenthetically, this would not preclude the methyl ester from cyclisation, but would slow down the rate of the reaction by several orders of magnitude, as was observed by Haslett.<sup>56</sup> The ability to compare the two substrates would prove beneficial to greater mechanistic understanding of the IOCC, even if it does not affect the desired cyclisation.

The inability to screen a variety of Michael acceptors was a consequence of a the protected  $\alpha$ -hydroxy- $\beta,\gamma$ -unsaturated aldehyde (**229 / 254**) causing difficulties in the lactate aldol reaction necessary to obtain the desired stereochemistry. A solution was developed by Eustache in the context of fumagillol.<sup>163</sup> To avoid the double bond moving into conjugation, a selenium derivative **330** was prepared, masking the olefin and allowing the aldol reaction to take place without the concern of the alkene migration (**Scheme 6.1-B**). Post-aldol, once the aldehyde has been converted to the alcohol, the phenylselenyl group may be eliminated to give the desired terminal olefin. While this method achieved the desired result (obtaining the aldol adduct without migration of the double bond), it would introduce several undesirable steps, notably the use of diazomethane needed to isolate ester **329\***, and the highly forcing conditions ( $\text{NBu}_4\text{IO}_4$ , reflux) needed to eliminate the phenylselenyl group to the desired alkene which may not be compatible with the other functionality present in the substrate.

\* The use of TMS-diazomethane would be a safer alternative, which may prove tractable.



**Reagents & conditions:** [a] i. PhSeSePh, NaBH<sub>4</sub>, DMF, 90 °C. ii. CH<sub>2</sub>N<sub>2</sub>, 20 °C. [b] PMB-TCA, CSA, CH<sub>2</sub>Cl<sub>2</sub>, 20 °C. [c] DIBAL, PhMe, -78 °C.

**Scheme 6.1:** **[A]** Synthetic strategy for screening Michael acceptors based on a cross-metathesis of allylic alcohol **325**. **[B]** Alternative to protected  $\alpha$ -hydroxy- $\beta,\gamma$ -unsaturated aldehyde **330** to prevent migration of the double bond (**Eustache**).<sup>163</sup> **[C]** Proposed lactate aldol incorporating aldehyde **330** which masks the  $\beta,\gamma$  alkene until after the aldol has taken place.

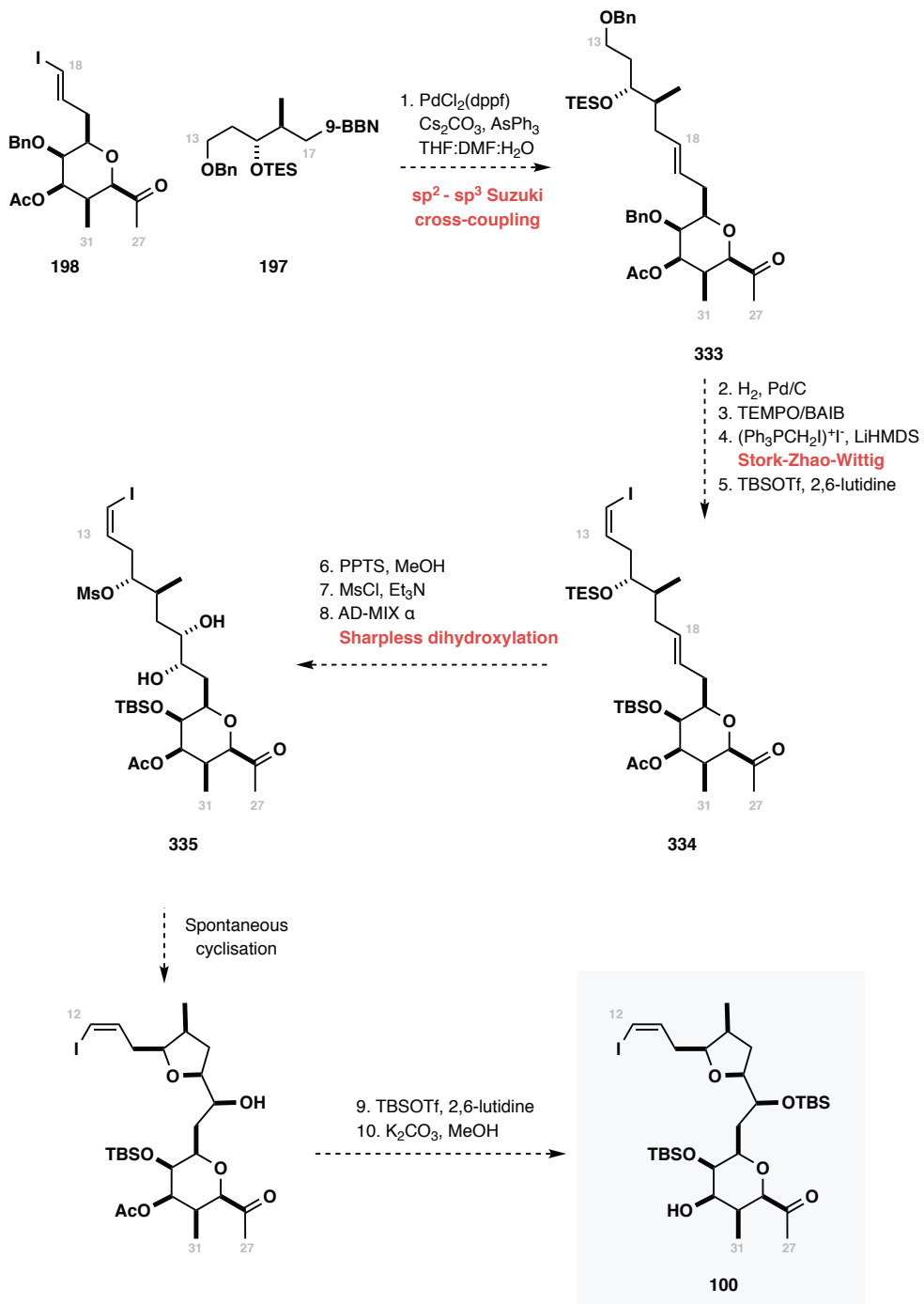
The preparation of allylic alcohol **325** as a single diastereomer would have the added benefit of permitting further investigations into the Pd(II) catalysed carbonylative cyclisation (§5.4), with initial investigations severely complicated by the epimeric mixture at C22.

The surprising lack of reactivity observed thus far (including work carried out previously by Haslett) may be indicative of a larger problem with the strategy of cyclising a fully elaborated linear precursor. Given this, it may be judicious to abandon the de novo approach to the THP ring in favour of a more stepwise approach. As described in §2.3.1.1, Fearnley was successful in developing the synthesis of a dihydropyran which lacked the C22 – C23 diol, although he

was unable to affect the necessary dihydroxylation, there is much work for future studies in this area.

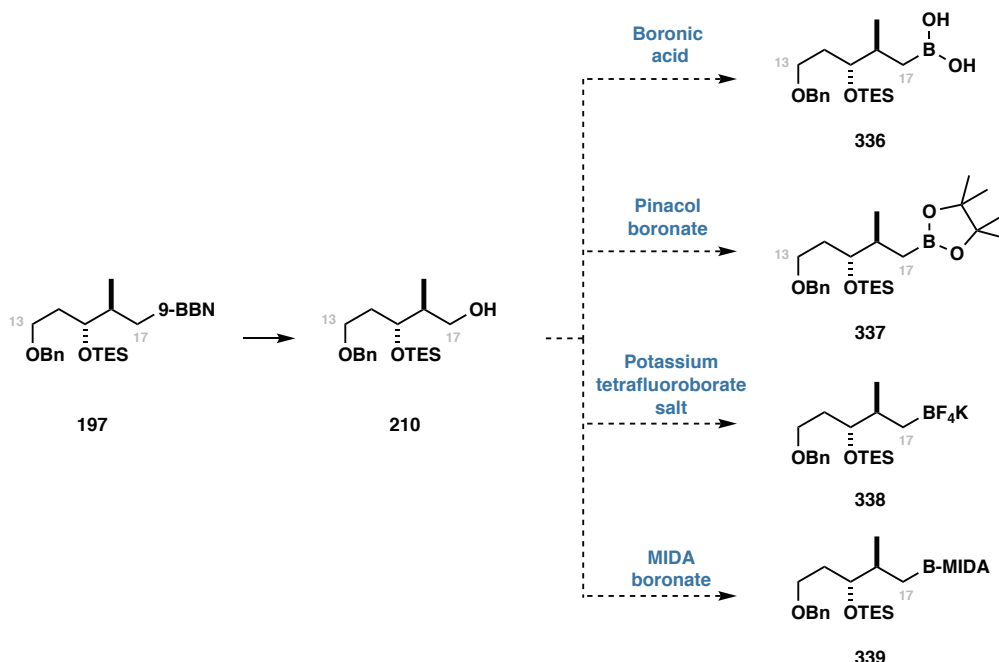
#### 6.2.1.2 FRAGMENT UNION AND ELABORATION INTO THE COMPLETE C12 – C27

##### FRAGMENT



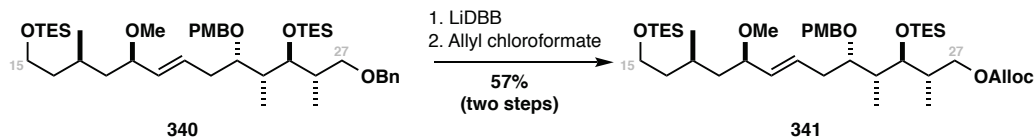
**Scheme 6.2:** Proposed union of the C13 – C17 fragment **198** and C18– C27 fragment **197** and elaboration to the protected C12 – C27 eastern fragment **100** of madeirolide A.

The proposed route for the synthesis of the protected C12 – C27 eastern fragment **100** is shown in **Scheme 6.2**. Key to the strategy is the union of the C13 – C17 organoborane **197** and the C18 – C27 vinyl iodide **198** using an  $sp^2$  –  $sp^3$  Suzuki cross coupling to form the C18 – C19 (*E*-alkene **333**. Early investigations into this cross-coupling using a model system were promising (see §4.2.2), however the option remains open to investigate more stable coupling partners should the need arise (**Scheme 6.3**):



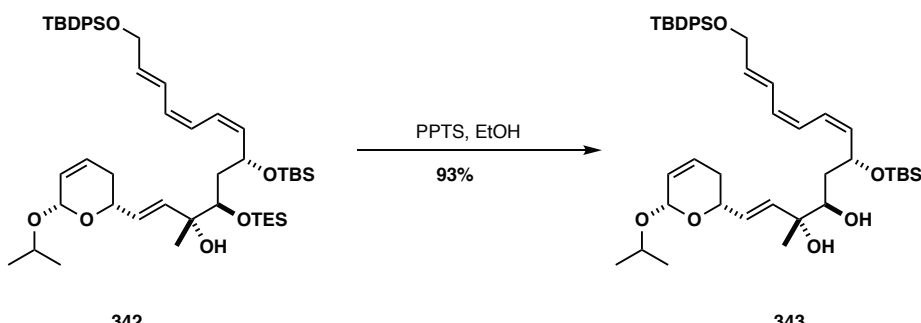
**Scheme 6.3:** Conversion of organoborane **197** into more stable derivatives for use in the  $sp^2$  –  $sp^3$  Suzuki cross-coupling.

The (*Z*)-vinyl iodide is proposed to be installed in three steps from **333** through removal of the benzyl ethers at C13 and C22, chemoselective oxidation of the primary C13 alcohol (TEMPO/BAIB), and a Stork-Zhao-Wittig olefination to complete the sequence. Finally, the C22 hydroxyl would be protected as a TBS ether to prevent reactivity in the subsequent steps. The presence of the internal alkene precludes the use of catalytic hydrogenation over palladium for removal of the benzyl ethers at C13 and C22, however LiDBB was utilised successfully in the second-generation synthesis of apllyronine A by Paterson, cleaving the C27 benzyl ether in the presence of an alkene and several other protecting groups (**Scheme 6.4**).<sup>164</sup> This sequence of reactions may, on initial inspection, show close parallels to those used by Haslett in the synthesis of the original C1 – C11 fragment of madeirolide A (see §2.3.1). However, the aldehyde used in this case has no  $\alpha$ -stereocentre, and as such is not prone to epimerisation. If necessary, the C13 – C17 fragment could be prepared with a PMB ether at C13, which would enable completely regioselective cleavage. This was not investigated further as without the C18 – C27 fragment prepared, the complete protecting group strategy cannot be fully elucidated.



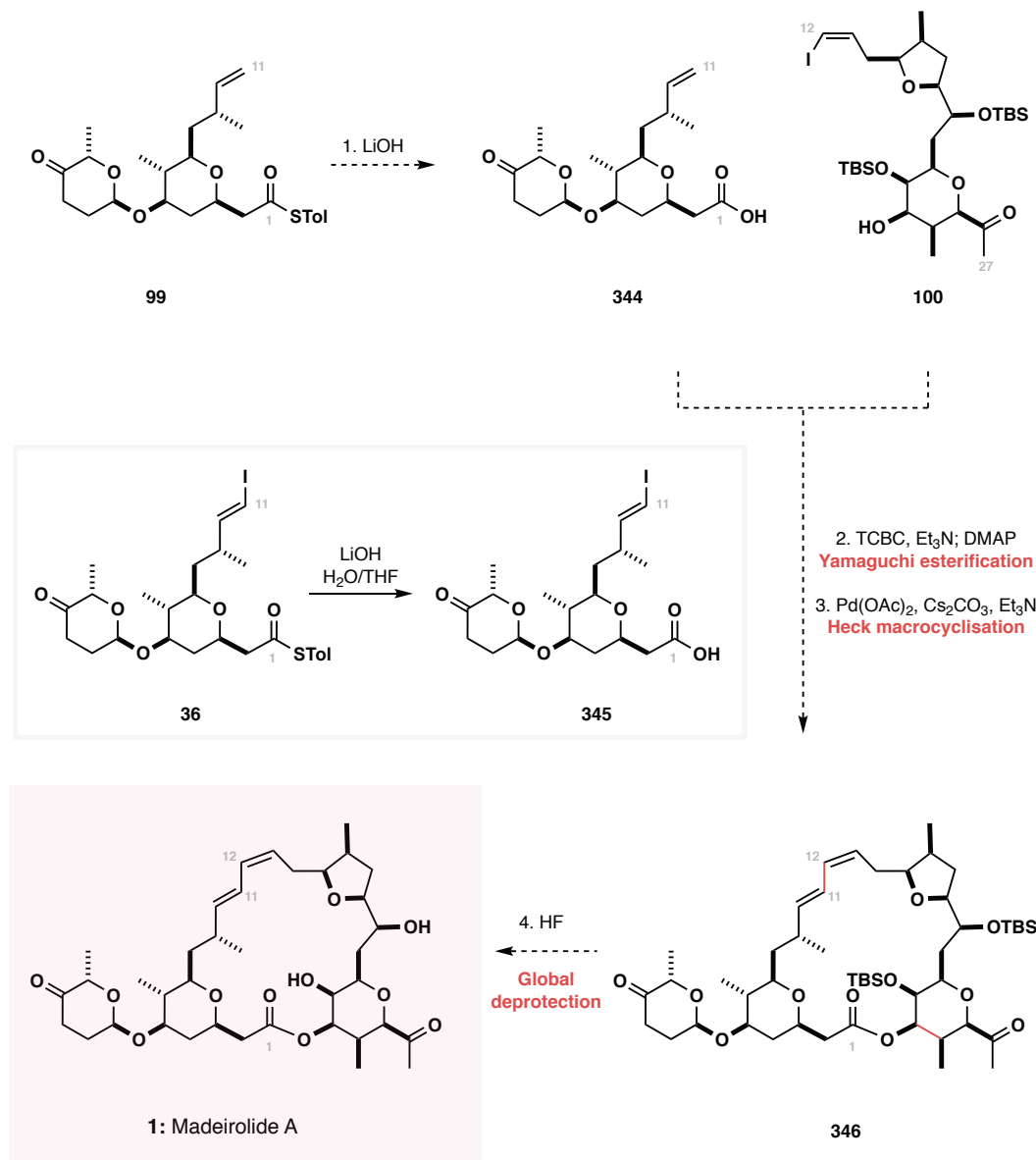
**Scheme 6.4:** Precedent for selective debenzylation in the presence of a disubstituted alkene and silyl ethers (**Paterson**).<sup>164</sup>

The THF is anticipated to form from an in situ Williamson etherification of mesylate **335**, similar to that used in Reddy's synthesis of the mandelalide A aglycone.<sup>58</sup> Selective removal of the C15 TES ether using PPTS should be possible in the presence of the secondary TBS using conditions developed by Boger (**Scheme 7.5**),<sup>165</sup> with mesylation of the ensuing hydroxyl converting it into a good leaving group. A Sharpless dihydroxylation (SAD) would thus introduce the C18 and C19 stereocentres with high-levels of selectivity under reagent control. Upon dihydroxylation it is anticipated that mesylate **335** will undergo rapid in situ cyclisation to the resulting THF, however it may be necessary to heat **335** in the presence of a weak amine base (i.e. pyridine) to facilitate the desired ring closure. Finally, the completion of the fully protected C12 – C27 fragment **100** ready for fragment union requires conversion of the C18 hydroxyl to the TBS ether and hydrolysis of the C23 acetate.



**Scheme 6.5:** Precedent for deprotection of a secondary TES ether in the presence of a secondary TBS ether and primary TBDPS ether (**Boger**).<sup>165</sup>

### 6.2.2 END-GAME AND COMPLETION OF MADEIROLIDE A



**Scheme 6.6:** Completion of madeirolide A through convergent union of the C1 – C11 western fragment **99** and the C12 – C27 eastern fragment **100**.

The convergent union of the eastern and western fragments of madeirolide A is anticipated to arise from a Yamaguchi esterification followed by Heck macrocyclisation, as discussed in §3.1. Thus, thioester **99** would initially be hydrolysed to carboxylic acid **344** to enable formation of the C1 – OC<sub>22</sub> ester;\* this has been demonstrated on a small scale using Haslett's C1 – C11 fragment **38** and occurred without any deleterious effects to the remainder of the fragment

\* The formation of an ester directly from a thioester has been reported, however strong alkoxide nucleophiles are required. Hydrolysis of the thioester to the carboxylic acid enables for milder esterifications to be investigated.

**(Scheme 6.6).** With the two fragments tethered together by the ester, the C11 – C12 bond could be forged using the conditions developed by Smith III in the total synthesis of mandelalide A ( $\text{Pd}(\text{OAc})_2$ ,  $\text{Cs}_2\text{CO}_3$ ,  $\text{Et}_3\text{N}$ ).<sup>69</sup> The proposed route leaves some flexibility as to the order of steps, such that a Heck reaction could first be used to join **344** and **100**, using a Yamaguchi esterification to close the macrocycle. Finally, the C18 and C21 protecting groups will be removed, completing the total synthesis and providing access to madeirolide A **1**. The exact conditions required to achieve this deprotection will be determined in due course, however, the ideal scenario would involve the C18 and C21 hydroxyls both being protected with silyl ethers, thus allowing a single-step deprotection with  $\text{HF} \cdot \text{Py}$ .

### 6.3 CONCLUSIONS

Madeirolide A **1** remains an important target for total synthesis. It is hoped that the completed synthetic work coupled with lessons learnt from unsuccessful attempts at forming the eastern THP may facilitate the first total synthesis. The availability of synthetic material would not only permit much-needed biological evaluation, but also serve to validate the stereochemical configuration of the molecule.







# A

## APPENDIX A: EXPERIMENTAL

### GENERAL EXPERIMENTAL DETAILS

#### NMR spectroscopy:

NMR spectra were recorded with an internal deuterium lock and referenced to the residual non-deuterated solvent peak ( $\text{CHCl}_3$ :  $\delta_{\text{H}}$  7.26 ppm,  $\delta_{\text{C}}$  77.16 ppm;  $\text{C}_6\text{H}_6$ :  $\delta_{\text{H}}$  7.16 ppm,  $\delta_{\text{C}}$  128.06 ppm)<sup>166</sup> using one of the following spectrometers: Bruker Avance BB (500 MHz), Bruker Avance TCI (500 MHZ) and Bruker DRX (400 MHz).  $^1\text{H}$  NMR data are presented as follows: chemical shift (in ppm), multiplicity (s = singlet, d = doublet, t = triplet, q = quartet, quint. = quintet, sext. = sextet, sept. = septet, m = multiplet, br. = broad, obs. = obscured, app. = apparent), coupling constants (J / Hz), integration and assignment. Diastereotopic protons are indicated as (‘) or (‘‘). Proton shift assignments were determined on the basis of unambiguous chemical shift data, coupling constants, and 2D experiments (COSY, HSQC, HMBC, NOESY), or by analogy to fully interpreted spectra for known compounds.

#### IR spectroscopy:

Infrared spectra were recorded neat as thin films on a Perkin Elmer Spectrum One (FT-IR) machine fitted with an ATR accessory with wavelengths of maximum absorbance ( $\nu_{\text{max}}$ ) quoted in wavenumbers ( $\text{cm}^{-1}$ ).

#### Optical rotation measurements:

Optical rotations were measured using either a Perkin-Elmer 343 polarimeter or an Anton Parr MCP100 polarimeter at the sodium D-line (589 nm) in chloroform and are reported as an  $[\alpha]$  value together with the concentration of solution (c in g/100 mL).

#### Melting points:

Melting points were measured on a hot-stage apparatus and are uncorrected.

## Appendix A: Experimental

### Mass spectrometry:

High-resolution mass spectra (HRMS) were recorded by the EPSRC Mass Spectrometry Service (Swansea, UK) or Department of Chemistry (Cambridge, UK) using electrospray (ES+) and electron ionisation (EI) techniques. The parent ion ( $M^+$ ) is quoted with the indicated cation where applicable.

### Chromatography:

All solvent mixtures are reported as %vol unless otherwise stated. Analytical thin layer chromatography (TLC) was carried out on Merck Kieselgel 60 F<sub>254</sub> plates, with visualisation using Goofy's dip (phosphomolybdic acid/Ce<sub>2</sub>(SO<sub>4</sub>)<sub>3</sub>), potassium permanganate (KMnO<sub>4</sub>) dip, vanillin dip (vanillin, EtOH, H<sub>2</sub>SO<sub>4</sub>) or ultra-violet light. Preparative thin layer chromatography (PLC) was carried out using either Merck Kieselgel 60 F<sub>254</sub> plates. Unless otherwise stated flash column chromatography was carried out using Merck Kieselgel 60 (230-400 mesh) silica gel under a positive pressure by means of compressed air.

### Purification of reagents and solvents:

Reagents and solvents were purified by standard methods where appropriate.<sup>167</sup> All solvents used for reactions, chromatograph and workup were distilled prior to use. Tetrahydrofuran (THF) and diethyl ether (Et<sub>2</sub>O) were pre-dried over sodium wire and distilled from potassium/benzophenone or sodium wire/benzophenone ketyl respectively. Dichloromethane (CH<sub>2</sub>Cl<sub>2</sub>), triethylamine (Et<sub>3</sub>N), hexamethylphosphoramide (HMPA), benzene and toluene were distilled from CaH<sub>2</sub>. DMSO was distilled from MgSO<sub>4</sub> and stored over molecular sieves. Diisopropylethylamine (*i*-Pr<sub>2</sub>NEt) was distilled sequentially from ninhydrin and KOH before being stored over molecular sieves. *N,N'*-Dimethylformamide (DMF) was distilled from and stored over activated 4Å molecular sieves. DDQ was recrystallised from a saturated solution of refluxing CHCl<sub>3</sub> or benzene. Proton sponge was recrystallised from anhydrous ethanol. Lithium chloride (LiCl) was dried by heating under high vacuum and cooling under argon. All other chemicals were used as received, unless otherwise noted. Molecular sieves were activated by heating in a microwave and allowing to cool under high vacuum.

### Reaction setup:

All non-aqueous reactions were carried out at room temperature (rt) under an argon atmosphere using glassware flame dried under vacuum and allowed to cool under a stream of argon. Standard techniques were followed for handling air/moisture sensitive reagents.

Ozone was generated using a Peak Scientific Ozone Generator using oxygen pre-dried through a column of drierite. Quenching of excess ozone was affected by purging the solution with a stream of oxygen.

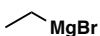
## PREPARATION OF REAGENTS

*iso*-Propyl magnesium chloride



Magnesium turnings (9.70 g, 400 mmol) and iodine (1 crystal) were suspended in dry THF (200 mL) and the reaction heated under reflux until the colour dissipated. 2-Chloropropane (36.6 mL, 400 mmol) was added dropwise over 15 min and reflux maintained for a further 2 h to give a black solution of the Grignard reagent in THF. Titration against menthol in the presence of 1,10-phenanthroline gave an effective concentration of 1.7 M.

Ethyl magnesium bromide



To a suspension of magnesium turnings (7.00 g, 270 mmol) and iodine (1 crystal) in dry THF (60 mL) was added EtBr (19.0 mL, 250 mmol) dropwise over 15 min. Reflux was maintained for 1 h to give a grey solution of the Grignard reagent in THF. Titration against menthol in the presence of 1,10-phenanthroline gave an effective concentration of 3.0 M.

Divinyl zinc<sup>168</sup>

Vinyl magnesium bromide (3.40 mL, 1 M soln in THF, 3.40 mmol) was added dropwise to a suspension of ZnCl<sub>2</sub> (250 mg, 1.83 mmol) THF (1.1 mL). The deep-orange reaction mixture was stirred for 1 h before being used in the subsequent reaction directly.

Samarium diiodide

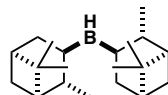
1,2-diiodoethane (0.362 g, 1.28 mmol) and powdered Sm (0.378 g, 2.52 mmol) were suspended in THF (6.8 mL) in a Schlenk tube under Ar. The mixture was sonicated for 1.5 h to give a deep-blue solution of SmI<sub>2</sub> which was treated as a 0.4 M solution in THF and used immediately in the subsequent reaction.

## Appendix A: Experimental

### Stryker's solution

To a solution of Cu(OAc)<sub>2</sub> (25 mg, 0.13 mmol) and PPh<sub>3</sub> (65 mg, 0.25 mmol) in benzene (2 mL) was added (Me<sub>2</sub>SiH)<sub>2</sub>O. The resulting blue solution was stirred vigorously for 18 h to give a red/wine coloured solution (ca. 0.06 M in Cu(OAc)<sub>2</sub>).

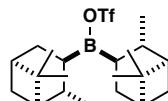
### (-)-diisopinocampheyl borane



To a solution (+)- $\alpha$ -pinene (47.1 mL, 296 mmol, 98% ee, freshly distilled from CaH<sub>2</sub>) in THF (40 mL) was added BH<sub>3</sub>·DMS (11.7 mL, 124 mmol) in a single portion at rt. Following addition, the solution was left standing without stirring for 17 h over which time a white crystalline solid precipitated. The solvent was removed via cannula and the crystals washed with *n*-pentane (5 x 15 mL) before being dried under high-vacuum to give (-)-ipc<sub>2</sub>BH (32.5 g, 114 mmol, 92%). The ipc<sub>2</sub>BH was able to be stored at -20 °C under Ar without appreciable loss of activity.

The enantiomeric (+)-ipc<sub>2</sub>BH was prepared from (-)- $\alpha$ -pinene using an analogous procedure.

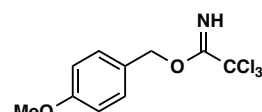
### (-)-diisopinocampheyl boron triflate



To a suspension of (-)-ipc<sub>2</sub>BH (7.60 g, 26.6 mmol) in hexane (13 mL) was added TfOH\* (2.35 mL, 26.5 mmol) dropwise, resulting in a biphasic solution. The reaction mixture was stirred for 2.5 h, and the upper (clear) layer removed via cannula to give a solution of (-)-ipc<sub>2</sub>BOTf in hexane which was used immediately in the subsequent boron aldol reaction.

The enantiomeric (+)-ipc<sub>2</sub>BOTf was prepared from (+)-ipc<sub>2</sub>BH using an analogous procedure.

### 4-Methoxybenzyl-2,2,2-trichloroacetimidate (PMB-TCA)

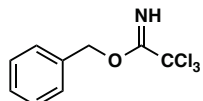


\* The quality of the TfOH was found to be critical to the successful preparation of ipc<sub>2</sub>BOTf, with best results obtained using a previously unopened bottle of TfOH showing no signs of decolouration.

To a solution of 4-methoxybenzyl alcohol (15.5 mL, 125 mmol) and tetrabutylammonium hydrogensulfate (424 mg, 1.25 mmol) in  $\text{CH}_2\text{Cl}_2$  at 0 °C was added KOH (150 mL, 50% wt in  $\text{H}_2\text{O}$ ) and 2,2,2-trichloroacetonitrile (14.4 mL, 144 mmol) sequentially. The reaction was warmed to rt and stirred for 2 h before the phases separated. The aqueous phase was extracted with EtOAc (3 x 50 mL) before the combined organic extracts dried ( $\text{Na}_2\text{SO}_4$ ) and concentrated in vacuo. The product was purified by flash column chromatography ( $\text{Al}_2\text{O}_3$ , 10% EtOAc:PE<sub>40-60</sub>) afforded 4-methoxymethyl-2,2,2-trichloroacetimidate (29.1 g, 82%) as a colourless oil.

**<sup>1</sup>H NMR** (500 MHz,  $\text{CDCl}_3$ ):  $\delta$  8.35 (br s, 1H, NH), 7.35 (d,  $J$  = 8.7 Hz, 2H, Ar-H), 6.93 (d,  $J$  = 8.7 Hz, 2H, Ar-H), 5.25 (s, 2H, Ar-CH<sub>2</sub>-O), 3.80 (s, 3H, Ar-OCH<sub>3</sub>).

Benzyl-2,2,2-trichloroacetimidate (Bn-TCA)



To a solution of benzyl (12.9 mL, 125 mmol) and tetrabutylammonium hydrogensulfate (424 mg, 1.25 mmol) in  $\text{CH}_2\text{Cl}_2$  at 0 °C was added KOH (150 mL, 50% wt in  $\text{H}_2\text{O}$ ) and 2,2,2-trichloroacetonitrile (14.4 mL, 144 mmol) sequentially. The reaction was warmed to rt and stirred for 2 h before the phases separated. The aqueous phase was extracted with EtOAc (3 x 50 mL) before the combined organic extracts dried ( $\text{Na}_2\text{SO}_4$ ) and concentrated in vacuo. The product was purified by flash column chromatography ( $\text{Al}_2\text{O}_3$ , 5% EtOAc:PE<sub>40-60</sub>) afforded benzyl-2,2,2-trichloroacetimidate (25.2 g, 80%) as a colourless oil.

**<sup>1</sup>H NMR** (500 MHz,  $\text{CDCl}_3$ ):  $\delta$  8.39 (br s, 1H, NH), 7.45 – 7.20 (m, 5H, ArH), 5.32 (s, 2H, Ar-CH<sub>2</sub>-O).

$[\text{RuCl}_2(\text{p-cymene})]_2$ <sup>169</sup>

A solution of  $\text{RuCl}_3 \cdot x\text{H}_2\text{O}$  (3.6 g, 17.4 mmol) and  $\alpha$ -phellandrene (18 mL, 112 mmol) in EtOH (180 mL) was heated under reflux for 4 h before EtOH (ca. 100 mL) was distilled off and the solution allowed to cool to rt. Et<sub>2</sub>O (100 mL) was added and reaction filtered under vacuum. After drying the resulting solid in vacuo,  $[\text{RuCl}_2(\text{p-cymene})]_2$  (5.86 g, 55%) was obtained as an amorphous red solid.

**<sup>1</sup>H NMR** (500 MHz,  $\text{CDCl}_3$ ):  $\delta$  5.50 (d,  $J$  = 5.8 Hz, 2H), 5.36 (d,  $J$  = 5.8 Hz, 2H), 2.94 (hept,  $J$  = 7.0 Hz, 1H), 2.18 (s, 3H), 1.30 (d,  $J$  = 7.0 Hz, 6H).

## Appendix A: Experimental

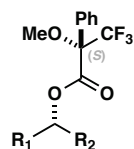
### (*S,S*)-Noyori catalyst for transfer hydrogenation

Powdered KOH (0.195 g, 3.48 mmol) was added to a solution of (*S,S*)-TsDPEN (0.180 g, 0.490 mmol) and  $[\text{RuCl}_2(p\text{-cymene})]_2$  (0.150 g, 0.145 mmol) in  $\text{CH}_2\text{Cl}_2$  to give a deep-orange solution. After 10 min,  $\text{H}_2\text{O}$  (3.5 mL) was added resulting in a purple suspension. The layers were separated and the organic phase dried over  $\text{CaH}_2$ , filtered, and concentrated in vacuo to give the Noyori catalyst as a free-flowing purple crystalline solid (279 mg g, 95%).

The enantiomeric catalyst was prepared from (*R,R*)-TsDPEN using an analogous procedure.

## GENERAL PROCEDURES

### General procedure 1: MTPA ester formation

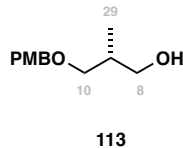


For the (*S*)-MTPA ester: To a solution of the chiral alcohol in  $\text{CH}_2\text{Cl}_2$  (0.1 M) was added (*S*)-3,3,3-trifluoro-2-methoxy-2-phenylpropanoic acid (5 eq), DCC (5 eq) and DMAP (0.1 eq). The reaction mixture was stirred for 18 h at rt before  $\text{Et}_2\text{O}$  (0.5 mL) was added. The reaction mixture was filtered through a plug of cotton wool and concentrated in vacuo. Unless otherwise stated, the crude MTPA ester was used in the analysis directly without purification.

The (*R*)-MTPA ester was prepared following an analogous procedure, using (*R*)-3,3,3-trifluoro-2-methoxy-2-phenylpropanoic acid.

## EXPERIMENTAL PROCEDURES FOR THE WESTERN FRAGMENT OF MADEIROLIDE A

(*R*)-3-((4-methoxybenzyl)oxy)-2-methylpropan-1-ol

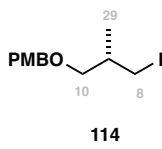


Methyl-(*S*)-3-((4-methoxybenzyl)oxy)-2-methylpropanoate (20.0 g, 83.9 mmol) was added to a slurry of LiAlH<sub>4</sub> (3.50 g, 92.3 mmol) in THF (200 mL) at -78 °C. The reaction mixture was allowed to warm to rt and stirred for a further 2.5 h before addition of EtOAc (100 mL) and Na/K tartrate (100 mL). After 18 h the supernatant was decanted from the grey precipitate, diluted with H<sub>2</sub>O (100 mL) and extracted with EtOAc (3 x 100 mL). The combined organic extracts were dried (MgSO<sub>4</sub>), concentrated in vacuo, and purified by flash column chromatography (SiO<sub>2</sub>, 30% EtOAc:PE<sub>40-60</sub>) to give alcohol **113** as a pale-yellow oil (14.7 g, 83%).

**<sup>1</sup>H NMR** (500 MHz, CDCl<sub>3</sub>) δ 7.24 (d, *J* = 8.6 Hz, 2H, PMB Ar-H), 6.88 (d, *J* = 8.7 Hz, 2H, PMB Ar-H), 4.44 (s, 2H, PMB Ar-CH<sub>2</sub>O-), 3.80 (s, 3H, PMB O-CH<sub>3</sub>), 3.60 (dd, *J* = 10.8, 4.6 Hz, 1H, H8'), 3.57 (dd, *J* = 10.8, 7.1 Hz, 1H, H8''), 3.51 (dd, *J* = 9.1, 4.7 Hz, 1H, H10'), 3.89 (dd, *J* = 9.0, 8.1 Hz, 1H, H10''), 2.64 (br. s, 1H, C8-OH), 2.01-2.09 (m, 1H, H9), 0.87 (d, *J* = 7.1 Hz, 3H, H29).  
**HRMS** (ES+) calcd for C<sub>12</sub>H<sub>19</sub>O<sub>3</sub> [M+NH<sub>4</sub>]<sup>+</sup> 211.1329, found 211.1330.

Data consistent with that reported in the literature.<sup>53</sup>

(*S*)-1-((3-iodo-2-methylpropoxy)methyl)-4-methoxybenzene



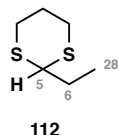
Alcohol **113** (8.00 g, 38.1 mmol) in CH<sub>2</sub>Cl<sub>2</sub> (80 mL) was added to a pre-stirred suspension of I<sub>2</sub> (10.6 g, 41.9 mmol), PPh<sub>3</sub> (11.9 g, 45.6 mmol) and imidazole (3.90 g, 57.1 mmol) in CH<sub>2</sub>Cl<sub>2</sub> (300 mL) at 0 °C. The reaction mixture was stirred for 1 h before Et<sub>2</sub>O (100 mL) added and the reaction mixture filtered. Na<sub>2</sub>S<sub>2</sub>O<sub>4</sub> (100 mL) was added and the layers separated. The aqueous phase was back-extracted with Et<sub>2</sub>O (3 x 100 mL) and the combined organic extracts dried (MgSO<sub>4</sub>), concentrated in vacuo, and the crude residue purified by flash column chromatography (SiO<sub>2</sub>, 30% EtOAc:PE<sub>40-60</sub>) to give **114** as a pale-yellow oil (8.53 g, 70%).

## Appendix A: Experimental

**<sup>1</sup>H-NMR** (400 MHz, CDCl<sub>3</sub>) δ 7.29 (d, *J*= 8.6 Hz, 2H, PMB Ar-H), 6.91 (d, *J*= 8.6 Hz, 2H, PMB Ar-H), 4.48 (s, 2H, PMB Ar-CH<sub>2</sub>O-), 3.84 (s, 3H, PMB O-CH<sub>3</sub>), 3.27-3.41 (m, 4H, H8, H10), 1.79 (m, 1H, H9), 1.01 (d, *J*= 6.7 Hz, 3H, H29). **HRMS** (ES+) calcd for C<sub>12</sub>H<sub>21</sub>O<sub>2</sub>NI [M+NH<sub>4</sub>]<sup>+</sup> 338.0611, found 388.0612.

Data consistent with that reported in the literature.<sup>53</sup>

2-ethyl-1,3-dithiane

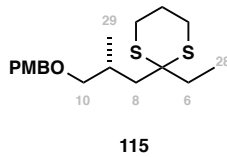


To a solution of propanal (5.00 mL, 69.3 mmol) in THF (5 mL) at -78 °C was added BF<sub>3</sub>·OEt<sub>2</sub> (8.60 mL, 69.3 mmol) and 1,3-propanedithiol (7.00 mL, 69.3 mmol). The reaction mixture was warmed to rt over 2 h before Et<sub>3</sub>N (1 mL) added and the solution concentrated in vacuo. Purification by flash column chromatography (SiO<sub>2</sub>, 15% EtOAc:PE<sub>40-60</sub>) afforded **112** as a colourless oil (7.85 g, 90%).

**<sup>1</sup>H-NMR** (500 MHz, CDCl<sub>3</sub>) δ 3.99 (t, *J*= 6.8 Hz, 1H, C5-H), 2.80-2.91 (m, 4H, -S-CH<sub>2</sub>-CH<sub>2</sub>-CH<sub>2</sub>-S-), 2.08-2.15 (m, 1H, -S-CH<sub>2</sub>-CH<sub>2</sub>'-CH<sub>2</sub>-S-), 1.82-1.90 (m, 1H, -S-CH<sub>2</sub>-CH<sub>2</sub>"-CH<sub>2</sub>-S-), 1.79 (quin, *J*= 6.8 Hz, 2H, H6), 1.08 (t, *J*= 7.5 Hz, 3H, H28). **HRMS** (ES+) calcd for C<sub>6</sub>H<sub>13</sub>S<sub>2</sub> [M+H]<sup>+</sup> 149.0453, found 149.0450.

Data consistent with that reported in the literature.<sup>53</sup>

(R)-2-ethyl-2-(3-((4-methoxybenzyl)oxy)-2-methylpropyl)-1,3-dithiane

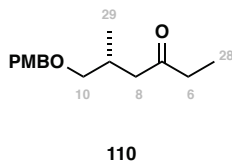


Iodide **114** (8.53 g, 26.6 mmol) in THF (20 mL) was added to a solution of dithiane **112** (5.93 g, 40.0 mmol), *t*-BuLi (21 mL, 1.4 M in pentane, 29.3 mmol) and HMPA (6 mL) in THF (100 mL) at -78 °C. Stirring was continued at this temperature for 4 h before the addition of NH<sub>4</sub>Cl (100 mL). After warming to rt, the mixture was diluted with EtOAc (80 mL) and the layers separated. The aqueous phase was extracted sequentially with EtOAc (3 x 80 mL) and CH<sub>2</sub>Cl<sub>2</sub> (80 mL) before the combined organic extracts dried (Na<sub>2</sub>SO<sub>4</sub>), concentrated in vacuo and the crude residue purified by flash column chromatography (SiO<sub>2</sub>, 10% EtOAc:PE<sub>40-60</sub>) to give **115** as a viscous colourless oil (8.52 g, 94%).

**<sup>1</sup>H NMR** (400 MHz, CDCl<sub>3</sub>) δ 7.26 (d, *J* = 8.4 Hz, 2H, PMB Ar-H), 6.87 (d, *J* = 8.4 Hz, 2H, PMB Ar-H), 4.44 (s, 2H, PMB Ar-CH<sub>2</sub>O-), 3.80 (s, 3H, PMB ArO-CH<sub>3</sub>), 3.34 (dd, *J* = 9.1, 5.7 Hz, 1H, H10'), 3.27 (dd, *J* = 9.1, 6.2 Hz, 1H, H10''), 2.73 – 2.83 (m, 4H, -S-CH<sub>2</sub>-CH<sub>2</sub>-CH<sub>2</sub>-S-), 2.03 – 2.12 (m, 2H, H9, H8'), 1.87 – 2.00 (m, 4H, H6, -S-CH<sub>2</sub>-CH<sub>2</sub>-CH<sub>2</sub>-S-), 1.63 (dd, *J* = 15.6, 6.6 Hz, 1H, H8''), 1.06 (d, *J* = 6.6 Hz, 3H, H29), 0.99 (t, *J* = 7.4 Hz, 3H, H28). **HRMS** (ES+) calcd for C<sub>18</sub>H<sub>32</sub>O<sub>2</sub>S<sub>2</sub>N [M+NH<sub>4</sub>]<sup>+</sup> 358.1860, found 358.1863.

Data consistent with that reported in the literature.<sup>53</sup>

(*R*)-6-((4-methoxybenzyl)oxy)-5-methylhexan-3-one

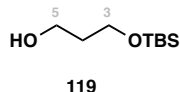


Dithiane **115** (55.8 g, crude) was added to a solution of I<sub>2</sub> (80.0 g, 315 mmol) in MeCN (1500 mL) and NaHCO<sub>3</sub> (1000 mL). After 2.5 h, the reaction mixture was diluted with CHCl<sub>3</sub>\* (500 mL) and solid Na<sub>2</sub>S<sub>2</sub>O<sub>3</sub> (ca. 250 g) was added until a colour change from brown to colourless was observed. The layers were separated and the aqueous phase extracted with CHCl<sub>3</sub> (3 x 500 mL) before the combined organic extracts dried (Na<sub>2</sub>SO<sub>4</sub>), concentrated in vacuo and the crude residue purified by flash column chromatography (SiO<sub>2</sub>, 10 → 30% EtOAc:PE<sub>40-60</sub>) to give **110** as a yellow oil (20.1 g, 49% over two steps) plus starting material **110** (10.2 g) which was able to be resubjected to the reaction conditions to obtain a further 6.2 g of product.

**<sup>1</sup>H NMR** (400 MHz, CDCl<sub>3</sub>) δ 7.23 (d, *J* = 8.7 Hz, 2H, PMB Ar-H), 6.87 (d, *J* = 8.6 Hz, 2H, PMB Ar-H), 4.39 (s, 2H, PMB Ar-CH<sub>2</sub>O-), 3.80 (s, 3H, PMB Ar-CH<sub>3</sub>), 3.32 (dd, *J* = 9.2, 5.4 Hz, 1H, H10'), 3.22 (dd, *J* = 9.2, 7.0 Hz, 1H, H10''), 2.56 (dd, *J* = 15.9, 5.7 Hz, 1H, H8'), 2.29–2.46 (m, 3H, H9, H6), 2.22 (dd, *J* = 15.9, 7.6 Hz, 1H, H8''), 1.01 (t, *J* = 7.3 Hz, 3H, H28), 0.92 (d, *J* = 6.8 Hz, 3H, H29). **HRMS** (ES+) calcd for C<sub>15</sub>H<sub>22</sub>O<sub>3</sub>Na [M+Na]<sup>+</sup> 273.1461, found 273.1458.

Data consistent with that reported in the literature.<sup>53</sup>

3-((*tert*-butyldimethylsilyl)oxy)propan-1-ol



\* CHCl<sub>3</sub> was used in place of CH<sub>2</sub>Cl<sub>2</sub> owing to the increased density which aided in the separation of the phases during workup.

## Appendix A: Experimental

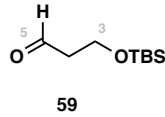
1,3-propanediol (9.00 g, 118 mmol) was added dropwise to a slurry of NaH (4.70 g, 60% wt dispersion in mineral oil, 118 mmol) in THF (200 mL) at 0 °C. Upon complete addition the cooling bath was removed and TBS-Cl (16.0 g, 107 mmol) added portion-wise. After stirring for 2 h, NaHCO<sub>3</sub> (50 mL) and EtOAc (100 mL) were added and the layers separated. The aqueous phase was extracted with EtOAc (3 x 100 mL) and the combined organic extracts dried (Na<sub>2</sub>SO<sub>4</sub>) and concentrated in vacuo to afford the mono-TBS protected diol **119** as a colourless oil (21.2 g, ca. 94%) which was used directly in the subsequent step without additional purification.

For the purposes of characterisation, an analytical sample was purified by flash column chromatography (SiO<sub>2</sub>, 5% EtOAc:PE<sub>40-60</sub>) to provide the following data:

**<sup>1</sup>H NMR** (400 MHz, CDCl<sub>3</sub>) δ 3.91 – 3.72 (m, 4H, H<sub>5</sub>, H<sub>3</sub>), 2.60 (t, J = 5.4 Hz, 1H, OH), 1.78 (p, J = 5.5 Hz, 2H, H<sub>4</sub>), 0.90 (s, 9H, Si-C(CH<sub>3</sub>)<sub>3</sub>), 0.08 (s, 6H, Si-(CH<sub>3</sub>)<sub>2</sub>). **HRMS** (ES+) calcd for C<sub>9</sub>H<sub>23</sub>SiO<sub>2</sub> [M+H]<sup>+</sup> 191.1462, found 191.1460.

Data consistent with that reported in the literature.<sup>53</sup>

3-((*tert*-butyldimethylsilyl)oxy)propanal

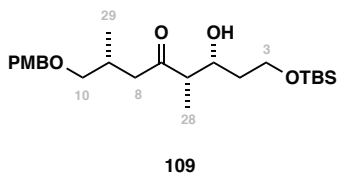


DMSO (3.50 mL, 49.8 mmol) was added dropwise to a solution of (COCl)<sub>2</sub> (2.10 mL, 24.9 mmol) in CH<sub>2</sub>Cl<sub>2</sub> at -78 °C and the reaction mixture stirred for 10 min before a solution of **119** (2.50 g, 13.1 mmol) in CH<sub>2</sub>Cl<sub>2</sub> (20 mL) was added dropwise, followed immediately by Et<sub>3</sub>N (15.8 mL, 113.1 mmol). The cooling bath was removed and the reaction mixture stirred for 20 min while warming to rt. Water (30 mL) was added and the layers separated. The aqueous phase was extracted with EtOAc (3 x 20 mL) before the combined organics layers dried (Na<sub>2</sub>SO<sub>4</sub>) and concentrated in vacuo. Purification by flash column chromatography (SiO<sub>2</sub>, 5% EtOAc:PE<sub>30-40</sub>) afforded **59** (2.40 g, 96%) as a colourless oil.

**<sup>1</sup>H NMR** (400 MHz, CDCl<sub>3</sub>) δ 9.78 (t, J = 2.0 Hz, 1H, H<sub>5</sub>), 3.96 (t, J = 6.0 Hz, 2H, H<sub>3</sub>), 2.58 (td, J = 6.0, 2.1 Hz, 2H, H<sub>4</sub>), 0.86 (s, 9H, Si-C(CH<sub>3</sub>)<sub>3</sub>), 0.05 (s, 6H, Si-(CH<sub>3</sub>)<sub>2</sub>). **HRMS** (ES+) calcd for C<sub>9</sub>H<sub>21</sub>SiO<sub>2</sub> [M+H]<sup>+</sup> 189.1305, found 189.1307.

Data consistent with that reported in the literature.<sup>53</sup>

(2*R*,5*S*,6*R*)-8-((*tert*-butyldimethylsilyl)oxy)-6-hydroxy-1-((4-methoxybenzyl)oxy)-2,5-dimethyloctan-4-one

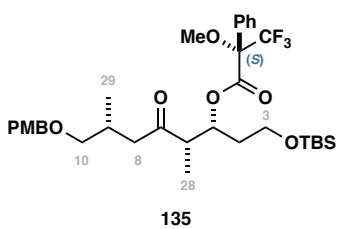


A solution of ketone **110** (2.00 g, 7.90 mmol) in CH<sub>2</sub>Cl<sub>2</sub> (8 mL) was added dropwise to a pre-stirred solution of (-)-ip*c*<sub>2</sub>BOTf (10.0 mL, ca. 1.2 M in hexane, 12.0 mmol) and *i*-Pr<sub>2</sub>NEt (4.20 mL, 23.9 mmol) in CH<sub>2</sub>Cl<sub>2</sub> (5 mL) at -78 °C, and the resulting mixture stirred for 2.5 h while warming to -30 °C. A solution of aldehyde **59** (4.50 g, 23.9 mmol) in CH<sub>2</sub>Cl<sub>2</sub> (5 mL) was dried over CaH<sub>2</sub> before being added to the enolate solution at -78 °C and stirred for a further 18 h at this temperature. MeOH (5 mL), pH 7 buffer (5 mL) and H<sub>2</sub>O<sub>2</sub> (2 mL) were added and the reaction stirred vigorously while warming to rt. The layers were separated and the aqueous phase extracted with CH<sub>2</sub>Cl<sub>2</sub> (3 x 10 mL) before the combined organic extracts dried (MgSO<sub>4</sub>), concentrated in vacuo, and the crude residue purified by flash column chromatography (SiO<sub>2</sub>, 10% EtOAc:PE<sub>40-60</sub> then 25% Et<sub>2</sub>O:CH<sub>2</sub>Cl<sub>2</sub> + 0.1% AcOH) to give **109** as a colourless oil (2.30 g, 65%).

<sup>1</sup>H-NMR (500 MHz, CDCl<sub>3</sub>) δ 7.23 (d, *J* = 8.6 Hz, 2H, PMB Ar-H), 6.86 (d, *J* = 8.6 Hz, 2H, PMB Ar-H), 4.41 (s, 2H, PMB Ar-CH<sub>2</sub>O-), 4.04-4.09 (m, 1H, H5), 3.80 (s, 3H, PMB Ar-OCH<sub>3</sub>), 3.70-3.83 (m, 2H, H2), 3.44 (s, 1H, C5-OH), 3.32 (dd, *J* = 9.3, 5.3 Hz, 1H, H10'), 3.23 (dd, *J* = 9.3, 6.8 Hz, 1H, H10''), 2.67 (d, *J* = 5.1 Hz, 1H, H8'), 2.57-2.65 (m, 1H, H6), 2.32-2.41 (m, 1H, H9), 2.31 (d, *J* = 7.6 Hz, 1H, H8''), 1.60-1.69 (m, 1H, H4'), 1.51-1.58 (m, 1H, H4''), 1.12 (d, *J* = 7.2 Hz, 3H, H8), 0.92 (d, *J* = 6.6 Hz, 3H, H29), 0.9 (s, 9H, Si-C(CH<sub>3</sub>)<sub>3</sub>), 0.1 (s, 6H, Si-(CH<sub>3</sub>)<sub>2</sub>). HRMS (ES+) calcd for C<sub>24</sub>H<sub>42</sub>O<sub>3</sub>SiNa [M+Na]<sup>+</sup> 461.2694, found 461.2682.

Data consistent with that reported in the literature.<sup>53</sup>

(3*R*,4*S*,7*R*)-1-((tert-butyldimethylsilyl)oxy)-8-((4-methoxybenzyl)oxy)-4,7-dimethyl-5-oxooctan-3-yl (*S*)-3,3,3-trifluoro-2-methoxy-2-phenylpropanoate



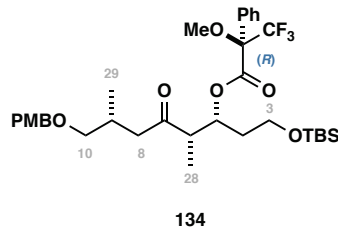
(*S*)-MTPA ester **135** was prepared from aldol adduct **109** (10.0 mg, 0.02 mmol) following general procedure A and purified by preparative layer chromatography (SiO<sub>2</sub>, 20% EtOAc:Hexanes) to give (*S*)-MTPA ester **135** (5.2 mg, 81%) as a colourless residue (7.2 mg, 55%).

## Appendix A: Experimental

**<sup>1</sup>H NMR** (500 MHz, CDCl<sub>3</sub>) δ 7.54 (dd, *J* = 7.0, 3.0 Hz, 2H, MTPA Ar-H), 7.41 – 7.35 (m, 3H, MTPA Ar-H), 7.25 – 7.19 (m, 2H, PMB Ar-H), 6.89 – 6.83 (m, 2H, PMB Ar-H), 5.56 (dt, *J* = 7.4, 5.0 Hz, 1H, H<sub>5</sub>), 4.38 (s, 2H, PMB Ar-CH<sub>2</sub>O-), 3.80 (s, 3H, PMB-OCH<sub>3</sub>), 3.69 – 3.56 (m, 2H, H<sub>3</sub>), 3.52 (d, *J* = 1.2 Hz, 3H, MTPA -OCH<sub>3</sub>), 3.25 (dd, *J* = 9.2, 5.6 Hz, 1H, H<sub>10'</sub>), 3.18 (dd, *J* = 9.2, 6.6 Hz, 1H, H<sub>10''</sub>), 2.81 (qd, *J* = 7.0, 4.5 Hz, 1H, H<sub>6</sub>), 2.53 (dd, *J* = 16.7, 5.2 Hz, 1H, H<sub>8'</sub>), 2.35 – 2.25 (m, 1H, H<sub>9</sub>), 2.21 (dd, *J* = 16.4, 7.8 Hz, 1H, H<sub>8''</sub>), 1.90 – 1.79 (m, 2H, H<sub>4</sub>), 1.04 (d, *J* = 7.1 Hz, 3H, H<sub>28</sub>), 0.88 (s, 9H, Si-C(CH<sub>3</sub>)<sub>3</sub>), 0.86 (d, *J* = 6.6 Hz, 3H, H<sub>29</sub>), 0.03 (s, 6H, Si-(CH<sub>3</sub>)<sub>2</sub>). **HRMS** (ES+) calcd for C<sub>34</sub>H<sub>53</sub>O<sub>7</sub>NF<sub>3</sub>Si [M+NH<sub>4</sub>]<sup>+</sup> 672.3538, found 672.3537.

Data consistent with that reported in the literature.<sup>53</sup>

(3*R*,4*S*,7*R*)-1-((tert-butyldimethylsilyl)oxy)-8-((4-methoxybenzyl)oxy)-4,7-dimethyl-5-oxooctan-3-yl (*R*)-3,3,3-trifluoro-2-methoxy-2-phenylpropanoate



(*R*)-MTPA ester **134** was prepared following an analogous procedure to that used for the (*S*)-MTPA ester **135** using the enantiomeric (*R*)-(+) $\alpha$ -methoxy- $\alpha$ -trifluoromethylphenylacetic acid to give **134** as a colourless residue (8.5 mg, 65%).

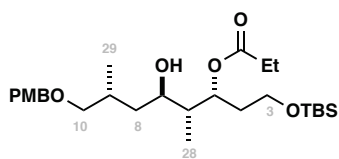
**<sup>1</sup>H NMR** (500 MHz, CDCl<sub>3</sub>) δ 7.53 (dd, *J* = 6.8, 3.0 Hz, 2H, MTPA Ar-H), 7.42 – 7.35 (m, 3H, MTPA Ar-H), 7.22 (d, *J* = 8.6 Hz, 2H, PMB Ar-H), 6.86 (d, *J* = 8.6 Hz, 2H, PMB Ar-H), 5.59 (dt, *J* = 7.6, 4.7 Hz, 1H, H<sub>5</sub>), 4.39 (s, 2H, PMB Ar-CH<sub>2</sub>O-), 3.80 (s, 3H, PMB-OCH<sub>3</sub>), 3.59 – 3.44 (m, 2H, H<sub>3</sub>), 3.50 (s, 3H, MTPA -OCH<sub>3</sub>), 3.28 (dd, *J* = 9.2, 5.2 Hz, 1H, H<sub>10'</sub>), 3.22 (dd, *J* = 9.2, 6.2 Hz, 1H, H<sub>10''</sub>), 2.86 (qd, *J* = 7.1, 4.2 Hz, 1H, H<sub>6</sub>), 2.68 – 2.56 (m, 1H, H<sub>8'</sub>), 2.40 – 2.29 (m, 2H, H<sub>9</sub>, H<sub>8''</sub>), 1.84 – 1.73 (m, 2H, H<sub>4</sub>), 1.08 (d, *J* = 7.1 Hz, 3H, H<sub>28</sub>), 0.91 (d, *J* = 6.3 Hz, 3H, H<sub>29</sub>), 0.88 (s, 9H, Si-C(CH<sub>3</sub>)<sub>3</sub>), 0.02 (s, 3H, Si-CH<sub>3</sub>), 0.01 (s, 3H, Si-CH<sub>3</sub>). **HRMS** (ES+) calcd for C<sub>34</sub>H<sub>53</sub>O<sub>7</sub>NF<sub>3</sub>Si [M+NH<sub>4</sub>]<sup>+</sup> 672.3538, found 672.3533.

Data consistent with that reported in the literature.<sup>53</sup>

Proton	$\delta_{S}$ -MTPA	$\delta_{R}$ -MTPA	$\delta_{(S-R)}$
3	3.61	3.52	+0.09
4	1.83	1.79	+0.04
6	2.81	2.86	-0.05
8'	2.53	2.62	-0.09
8''	2.21	2.33	-0.12
9	2.28	2.33	-0.05
10'	3.18	3.22	-0.04
10''	2.35	3.28	-0.03
28	1.04	1.08	-0.04
29	0.86	0.91	-0.05

Chemical shifts are taken as the midpoint of multiplets for the purpose of the MTPA analysis.

(3*R*,4*R*,5*R*,7*R*)-1-((tert-butyldimethylsilyl)oxy)-5-hydroxy-8-((4-methoxybenzyl)oxy)-4,7-dimethyloctan-3-yl propionate



Aldol adduct **109** (1.00 g, 2.30 mmol) in THF (11 mL) was added dropwise to a pre-stirred solution of SmI<sub>2</sub> (5.00 mL, 0.1 M soln in THF, 0.50 mmol) and EtCHO (1.72 mL, 10mmol) at -30 °C. The reaction mixture was stirred at -30 °C for 18 h before being quenched by addition of NaHCO<sub>3</sub> (10 mL) and diluted with EtOAc (20 mL). They layers were separated, the aqueous phase extracted with EtOAc (3 x 20 mL), dried (Na<sub>2</sub>SO<sub>4</sub>) and concentrated in vacuo to afford propionate ester **136** a yellow oil (1.10 g) which was used directly in the subsequent step without additional purification due to observed migration of the propionate ester during flash column chromatography.

For the purposes of characterisation, an analytical sample was purified by flash column chromatography (SiO<sub>2</sub>, 10% EtOAc:PE<sub>40-60</sub>) to provide the following data:

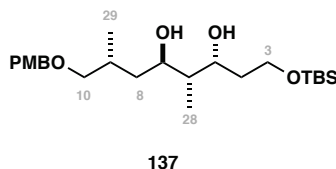
**<sup>1</sup>H NMR** (500 MHz, CDCl<sub>3</sub>) δ 7.25 (d, *J* = 8.7 Hz, 2H, PMB Ar-H), 6.86 (d, *J* = 8.7 Hz, 2H, PMB Ar-H), 5.40 (ddd, *J* = 9.4, 3.7, 2.2 Hz, 1H, H5), 4.44 (s, 2H, PMB Ar-CH<sub>2</sub>O-), 3.81 (s, 3H, PMB OCH<sub>3</sub>), 3.65 – 3.63 (m, 2H, H3), 3.32 (dd, *J* = 9.2, 6.6 Hz, 2H, H10'), 3.28 (dd, *J* = 9.2, 6.3 Hz, 2H, H10''), 3.25 – 3.21 (m, 1H, H7), 2.35 – 2.32 (m, 2H, -CH<sub>2</sub>CH<sub>3</sub>), 2.12 – 2.06 (m, 1H, H9), 1.94

## Appendix A: Experimental

– 1.89 (m, 1H, H4'), 1.75 – 1.64 (m, 1H, H4''), 1.55 – 1.50 (m, 1H, H6), 1.42 (ddd,  $J = 14.0, 10.1, 4.4$  Hz, 1H, H8'), 1.33 (ddd,  $J = 14.0, 8.9, 2.2$  Hz, 1H, H8''), 1.14 (t,  $J = 7.5$  Hz, -CH<sub>2</sub>CH<sub>3</sub>), 0.91 (d,  $J = 6.8$  Hz, H29), 0.88 (s, 9H, Si-C(CH<sub>3</sub>)<sub>3</sub>), 0.84 (d,  $J = 6.8$  Hz, 3H, H28), 0.03 (s, 6H, Si-(CH<sub>3</sub>)<sub>2</sub>). **HRMS** (ES+) calcd for C<sub>26</sub>H<sub>47</sub>O<sub>6</sub>Si [M+H]<sup>+</sup> 497.3293, found 497.3283.

Data consistent with that reported in the literature.<sup>53</sup>

(3*R*,4*R*,5*R*,7*R*)-1-((tert-butyldimethylsilyl)oxy)-8-((4-methoxybenzyl)oxy)-4,7-dimethyloctane-3,5-diol



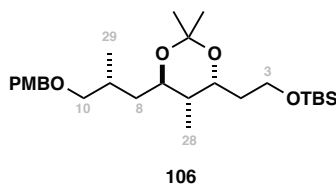
To a solution of crude ester **136** (1.10 g) in MeOH (10 mL) was added K<sub>2</sub>CO<sub>3</sub> (500 mg, 3.60 mmol). The suspension was stirred for 48 h before being filtered through a plug of cotton wool. Concentration of the organic filtrate in vacuo afforded diol **137** as a colourless oil (987 mg) which was used directly in the subsequent step without additional purification.

For the purposes of characterisation, an analytical sample was purified by flash column chromatography (SiO<sub>2</sub>, 50% EtOAc:PE<sub>40-60</sub>) to provide the following data:

**<sup>1</sup>H NMR** (500 MHz, CDCl<sub>3</sub>) δ 7.26 (d,  $J = 8.6$  Hz, 2H, Ar-H), 6.90 (d,  $J = 8.6$  Hz, 2H, Ar-H), 4.47 (s, 2H, Ar-CH<sub>2</sub>-O), 4.15 (d,  $J = 9.7$  Hz, 1H, H5), 3.90 – 3.79 (m, 2H, H3), 3.81 (s, 3H, Ar-OCH<sub>3</sub>), 3.70 – 3.66 (m, 1H, H7), 3.37 (dd,  $J = 9.0, 5.3$  Hz, 1H, H10'), 3.28 (dd,  $J = 9.0, 8.1$  Hz, 1H, H10''), 2.03 – 1.97 (m, 1H, H9), 1.88 – 1.81 (m, 1H, H4'), 1.64 – 1.50 (m, 3H, H8', H6, H4''), 1.42 – 1.40 (m, 1H, H8''), 0.95 (d,  $J = 6.9$  Hz, 3H, H29), 0.93 (d,  $J = 6.9$  Hz, 3H, H28), 0.91 (s, 9H, Si-C(CH<sub>3</sub>)<sub>3</sub>), 0.09 (s, 6H, Si-(CH<sub>3</sub>)<sub>2</sub>). **HRMS** (ES+) calcd for C<sub>24</sub>H<sub>45</sub>O<sub>5</sub>Si [M+H]<sup>+</sup> 441.3031, found 441.3020.

Data consistent with that reported in the literature.<sup>53</sup>

tert-butyl(2-((4*R*,5*R*,6*R*)-6-((*R*)-3-((4-methoxybenzyl)oxy)-2-methylpropyl)-2,2,5-trimethyl-1,3-dioxan-4-yl)ethoxy)dimethylsilane

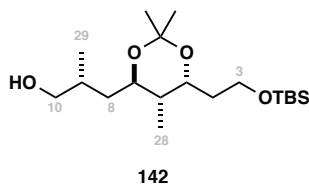


To a solution of crude diol **137** (850 mg) in CH<sub>2</sub>Cl<sub>2</sub> (5 mL) and Me<sub>2</sub>C(OMe)<sub>2</sub> (5 mL, 40.6 mmol) was added PPTS (cat.) and the reaction stirred for 2.5 h. NaHCO<sub>3</sub> (5 mL) was added, the layers separated and the aqueous phase extracted with CH<sub>2</sub>Cl<sub>2</sub> (4 x 5 mL). The combined organic extracts were dried (MgSO<sub>4</sub>), concentrated in vacuo and purified by flash column chromatography (SiO<sub>2</sub>, 30% EtOAc:PE<sub>40-60</sub>) to afford acetonide **106** as a colourless oil (942 mg, 86% over three steps from aldol adduct **109**).

**<sup>1</sup>H NMR** (500 MHz, CDCl<sub>3</sub>) δ 7.26 (d, *J* = 8.6 Hz, 2H, Ar-H), 6.87 (d, *J* = 8.7 Hz, 2H, Ar-H), 4.43 (s, 2H, Ar-CH<sub>2</sub>-O), 4.04 (ddd, *J* = 9.4, 5.2, 3.7 Hz, 1H, H5), 3.80 (s, 3H, Ar-OCH<sub>3</sub>), 3.72 – 3.55 (m, 2H, H3), 3.35 (dd, *J* = 9.1, 5.6 Hz, 1H, H10''), 3.30 (ddd, *J* = 10.5, 8.1, 2.4 Hz, 1H, H7), 3.21 (dd, *J* = 9.1, 7.0 Hz, 1H, H10'), 2.10 – 1.93 (m, 1H, H9), 1.73 – 1.48 (m, 5H, H6, H8, H4), 1.31 (s, 3H, C(CH<sub>3</sub>)<sub>2</sub>), 1.30 (s, 3H, C(CH<sub>3</sub>)<sub>2</sub>), 0.94 (d, *J* = 6.7 Hz, 3H, H28), 0.89 (s, 9H, Si-C(CH<sub>3</sub>)<sub>3</sub>), 0.81 (d, *J* = 6.9 Hz, 3H, H29), 0.04 (s, 6H, Si-(CH<sub>3</sub>)<sub>2</sub>). **<sup>13</sup>C NMR** (126 MHz, CDCl<sub>3</sub>) δ 159.18, 131.05, 129.29, 113.84, 100.58, 76.10, 72.70, 72.47, 65.53, 59.85, 55.41, 40.73, 38.57, 34.05, 30.19, 26.10, 25.09, 23.98, 18.42, 16.62, 11.86, -5.17, -5.21. **HRMS** (ES+) calcd for C<sub>27</sub>H<sub>49</sub>O<sub>5</sub>Si [M+H]<sup>+</sup> 481.3344, found 481.3336.

Data consistent with that reported in the literature.<sup>53</sup>

(R)-3-((4*R*,5*R*,6*R*)-6-(2-((tert-butyldimethylsilyl)oxy)ethyl)-2,2,5-trimethyl-1,3-dioxan-4-yl)-2-methylpropan-1-ol



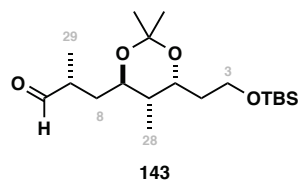
To a solution of PMB ether **106** (150 mg, 0.312 mmol) in CH<sub>2</sub>Cl<sub>2</sub> (15 mL) and pH 7 buffer (0.75 mL) was added DDQ (105 mg, 0.468 mmol). The resulting deep-red suspension was stirred for 2 h before being quenched by addition of NaHCO<sub>3</sub> (2 mL). The reaction mixture was diluted with H<sub>2</sub>O (30 mL), EtOAc (30 mL) and MeOH (0.5 mL) and the layers separated. The aqueous phase was extracted with EtOAc (5 x 10 mL) before the combined organic layers dried (MgSO<sub>4</sub>), concentrated in vacuo, and the resulting orange residue purified by flash column chromatography (SiO<sub>2</sub>, 10 → 25% EtOAc:PE<sub>40-60</sub> then 10% CH<sub>2</sub>Cl<sub>2</sub>:PhMe) to afford **142** as a colourless oil (115 mg, 77%).

**R<sub>f</sub>** (SiO<sub>2</sub>, 10% EtOAc:PE<sub>40-60</sub>) 0.2. **<sup>1</sup>H NMR** (500 MHz, CDCl<sub>3</sub>) δ 4.05 (ddd, *J* = 9.4, 5.2, 3.7 Hz, 1H, H5), 3.73 – 3.61 (m, 2H, H3), 3.58 – 3.51 (m, 1H, H10''), 3.44 – 3.34 (m, 1H, H10'), 3.29 (ddd, *J* = 10.2, 8.1, 1.9 Hz, 1H, H7), 1.81 – 1.71 (m, 1H, H9), 1.57 – 1.53 (m, 5H, H6, H4, H8), 1.35 (s, 3H, C(CH<sub>3</sub>)<sub>2</sub>), 1.33 (s, 3H, C(CH<sub>3</sub>)<sub>2</sub>), 0.94 (d, *J* = 6.9 Hz, 3H, H28), 0.89 (s, 9H, Si-C(CH<sub>3</sub>)<sub>3</sub>), 0.84 (d,

## Appendix A: Experimental

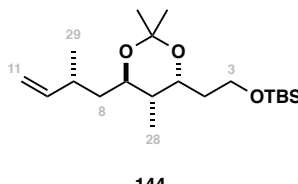
*J* = 6.8 Hz, 3H, H<sub>29</sub>), 0.04 (s, 6H, Si-(CH<sub>3</sub>)<sub>2</sub>). **<sup>13</sup>C NMR** (126 MHz, CDCl<sub>3</sub>) δ 100.97, 77.16, 74.50, 68.48, 65.57, 59.71, 40.93, 39.78, 34.71, 33.95, 26.10, 24.99, 23.90, 18.42, 18.15, 11.97, -5.18, -5.21. **HRMS** (ES+) calcd for C<sub>19</sub>H<sub>41</sub>O<sub>4</sub>Si [M+H]<sup>+</sup> 361.2769, found 361.2774. **IR** (thin film)  $\nu_{\text{max}}$  3438, 2987, 2955, 2906, 1514, 1502, 1305, 1219, 1182, 1094, 1053, 952, 934, 820 cm<sup>-1</sup>.  $[\alpha]_D^{25}$  (c 0.50, CHCl<sub>3</sub>) -16.2.

(*R*)-3-((4*R*,5*R*,6*R*)-6-(2-((tert-butyldimethylsilyl)oxy)ethyl)-2,2,5-trimethyl-1,3-dioxan-4-yl)-2-methylpropanal



To a solution of alcohol **142** (92 mg, 0.255 mmol) in CH<sub>2</sub>Cl<sub>2</sub> (20 mL) and H<sub>2</sub>O (0.1 mL) was added solid NaHCO<sub>3</sub> (171 mg, 2.04 mmol) and DMP (432 mg, 1.02 mmol) sequentially and the resulting suspension stirred for 1 h. Na<sub>2</sub>S<sub>2</sub>O<sub>3</sub> (5 mL) was added and the layers separated. The aqueous phase was extracted with CH<sub>2</sub>Cl<sub>2</sub> (3 x 15 mL) before the combined organic layers washed with NaHCO<sub>3</sub>, dried (Na<sub>2</sub>SO<sub>4</sub>) and concentrated in vacuo to give **143** as a colourless oil (106 mg) that was used directly in the subsequent reaction without additional purification owing to rapid epimerisation of the C9 stereocentre.

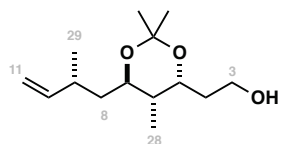
tert-butyldimethyl(2-((4*R*,5*R*,6*R*)-2,2,5-trimethyl-6-((*R*)-2-methylbut-3-en-1-yl)-1,3-dioxan-4-yl)ethoxy)silane



*n*-BuLi (0.52 mL, 1.6 M in hexane, 0.832 mmol) was added to a suspension of Ph<sub>3</sub>PMeBr (297 mg, 0.832 mmol) in THF (8 mL) at 0 °C to give a bright yellow solution which was stirred for 2 h. After cooling to -78 °C, a solution of aldehyde **143** (106 mg, crude) in THF (10 mL) was added and the reaction stirred overnight whilst warming to rt. NH<sub>4</sub>Cl (10 mL) was added and the layers separated. The aqueous phase was extracted with EtOAc (3 x 20 mL) before the combined organic phases dried (MgSO<sub>4</sub>), concentrated in vacuo, and the resulting residue purified by flash column chromatography (SiO<sub>2</sub>, 10 → 30% EtOAc:PE<sub>40-60</sub>) to afford **144** as a colourless oil (65 mg, 78% over two steps from **142**).

**R<sub>f</sub>** (SiO<sub>2</sub>, 10% EtOAc:PE<sub>40-60</sub>) 0.35. **<sup>1</sup>H NMR** (500 MHz, CDCl<sub>3</sub>) δ 5.83 (ddd, *J* = 17.2, 10.4, 6.8 Hz, 1H, H10), 5.00 (dt, *J* = 17.3, 1.6 Hz, 1H, H11'), 4.92 (dt, *J* = 10.4, 1.5 Hz, 1H, H11''), 4.08 (ddd, *J* = 9.4, 5.1, 3.7 Hz, 1H, H5), 3.74 – 3.62 (m, 2H, H3), 3.33 (ddd, *J* = 10.4, 7.9, 2.9 Hz, 1H, H7), 2.46 – 2.35 (m, 1H, H9), 1.72 – 1.51 (m, 5H, H8, H6, H4), 1.35 (s, 6H, C(CH<sub>3</sub>)<sub>2</sub>), 1.01 (d, *J* = 6.8 Hz, 3H, H29), 0.91 (s, 9H, Si-C(CH<sub>3</sub>)<sub>3</sub>), 0.88 – 0.76 (m, 3H, H28), 0.06 (s, 6H, Si-(CH<sub>3</sub>)<sub>2</sub>). **<sup>13</sup>C NMR** (125 MHz, CDCl<sub>3</sub>) δ 144.93, 111.87, 100.45, 72.42, 65.36, 59.68, 41.33, 40.48, 33.92, 33.53, 25.95, 25.02, 23.93, 18.54, 18.26, 11.76, -5.32, -5.36. **HRMS** (ES+) calcd for C<sub>20</sub>H<sub>40</sub>O<sub>4</sub>Si [M+H]<sup>+</sup> 357.2819, found 357.2821. **IR** (thin film)  $\nu_{\text{max}}$  2955, 2899, 1642, 1276, 1135, 1104, 997, 913, 847, 840, 677, 669 cm<sup>-1</sup>.  $[\alpha]_D^{25}$  (c 0.50, CHCl<sub>3</sub>) -22.3.

2-((4*R*,5*R*,6*R*)-2,2,5-trimethyl-6-((*R*)-2-methylbut-3-en-1-yl)-1,3-dioxan-4-yl)ethan-1-ol

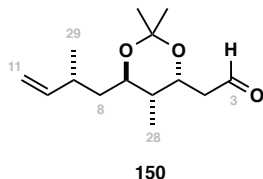


To a solution of **144** (65.3 mg, 0.183 mmol) in THF (10 mL) was added TBAF (1 mL, 1 M in THF, 1 mmol). The reaction was stirred at rt for 1 h before NaHCO<sub>3</sub> (5 mL) and CH<sub>2</sub>Cl<sub>2</sub> (10 mL) added and the phases separated. The aqueous phase was extracted with CH<sub>2</sub>Cl<sub>2</sub> (3 x 10 mL) before the combined organic layers dried (Na<sub>2</sub>SO<sub>4</sub>), concentrated in vacuo and purified by flash column chromatography (SiO<sub>2</sub>, 20% EtOAc:PE<sub>40-60</sub>) to give the title compound (41.0 mg, 93%) as a colourless residue.

**R<sub>f</sub>** (SiO<sub>2</sub>, 20% EtOAc:PE<sub>40-60</sub>) 0.30. **<sup>1</sup>H NMR** (500 MHz, CDCl<sub>3</sub>) δ 5.82 (ddd, *J* = 17.2, 10.4, 6.8 Hz, 1H, H10), 5.00 (dt, *J* = 17.3, 1.6 Hz, 1H, H11'), 4.93 (dt, *J* = 10.4, 1.5 Hz, 1H, H11''), 4.12 (ddd, *J* = 10.9, 5.1, 2.7 Hz, 1H, H5), 3.84 – 3.64 (m, 2H, H3), 3.35 (ddd, *J* = 9.9, 7.9, 2.8 Hz, 1H, H7), 2.51 – 2.44 (m, 1H, H9), 2.43 – 2.33 (m, 1H, H6), 1.81 (dddd, *J* = 14.5, 10.9, 7.7, 4.9 Hz, 1H, H4'), 1.70 – 1.57 (m, 2H, H8), 1.53 (dddd, *J* = 14.5, 5.5, 4.1, 2.7 Hz, 1H, H4''), 1.40 (s, 3H, C(CH<sub>3</sub>)<sub>2</sub>), 1.36 (s, 3H, C(CH<sub>3</sub>)<sub>2</sub>), 1.01 (d, *J* = 6.8 Hz, 3H, H29), 0.87 (d, *J* = 6.9 Hz, 3H, H28). **<sup>13</sup>C NMR** (125 MHz, CDCl<sub>3</sub>) δ 144.98, 112.16, 100.81, 72.50, 69.75, 62.20, 41.49, 40.78, 33.68, 32.86, 25.28, 24.01, 18.76, 12.05. **HRMS** (ES+) calcd for C<sub>14</sub>H<sub>30</sub>O<sub>3</sub>N [M+NH<sub>4</sub>]<sup>+</sup> 260.2220, found 260.2216. **IR** (thin film)  $\nu_{\text{max}}$  3360, 3335, 2950, 2887, 1642, 1633, 1271, 1135, 1075, 989, 918, 840, 678, 669, 625 cm<sup>-1</sup>.  $[\alpha]_D^{25}$  (c 0.10, CHCl<sub>3</sub>) -2.8.

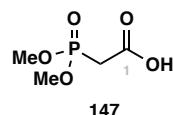
## Appendix A: Experimental

### 2-((4*R*,5*R*,6*R*)-2,2,5-trimethyl-6-((*R*)-2-methylbut-3-en-1-yl)-1,3-dioxan-4-yl)acetaldehyde



Alcohol (41.0 mg, 0.169 mmol) in CH<sub>2</sub>Cl<sub>2</sub> (1.5 mL) was added to a pre-mixed solution of (COCl)<sub>2</sub> (87 µL, 1.01 mmol) and DMSO (144 µL, 2.03 mmol) in CH<sub>2</sub>Cl<sub>2</sub> (2.5 mL) at -78 °C. After 15 min, Et<sub>3</sub>N (0.5 mL, 4.05 mmol) was added and the reaction mixture stirred for 30 min at -78 °C then 30 min at rt. H<sub>2</sub>O (2 mL) was added, the layers separated, and the organic layer concentrated in vacuo to give **150** (47 mg) as a yellow oil that was used directly in the subsequent Horner-Wadsworth-Emmons reaction without additional purification.

### 2-(dimethoxyphosphoryl)acetic acid



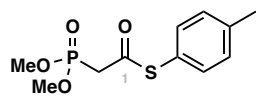
Trimethyl phosphonoacetate (16.0 mL, 111 mmol) was added to a solution of NaOH (4.88 g, 122 mmol) in H<sub>2</sub>O (40 mL) and the reaction mixture stirred for 18 h before the addition of HCl (10 mL, 37% aq.) at 0 °C. The solution was extracted with EtOAc (6 x 20 mL), the combined organic layers dried (MgSO<sub>4</sub>) and concentrated in vacuo to give carboxylic acid **147** (13.0 g, 77.3 mmol, 70%) which was used without further purification.

An analytical sample was purified by flash column chromatography (SiO<sub>2</sub>, 80% EtOAc:PE<sub>40-60</sub>) to provide the following data:

**<sup>1</sup>H NMR** (500 MHz, CDCl<sub>3</sub>) δ 10.55 (br s, 1H, OH), 3.80 (d, <sup>3</sup>J<sub>P-H</sub> = 11.6 Hz, 6H, O-CH<sub>3</sub>), 3.00 (d, <sup>2</sup>J<sub>P-H</sub> = 21.8 Hz, 2H, H2). **HRMS** (ES+) calcd for C<sub>4</sub>H<sub>10</sub>PO<sub>5</sub> [M+H]<sup>+</sup> 169.0260, found 169.0256.

Data consistent with that reported in the literature.<sup>53</sup>

### S-(*p*-tolyl)-2-(dimethoxyphosphoryl)ethanethioate



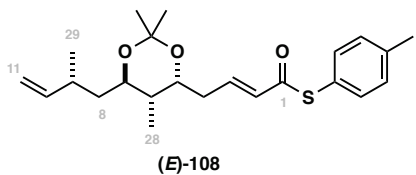
To a solution of acid **147** (10.0 g, 59.4 mmol) and 4-methylbenzenethiol (7.38 g, 59.4 mmol) in CH<sub>2</sub>Cl<sub>2</sub> (120 mL) was added DCC (12.3 g, 59.4 mmol) and DMAP (cat.). The resulting

suspension was stirred for 18 h before being diluted with Et<sub>2</sub>O (100 mL) and filtered through a short plug of celite. The filtrate was concentrated in vacuo, with the resulting residue purified by flash column chromatography (SiO<sub>2</sub>, 40 → 60% EtOAc:PE<sub>40-60</sub>) to give thiophosphonate **149** (12.8 g, 46.7 mmol, 79%) as a colourless oil.

**<sup>1</sup>H NMR** (500 MHz, CDCl<sub>3</sub>) δ 7.30 (d, *J* = 8.2 Hz, 2H, Ar-H), 7.22 (d, *J* = 8.2 Hz, 2H, Ar-H), 3.82 (d, <sup>3</sup>J<sub>P-H</sub> = 11.3 Hz, 6H, O-CH<sub>3</sub>), 3.30 (d, <sup>2</sup>J<sub>P-H</sub> = 21.2 Hz, 2H, H<sub>2</sub>), 2.37 (s, 3H, Ar-CH<sub>3</sub>). **HRMS** (ES+) calcd for C<sub>11</sub>H<sub>16</sub>PO<sub>4</sub>S [M+H]<sup>+</sup> 275.0507, found 275.0502.

Data consistent with that reported in the literature.<sup>53</sup>

S-(*p*-tolyl)-(E)-4-((4*R*,5*S*,6*R*)-2,2,5-trimethyl-6-((*R*)-2-methylbut-3-en-1-yl)-1,3-dioxan-4-yl)but-2-enethioate

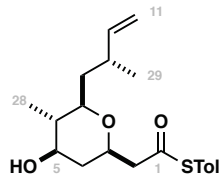


Phosphonate **149** (41.0 mg, 0.156 mmol) in THF (0.5 mL) was added dropwise to a suspension of LiCl (6 mg, 0.156 mmol) in THF (1.5 mL) at -10 °C, followed immediately by Et<sub>3</sub>N (0.02 mL, 0.156 mmol). After 20 min, a solution of aldehyde **150** (25.0 mg, 0.104 mmol) in THF (2 mL) was added dropwise and the reaction mixture stirred at -10 °C for 23 h. EtOAc (5 mL) and H<sub>2</sub>O (5 mL) were added and the phases separated. The aqueous layer was extracted sequentially with EtOAc (2 x 10 mL) and CH<sub>2</sub>Cl<sub>2</sub> (10 mL) before the combined organic extracts dried (Na<sub>2</sub>SO<sub>4</sub>), concentrated in vacuo and purified by flash column chromatography (SiO<sub>2</sub>, 10 → 30% EtOAc:hexanes) to give **108** (45 mg, 74%) as a white solid.

**R<sub>f</sub>** (SiO<sub>2</sub>, 20% EtOAc:PE<sub>40-60</sub>) 0.10. **<sup>1</sup>H NMR** (400 MHz, CDCl<sub>3</sub>) δ 7.33 (d, *J* = 8.1 Hz, 2H, Ar-H), 7.23 (d, *J* = 7.9 Hz, 2H, Ar-H), 6.95 (ddd, *J* = 15.6, 7.5, 6.4 Hz, 1H, H<sub>3</sub>), 6.30 – 6.20 (m, 1H, H<sub>2</sub>), 5.81 (ddd, *J* = 17.2, 10.4, 6.8 Hz, 1H, H<sub>10</sub>), 4.99 (dd, *J* = 17.3, 1.6 Hz, 1H, H<sub>11'</sub>), 4.93 – 4.76 (m, 1H, H<sub>11''</sub>), 3.99 (dt, *J* = 9.5, 5.0 Hz, 1H, H<sub>5</sub>), 3.44 – 3.25 (m, 1H, H<sub>7</sub>), 2.39 – 2.35 (m, 1H, H<sub>9</sub>), 2.38 (s, 3H, Ar-CH<sub>3</sub>), 2.30 – 2.19 (m, 1H, H<sub>6</sub>), 1.71 – 1.59 (m, 2H, H<sub>4</sub>), 1.35 – 1.29 (m, 8H, H<sub>8</sub>, C(CH<sub>3</sub>)<sub>2</sub>), 1.00 (d, *J* = 6.7 Hz, 3H, H<sub>29</sub>), 0.86 (d, *J* = 6.8 Hz, 3H, H<sub>28</sub>). **<sup>13</sup>C NMR** (126 MHz, CDCl<sub>3</sub>) δ 189.15, 144.95, 141.00, 139.01, 134.52, 133.83, 130.15, 125.48, 113.05, 100.78, 71.80, 71.59, 40.93, 37.76, 36.54, 35.92, 25.46, 24.19, 18.97, 12.07. **HRMS** (ES+) calcd for C<sub>23</sub>H<sub>33</sub>O<sub>3</sub>S [M+H]<sup>+</sup> 389.2145, found 389.2142. **IR** (thin film)  $\nu_{\text{max}}$  3021, 2950, 2887, 1945, 1854, 1730, 1690, 1649, 1631, 1623, 1271, 1195, 1135, 1075, 989, 918, 840, 678, 669, 625 cm<sup>-1</sup>.  $[\alpha]_D^{25}$  (c 1.05, CHCl<sub>3</sub>) -7.6

## Appendix A: Experimental

S-(*p*-tolyl)-2-((2*R*,4*R*,5*S*,6*R*)-4-hydroxy-5-methyl-6-((*R*)-2-methylbut-3-en-1-yl)tetrahydro-2*H*-pyran-2-yl)ethanethioate

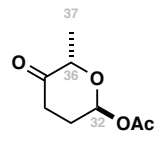


**107**

To a solution of **108** (37 mg, 0.145 mmol) in CH<sub>2</sub>Cl<sub>2</sub> (5 mL) was added *p*-TsOH (2 mg, 0.011 mmol) and *i*-PrOH (0.1 mL). The reaction was stirred for 36 h before H<sub>2</sub>O (5 mL) added and the phases separated. The organic layer was dried (Na<sub>2</sub>SO<sub>4</sub>), concentrated in vacuo and purified by flash column chromatography (SiO<sub>2</sub>, 10% Me<sub>2</sub>CO:PhMe) to afford **107** (23 mg, 70%) as a colourless residue.

**R<sub>f</sub>** (SiO<sub>2</sub>, 10% Me<sub>2</sub>CO:PhMe + 0.1% HCOOH) 0.40. **<sup>1</sup>H NMR** (500 MHz, CDCl<sub>3</sub>) δ 7.29 (d, *J* = 7.2 Hz, 2H, Ar-H), 7.24 (d, *J* = 8.1 Hz, 2H, Ar-H), 5.85 (ddd, *J* = 17.2, 10.4, 6.7 Hz, 1H, H10), 5.01 (dd, *J* = 17.3, 1.6 Hz, 1H, H11'), 4.92 (dd, *J* = 10.4, 1.5 Hz, 1H, H11''), 3.88 (dddd, *J* = 15.7, 13.9, 6.9, 4.3 Hz, 1H, H3), 3.44 – 3.35 (m, 1H, H5), 3.07 (td, *J* = 9.9, 2.9 Hz, 1H, H7), 2.94 (dd, *J* = 14.6, 8.6 Hz, 1H, H2''), 2.70 (dd, *J* = 14.6, 4.5 Hz, 1H, H2'), 2.60 – 2.50 (m, 1H, H9), 2.40 (s, 3H, Ar-CH<sub>3</sub>), 2.11 – 1.97 (m, 1H, H6), 1.64 – 1.43 (m, 2H, H4), 1.41 – 1.31 (m, 2H, H8), 0.98 (m, 6H, H29, H28). **<sup>13</sup>C NMR** (126 MHz, CDCl<sub>3</sub>) δ 195.65, 145.24, 139.72, 134.60, 134.39, 130.04, 124.19, 111.73, 78.43, 73.35, 72.36, 44.27, 40.65, 39.64, 33.12, 21.35, 18.20, 12.78. **HRMS** (ES+) calcd for C<sub>20</sub>H<sub>28</sub>O<sub>3</sub>Na [M+Na]<sup>+</sup> 371.1561, found 371.1558. **IR** (thin film)  $\nu_{\text{max}}$  3411, 2980, 2957, 2930, 2901, 2869, 2848, 1853, 1703, 1622, 1514, 1464, 1303, 1247, 1173, 1058, 1022, 1014, 975, 809, 743 cm<sup>-1</sup>.  $[\alpha]_D^{25}$  (c 0.50, CHCl<sub>3</sub>) -12.2.

(6*S*)-6-methyl-5-oxotetrahydro-2*H*-pyran-2-yl acetate



**42**

To (6*S*)-6-methyl-5-oxo-5,6-dihydro-2*H*-pyran-2-yl acetate **190** (485 mg, 2.85 mmol) was added Strykers reagent solution (8.0 mL, 0.025 M in copper/0.46 M in hydride) and *t*-BuOH (1.20 mL, 12.5 mmol) sequentially. After 3.5 h, the reaction was diluted with pentane (15 mL) and passed through a plug of SiO<sub>2</sub>, eluting with pentane (10 mL) then Et<sub>2</sub>O (60 mL). The filtrate was carefully concentrated in vacuo and purified by flash column chromatography

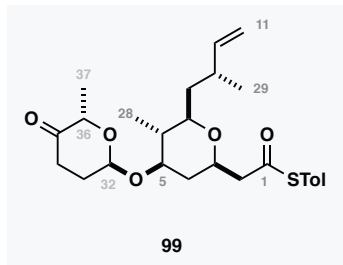
(SiO<sub>2</sub>, 30% Et<sub>2</sub>O:PE<sub>30-40</sub>) to give **42** (118 mg, >15:1  $\alpha$ : $\beta$ ; 141 mg, 1:1  $\alpha$ : $\beta$ , 62% total) as colourless residues.

The following data is provided for the major  $\alpha$ -anomer:

**<sup>1</sup>H NMR** (500 MHz, CDCl<sub>3</sub>)  $\delta$  6.27 (t,  $J$  = 5.1 Hz, 1H, H<sub>32</sub>), 4.35 (q,  $J$  = 6.7 Hz, 1H, H<sub>36</sub>), 2.58 – 2.47 (m, 2H, H<sub>34</sub>), 2.44 – 2.38 (m, 1H, H<sub>33'</sub>), 2.13 – 2.05 (m, 1H, H<sub>33''</sub>), 2.11 (s, 3H, Ac CH<sub>3</sub>), 1.30 (d,  $J$  = 6.7 Hz, 3H, H<sub>37</sub>). **HRMS** (ES+) calcd for C<sub>8</sub>H<sub>12</sub>O<sub>4</sub>Na [M+Na]<sup>+</sup> 15.0628, found 195.0625.

Data consistent with that reported in the literature.<sup>53</sup>

S-(4-methylphenyl) ((2*R*,4*R*,5*R*,6*R*)-5-methyl-6-((2*R*)-2-methylbut-3-en-1-yl)-4-(((2*R*,6*S*)-6-methyl-5-oxooxan-2-yl)oxy)oxan-2-yl)ethanethioate



A mixture of **107** (100 mg, 0.29 mmol) and **42** (197 mg, 1.15 mmol) were azeotroped with PhH (5 x 10mL), dissolved in THF (10 mL), cannulated onto powdered molecular sieves, and stirred for 1 h. The solution was cooled to -78 °C and freshly distilled BF<sub>3</sub>·Et<sub>2</sub>O (one drop) added. The reaction mixture was stirred for 16 h at -78 °C then quenched by addition of Et<sub>3</sub>N (0.5 mL). Concentration in vacuo and purification by flash column chromatography (SiO<sub>2</sub>, 40% EtOAc:hexanes) afforded the modified C1 – C11 fragment **99** (85 mg, 64%, dr 7:1) as a colourless oil.

**R<sub>f</sub>** (SiO<sub>2</sub>, 40% EtOAc:PE<sub>40-60</sub>) 0.5. **<sup>1</sup>H NMR** (500 MHz, CDCl<sub>3</sub>)<sup>\*</sup>  $\delta$  7.25 (d,  $J$  = 7.2 Hz, 2H, Ar-H), 7.20 (d,  $J$  = 8.1 Hz, 2H, Ar-H), 5.80 (ddd,  $J$  = 17.2, 10.4, 6.8 Hz, 1H, H<sub>10</sub>), 5.14 (t,  $J$  = 5.4 Hz, 1H, H<sub>32</sub>), 4.97 (dd,  $J$  = 17.3, 1.6 Hz, 1H, H<sub>11'</sub>), 4.88 (dd,  $J$  = 10.4, 1.5 Hz, 1H, H<sub>11''</sub>), 4.27 (q,  $J$  = 6.7 Hz, 1H, H<sub>36</sub>), 3.86 – 3.78 (m, 1H, H<sub>3</sub>), 3.52 (td,  $J$  = 10.6, 4.6 Hz, 1H, H<sub>5</sub>), 3.08 (td,  $J$  = 9.9, 2.9 Hz, 1H, H<sub>7</sub>), 2.92 (dd,  $J$  = 14.6, 8.3 Hz, 1H, H<sub>2''</sub>), 2.67 (dd,  $J$  = 14.6, 4.7 Hz, 1H, H<sub>2'</sub>), 2.56 – 2.47 (m, 1H, H<sub>9</sub>), 2.49 – 2.41 (m, 2H, H<sub>34</sub>), 2.35 (s, 3H, Ar-CH<sub>3</sub>), 2.30 – 2.23 (m, 1H, H<sub>33'</sub>), 2.14 (ddd,  $J$  = 12.1, 4.5, 1.9 Hz, 1H, H<sub>4''</sub>), 1.93 (ddt,  $J$  = 14.8, 9.5, 5.6 Hz, 1H, H<sub>33''</sub>), 1.54 – 1.50 (m, 1H, H<sub>8'</sub>),

\* NMR spectra were recorded with an internal deuterium lock and referenced to the residual non-deuterated solvent peak using modified values to allow comparison with the spectral data recorded by Winder (CHCl<sub>3</sub>:  $\delta$ <sub>H</sub> 7.24 ppm,  $\delta$ <sub>C</sub> 77.23 ppm). <sup>40</sup> All other compounds are referenced to standard values.

## Appendix A: Experimental

1.46 (dd,  $J = 10.3, 3.0$  Hz, 1H, H8''), 1.37 (ddq,  $J = 9.8, 6.4, 3.4$  Hz, 1H, H6), 1.26 (d,  $J = 6.8$  Hz, 3H, H37), 1.24 – 1.22 (m, 1H, 4') (s, 1H, H4'), 0.94 (d,  $J = 6.7$  Hz, 3H, H29), 0.91 (d,  $J = 6.5$  Hz, 3H, H28). **<sup>13</sup>C NMR** (126 MHz, CDCl<sub>3</sub>) δ 211.24 (C35), 195.78 (C1), 145.44 (C10), 140.00, 134.62, 130.29, 124.35, 112.00 (C11), 92.59 (C32), 78.87 (C7), 77.44, 77.23, 76.04 (C5), 72.44 (C3), 71.34 (C36), 49.92 (C2), 42.13 (C6), 39.98 (C8), 36.38 (C4), 33.84 (C34), 33.32 (C9), 28.85 (C33), 21.57, 18.44 (C29), 15.09 (C37), 13.31 (C28). **HRMS** (ASAP, +) calcd for C<sub>26</sub>H<sub>37</sub>O<sub>5</sub>S [M+H]<sup>+</sup> 461.2356, found 461.2349 also C<sub>26</sub>H<sub>40</sub>O<sub>5</sub>SN [M+NH<sub>4</sub>]<sup>+</sup> 478.2622, found 478.2614. **IR** (thin film)  $\nu_{\text{max}}$  3011, 2953, 2889, 2850, 1730, 1708, 1483, 1451, 1449, 1390, 1324, 1221, 1139, 1123, 1109, 1100, 1072, 1053, 724, 630, 625 cm<sup>-1</sup>.  $[\alpha]_D^{25}$  (c 2.00, CHCl<sub>3</sub>) -35.6.

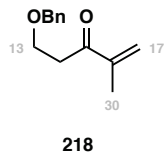
NMR data for madeirolide A and the C1 - C11 fragment **99**:

	Natural madeirolide A <b>1</b>				Synthetic C1 - C11 fragment <b>99</b>			
	<sup>13</sup> C [ppm]	<sup>1</sup> H [ppm]	mult	J [Hz]	<sup>13</sup> C [ppm]	<sup>1</sup> H [ppm]	mult	J [Hz]
1	170.9	-	-	-	195.9	-	-	-
2'	41.6	2.45	m	-	49.9	2.67	dd	14.6, 4.7
2''		2.58	m	-		2.92	dd	14.6, 8.3
3	74.2	3.80	m	-	72.4	3.82	m	-
4'	36.2	1.26	m	-	36.4	1.23	m	-
4''		2.14	m	-		2.14	ddd	12.1, 4.5, 1.9
5	75.9	3.56	td	10, 4	76.0	3.52	td	10.6, 4.6
6	42.9	1.32	m	-	42.1	1.37	ddq	9.8, 6.4, 3.4
7	77.9	3.07	td	78.9	78.9	3.08	td	9.9, 2.9
8'	40.5	1.44	m	40.0	40.0	1.52	m	-
8''						1.46	dd	10.3, 3.0
9	34.3	2.37	m	-	33.3	2.51	m	-
10	142.3	5.48	dd	15, 10	145.4	5.80	ddd	17.2, 10.4, 6.8
11'	122.8	6.24	dd	15, 11	112.0	4.97	dd	17.3, 1.6
11''						4.88	dd	10.4, 1.5
28	13.0	0.90	d	7	13.3	0.91	d	6.5
29	18.0	0.85	d	7	18.4	0.94	d	6.7
32	92.6	5.15	t	6	92.6	5.15	t	5.4
33'	28.8	1.93	m	-	28.9	1.93	ddt	14.8, 9.5, 5.6
33''		2.28	m	-		2.36	m	-
34	33.8	2.46	m	-	33.8	2.45	m	-
35	211.0	-	-	-	211.2	-	-	-
36	71.5	4.26	q	7	71.3	4.27	q	6.7
37	15.0	1.26	d	7	15.1	1.27	d	6.8

**EXPERIMENTAL PROCEDURES FOR THE EASTERN FRAGMENT OF  
MADEIROLIDE A**

**COMPOUNDS TOWARDS THE THF**

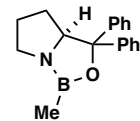
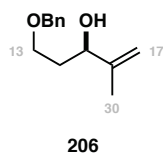
5-(benzyloxy)-2-methylpent-1-en-3-one



To a solution of DMSO (1.38 mL, 19.4 mmol) in  $\text{CH}_2\text{Cl}_2$  (5 mL) at  $-78^\circ\text{C}$  was added  $(\text{COCl})_2$  (0.83 mL, 9.70 mmol). After stirring for 15 min, a solution of  $(\pm)$ -5-(benzyloxy)-2-methylpent-1-en-3-ol (1.00 g, 4.85 mmol) in  $\text{CH}_2\text{Cl}_2$  (5 mL) was added. The reaction mixture was stirred for 30 min then  $\text{Et}_3\text{N}$  (4.50 mL, 29.1 mmol) was added. The reaction mixture was stirred for 10 min at  $-78^\circ\text{C}$  then warmed to rt before being quenched by addition of  $\text{H}_2\text{O}$  (50 mL). The layers were separated and the aqueous phase extracted with  $\text{Et}_2\text{O}$  ( $3 \times 50$  mL) before the combined organic extracts were dried ( $\text{Na}_2\text{SO}_4$ ), concentrated in vacuo and purified by flash column chromatography ( $\text{SiO}_2$ , 5% EtOAc:PE<sub>40-60</sub>) to give ketone **218** (860 mg, 87%) as a colourless oil.

**R<sub>f</sub>** ( $\text{SiO}_2$ , 30% EtOAc:PE<sub>40-60</sub>) 0.6. **<sup>1</sup>H NMR** (500 MHz,  $\text{CDCl}_3$ )  $\delta$  7.39 – 7.28 (m, 5H, Ar-H), 6.01 (s, 1H, H17'), 5.83 (s, 1H, H17''), 4.56 (s, 2H, -O-CH<sub>2</sub>-Ar), 3.83 (t,  $J = 6.5$  Hz, 2H, H13), 3.04 (t,  $J = 6.5$  Hz, 2H, H14), 1.91 (s, 3H, H30). **<sup>13</sup>C NMR** (126 MHz,  $\text{CDCl}_3$ )  $\delta$  200.05, 144.76, 138.34, 128.51, 127.83, 125.29, 73.42, 65.92, 37.92, 17.61. **HRMS** (ES+) calcd for  $\text{C}_{13}\text{H}_{17}\text{O}_2$  [ $\text{M}+\text{H}]^+$  205.1223, found 205.1221. **IR** (thin film,  $\nu_{\text{max}}$ ) 3540, 2933, 1700, 1453, 1365, 1274, 1204, 1099, 1073, 1004, 743.

(R)-5-(benzyloxy)-2-methylpent-1-en-3-ol



(S)-CBS catalyst

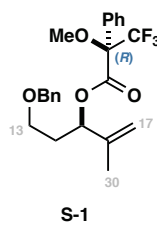
(S)-CBS catalyst (0.25 mL, 1 M soln in PhMe, 0.250 mmol) was added to a solution of enone **218** (691 mg, 3.38 mmol) in THF (5 mL) at  $-78^\circ\text{C}$ .  $\text{BH}_3 \cdot \text{DMS}$  (0.64 mL, 6.74 mmol) was added dropwise, and the reaction mixture stirred at  $-78^\circ\text{C}$  for 10 min then  $-50^\circ\text{C}$  for 12 h before

being quenched by addition of MeOH (5mL). The solution was warmed to rt and concentrated in vacuo. The resulting residue was redissolved in MeOH (10 mL) and concentrated in vacuo – this procedure was repeated five times. Purification by flash column chromatography (SiO<sub>2</sub>, 25% EtOAc:PE<sub>40-60</sub>) afforded allylic alcohol **206** (592 mg, 89%, er 97:3) as a pale-yellow oil.

**<sup>1</sup>H NMR** (500 MHz, CDCl<sub>3</sub>) δ 7.37 – 7.27 (m, 5H, Ar-H), 5.05 – 4.98 (m, 1H, H17'), 4.90 – 4.81 (m, 1H, H17''), 4.52 (s, 2H, -O-CH<sub>2</sub>-Ar), 4.26 (dd, *J* = 7.3, 4.3 Hz, 1H, H15), 3.70 (ddd, *J* = 9.4, 6.3, 5.0 Hz, 1H, H13'), 3.63 (ddd, *J* = 9.4, 7.0, 5.0 Hz, 1H, H13''), 1.86 (m, 2H, H14), 1.73 (s, 3H, H30). **HRMS** (ES+) calcd for C<sub>13</sub>H<sub>19</sub>O<sub>2</sub> [M+H]<sup>+</sup> 207.1380, found 207.1379. **Chiral HPLC** (Chiraldak-IA, 2% *i*-PrOH:*n*-hex, 1 μL/min) R<sub>t</sub> (major) = 12.2 min, R<sub>t</sub> (major) = 13.1 min, er 97:3. [α]<sub>D</sub><sup>25</sup> (c 1.05, CHCl<sub>3</sub>) +5.9 (lit. -5.54 for *ent*-**206**).\*

Data consistent with that reported in the literature.<sup>125</sup>

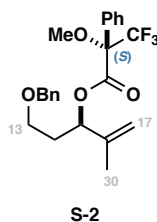
(*R*)-5-(benzyloxy)-2-methylpent-1-en-3-yl (*R*)-3,3,3-trifluoro-2-methoxy-2-phenylpropanoate



The (*R*)-MTPA ester **S-1** was prepared from **206** (3.1 mg, 0.015 mmol) following general procedure A and purified by flash column chromatography (SiO<sub>2</sub>, 0 → 10% EtOAc:PE<sub>40-60</sub>) to give (*R*)-MTPA ester **S-1** (4.9 mg, 77%) as a colourless residue.

**<sup>1</sup>H NMR** (500 MHz, CDCl<sub>3</sub>) δ 7.54 – 7.27 (m, 10H, Ar-H), 5.63 (dd, *J* = 8.5, 5.2 Hz, 1H, H15), 5.12 – 5.05 (m, 1H, H17'), 5.01 – 4.92 (m, 1H, H17''), 4.45 – 4.34 (m, 2H, -O-CH<sub>2</sub>-Ar), 3.51 (s, 3H, MTPA O-CH<sub>3</sub>), 3.44 – 3.28 (m, 2H, H13), 2.07 – 1.95 (m, 2H, H14), 1.74 (s, 3H, H30). **HRMS** (ES+) calcd for C<sub>23</sub>H<sub>29</sub>F<sub>3</sub>O<sub>4</sub>N [M+NH<sub>4</sub>]<sup>+</sup> 440.2043, found 440.2034.

(*R*)-5-(benzyloxy)-2-methylpent-1-en-3-yl (*S*)-3,3,3-trifluoro-2-methoxy-2-phenylpropanoate



\* Chiral HPLC analysis was conducted by Dr Michael Housden.

## Appendix A: Experimental

(S)-MTPA ester **S-2** was prepared from **206** (3.1 mg, 0.015 mmol) following general procedure A and purified by flash column chromatography ( $\text{SiO}_2$ , 0 → 10% EtOAc:PE<sub>40-60</sub>) to give (S)-MTPA ester **S-2** (5.2 mg, 81%) as a colourless residue.

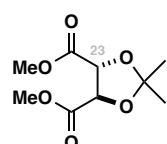
**<sup>1</sup>H NMR** (500 MHz,  $\text{CDCl}_3$ )  $\delta$  7.52 – 7.47 (m, 2H, Ar-H), 7.44 – 7.41 (m, 1H, Ar-H), 7.40 – 7.27 (m, 7H, Ar-H), 5.58 (dd,  $J$  = 8.3, 5.4 Hz, 1H, H15), 5.00 – 4.96 (m, 1H, H17'), 4.94 – 4.90 (m, 1H, H17''), 4.47 (s, 2H, -O-CH<sub>2</sub>-Ar), 3.49 (s, 3H, MTPA O-CH<sub>3</sub>), 3.49 – 3.43 (m, 2H, H13), 2.08 – 1.92 (m, 2H, H14), 1.61 (s, 3H, H30). **HRMS** (ES+) calcd for  $\text{C}_{23}\text{H}_{29}\text{F}_3\text{O}_4\text{N} [\text{M}+\text{NH}_4]^+$  440.2043, found 440.2033.

Proton	$\delta_{\text{S-MTPA}}$	$\delta_{\text{R-MTPA}}$	$\delta_{(\text{S-R})}$
13	3.47	3.36	+0.38
14	2.05	2.03	+0.02
15	5.58	5.63	-0.05
17'	4.98	5.08	-0.10
17''	4.92	4.98	-0.06
30	1.61	1.74	-0.13

Chemical shifts are taken as the midpoint of multiplets for the purpose of the MTPA analysis.

### 6.3.1 COMPOUNDS TOWARDS THE THP

Dimethyl (4*R*,5*R*)-2,2-dimethyl-1,3-dioxolane-4,5-dicarboxylate



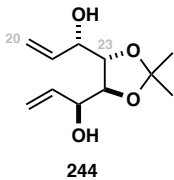
**242**

To a solution of L-(+)-dimethyltartrate (15.0 g, 84.2 mmol) in  $\text{CH}_2\text{Cl}_2$  (170 mL) was added 2,2-dimethoxypropane (20.0 mL, 168 mmol) and *p*-TsOH (8.00 g, 42.1 mmol). The reaction mixture was heated under reflux for 72 h before being diluted with  $\text{H}_2\text{O}$  (200 mL) and the layers separated. The organic layer was dried ( $\text{Na}_2\text{SO}_4$ ), concentrated in vacuo and purified by flash column chromatography ( $\text{SiO}_2$ , 30 → 70% EtOAc:PE<sub>40-60</sub>) to give **242** (7.31 g, 60%) as a yellow oil.

**<sup>1</sup>H NMR** (500 MHz,  $\text{CDCl}_3$ )  $\delta$  4.77 (s, 2H, CH), 3.78 (s, 6H, O-CH<sub>3</sub>), 1.45 (s, 6H, C(CH<sub>3</sub>)<sub>2</sub>). **<sup>13</sup>C NMR** (125 MHz,  $\text{CDCl}_3$ )  $\delta$  170.11, 113.90, 77.04, 52.86, 26.35. **HRMS** (ES+) calcd for  $\text{C}_9\text{H}_{14}\text{O}_6\text{Na} [\text{M}+\text{Na}]^+$  241.0683, found 241.0684.

Data consistent with that reported in the literature.<sup>170</sup>

(1*S*,1'*S*)-1,1'-((4*S*,5*S*)-2,2-dimethyl-1,3-dioxolane-4,5-diyl)bis(prop-2-en-1-ol)



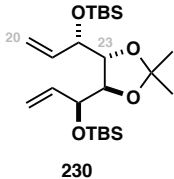
To a solution of **242** (1.00 g, 4.58 mmol) in PhMe (12 mL) at -78 °C was added DIBAL (9.16 mL, 1 M soln in hexane, 0.92 mmol) dropwise. The reaction mixture was stirred for 3 h at -78 °C before a solution of divinyl zinc (40.0 mL, 0.3 M soln in THF, 12.0 mmol) was added dropwise. The reaction mixture was warmed to rt and stirred for 18 h before the addition of NH<sub>4</sub>Cl (30 mL), Na/K tartrate (30 mL) and EtOAc (50 mL) sequentially. The layers were separated and the aqueous phase extracted with EtOAc (3 x 50 mL) before the combined organics dried (Na<sub>2</sub>SO<sub>4</sub>), concentrated in vacuo and purified by flash column chromatography (SiO<sub>2</sub>, 30% EtOAc:PE<sub>40-60</sub>) to give **244** (590 mg, 60%, dr 11:1) as a viscous yellow oil.

The following data was collected for the major diastereomer:

**<sup>1</sup>H NMR** (500 MHz, CDCl<sub>3</sub>) δ 5.99 (ddd, *J* = 17.2, 10.5, 6.0 Hz, 2H, H21), 5.39 (dt, *J* = 17.3, 1.5 Hz, 2H, H20'), 5.29 (dt, *J* = 10.5, 1.4 Hz, 2H, H20''), 4.25 – 4.15 (m, 2H, H22), 3.95 – 3.86 (m, 2H, H23), 2.58 (s, 2H, OH), 1.41 (s, 6H, C(CH<sub>3</sub>)<sub>2</sub>). **HRMS** (ES+) calcd. for C<sub>11</sub>H<sub>22</sub>O<sub>4</sub>N [M+NH<sub>4</sub>]<sup>+</sup> 232.1543, found 232.1547.

Data consistent with that reported in the literature.<sup>171</sup>

((1*S*,1'*S*)-((4*R*,5*R*)-2,2-dimethyl-1,3-dioxolane-4,5-diyl)bis(prop-2-ene-1,1-diyl))bis(tert-butyldimethylsilane)

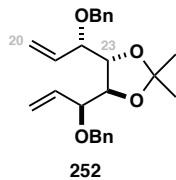


To a solution of **244** (100 mg, 0.47 mmol) in CH<sub>2</sub>Cl<sub>2</sub> (5 mL) was added TBSOTf (200 μL, 1.12 mmol) and 2,6-lutidine (160 μL, 1.40 mmol) sequentially. The reaction mixture was stirred at rt for 1.5 h then quenched by addition of NaHCO<sub>3</sub> (5 mL). The layers were separated and the aqueous phase extracted with CH<sub>2</sub>Cl<sub>2</sub> (3 x 5 mL) before the combined organics dried (Na<sub>2</sub>SO<sub>4</sub>), concentrated in vacuo, and purified by flash column chromatography (SiO<sub>2</sub>, 5% EtOAc:PE<sub>40-60</sub>) to give **230** (175 mg, 84%) as a yellow oil.

## Appendix A: Experimental

**R<sub>f</sub>** (SiO<sub>2</sub>, 10% EtOAc:PE<sub>40-60</sub>) 0.7. **<sup>1</sup>H NMR** (500 MHz, CDCl<sub>3</sub>) δ 5.87 (ddd, *J* = 17.1, 10.4, 6.5 Hz, 1H, H<sub>21</sub>), 5.23 (d, *J* = 17.1 Hz, 1H, H<sub>20'</sub>), 5.19 (d, *J* = 10.4 Hz, 1H, H<sub>20''</sub>), 4.23 (d, *J* = 6.5 Hz, 1H, H<sub>22</sub>), 3.96 (s, 1H, H<sub>23</sub>), 1.38 (s, 3H, C-CH<sub>3</sub>), 0.91 (s, 9H, Si-C(CH<sub>3</sub>)<sub>3</sub>), 0.08 (s, 3H, Si-CH<sub>3</sub>), 0.04 (s, 3H, Si-CH<sub>3</sub>). **<sup>13</sup>C NMR** (126 MHz, CDCl<sub>3</sub>) δ 138.04, 116.78, 109.18, 80.77, 74.42, 27.79, 26.17, 18.48, -4.06, -4.36. **HRMS** (ES+) calcd. for C<sub>23</sub>H<sub>50</sub>O<sub>4</sub>Si<sub>2</sub>N [M+NH<sub>4</sub>]<sup>+</sup> 460.3273, found 460.3271. **IR** (thin film,  $\nu_{\text{max}}$ ) 2899, 2875, 2164, 1640, 1300, 1294, 1241, 1235, 1200, 1164, 1076, 924, 725, 643 cm<sup>-1</sup>.  $[\alpha]_D^{25}$  (*c* 1.00, CHCl<sub>3</sub>) -30.9.

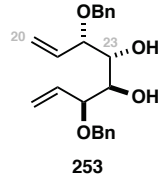
(4S,5S)-4,5-bis((S)-1-(benzyloxy)allyl)-2,2-dimethyl-1,3-dioxolane



NaH (34.0 mg, 60% dispersion in mineral oil, 1.40 mmol) was added to a solution of diol **244** (100 mg, 0.467 mmol) in THF (5 mL) at 0 °C. The reaction mixture was stirred for 30 min before BnBr (0.16 mL, 1.40 mmol) and TBAI (8 mg, 0.023 mmol) were added sequentially and the reaction warmed to rt. The reaction mixture was stirred for a further 18 h then concentrated in vacuo and purified by flash column chromatography (SiO<sub>2</sub>, 10% EtOAc:PE<sub>40-60</sub>) to give **252** (156 mg, 85%) as a yellow oil.

**R<sub>f</sub>** (SiO<sub>2</sub>, 10% EtOAc:PE<sub>40-60</sub>) 0.5. **<sup>1</sup>H NMR** (400 MHz, CDCl<sub>3</sub>) δ 7.37 – 7.19 (m, 5H, Ar-H), 5.83 (ddd, *J* = 17.4, 10.4, 8.0 Hz, 1H, H<sub>21</sub>), 5.35 (dd, *J* = 10.4, 1.8 Hz, 1H, H<sub>20'</sub>), 5.23 (dd, *J* = 17.3, 1.8 Hz, 1H, H<sub>20''</sub>), 4.60 (d, *J* = 12.0 Hz, 1H, Ar-O-CH<sub>2</sub>), 4.34 (d, *J* = 12.1 Hz, 1H, Ar-O-CH<sub>2</sub>'), 3.98 (dd, *J* = 2.9, 1.5 Hz, 1H, H<sub>22</sub>), 3.89 – 3.81 (m, 1H, H<sub>23</sub>), 1.36 (s, 3H, C(CH<sub>3</sub>)<sub>2</sub>). **<sup>13</sup>C NMR** (126 MHz, CDCl<sub>3</sub>) δ 138.26, 134.67, 128.43, 128.02, 127.67, 120.44, 110.10, 81.13, 80.44, 70.38, 27.20. **HRMS** (ES+) calcd for C<sub>25</sub>H<sub>34</sub>O<sub>4</sub>N [M+NH<sub>4</sub>]<sup>+</sup> 412.2482, found 412.2475. **IR** (thin film,  $\nu_{\text{max}}$ ) 2891, 1642, 1369, 1243, 1217, 1213, 1164, 1076, 924 cm<sup>-1</sup>.  $[\alpha]_D^{25}$  (*c* 1.00, CHCl<sub>3</sub>) +29.9

(3*S*,4*R*,5*R*,6*S*)-3,6-bis(benzyloxy)octa-1,7-diene-4,5-diol

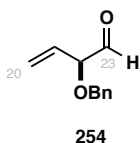


To a solution of **252** (40.0 mg, 0.101 mmol) in MeOH (2 mL) was added HCl (1 mL, 12 M aq., 12 mmol) and the reaction mixture stirred at 35 °C for 3 h then rt for 1 h. NaHCO<sub>3</sub> (20 mL) was added dropwise and the reaction mixture extracted with EtOAc (5 x 20 mL). The combined

organics were dried ( $\text{Na}_2\text{SO}_4$ ), concentrated in vacuo, and purified by flash column chromatography ( $\text{SiO}_2$ , 20% EtOAc:PE<sub>40-60</sub>) to give diol **253** (22 mg, 60%).

**R<sub>f</sub>** ( $\text{SiO}_2$ , 30% EtOAc:PE<sub>40-60</sub>) 0.3. **<sup>1</sup>H NMR** (400 MHz,  $\text{CDCl}_3$ )  $\delta$  7.39 – 7.27 (m, 5H, Ar-H), 5.84 (ddd,  $J$  = 17.1, 10.6, 7.3 Hz, 1H, H<sub>21</sub>), 5.44 – 5.30 (m, 2H, H<sub>20</sub>), 4.64 (d,  $J$  = 11.5 Hz, 1H, Ar-O-CH'<sub>2</sub>), 4.39 (d,  $J$  = 11.5 Hz, 1H, Ar-O-CH'<sub>2</sub>), 4.11 – 4.00 (m, 1H, H<sub>22</sub>), 3.94 – 3.79 (m, 1H, H<sub>23</sub>), 2.98 (d,  $J$  = 5.5 Hz, 1H, C<sub>23</sub>-OH). **<sup>13</sup>C NMR** (126 MHz,  $\text{CDCl}_3$ )  $\delta$  138.10, 134.00, 128.49, 128.03, 127.98, 120.90, 81.51, 73.27, 71.82. **HRMS** (ES+) calcd for  $\text{C}_{25}\text{H}_{34}\text{O}_4\text{N} [\text{M}+\text{NH}_4]^+$  412.2482, found 412.2475. **IR** (thin film,  $\nu_{\text{max}}$ ) 3510 (br), 3021, 2820, 1945, 1864, 1840, 1808, 1622, 1449, 1372, 895, 760, 690  $\text{cm}^{-1}$ .  $[\alpha]_D^{25}$  (*c* 1.00,  $\text{CHCl}_3$ ) +25.1

(S)-2-(benzyloxy)but-3-enal

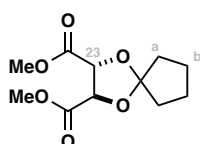


To a solution of diol **253** (10 mg, 0.028 mmol) in  $\text{CH}_2\text{Cl}_2$  (1 mL) was added  $\text{NaIO}_4/\text{SiO}_2$  (30 mg) and pH 4 buffer (0.05 mL). The reaction mixture was stirred for 1 h before being filtered through a plug of cotton wool and concentrated in vacuo to give a colourless oil (7.3 mg, ca. 73%).

The following data was obtained from the crude product:

**<sup>1</sup>H NMR** (400 MHz,  $\text{CDCl}_3$ )  $\delta$  10.02 (s, 1H, CHO), 7.43 – 7.11 (m, 5H, Ar-H), 6.16 (ddd,  $J$  = 16.5, 10.3, 6.2 Hz, 1H, H<sub>21</sub>), 5.32 – 5.06 (m, 2H, H<sub>20</sub>), 4.90 (d,  $J$  = 6.3 Hz, 1H, H<sub>22</sub>), 4.47 (d,  $J$  = 11.8 Hz, 1H, Ar-O-CH<sub>2</sub>'), 4.07 (d,  $J$  = 11.8 Hz, 1H, Ar-O-CH<sub>2</sub>''). **HRMS** (ES+) calcd for  $\text{C}_{11}\text{H}_{12}\text{O}_2 [\text{M}+\text{H}]^+$  177.0910, found 177.0919.

dimethyl (2*R*,3*R*)-1,4-dioxaspiro[4.4]nonane-2,3-dicarboxylate



**248**

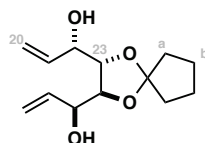
To a solution of L-(+)-dimethyltartrate (10 g, 57.1 mmol) in PhMe (120 mL) was added cyclopentanone (22 mL, 261 mmol) and 10-( $\pm$ )-CSA (1.10 g, 4.74 mmol). The reaction mixture was heated under reflux for 5 h, during which time the liberated  $\text{H}_2\text{O}$  was removed by azeotropic distillation. After cooling to rt,  $\text{NaHCO}_3$  (250 mL) was added and the layers

## Appendix A: Experimental

separated. The organic phase was dried ( $\text{MgSO}_4$ ), concentrated in vacuo and purified by flash column chromatography ( $\text{SiO}_2$ , 10% EtOAc:PE<sub>40-60</sub>) to give cyclopentylidene acetal **248** (2.6 g, 19%) as a colourless oil. The remaining mass was accounted for by recovered L-(+)-dimethyltartrate.

**R<sub>f</sub>** ( $\text{SiO}_2$ , 10% EtOAc:PE<sub>40-60</sub>) 0.2. **<sup>1</sup>H NMR** (500 MHz,  $\text{CDCl}_3$ )  $\delta$  4.78 (s, 1H, H23), 4.14 – 3.43 (m, 3H, O-CH<sub>3</sub>), 2.05 – 1.93 (m, 1H, Ha'), 1.92 – 1.82 (m, 1H, Ha''), 1.77 – 1.68 (m, 2H, Hb). **<sup>13</sup>C NMR** (126 MHz,  $\text{CDCl}_3$ )  $\delta$  170.03, 123.18, 76.80 (obscured by  $\text{CDCl}_3$ ), 52.78, 38.34, 23.45. **HRMS** (ES+) calcd for  $\text{C}_{11}\text{H}_{17}\text{O}_6$  [M+H]<sup>+</sup> 245.1020, found 245.1018. **IR** (thin film,  $\nu_{\text{max}}$ ) 2958, 2876, 1760, 1741, 1437, 1338, 1206, 1125, 973, 867 cm<sup>-1</sup>.  $[\alpha]_D^{25}$  (c 1.06,  $\text{CHCl}_3$ ) -28.1.

(1*S*,1'*S*)-1,1'-(*(2S,3S)*-1,4-dioxaspiro[4.4]nonane-2,3-diyl)bis(prop-2-en-1-ol)

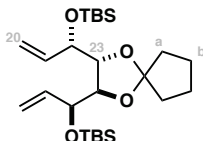


**250**

To a solution of **248** (2.00 g, 8.19 mol) in PhMe (24 mL) at -78 °C was added DIBAL (16.3 mL, 1 M soln in hexane, 16.3 mmol) dropwise. The reaction mixture was stirred for 5 h at -78 °C before a solution of divinyl zinc (80 mL, 0.3 M soln in THF, 24.0 mmol) was added dropwise. The reaction mixture was warmed to rt and stirred for 2 h before the addition of NH<sub>4</sub>Cl (70 mL), Na/K tartrate (30 mL) and EtOAc (50 mL) sequentially. The layers were separated and the aqueous phase extracted with EtOAc (3 x 150 mL) before the combined organics dried ( $\text{Na}_2\text{SO}_4$ ), concentrated in vacuo and purified by flash column chromatography ( $\text{SiO}_2$ , 10 → 50% EtOAc:PE<sub>40-60</sub>) to give **250** as a pale-yellow oil (1.56 g, 79%, dr 8:1).

The following data was collected for the major diastereomer:

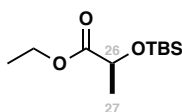
**R<sub>f</sub>** ( $\text{SiO}_2$ , 30% EtOAc:PE<sub>40-60</sub>) 0.15. **<sup>1</sup>H NMR** (500 MHz,  $\text{CDCl}_3$ )  $\delta$  5.98 (ddd, *J* = 17.3, 10.5, 5.9 Hz, 1H, H21), 5.38 (dd, *J* = 17.3, 1.5 Hz, 1H, H20'), 5.28 (dd, *J* = 10.5, 1.5 Hz, 1H, H20''), 4.20 – 4.10 (m, 1H, H23), 3.92 – 3.81 (m, 1H, H22), 1.89 – 1.81 (m, 1H, Ha'), 1.80 – 1.72 (m, 1H, Ha''), 1.71 – 1.60 (m, 2H, Hb). **<sup>13</sup>C NMR** (126 MHz,  $\text{CDCl}_3$ )  $\delta$  137.13, 119.76, 117.22, 81.46, 73.62, 37.42, 23.66. **HRMS** (ES+) calcd for  $\text{C}_{13}\text{H}_{20}\text{O}_4\text{Na}$  [M+Na]<sup>+</sup> 263.1254, found 263.1254. **IR** (thin film,  $\nu_{\text{max}}$ ) 3412, 2960, 2880, 2873, 1645, 1433, 1336, 1205, 994, 926 cm<sup>-1</sup>.  $[\alpha]_D^{25}$  (c 1.00,  $\text{CHCl}_3$ ) -46.2

(2*R*,3*R*)-2,3-bis((*S*)-1-((tert-butyldimethylsilyl)oxy)allyl)-1,4-dioxaspiro[4.4]nonane**251**

To a solution of **250** (250 mg, 1.04 mmol) in CH<sub>2</sub>Cl<sub>2</sub> (12 mL) at -78 °C was added TBSOTf (0.079 mL, 3.12 mmol) and 2,6-lutidine (0.48 mL, 4.16 mmol) sequentially. The reaction mixture was warmed to rt and stirred for 6 h then MeOH (1 mL) added and the solvent removed in vacuo. Purification by flash column chromatography (SiO<sub>2</sub>, 10% EtOAc:PE<sub>40-60</sub>) to afford **251** (410 mg, 84%) as a colourless oil.

**R<sub>f</sub>** (SiO<sub>2</sub>, 5% EtOAc:PE<sub>40-60</sub>) 0.2. **<sup>1</sup>H NMR** (400 MHz, CDCl<sub>3</sub>) δ 5.87 (ddd, *J* = 17.1, 10.4, 6.7 Hz, 1H, H<sub>21</sub>), 5.27 – 5.18 (m, 2H, H<sub>20</sub>), 4.18 – 4.12 (m, 1H, H<sub>23</sub>), 3.95 (dd, *J* = 3.9, 1.3 Hz, 1H, H<sub>22</sub>), 1.79 (td, *J* = 6.5, 5.9, 2.4 Hz, 2H, H<sub>a</sub>), 1.69 – 1.61 (m, 2H, H<sub>b</sub>), 0.91 (s, 9H, Si-C(CH<sub>3</sub>)<sub>3</sub>), 0.08 (s, 3H, Si-CH<sub>3</sub>), 0.04 (s, 3H, Si-CH<sub>3</sub>). **<sup>13</sup>C NMR** (126 MHz, CDCl<sub>3</sub>) δ 138.41, 119.39, 116.53, 80.90, 74.11, 38.20, 25.93, 23.51, 18.22, -4.13, -4.62. **HRMS** (ES+) calcd for C<sub>25</sub>H<sub>52</sub>O<sub>4</sub>Si<sub>2</sub>N [M+NH<sub>4</sub>]<sup>+</sup> 486.3249, found 486.3420. **IR** (thin film,  $\nu_{\text{max}}$ ) 2910, 2896, 2870, 2159, 2143, 1640, 1309, 1290, 1288, 1241, 1225, 1160, 1101, 1075, 924 cm<sup>-1</sup>.  $[\alpha]_D^{25}$  (c 1.00, CHCl<sub>3</sub>) +18.3

[All of the intermediates in this section are in the opposite enantiomeric series to the natural product due to the availability of (*S*)-ethyl lactate]

ethyl (*S*)-2-((tert-butyldimethylsilyl)oxy)propanoate**238**

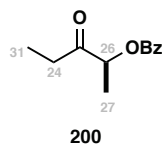
To a solution of ethyl (*S*)-2-hydroxypropanoate (31.0 g, 262 mmol) in CH<sub>2</sub>Cl<sub>2</sub> (1000 mL) was added TBSCl (56.0 g, 372 mmol) and imidazole (26.0 g, 382 mmol) sequentially. The reaction mixture was stirred for 18 h before being filtered through a plug of SiO<sub>2</sub> and concentrated in vacuo to give **238** as a colourless oil (90.4 g, 95%) which was used without additional purification.

An analytical sample was purified by flash column chromatography (SiO<sub>2</sub>, 10% EtOAc:PE<sub>40-60</sub>) to provide the following data:

## Appendix A: Experimental

**R<sub>f</sub>** (SiO<sub>2</sub>, 10% EtOAc:PE<sub>40-60</sub>) 0.35. **<sup>1</sup>H NMR** (500 MHz, CDCl<sub>3</sub>) δ 4.33 (q, *J* = 6.7 Hz, 1H, H<sub>26</sub>), 4.28 – 4.13 (m, 2H, OCH<sub>2</sub>), 1.42 (d, *J* = 6.8 Hz, 3H, H<sub>27</sub>), 1.30 (t, *J* = 7.1 Hz, 3H, OCH<sub>2</sub>CH<sub>3</sub>), 0.93 (s, 9H, Si-C(CH<sub>3</sub>)<sub>3</sub>), 0.16 (s, 3H, Si-CH<sub>3</sub>), 0.05 (s, 3H, Si-CH<sub>3</sub>). **<sup>13</sup>C NMR** (126 MHz, CDCl<sub>3</sub>) δ 174.06, 68.40, 60.60, 25.72, 21.20, 18.25, 14.39, -4.60. **HRMS** (ES+) calcd. for C<sub>11</sub>H<sub>25</sub>O<sub>3</sub>Si [M+H]<sup>+</sup> 233.1567, found 233.1567. **IR** (thin film,  $\nu_{\text{max}}$ ) 1732, 1730, 1455, 1310, 1211, 1093, 965, 801 cm<sup>-1</sup>.  $[\alpha]_D^{25}$  (c 1.00, CHCl<sub>3</sub>) -23.1.

(S)-3-oxopentan-2-yl benzoate

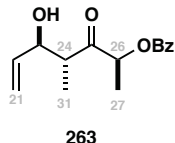


To a suspension of **238** (10.0 g, 43.0 mmol) and *N,O*-dimethylhydroxylamine hydrochloride (4.40 g, 45.1 mmol) in THF (200 mL) at 0 °C was added *i*-PrMgCl (44.0 mL of a 2.2 M solution in THF, 96.8 mmol) dropwise. The reaction mixture was stirred at 0 °C for 2 h then cooled to -20 °C and EtMgBr (40.0 mL of a 2.3 M solution in Et<sub>2</sub>O, 92.1 mmol) added dropwise. The reaction mixture was warmed rt and stirred for 18 h then quenched by cautious addition of NH<sub>4</sub>Cl (150 mL), extracted with EtOAc (3 x 150 mL), dried (MgSO<sub>4</sub>) and concentrated in vacuo to give (S)-2-((tert-butyldimethylsilyl)oxy)pentan-3-one. This material was used crude in the subsequent step.

To a solution of the crude (S)-2-((tert-butyldimethylsilyl)oxy)pentan-3-one (13 g) in THF (200 mL) was added TBAF (80.0 mL of a 1.0 M solution in THF, 80.0 mmol). The reaction mixture was stirred for 10 min before the sequential addition of Bz<sub>2</sub>O (20.0 g, 88.4 mmol), Et<sub>3</sub>N (12.0 mL, 86.1 mmol) and DMAP (cat.). After 18 h, NaHCO<sub>3</sub> (250 mL) was added and the reaction extracted with EtOAc (5 x 200 mL). The combined organic extracts were dried (Na<sub>2</sub>SO<sub>4</sub>) and concentrated in vacuo. Purification by flash column chromatography (SiO<sub>2</sub>, 20% EtOAc:PE<sub>40-60</sub>) afforded **200** (7.25 g, 82% over two steps) as a colourless oil.

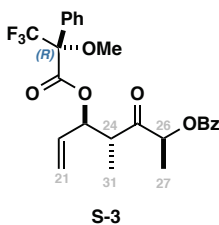
**<sup>1</sup>H NMR** (500 MHz, CDCl<sub>3</sub>) δ 8.12 – 8.03 (m, 2H, Ph-H), 7.63 – 7.56 (m, 1H, Ph-H), 7.51 – 7.41 (m, 2H, Ph-H), 5.36 (q, *J* = 7.0 Hz, 1H, H<sub>26</sub>), 2.66 (dq, *J* = 18.3, 7.3 Hz, 1H, H<sub>24''</sub>), 2.53 (dq, *J* = 18.3, 7.3 Hz, 1H, H<sub>24'</sub>), 1.53 (d, *J* = 7.1 Hz, 3H, H<sub>27</sub>), 1.10 (t, *J* = 7.3 Hz, 3H, H<sub>31</sub>). **HRMS** (ES+) calcd for C<sub>12</sub>H<sub>15</sub>O<sub>3</sub> [M+H]<sup>+</sup> 207.1016, found 207.1014.

Data consistent with that reported in the literature.<sup>135</sup>

(2*S*,4*R*,5*R*)-5-hydroxy-4-methyl-3-oxohept-6-en-2-yl benzoate

(*S*)-3-oxopentan-2-yl benzoate (*S*)-**200** (4.50 g, 21.8 mmol) in Et<sub>2</sub>O (10 mL) was added to a colourless solution of Cy<sub>2</sub>BCl (4.6 mL) and Et<sub>3</sub>N (4.0 mL) in Et<sub>2</sub>O (40 mL) at 0 °C. The mixture was held at this temperature for 2 h before being cooled to -78 °C and acrolein (6.0 mL, 89.9 mmol) added dropwise. Upon complete addition the reaction was warmed to -20 °C and held at this temperature for 36 h before the addition of MeOH (20 mL), pH 7 buffer (10 mL) and H<sub>2</sub>O<sub>2</sub> (2 mL, 30% aq.). The layers were separated and the aqueous phase extracted with Et<sub>2</sub>O (5 x 50 mL), with the combined organics dried (Na<sub>2</sub>SO<sub>4</sub>), filtered, and concentrated in vacuo. Sequential purification by flash column chromatography (SiO<sub>2</sub>, 10 → 20% EtOAc: PE<sub>40-60</sub>) and recrystallisation (hexanes:Et<sub>2</sub>O) afforded **263** (4.75 g, 85%) as white needle-like crystals.

**R<sub>f</sub>** (SiO<sub>2</sub>, 20% EtOAc:PE<sub>40-60</sub>) 0.2. **<sup>1</sup>H NMR** (400 MHz, CDCl<sub>3</sub>) δ 8.13 – 8.04 (m, 2H, Ph-H), 7.65 – 7.54 (m, 1H, Ph-H), 7.52 – 7.41 (m, 2H, Ph-H), 5.84 (ddd, *J* = 17.2, 10.4, 6.8 Hz, 1H, H<sub>22</sub>), 5.44 (q, *J* = 7.0 Hz, 1H, H<sub>26</sub>), 5.31 (dt, *J* = 17.1, 1.4 Hz, 1H, H<sub>21'</sub>), 5.22 (dt, *J* = 10.4, 1.2 Hz, 1H, H<sub>21''</sub>), 4.33 – 4.22 (m, 1H, H<sub>23</sub>), 3.00 – 2.86 (m, 1H, H<sub>24</sub>), 2.36 (d, *J* = 5.3 Hz, 1H, OH), 1.57 (d, *J* = 7.1 Hz, 3H, H<sub>27</sub>), 1.23 (d, *J* = 7.2 Hz, 3H, H<sub>31</sub>). **<sup>13</sup>C NMR** (125 MHz, CDCl<sub>3</sub>) δ 211.10, 165.85, 138.25, 133.36, 129.81, 129.46, 128.47, 117.17, 75.15, 74.78, 35.56, 15.69, 14.40. **HRMS** (ES+) calcd for C<sub>15</sub>H<sub>19</sub>O<sub>4</sub> [M+H]<sup>+</sup> 263.1278, found 263.1274. **IR** (thin film,  $\nu_{\max}$ ) 3345, 3110, 1813, 1732, 1727, 1718, 1430, 1377, 1104, 990, 905 cm<sup>-1</sup>.  $[\alpha]_D^{25}$  (c 1.00, CHCl<sub>3</sub>) +24.8. **mp** 122 °C dec.

(2*S*,4*R*,5*R*)-4-methyl-3-oxo-5-((*R*)-3,3,3-trifluoro-2-methoxy-2-phenylpropanoyl)oxy)hept-6-en-2-yl benzoate

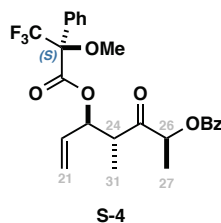
(*R*)-MTPA ester **S-3** was prepared from aldol adduct **263** (5 mg, 19 μmol) following general procedure A to give (*R*)-MTPA ester **S-3** (4 mg, 43%) as a white solid which was used crude in the MTPA analysis without additional purification.

**<sup>1</sup>H NMR** (500 MHz, CDCl<sub>3</sub>) δ 8.07 – 8.00 (m, 2H, Ar-H), 7.62 – 7.55 (m, 1H, Ar-H), 7.49 – 7.41 (m, 2H, Ar-H), 7.42 – 7.39 (m, 5H, MTPA Ar-H), 5.65 (ddd, *J* = 16.6, 10.0, 8.1, H<sub>22</sub>), 5.64 – 5.57

## Appendix A: Experimental

(m, 1H, H23) , 5.55 (dd,  $J = 16.6, 1.2$  Hz, 1H, H21'), 5.45 (dd,  $J = 9.9, 1.3$  Hz, 1H, H21''), 5.20 (q,  $J = 7.0$  Hz, 1H, H26), 3.52 (s, 3H, MTPA O-CH<sub>3</sub>), 3.11 – 3.02 (m, 1H, H24), 1.17 (d,  $J = 7.2$  Hz, 3H, H27), 1.15 (d,  $J = 7.0$  Hz, 3H, H31). **HRMS** (ES+) calcd for C<sub>25</sub>H<sub>26</sub>F<sub>3</sub>O<sub>6</sub> [M+H]<sup>+</sup> 479.1676, found 479.1680.

(2S,4R,5R)-4-methyl-3-oxo-5-(((S)-3,3,3-trifluoro-2-methoxy-2-phenylpropanoyl)oxy)hept-6-en-2-yl benzoate

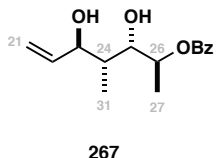


(S)-MTPA ester **S-4** was prepared following an analogous procedure to (R)-MTPA ester **S-3** using the enantiomeric MTPA acid to give **S-4** (7mg, 80%) as a white solid which was used crude in the MTPA analysis without additional purification.

**<sup>1</sup>H NMR** (500 MHz, CDCl<sub>3</sub>) δ 8.08 – 8.01 (m, 2H, Ph-H), 7.59 (ddt,  $J = 8.8, 7.4, 1.3$  Hz, 1H, Ph-H), 7.49 – 7.44 (m, 2H, Ph-H), 7.41 – 7.35 (m, 5H, MTPA Ph-H), 5.73 (ddd  $J = 16.7, 9.9, 8.1$ , H22), 5.71 – 5.65 (m, 1H, H23), 5.47 (dd,  $J = 16.6, 1.3$  Hz, 1H, H21'), 5.41 (dd,  $J = 9.9, 1.3$  Hz, 1H, H21''), 5.34 (q,  $J = 7.1$  Hz, 1H, H26), 3.43 (s, 3H, MTPA O-CH<sub>3</sub>), 3.10 – 3.04 (m, 1H, H24), 1.35 (d,  $J = 7.1$  Hz, 3H, H27), 1.21 (d,  $J = 7.2$  Hz, 3H, H31). **HRMS** (ES+) calcd for C<sub>25</sub>H<sub>26</sub>F<sub>3</sub>O<sub>6</sub> [M+H]<sup>+</sup> 479.1676, found 479.1679.

Proton	$\delta_{\text{S-MTPA}}$	$\delta_{\text{R-MTPA}}$	$\delta_{(\text{S-R})}$
21'	5.47	5.55	-0.08
21''	5.41	5.45	-0.04
22	5.73	5.65	+0.08
23	5.68	5.61	+0.07
24	3.07	3.07	0.00
31	1.21	1.15	+0.06
26	5.34	5.20	+0.14
27	1.35	1.17	+0.18

## (2S,3S,4R,5R)-3,5-dihydroxy-4-methylhept-6-en-2-yl benzoate

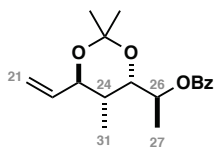
**267**

Aldol adduct **263** (1.90 g, 7.24 mmol) in MeCN (5 mL) was added to a solution of Me<sub>4</sub>NBH(OAc)<sub>3</sub> (9.50 g, 36.2 mmol) in MeCN (10 mL) and AcOH (15 mL) at -30 °C. The reaction mixture was stirred at -30 °C for 24 h then quenched by inverse addition into cold NaHCO<sub>3</sub> (100 mL). EtOAc (100 mL) was added and the layers separated before the aqueous phase extracted with EtOAc (3 x 100 mL). The combined organics were dried (Na<sub>2</sub>SO<sub>4</sub>) and concentrated in vacuo to afford **267** (1.55 g) as a crude residue which was used directly in the subsequent reaction without additional purification.

An analytical sample was purified by flash column chromatography (SiO<sub>2</sub>, 2% MeOH:CH<sub>2</sub>Cl<sub>2</sub> + 0.1% AcOH) to provide the following data:

**<sup>1</sup>H NMR** (400 MHz, CDCl<sub>3</sub>) δ 8.14 – 7.99 (m, 2H, Ar-H), 7.63 – 7.51 (m, 1H, Ar-H), 7.50 – 7.37 (m, Ar-H), 5.93 (ddd, *J* = 17.1, 10.5, 5.8 Hz, 1H, H<sub>22</sub>), 5.40 – 5.31 (m, 1H, H<sub>21'</sub>), 5.27 – 5.21 (m, 1H, H<sub>21''</sub>), 5.26 – 5.18 (m, 1H, H<sub>26</sub>), 4.21 – 4.15 (m, 1H, H<sub>25</sub>), 4.15 – 4.07 (m, 1H, H<sub>23</sub>), 1.84 – 1.73 (m, 1H, H<sub>24</sub>), 1.32 (d, *J* = 6.4 Hz, 3H, H<sub>27</sub>), 1.07 (d, *J* = 7.1 Hz, 3H, H<sub>31</sub>). **HRMS** (ES+) calcd for C<sub>15</sub>H<sub>20</sub>O<sub>4</sub>Na [M+Na]<sup>+</sup> 287.1254, found 287.1251.

## (S)-1-((4S,5R,6R)-2,2,5-trimethyl-6-vinyl-1,3-dioxan-4-yl)ethyl benzoate

**262**

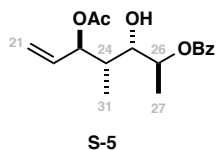
To a solution of diol **267** (1.55 g crude) in Me<sub>2</sub>C(OMe)<sub>2</sub> (20.0 mL, 163 mmol) and CH<sub>2</sub>Cl<sub>2</sub> (100 mL) was added *p*-TsOH (20 mg, 0.105 mmol). The reaction mixture was stirred for 18 h then diluted with H<sub>2</sub>O and the layers separated. The aqueous phase was extracted with CH<sub>2</sub>Cl<sub>2</sub> (3 x 150 mL) and the combined organics dried (MgSO<sub>4</sub>), concentrated in vacuo and purified by flash column chromatography (SiO<sub>2</sub>, 5 → 10% EtOAc: PE<sub>40-60</sub>) to afford **262** (1.9 g, 86% over two steps) as a colourless oil.

**R<sub>f</sub>** (SiO<sub>2</sub>, 10% EtOAc:PE<sub>40-60</sub>) 0.4. **<sup>1</sup>H NMR** (400 MHz, CDCl<sub>3</sub>) δ 8.07 – 7.97 (m, 2H, Ph-H), 7.59 – 7.51 (m, 1H, Ph-H), 7.44 (dd, *J* = 8.2, 7.0 Hz, 2H, Ph-H), 5.90 (ddd, *J* = 17.1, 10.4, 6.5 Hz, 1H, H<sub>22</sub>), 5.27 (d, *J* = 17.2 Hz, 1H, H<sub>21'</sub>), 5.24 – 5.20 (m, 1H, H<sub>26</sub>), 5.21 – 5.15 (m, 1H, H<sub>21''</sub>), 4.01

## Appendix A: Experimental

(dd,  $J = 9.0, 4.7$  Hz, 1H, H25), 3.79 (ddt,  $J = 7.7, 6.6, 1.2$  Hz, 1H, H23), 1.94 – 1.82 (m, 1H, H24), 1.39 (s, 3H, C(CH<sub>3</sub>)<sub>2</sub>), 1.35 (s, 2H, C(CH<sub>3</sub>)<sub>2</sub>), 1.33 (d,  $J = 6.3$  Hz, 3H, H27), 1.00 (d,  $J = 6.7$  Hz, 3H, H31). **<sup>13</sup>C NMR** (126 MHz, CDCl<sub>3</sub>) δ 166.16, 137.31, 132.84, 130.96, 129.68, 128.40, 116.07, 101.42, 76.73, 71.59, 70.36, 37.91, 24.63, 24.11, 16.61, 11.39. **HRMS** (ES+) calcd for C<sub>17</sub>H<sub>24</sub>O<sub>4</sub>Na [M+Na]<sup>+</sup> 327.1567, found 327.1567. **IR** (thin film,  $\nu_{\text{max}}$ ) 3327, 3112, 1735, 1729, 1633, 1415, 1233, 987, 950, 943, 939, 908, 880, 754 cm<sup>-1</sup>.  $[\alpha]_D^{25}$  (c 0.50, CHCl<sub>3</sub>) +6.2

(2S,3S,4S,5R)-5-acetoxy-3-hydroxy-4-methylhept-6-en-2-yl benzoate



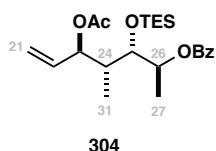
SmI<sub>2</sub> (6 mL, 0.1 M in THF, 0.6 mmol) was added to a solution of MeCHO (3 mL, 53.5 mmol) in THF (70 mL) at -50 °C. The reaction mixture was stirred at -50 °C for 15 min then cooled to -78 °C and a solution of **263** (1.50 g, 5.71 mmol) in THF (10 mL) added dropwise. The reaction mixture was stirred at -78 °C for 2 h, then 15 h at -50 °C. The reaction was quenched by addition of NH<sub>4</sub>Cl (60 mL), diluted with EtOAc (100 mL), and the layers separated. The aqueous phase was extracted with EtOAc (3 x 100 mL), dried (MgSO<sub>4</sub>), and concentrated in vacuo to give **S-5** (1.32 g, dr >20:1) as a white semi-solid. The crude product was used directly in the subsequent reaction without additional purification owing to observed migration of the O23 acetate.

The following data was collected on the crude material:

**<sup>1</sup>H NMR** (400 MHz, CDCl<sub>3</sub>) δ 8.05 (dd,  $J = 8.3, 1.4$  Hz, 2H, Ar-H), 7.62 – 7.51 (m, 1H, Ar-H), 7.45 (dd,  $J = 8.3, 7.0$  Hz, 2H, Ar-H), 5.79 (ddd,  $J = 17.0, 10.4, 7.4$  Hz, 1H, H22), 5.37 – 5.25 (m, 3H, 26, H21), 5.25 – 5.16 (m, 1H, H23), 3.82 (dd,  $J = 6.4, 3.6$  Hz, 1H, H25), 2.11 (s, 3H, Ac CH<sub>3</sub>), 1.96 – 1.83 (m, 1H, H24), 1.33 (d,  $J = 6.4$  Hz, 3H, H27), 0.96 (d,  $J = 7.0$  Hz, 3H, H31). **HRMS** (ES+) calcd for C<sub>17</sub>H<sub>23</sub>O<sub>5</sub> [M+H]<sup>+</sup> 307.1540, found 307.1541.

The position of the acetate was inferred based on the change in chemical shift of H23 in **S-5** relative to diol **267**.

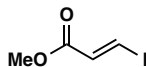
(2S,3S,4R,5R)-5-acetoxy-4-methyl-3-((triethylsilyl)oxy)hept-6-en-2-yl benzoate



To a solution of **S-5** (500 mg, crude) in THF (20 mL) was added TESOTf (0.54 mL, 2.40 mmol) and 2,6-lutidine (0.56 mL, 4.80 mmol) sequentially. The reaction mixture was stirred for 18 h then H<sub>2</sub>O (50 mL) and EtOAc (100 mL) added. The layers were separated and the aqueous phase extracted with EtOAc (3 x 100 mL). The combined organics were dried (Na<sub>2</sub>SO<sub>4</sub>), concentrated in vacuo and purified by flash column chromatography (SiO<sub>2</sub>, 5% EtOAc:PE<sub>40-60</sub>) to afford **304** (562 mg, 62% over two steps) as a pale-yellow oil.

**R<sub>f</sub>** (SiO<sub>2</sub>, 10% EtOAc:PE<sub>40-60</sub>) 0.7. **<sup>1</sup>H NMR** (500 MHz, CDCl<sub>3</sub>) δ 8.08 (dd, *J* = 8.3, 1.4 Hz, 2H, Ar-H), 7.58 (ddt, *J* = 8.7, 7.0, 1.3 Hz, 1H, Ar-H), 7.47 (t, *J* = 7.8 Hz, 2H, Ar-H), 5.70 (ddd, *J* = 17.4, 10.4, 7.2 Hz, 1H, H22), 5.30 – 5.26 (m, 1H, H21'), 5.23 (ddd, *J* = 10.4, 1.5, 0.8 Hz, 1H, H21''), 5.21 – 5.15 (m, 1H, H26), 5.14 – 5.10 (m, 1H, H23), 4.04 (dd, *J* = 6.5, 2.4 Hz, 1H, H25), 2.03 (s, 3H, Ac CH<sub>3</sub>), 2.02 – 1.96 (m, 1H, H24), 1.33 (d, *J* = 6.5 Hz, 3H, H27), 0.94 (d, *J* = 5.9 Hz, 3H, H31), 0.93 – 0.90 (m, 9H, Si-(CH<sub>2</sub>CH<sub>3</sub>)<sub>3</sub>), 0.64 – 0.51 (m, 6H, Si-(CH<sub>2</sub>CH<sub>3</sub>)<sub>3</sub>). **<sup>13</sup>C NMR** (126 MHz, CDCl<sub>3</sub>) δ 170.03, 166.09, 134.94, 132.89, 130.70, 129.60, 128.31, 118.78, 76.64, 74.41, 71.98, 38.37, 21.27, 15.69, 10.07, 6.90, 5.21. **IR** (thin film,  $\nu_{\text{max}}$ ) 3209, 2094, 1737, 1725, 1660, 1667, 1290, 1262, 1109, 1004, 865 cm<sup>-1</sup>. **HRMS** (ES+) calcd for C<sub>23</sub>H<sub>37</sub>O<sub>5</sub>Si [M+H]<sup>+</sup> 421.2405, found 421.2397.  $[\alpha]_D^{25}$  (c 1.2, CHCl<sub>3</sub>) +2.2.

Methyl (*E*)-3-iodoacrylate



259

To a solution of methyl propiolate (5.00 mL, 56.2 mmol) in AcOH (30 mL) was added NaI (17.0 g, 113 mmol) and the reaction mixture stirred at 70 °C for 18 h. After cooling to ambient temperature H<sub>2</sub>O (20 mL) and Et<sub>2</sub>O (20 mL) were added and the layers separated. The aqueous phase was extracted with Et<sub>2</sub>O (3 x 50 mL) before the combined organics neutralised with solid KOH (ca. 5 g), dried (MgSO<sub>4</sub>) and concentrated in vacuo to give a yellow oil (10.8 g, ca. 51 mmol).

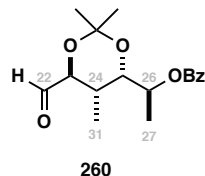
The crude product (10.8 g, ca. 51 mmol) was dissolved in benzene (100 mL) and HI (1.00 mL, 57% aq.) and the solution heated under reflux for 96 h. After cooling to ambient temperature H<sub>2</sub>O (20 mL) and Et<sub>2</sub>O (20 mL) were added and the layers separated. The aqueous phase was extracted with Et<sub>2</sub>O (3 x 50 mL) before the combined organic phase washed sequentially with NaHCO<sub>3</sub> (25 mL), Na<sub>2</sub>S<sub>2</sub>O<sub>4</sub> (25 mL) and brine (25 mL). Concentration in vacuo and purification by recrystallisation (hexanes:MeOH) gave geometrically pure **259** (10.2 g, 85% from methyl propiolate) as white needles.

## Appendix A: Experimental

**<sup>1</sup>H NMR** (500 MHz, CDCl<sub>3</sub>) δ 7.91 (d, *J* = 14.8 Hz, 1H, H<sub>21</sub>), 6.86 (d, *J* = 14.8 Hz, 1H, H<sub>20</sub>), 3.72 (s, 3H, O-CH<sub>3</sub>). **HRMS** (ES+) calcd for C<sub>4</sub>H<sub>6</sub>IO<sub>2</sub> [M+H]<sup>+</sup> 212.9412, found 212.9416.

Data consistent with that reported in the literature.<sup>172</sup>

(S)-1-((4*S*,5*S*,6*S*)-6-formyl-2,2,5-trimethyl-1,3-dioxan-4-yl)ethyl benzoate

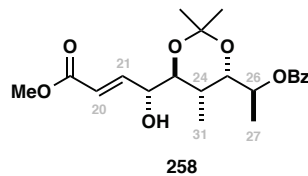


A solution of **262** (500 mg, 1.64 mmol) in CH<sub>2</sub>Cl<sub>2</sub> (80 mL) and MeOH (80 mL) was cooled to -78 °C and purged with O<sub>2</sub> for 1 min. O<sub>3</sub> was bubbled through the reaction mixture until a persistent deep-blue colour was achieved (ca. 5 min). The reaction mixture was purged with O<sub>2</sub> to remove excess O<sub>3</sub>, then quenched by addition of Me<sub>2</sub>S (0.5 mL) and warmed to rt. Filtration through cotton wool and concentration in vacuo afforded aldehyde **260** as a colourless oil which was used directly in the subsequent reaction without additional purification owing to rapid epimerisation of the C23 oxymethine.

The following data was collected on a mixture of the two C23 epimers:

**<sup>1</sup>H NMR** (500 MHz, CDCl<sub>3</sub>) δ 9.86 – 9.81 (m, 1H, CHO), 8.07 – 7.99 (m, 2H, Ar-H), 7.73 – 7.65 (m, 1H, Ar-H), 7.61 – 7.51 (m, 2H, Ar-H), 5.27 – 5.18 (m, 1H, H<sub>26</sub>), 3.96 – 3.90 (m, 1H), 3.89 – 3.85 (m, 1H), 3.79 – 3.74 (m, 1H), 2.33 – 2.25 (m, 1H), 1.43 – 1.38 (m, 6H, C(CH<sub>3</sub>)<sub>2</sub>), 1.36 – 1.31 (m, 3H, H<sub>27</sub>), 1.20 – 1.14 (m, 3H, H<sub>31</sub>).

(S)-1-((4*S*,5*R*,6*S*)-6-((*R,E*)-1-hydroxy-4-methoxy-4-oxobut-2-en-1-yl)-2,2,5-trimethyl-1,3-dioxan-4-yl)ethyl benzoate



A solution of aldehyde **260** (250 mg, 0.594 mmol) and iodide **259** (314 mg, 1.49 mmol) in degassed THF (15 mL) was added to a suspension of CrCl<sub>2</sub>\* (584 mg, 4.75 mmol) and NiCl<sub>2</sub> (cat.) in degassed DMF (15 mL). The emerald green solution was stirred for 16 h before being

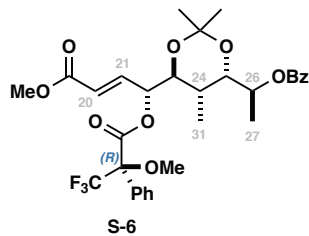
\* The quality of the CrCl<sub>2</sub> was found to be critical to the success of the NHK reaction, with best results obtained using a fresh commercial material manipulated in a glovebox and dried at 100 °C under high-vacuum for ~3 h immediately prior to use.

quenched with NaHCO<sub>3</sub> (50 mL) and diluted with Et<sub>2</sub>O (50 mL). The layers were separated and the aqueous phase extracted with Et<sub>2</sub>O (5 x 25 mL) before the combined organics washed with LiCl (50 mL of a satd aq soln), dried (Na<sub>2</sub>SO<sub>4</sub>), filtered, and concentrated in vacuo to give a yellow oil which was purified by flash column chromatography (SiO<sub>2</sub>, 10 → 50% EtOAc: PE<sub>40-60</sub>) to give **258** as a colourless oil (192 mg, 87%, 5:1 dr).

Data for the major isomer is provided below:

**R<sub>f</sub>** (SiO<sub>2</sub>, 20% EtOAc:PE<sub>40-60</sub>) 0.4. **<sup>1</sup>H NMR** (500 MHz, CDCl<sub>3</sub>) δ 8.11 – 8.01 (m, 2H, Ph-H), 7.62 – 7.53 (m, 1H, Ph-H), 7.52 – 7.42 (m, 2H, Ph-H), 6.98 (dd, J = 15.7, 4.5 Hz, 1H, H<sub>21</sub>), 6.23 (dd, J = 15.7, 2.0 Hz, 1H, H<sub>20</sub>), 5.28 – 5.15 (m, 1H, H<sub>22</sub>), 4.55 – 4.47 (m, 1H, H<sub>26</sub>), 3.86 (dd, J = 9.2, 4.1 Hz, 1H, H<sub>25</sub>), 3.80 (s, 3H, H<sub>28</sub>), 3.53 (dd, J = 6.9, 3.2 Hz, 1H, H<sub>23</sub>), 2.48 (s, 1H, OH), 2.19 – 2.03 (m, 1H, H<sub>24</sub>), 1.37 (s, 3H, C(CH<sub>3</sub>)<sub>2</sub>), 1.36 (s, 3H, C(CH<sub>3</sub>)<sub>2</sub>), 1.33 (d, J = 6.4 Hz, 3H, H<sub>27</sub>), 0.97 (d, J = 6.7 Hz, 3H, H<sub>31</sub>). **<sup>13</sup>C NMR** (126 MHz, CDCl<sub>3</sub>) δ 166.74, 166.09, 144.65, 132.86, 130.87, 129.65, 128.40, 122.17, 101.52, 77.56, 77.06, 72.36, 70.27, 51.86, 31.94, 24.73, 23.81, 16.38, 12.89. **IR** (thin film, ν<sub>max</sub>) 2905, 1736, 1729, 1713, 1624, 1605, 1510, 1390, 1125, 970, 850 cm<sup>-1</sup>. **HRMS** (ES+) calcd for C<sub>21</sub>H<sub>29</sub>O<sub>7</sub>[M+H]<sup>+</sup> 393.1908, found 393.1900. [α]<sub>D</sub><sup>25</sup> (c 1.50, CHCl<sub>3</sub>) +19.7.

(S)-1-((4S,5S,6S)-6-((R,E)-4-methoxy-4-oxo-1-(((R)-3,3,3-trifluoro-2-methoxy-2-phenylpropanoyl)oxy)but-2-en-1-yl)-2,2,5-trimethyl-1,3-dioxan-4-yl)ethyl benzoate

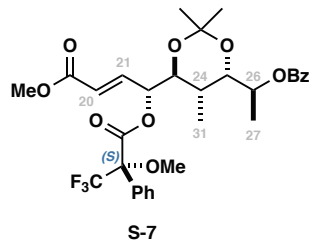


(R)-MTPA ester **S-6** was prepared from **258** (10 mg, 0.025 mmol) following general procedure A to give **S-6** (7 mg, 45%) as a white solid which was used crude in the MTPA analysis without additional purification.

**<sup>1</sup>H NMR** (500 MHz, CDCl<sub>3</sub>) δ 8.03 (dd, J = 8.3, 1.5 Hz, 2H, Ar-H), 7.67 – 7.61 (m, 1H, Ar-H), 7.60 – 7.52 (m, 2H, Ar-H), 7.51 – 7.41 (m, 5H, Ar-H). 6.91 (dd, J = 15.8, 5.0 Hz, 1H, H<sub>21</sub>), 5.98 (dd, J = 15.8, 1.7 Hz, 1H, H<sub>20</sub>), 5.82 (ddd, J = 5.0, 3.1, 1.8 Hz, 1H, H<sub>22</sub>), 5.20 – 5.10 (m, 1H, H<sub>26</sub>), 3.82 (dd, J = 9.3, 4.0 Hz, 1H, H<sub>25</sub>), 3.77 (s, 3H, O-CH<sub>3</sub>), 3.63 (dd, J = 6.8, 3.0 Hz, 1H, H<sub>23</sub>), 3.59 (s, 3H, MTPA O-CH<sub>3</sub>), 2.09 – 2.03 (m, 1H, H<sub>24</sub>), 1.35 (s, 3H, C(CH<sub>3</sub>)<sub>2</sub>), 1.32 (s, 3H, C(CH<sub>3</sub>)<sub>2</sub>), 1.23 (d, J = 6.4 Hz, 3H, H<sub>27</sub>), 0.95 (d, J = 6.8 Hz, 3H, H<sub>31</sub>). **HRMS** (ES+) calcd for C<sub>31</sub>H<sub>36</sub>F<sub>3</sub>O<sub>9</sub> [M+H]<sup>+</sup> 609.2306, found 609.2307.

## Appendix A: Experimental

(*S*)-1-((4*S*,5*S*,6*S*)-6-((*R,E*)-4-methoxy-4-oxo-1-(((*S*)-3,3,3-trifluoro-2-methoxy-2-phenylpropanoyl)oxy)but-2-en-1-yl)-2,2,5-trimethyl-1,3-dioxan-4-yl)ethyl benzoate

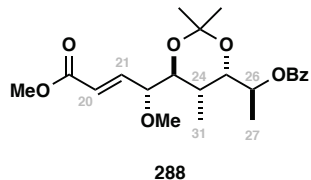


(*S*)-MTPA ester **S-7** was prepared following an analogous procedure to (*R*)-MTPA ester **S-6** using the enantiomeric MTPA acid to give **S7** (10.5 mg, 68%) as a white solid which was used crude in the MTPA analysis without additional purification.

**<sup>1</sup>H NMR** (500 MHz, CDCl<sub>3</sub>) δ 8.09 – 7.90 (m, 2H, Ar-H), 7.60 – 7.50 (m, 8H, Ar-H), 6.93 (dd, *J* = 15.8, 5.9 Hz, 1H, H21), 6.07 (dd, *J* = 15.8, 1.5 Hz, 1H, H20), 5.79 – 5.75 (m, 1H, H22), 5.10 (dq, *J* = 9.4, 6.5 Hz, 1H, H26), 3.78 (s, 3H, OCH<sub>3</sub>), 3.77 – 3.74 (m, 1H, H25), 3.57 (s, 3H, MTPA-OCH<sub>3</sub>), 3.55 – 3.49 (m, 1H, H23), 1.90 – 1.80 (m, 1H, H24), 1.27 (s, 3H, C(CH<sub>3</sub>)<sub>2</sub>), 1.21 (s, 3H, C(CH<sub>3</sub>)<sub>2</sub>), 1.19 (d, *J* = 6.4 Hz, 3H, H27), 0.86 (d, *J* = 6.9 Hz, 3H, H31). **HRMS** (ES+) calcd for C<sub>31</sub>H<sub>36</sub>F<sub>3</sub>O<sub>9</sub> [M+H]<sup>+</sup> 609.2306, found 609.2303.

Proton	$\delta_{\text{S-MTPA}}$	$\delta_{\text{R-MTPA}}$	$\delta_{(\text{S-R})}$
OMe (ester)	3.78	3.77	+0.01
20	6.07	5.98	+0.09
21	6.93	6.91	+0.02
22	5.77	5.82	-0.05
23	3.52	3.63	-0.11
24	1.85	2.06	-0.21
25	3.76	3.82	-0.06
26	5.10	5.15	-0.05
27	1.19	1.19	0
31	0.86	0.95	-0.09

(*S*)-1-((4*S*,5*S*,6*S*)-6-((*R,E*)-1,4-dimethoxy-4-oxobut-2-en-1-yl)-2,2,5-trimethyl-1,3-dioxan-4-yl)ethyl benzoate

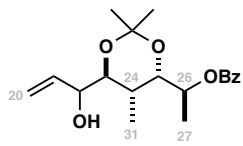


288

To a solution of  $(\text{MeO})_3\text{BF}_4$  [Meerwein salt] (282 mg, 1.91 mmol) and Proton Sponge™ (409 mg, 1.91 mmol) in  $\text{CH}_2\text{Cl}_2$  (5 mL) was added a solution **258** (0.05 g, 0.127 mmol) in  $\text{CH}_2\text{Cl}_2$  (5 mL). The reaction mixture was stirred for 3 h then quenched by addition of  $\text{NaHCO}_3$  (5 mL). EtOAc (20 mL) was added and the layers separated. The organic phase was washed with citric acid (10% wt aq., 3 x 10 mL), dried ( $\text{Na}_2\text{SO}_4$ ) and concentrated in vacuo. Purification by flash column chromatography ( $\text{SiO}_2$ , 10% EtOAc:PE<sub>40-60</sub>) afforded **288** as a yellow oil (40.3 mg, 78%).

**R<sub>f</sub>** ( $\text{SiO}_2$ , 20% EtOAc:PE<sub>40-60</sub>) 0.35. **<sup>1</sup>H NMR** (500 MHz,  $\text{CDCl}_3$ )  $\delta$  8.05 (dt,  $J$  = 8.4, 1.3 Hz, 2H, Ar-H), 7.60 – 7.52 (m, 1H, Ar-H), 7.49 – 7.41 (m, 2H, Ar-H), 6.94 (dd,  $J$  = 15.8, 6.3 Hz, 1H, H<sub>21</sub>), 6.10 (dd,  $J$  = 15.8, 1.3 Hz, 1H, H<sub>20</sub>), 5.20 (ddd,  $J$  = 9.1, 6.3, 2.5 Hz, 1H, H<sub>26</sub>), 3.92 (dd,  $J$  = 9.2, 4.1 Hz, 1H, H<sub>25</sub>), 3.82 – 3.78 (m, 4H, H<sub>22</sub>, O-CH<sub>3</sub>), 3.53 – 3.45 (m, 1H, H<sub>23</sub>), 3.41 (s, 3H, O-CH<sub>3</sub>), 2.04 – 1.93 (m, 1H, H<sub>24</sub>), 1.39 – 1.28 (m, 9H, H<sub>27</sub>, C(CH<sub>3</sub>)<sub>2</sub>), 1.02 (d,  $J$  = 6.7 Hz, 3H, H<sub>31</sub>). **<sup>13</sup>C NMR** (126 MHz,  $\text{CDCl}_3$ )  $\delta$  166.58, 166.15, 144.91, 132.83, 130.96, 129.68, 128.40, 123.54, 101.39, 82.66, 71.93, 70.40, 58.18, 58.16, 51.86, 34.23, 25.03, 23.53, 16.41, 12.85. **HRMS** (ES+) calcd for  $\text{C}_{22}\text{H}_{31}\text{O}_7$  [ $\text{M}+\text{H}]^+$  407.2064, found 407.2064. **IR** (thin film,  $\nu_{\text{max}}$ ) 3000, 2905, 1732, 1709, 1626, 1600, 1510, 1405, 1391, 1125, 970, 850, 733, 640  $\text{cm}^{-1}$ .  $[\alpha]_D^{25}$  (c 1.50,  $\text{CHCl}_3$ ) +11.0.

(*1S*)-1-((4*S*,5*R*,6*S*)-6-(1-hydroxyallyl)-2,2,5-trimethyl-1,3-dioxan-4-yl)ethyl benzoate



318

To a solution of **320** (100 mg, 0.329 mmol, crude) in THF (10 mL) at -78 °C was added vinyl MgBr (0.5 mL, 1 M in THF, 0.5 mmol). The reaction mixture was warmed to rt and stirred for 36 h before the addition of NH<sub>4</sub>Cl (10 mL) and EtOAc (10 mL) sequentially. The layers were separated and the aqueous phase extracted with EtOAc (3 x 25 mL) before the combined organics dried ( $\text{Na}_2\text{SO}_4$ ), concentrated in vacuo and purified by flash column chromatography ( $\text{SiO}_2$ , 10 → 30% EtOAc:PE<sub>40-60</sub>) to give **318** (46 mg, 42%, dr 2:1) as a colourless oil.

## Appendix A: Experimental

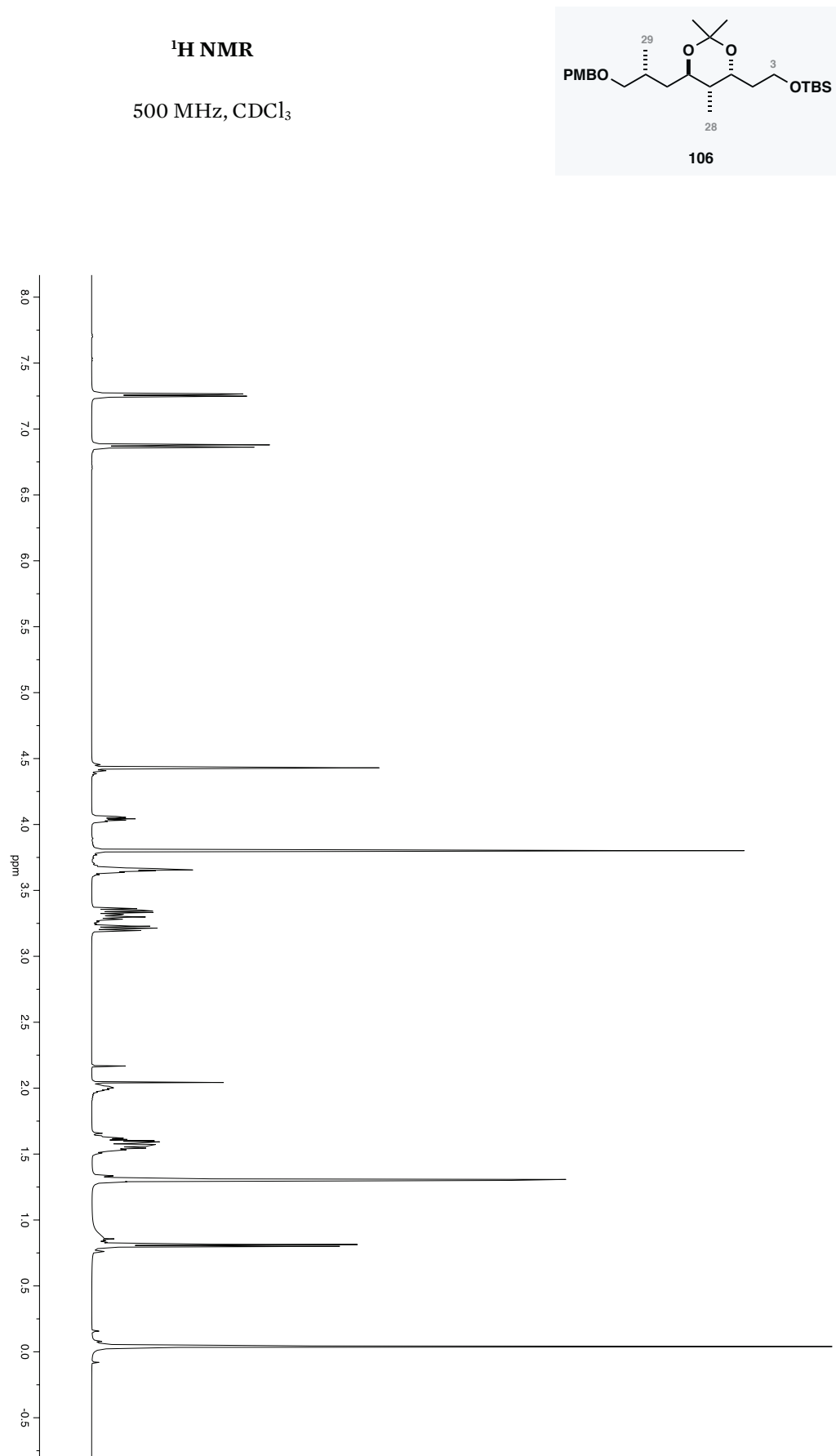
The following data was recorded on the mixture of C22 epimers:

**<sup>1</sup>H NMR** (500 MHz, CDCl<sub>3</sub>) δ 8.10 – 7.96 (m, 2H, Ar-H), 7.58 – 7.50 (m, 1H, Ar-H), 7.43 (td, *J* = 7.8, 1.6 Hz, 2H, Ar-H), 5.89 (dddd, *J* = 18.9, 17.0, 10.5, 6.2 Hz, 1H, H21 major + minor), 5.40 (d, *J* = 17.3 Hz, 0.64H, H20' major), 5.39 (d, *J* = 17.2 Hz, 0.36H, H20' minor), 5.27 (ddt, *J* = 10.4, 8.8, 1.5 Hz, 1H, H20'' major + minor), 5.19 (dq, *J* = 9.1, 6.5 Hz, 1H, H26 major + minor), 4.29 – 4.24 (m, 0.64H, H22 major), 4.06 – 4.00 (m, 0.34H, H22 minor), 3.91 (dd, *J* = 9.2, 4.2 Hz, 0.36H, H25 minor), 3.84 (dd, *J* = 9.2, 4.0 Hz, 0.64H, H25 major), 3.45 (dd, *J* = 6.8, 3.1 Hz, 0.64H, H23 major), 3.26 (dd, *J* = 7.1, 5.5 Hz, 0.36H, H23 minor), 2.50 (d, *J* = 5.1 Hz, 0.36H, OH minor), 2.28 (d, *J* = 4.4 Hz, 0.64H, OH major), 2.10 (ddq, *J* = 6.8, 4.1 Hz, 0.64H, H24 major + minor), 2.02 (ddq, *J* = 6.7, 4.1 Hz, 0.36H, H24 major + minor), 1.37 – 1.29 (m, 9H, H31 major + minor, C(CH<sub>3</sub>)<sub>2</sub>), 0.98 (dd, *J* = 6.8, 1.7 Hz, 3H, H31 major + minor). **HRMS** (ES+) calcd for C<sub>19</sub>H<sub>26</sub>O<sub>5</sub>Na [M+Na]<sup>+</sup> 357.1673, found 357.1679.

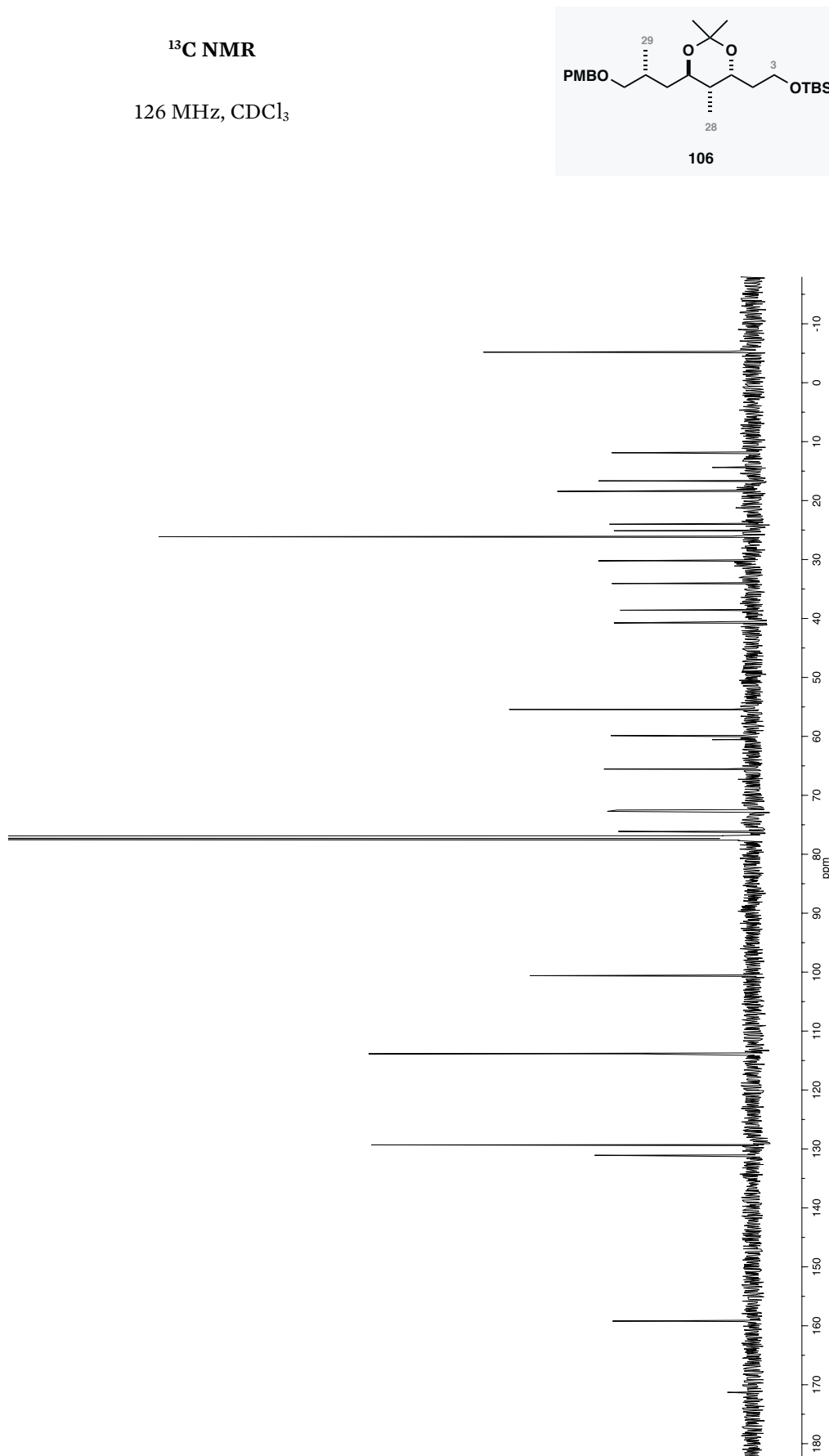
# B

## APPENDIX B: SELECTED NMR SPECTRA

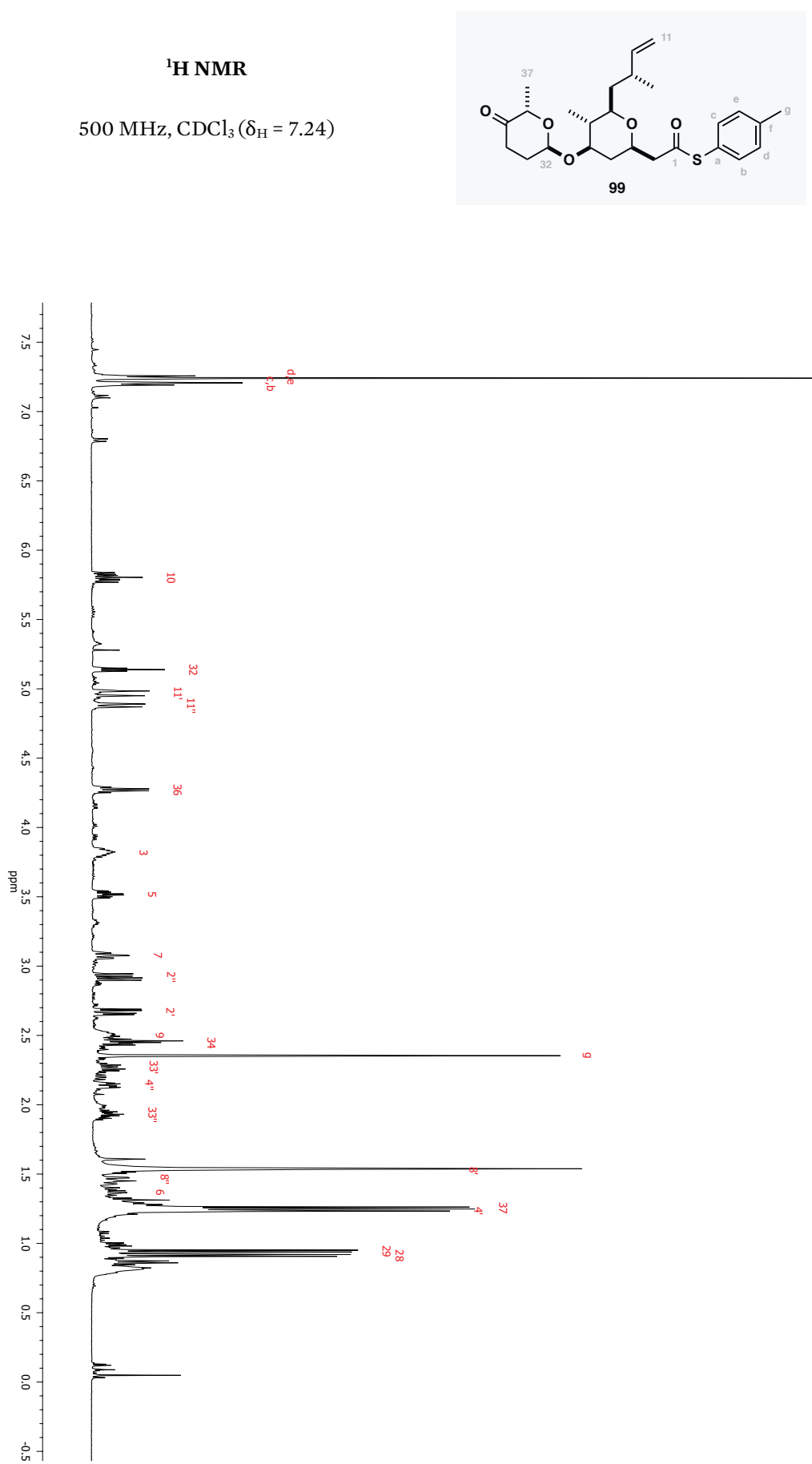
Appendix B: Selected NMR spectra



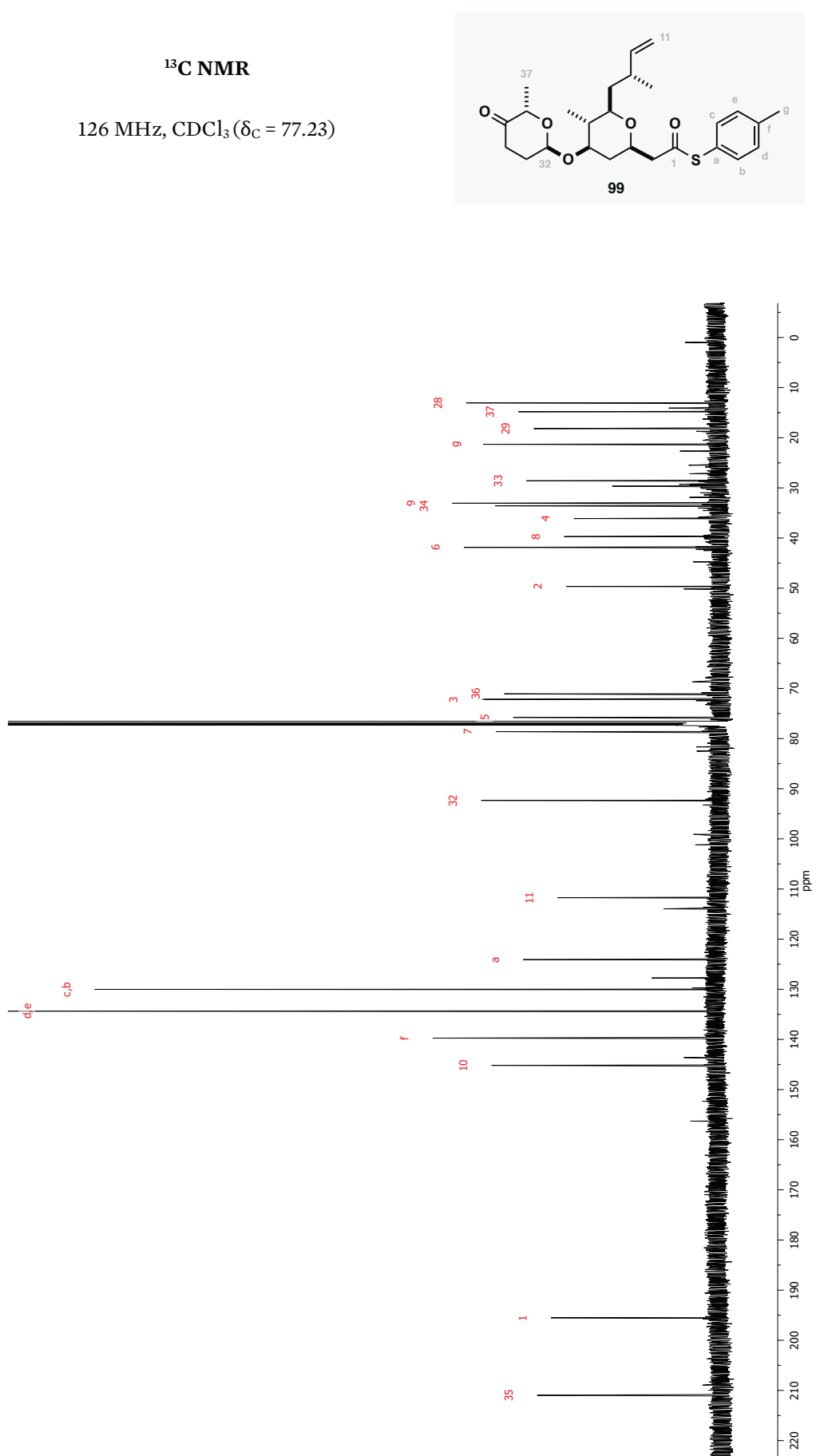
Appendix B: Selected NMR spectra



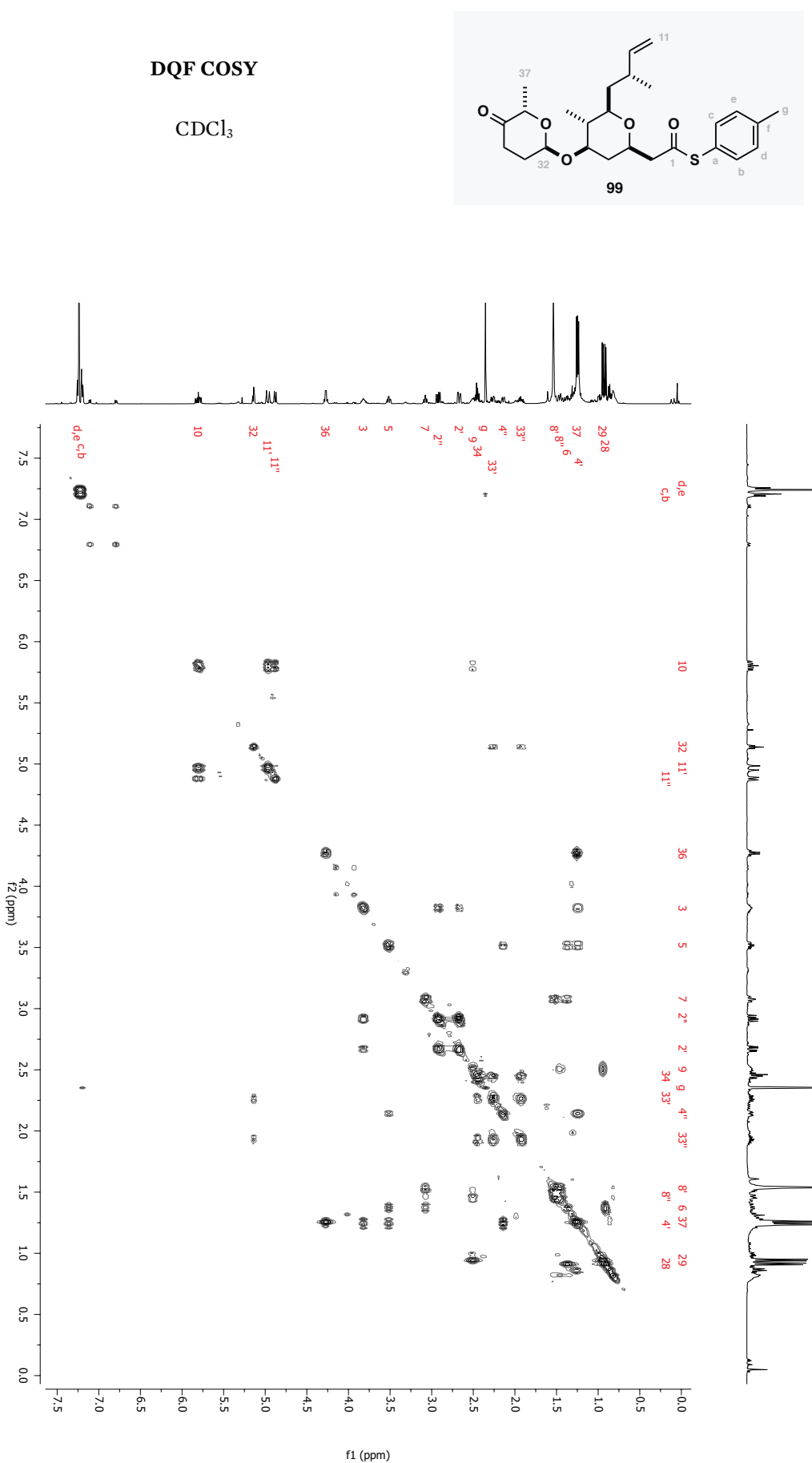
Appendix B: Selected NMR spectra



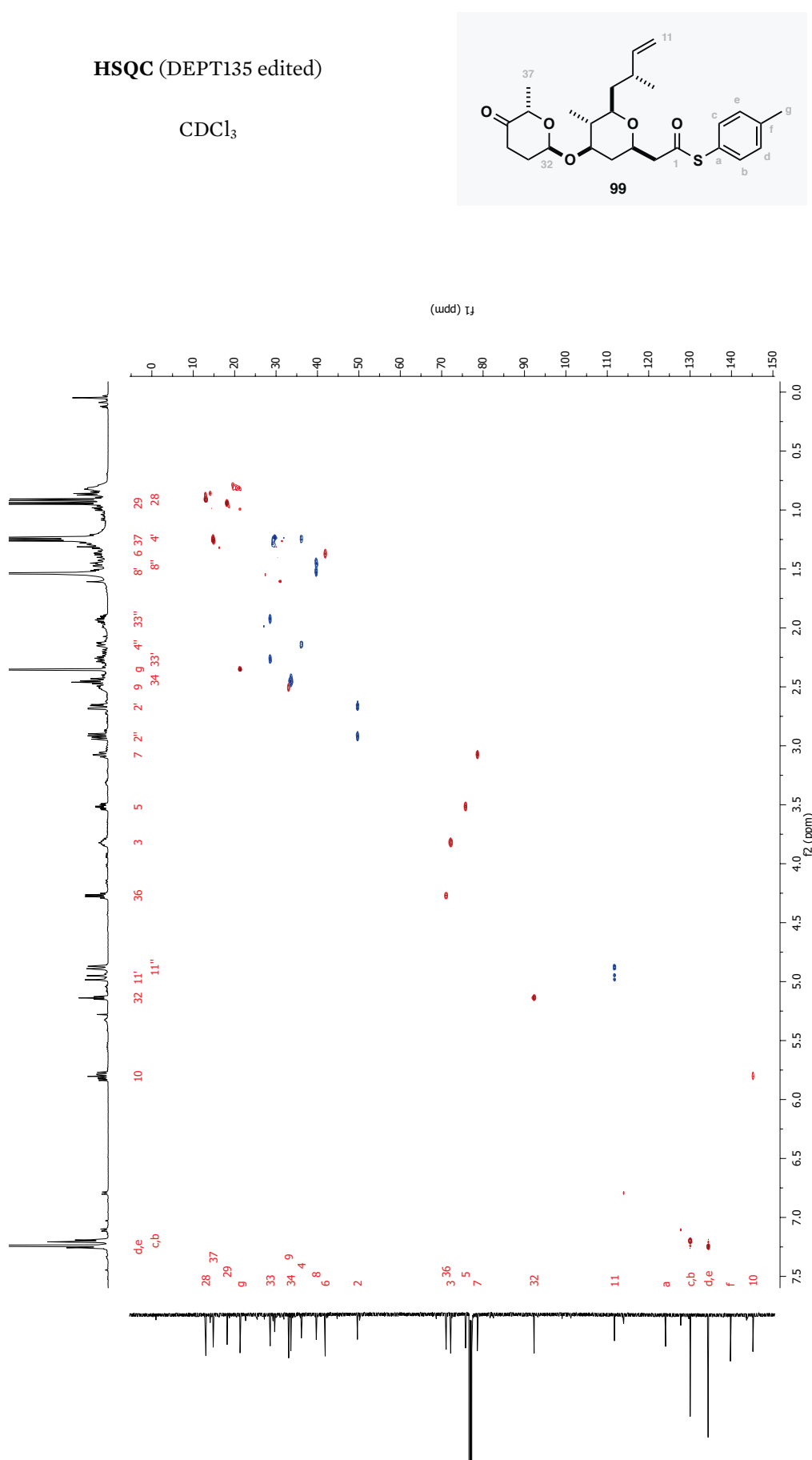
Appendix B: Selected NMR spectra



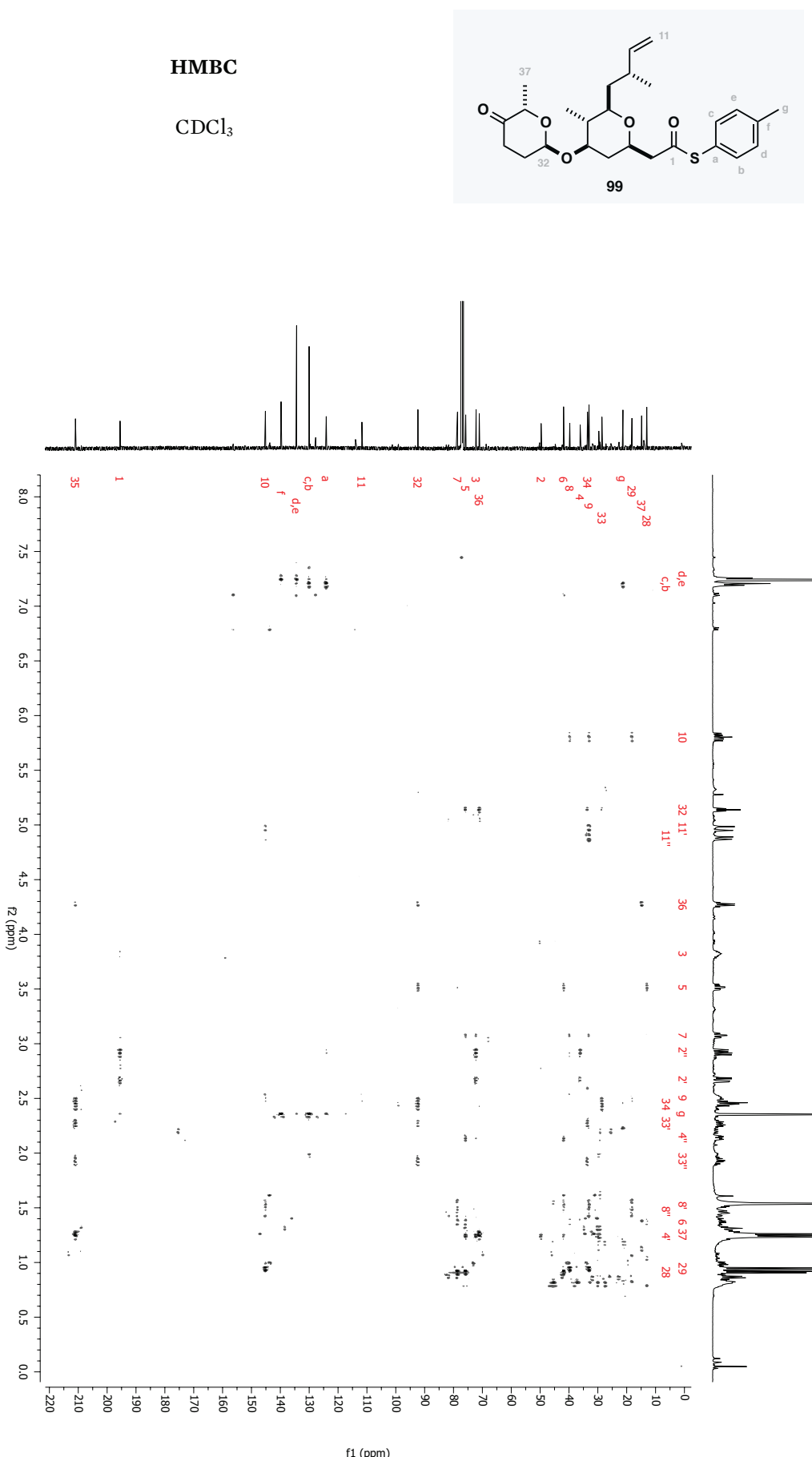
Appendix B: Selected NMR spectra

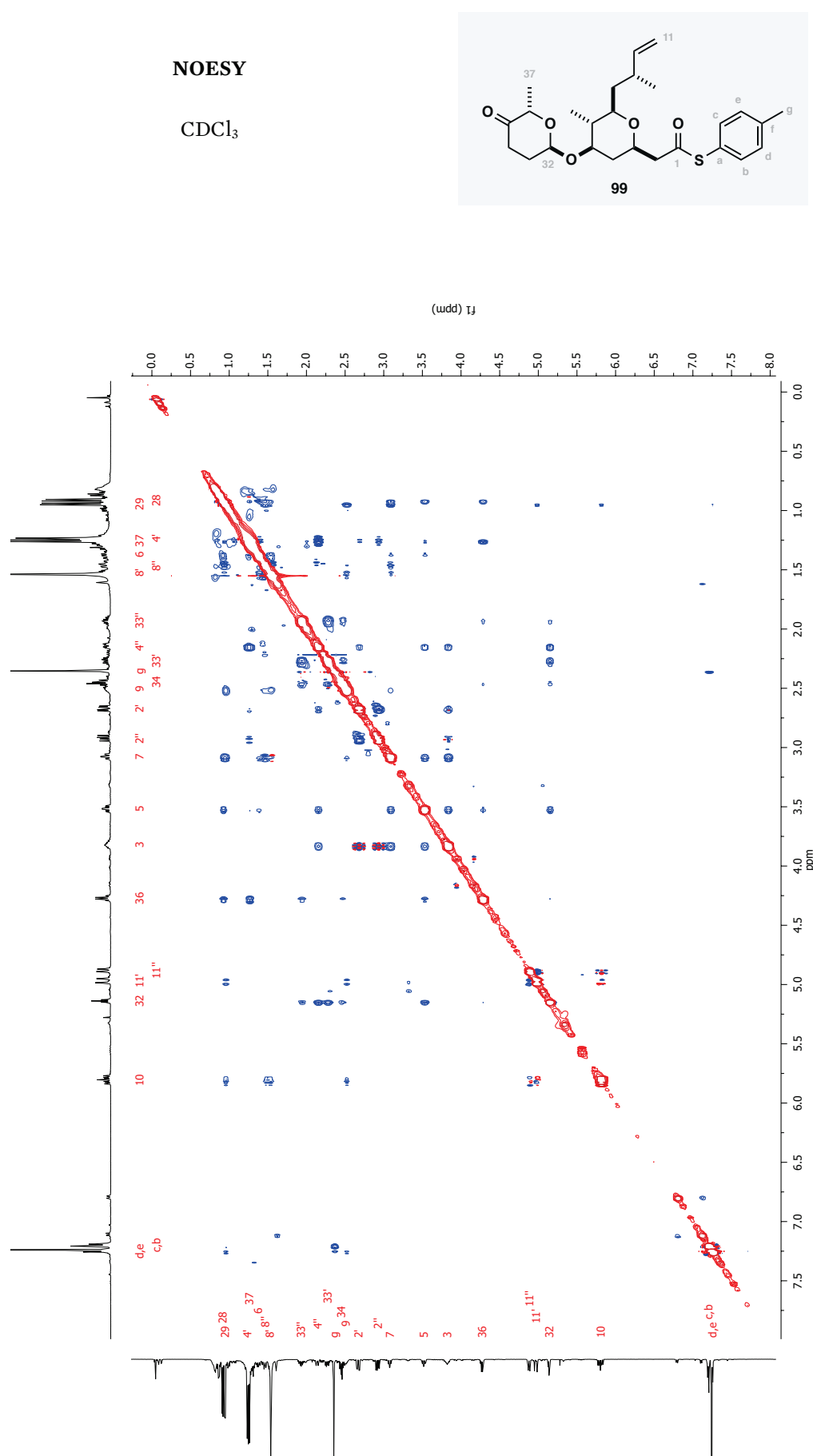


Appendix B: Selected NMR spectra

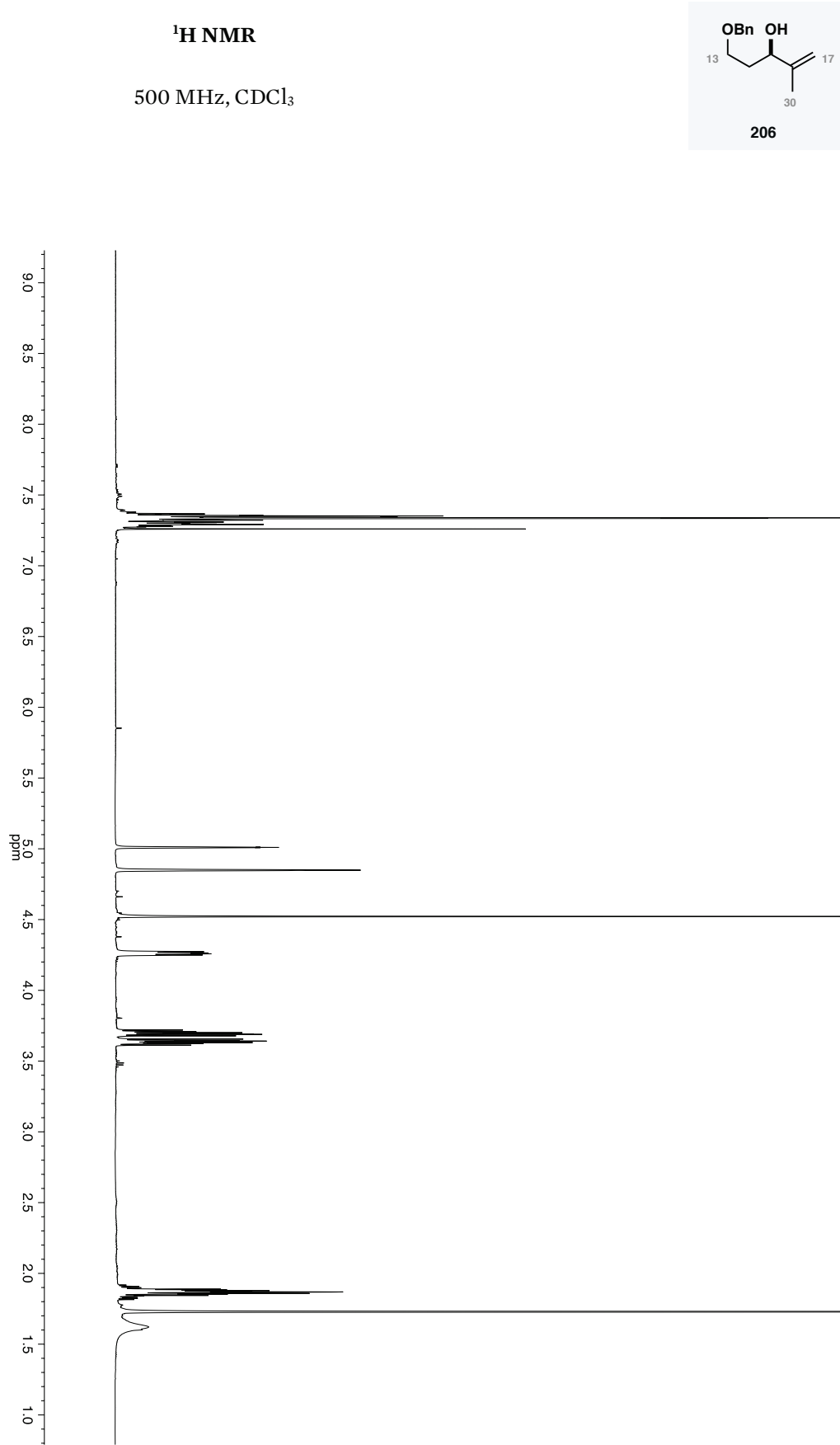


Appendix B: Selected NMR spectra

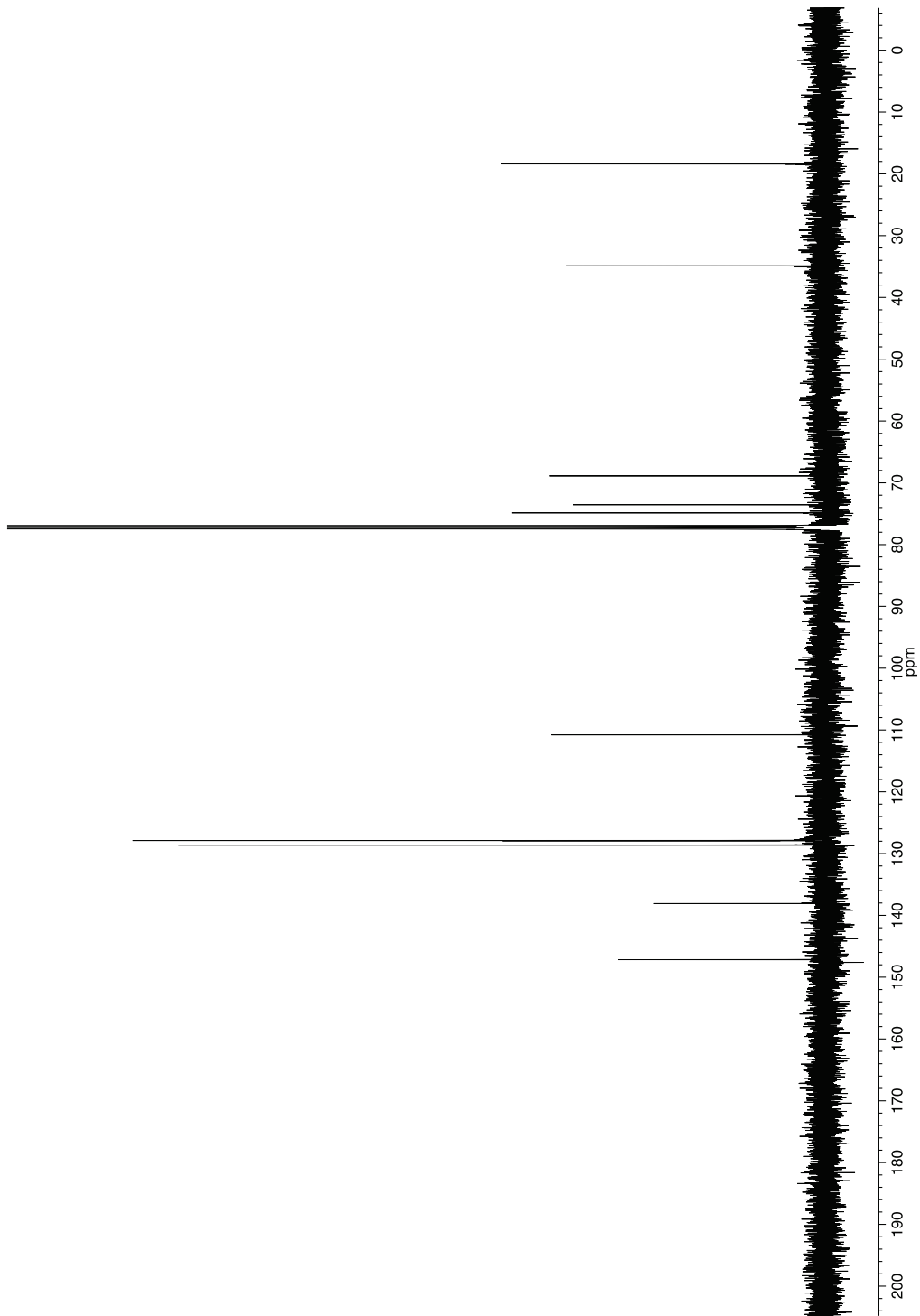
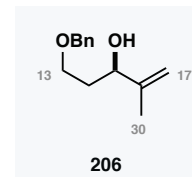




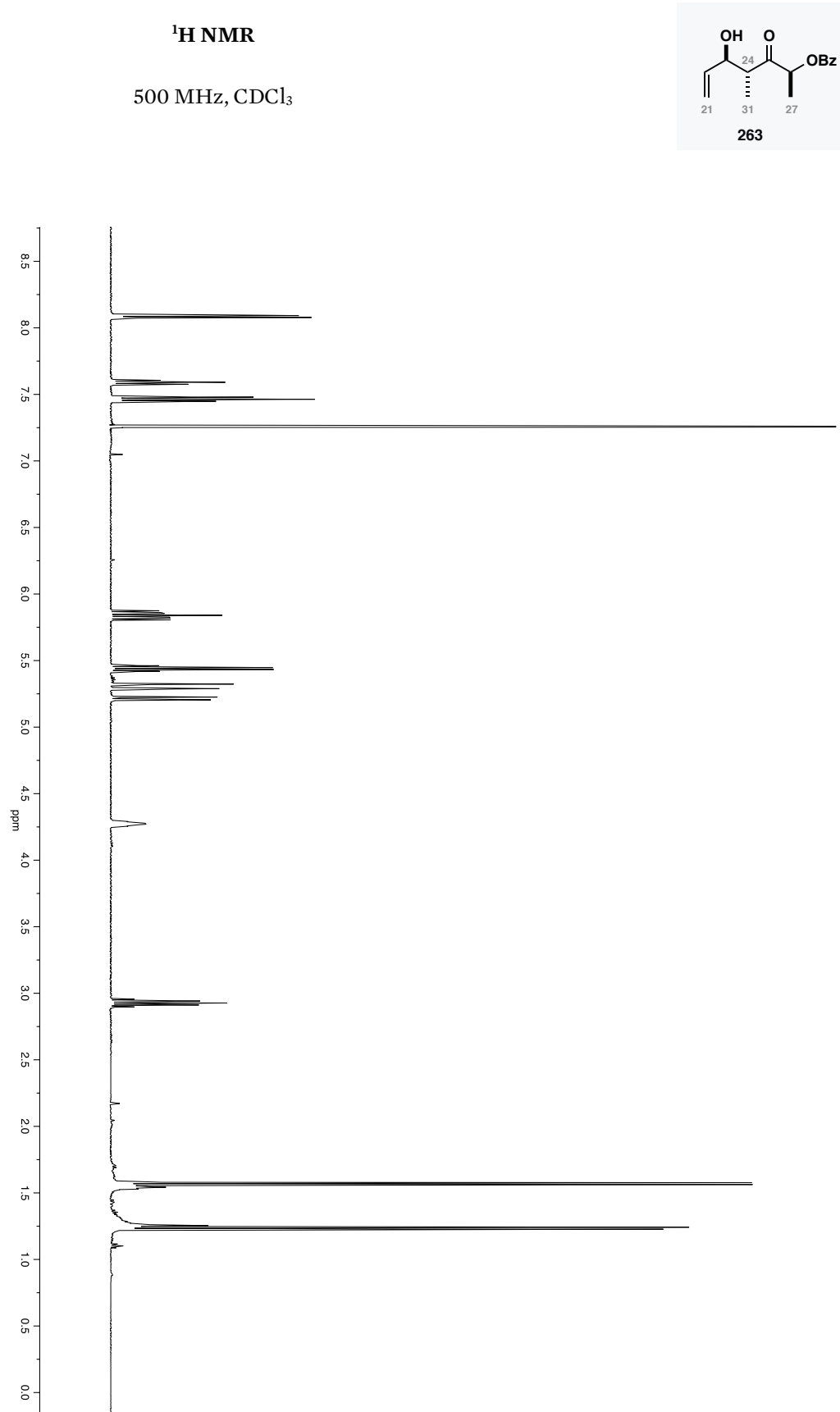
Appendix B: Selected NMR spectra



**<sup>13</sup>C NMR**  
126 MHz, CDCl<sub>3</sub>

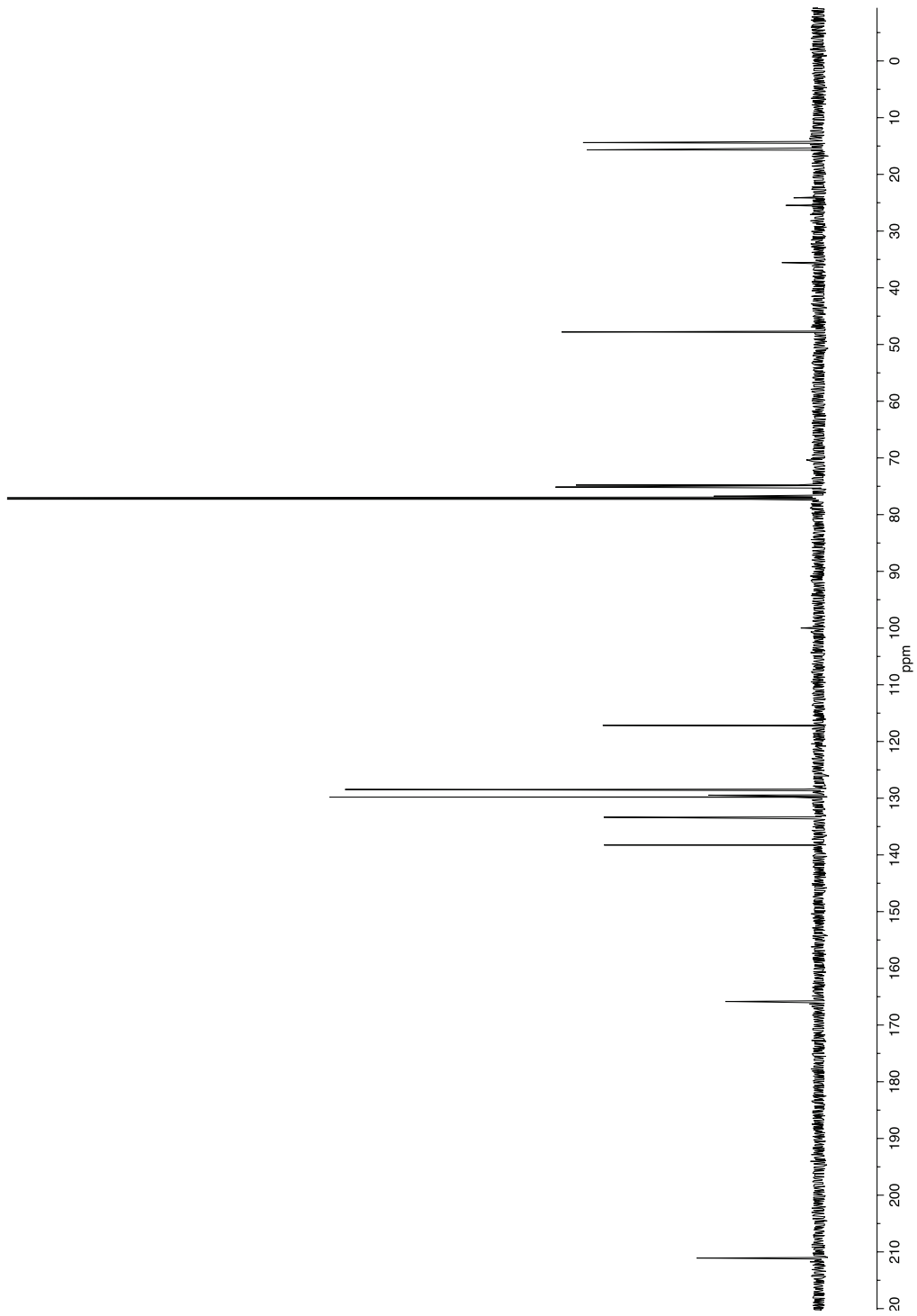
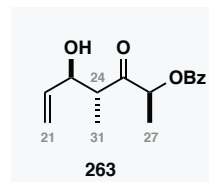


Appendix B: Selected NMR spectra



### **<sup>13</sup>C NMR**

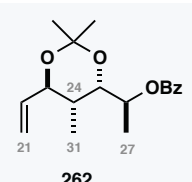
126 MHz, CDCl<sub>3</sub>



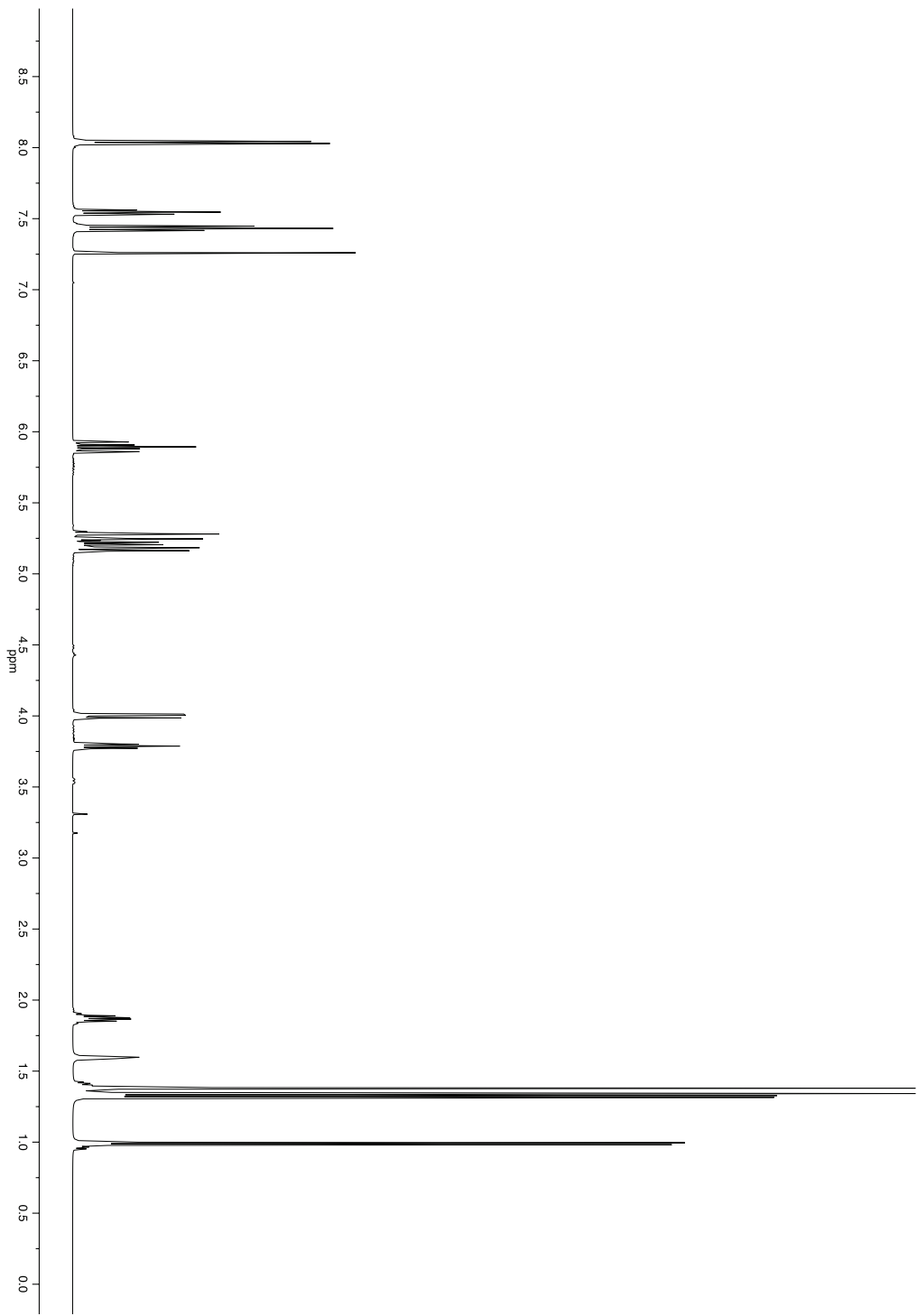
Appendix B: Selected NMR spectra

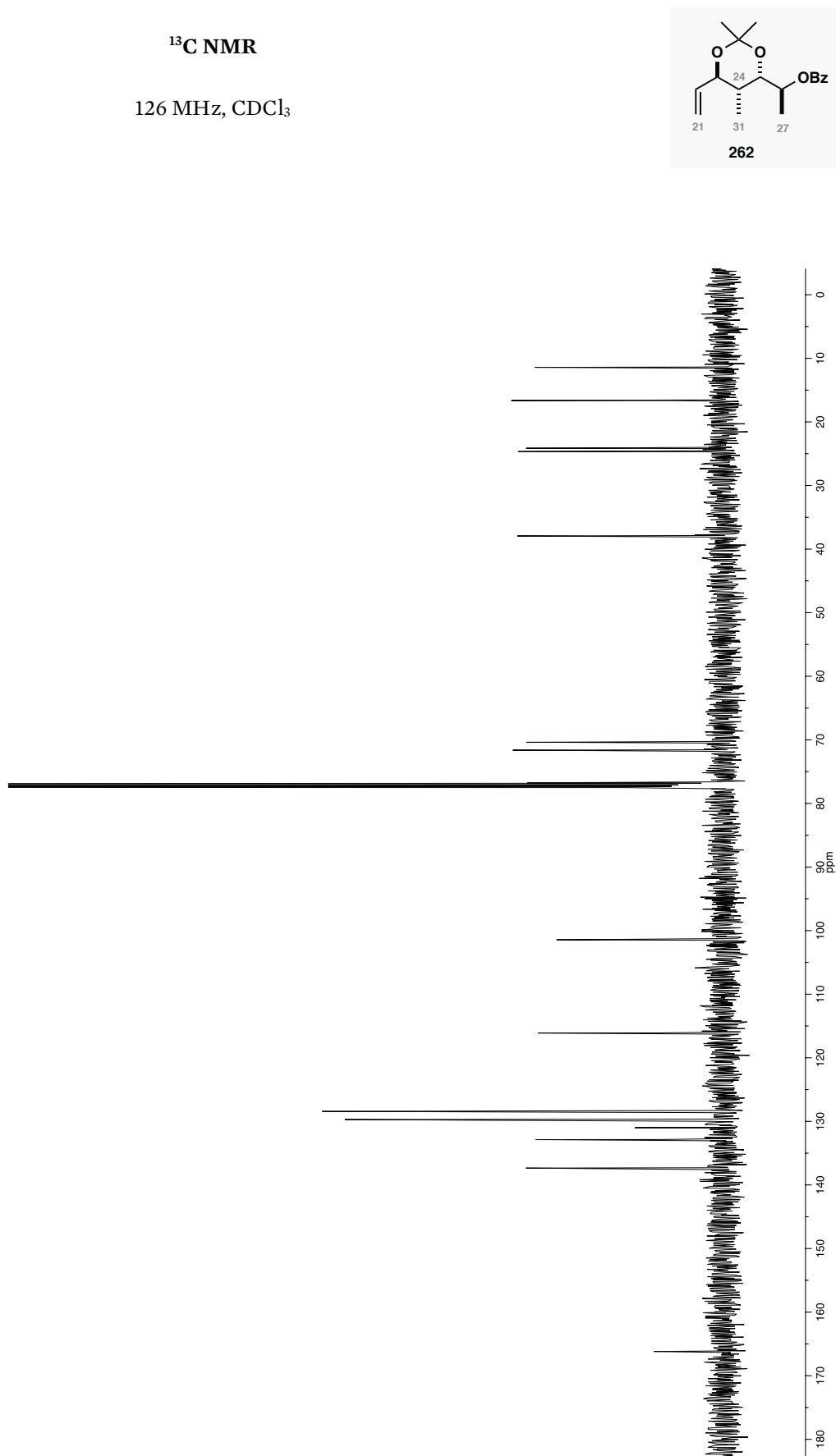
<sup>1</sup>H NMR

500 MHz, CDCl<sub>3</sub>

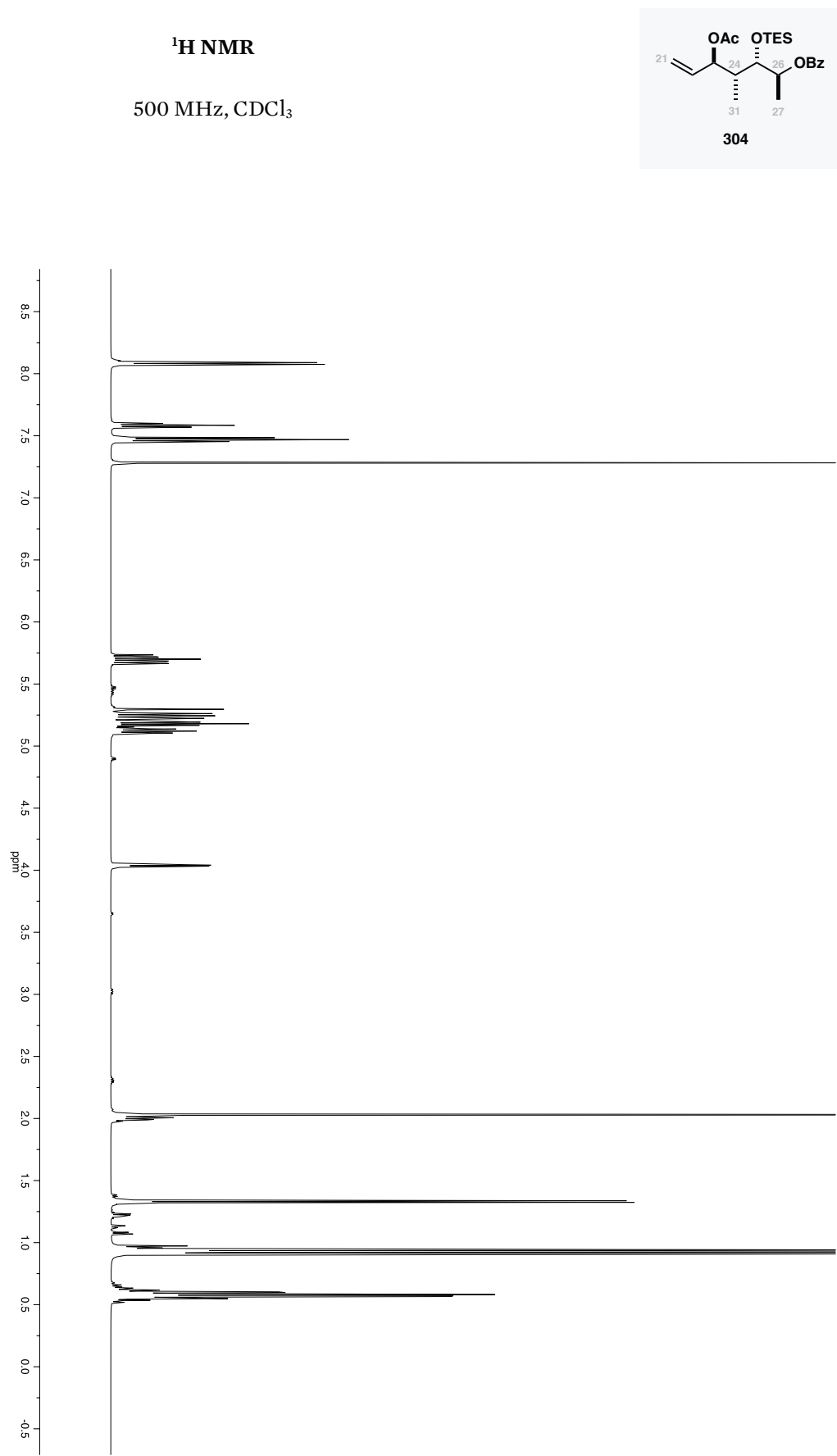


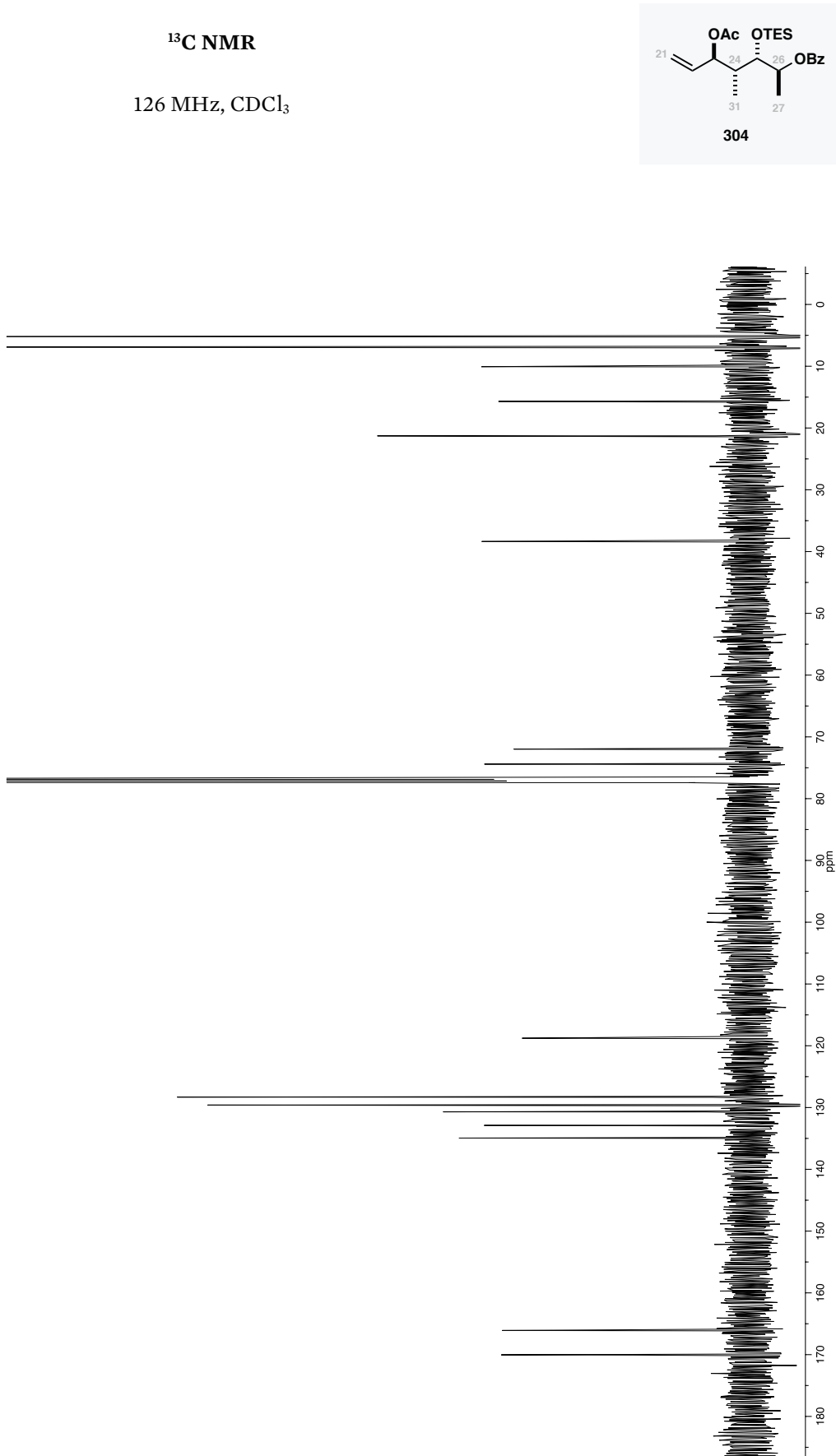
**262**



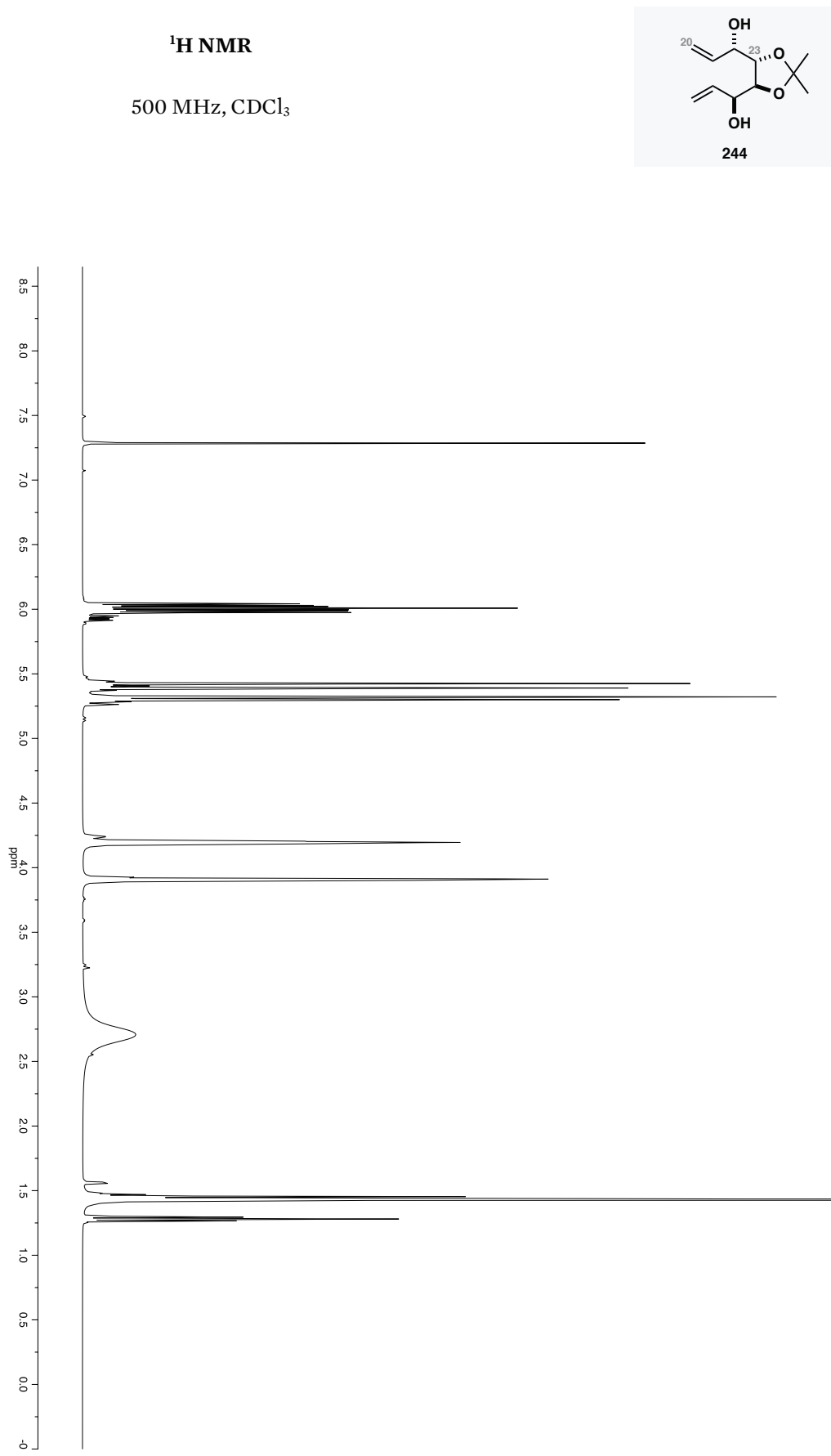


Appendix B: Selected NMR spectra



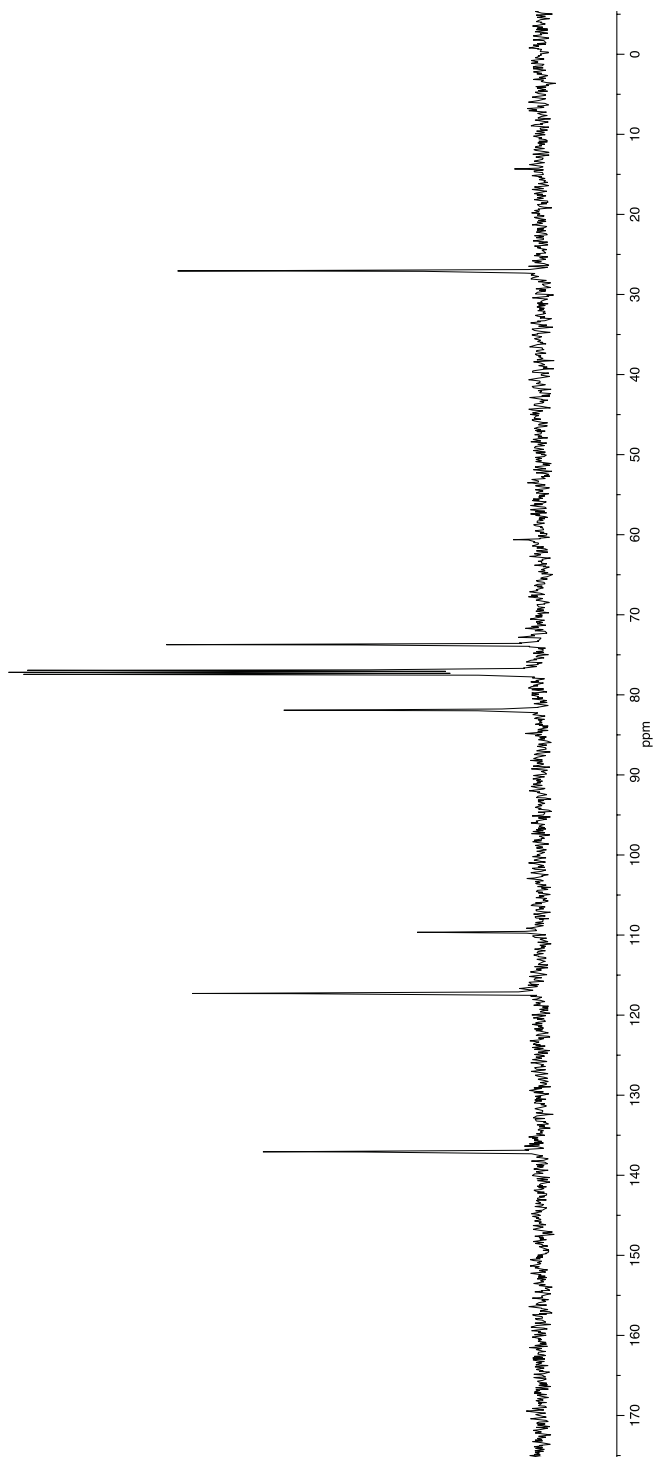
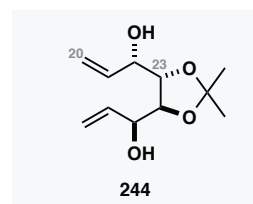


Appendix B: Selected NMR spectra

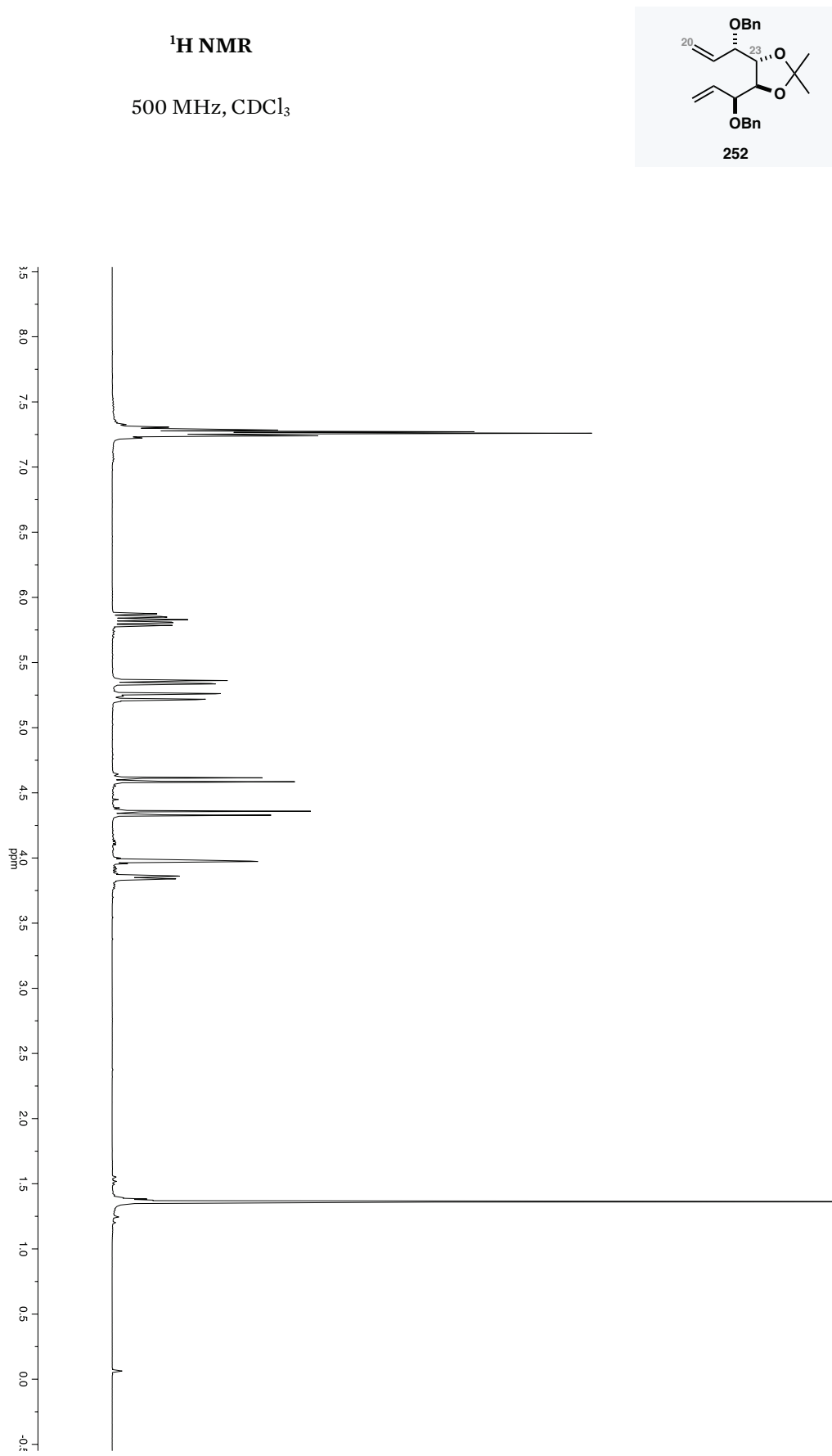


Appendix B: Selected NMR spectra

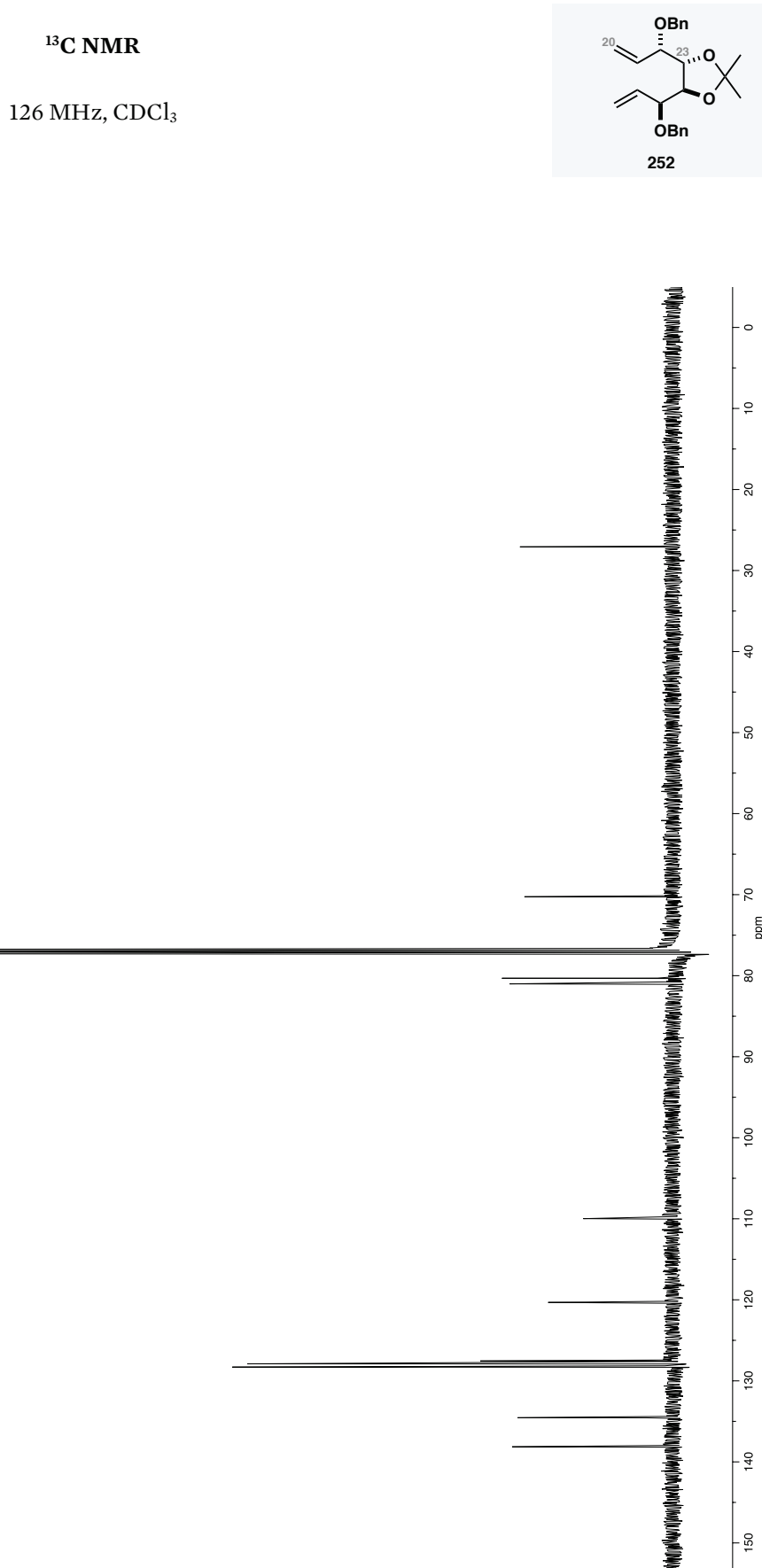
<sup>13</sup>C NMR  
126 MHz, CDCl<sub>3</sub>



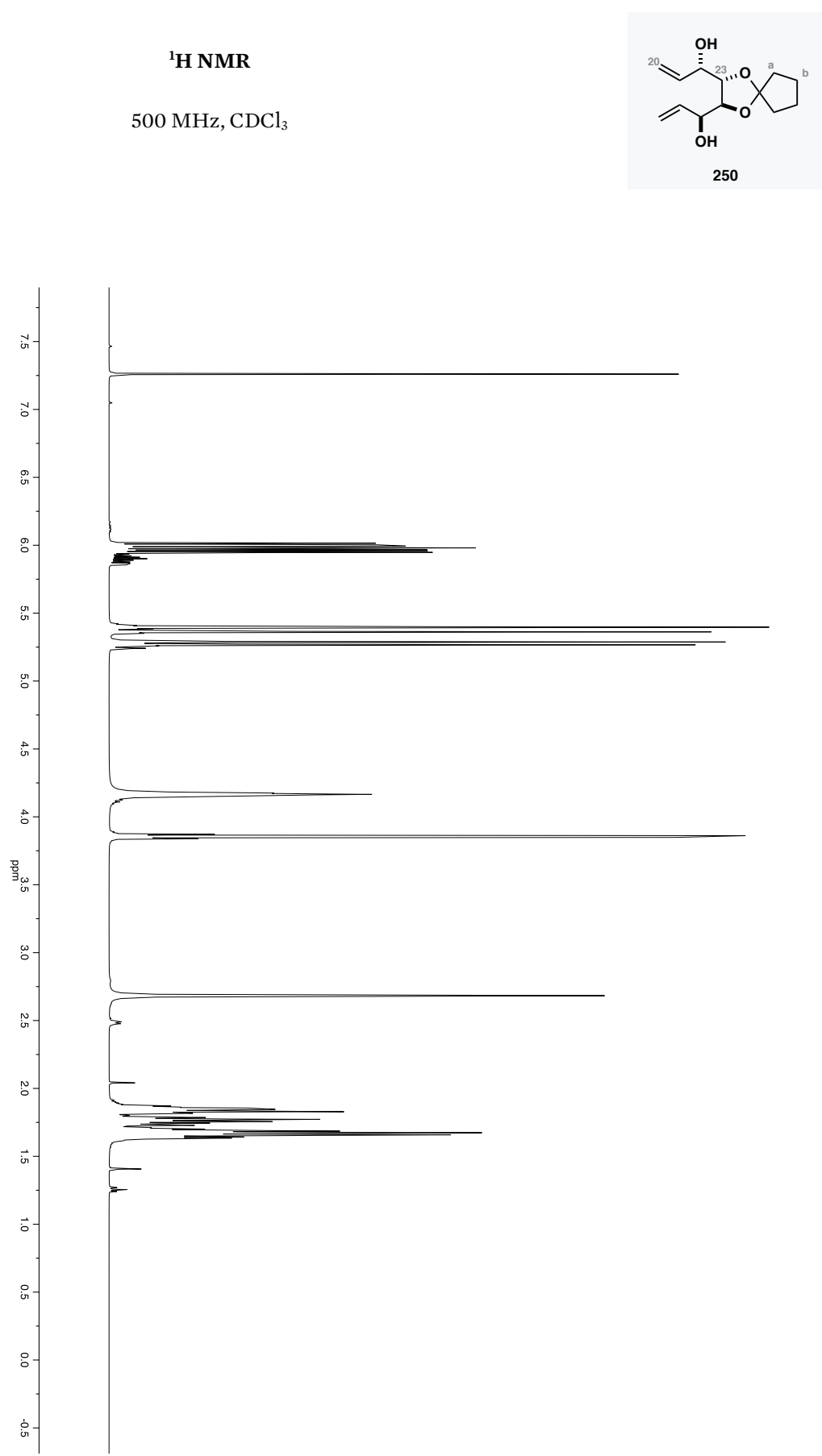
Appendix B: Selected NMR spectra



Appendix B: Selected NMR spectra

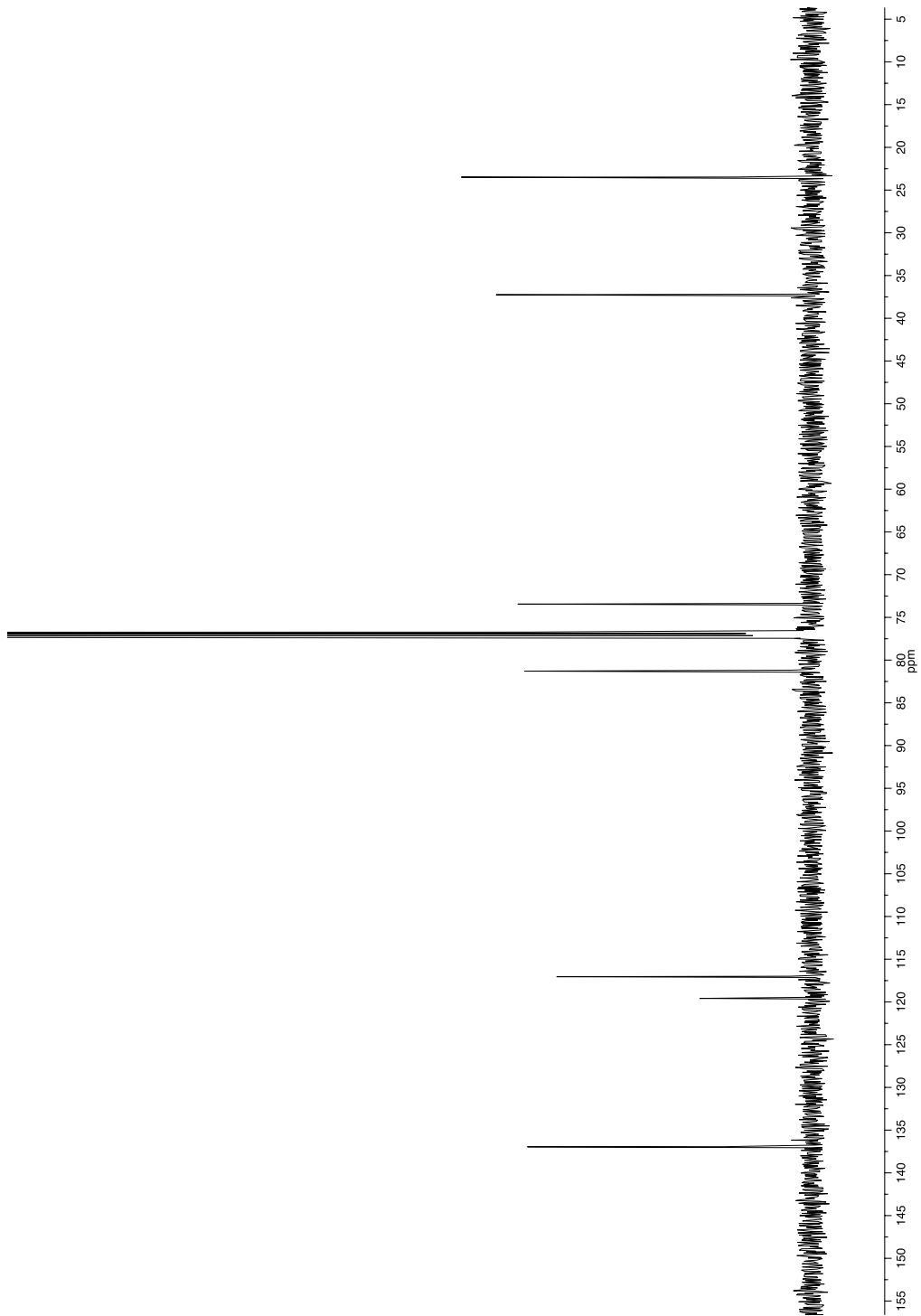
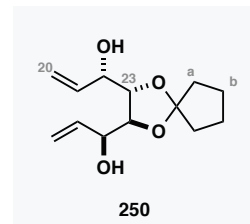


Appendix B: Selected NMR spectra

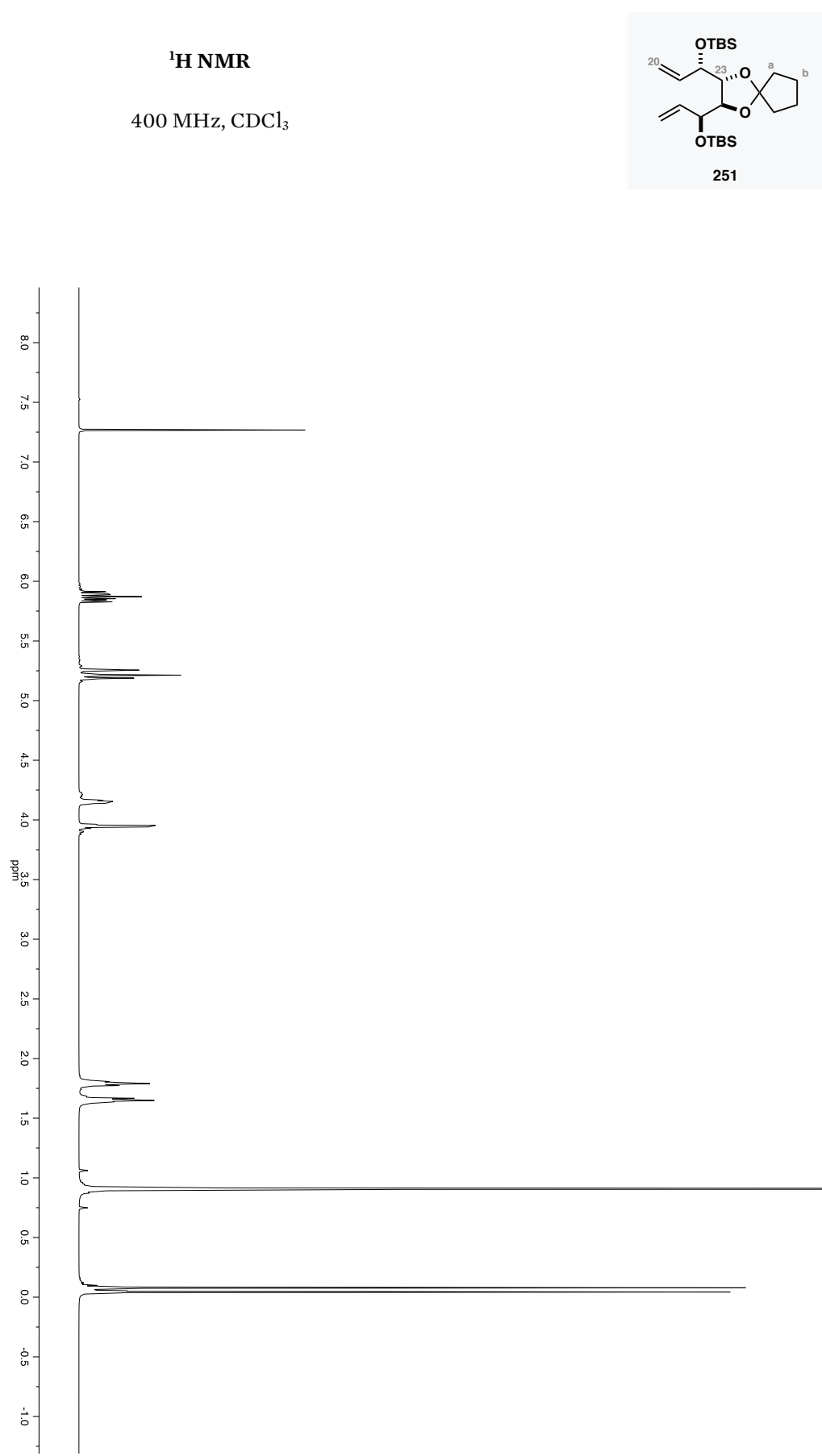


Appendix B: Selected NMR spectra

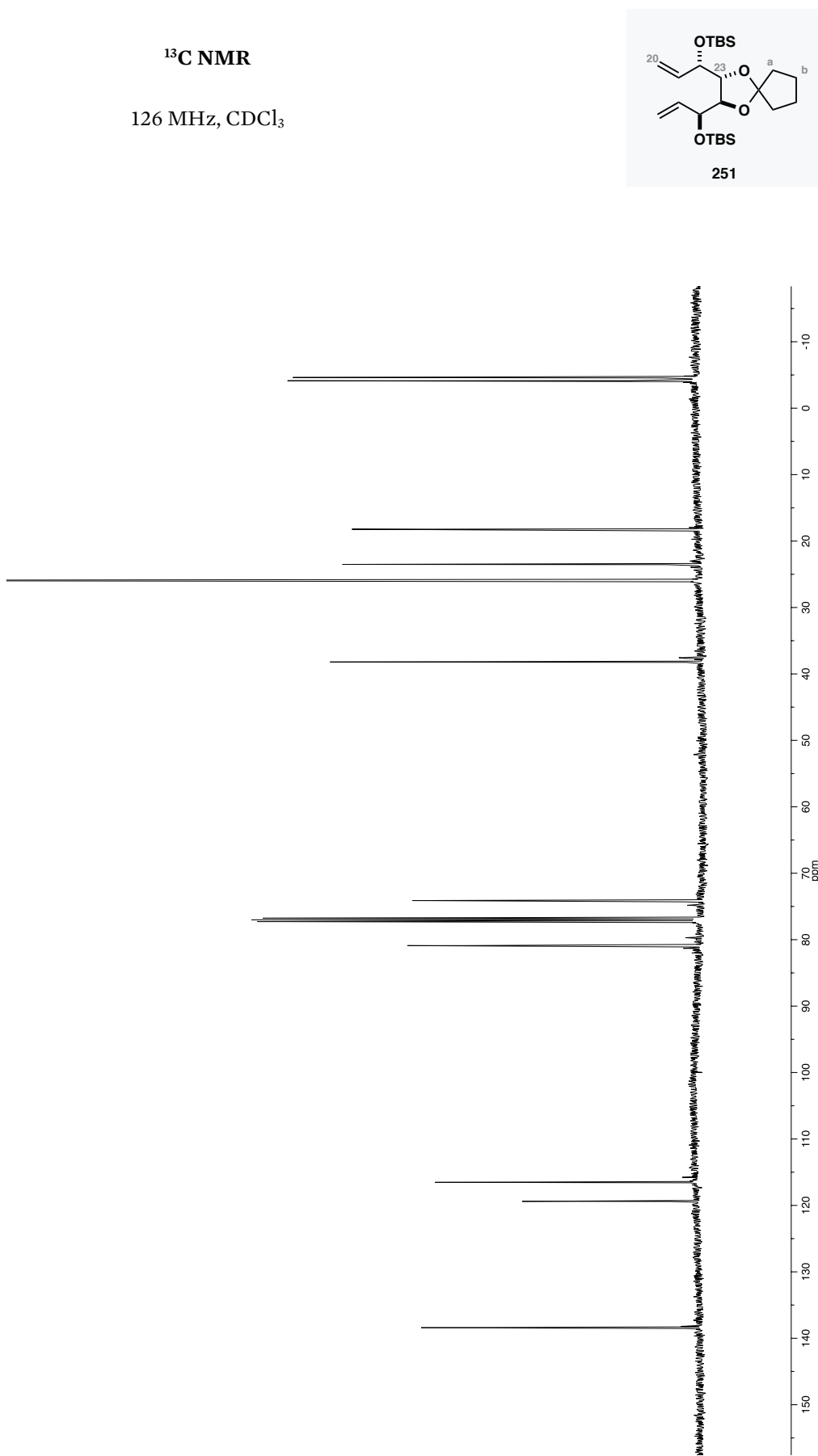
<sup>13</sup>C NMR  
126 MHz, CDCl<sub>3</sub>



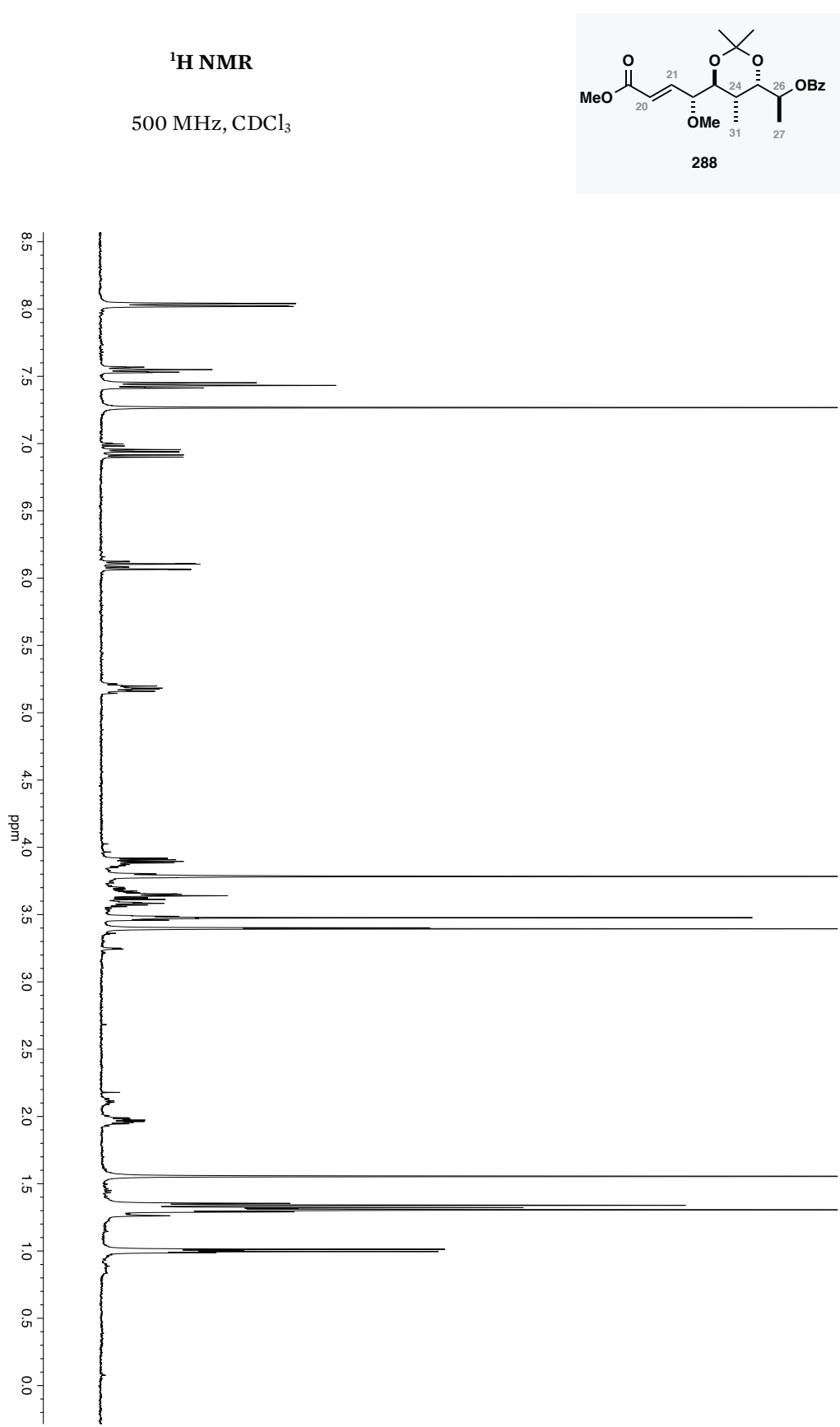
Appendix B: Selected NMR spectra

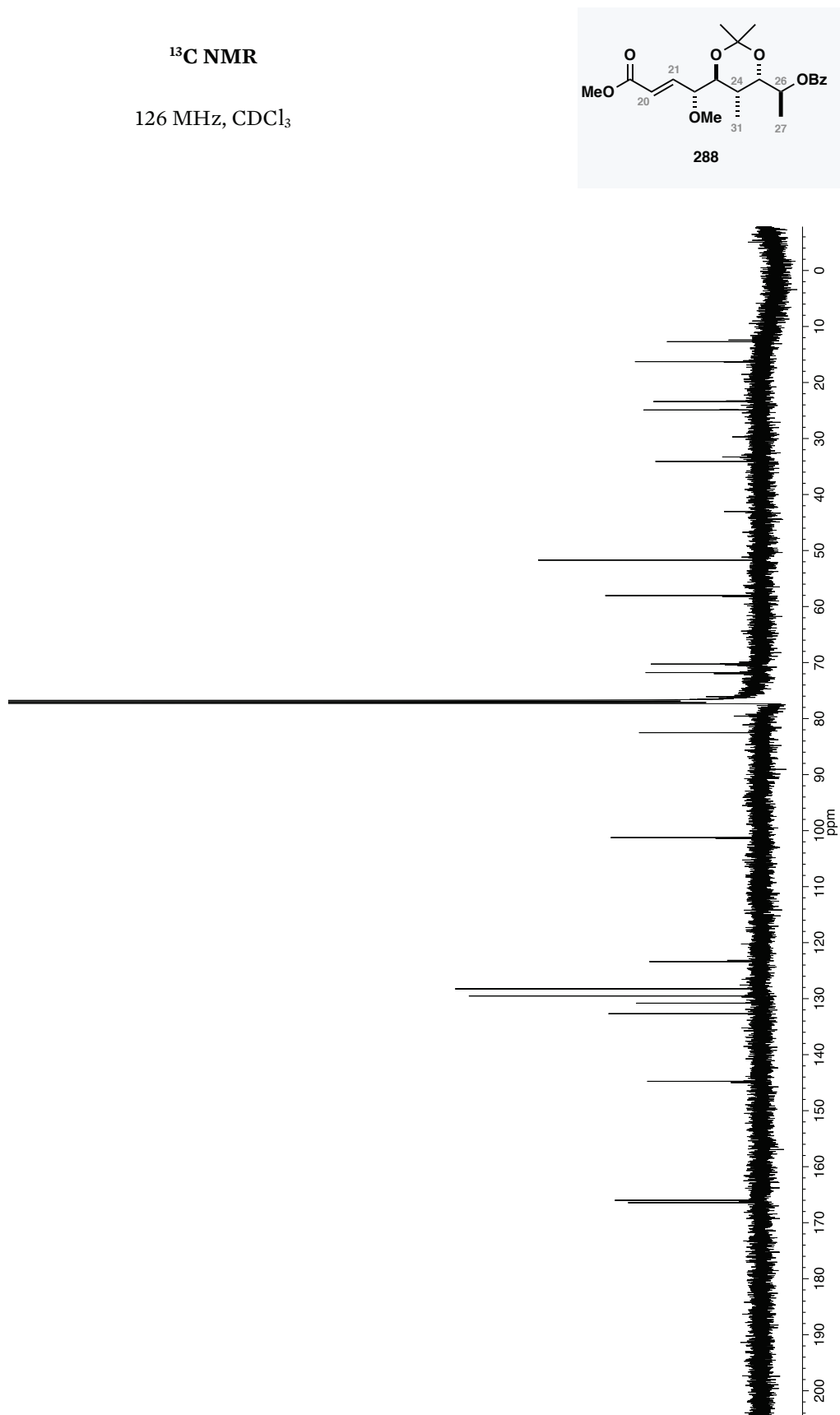


Appendix B: Selected NMR spectra



Appendix B: Selected NMR spectra

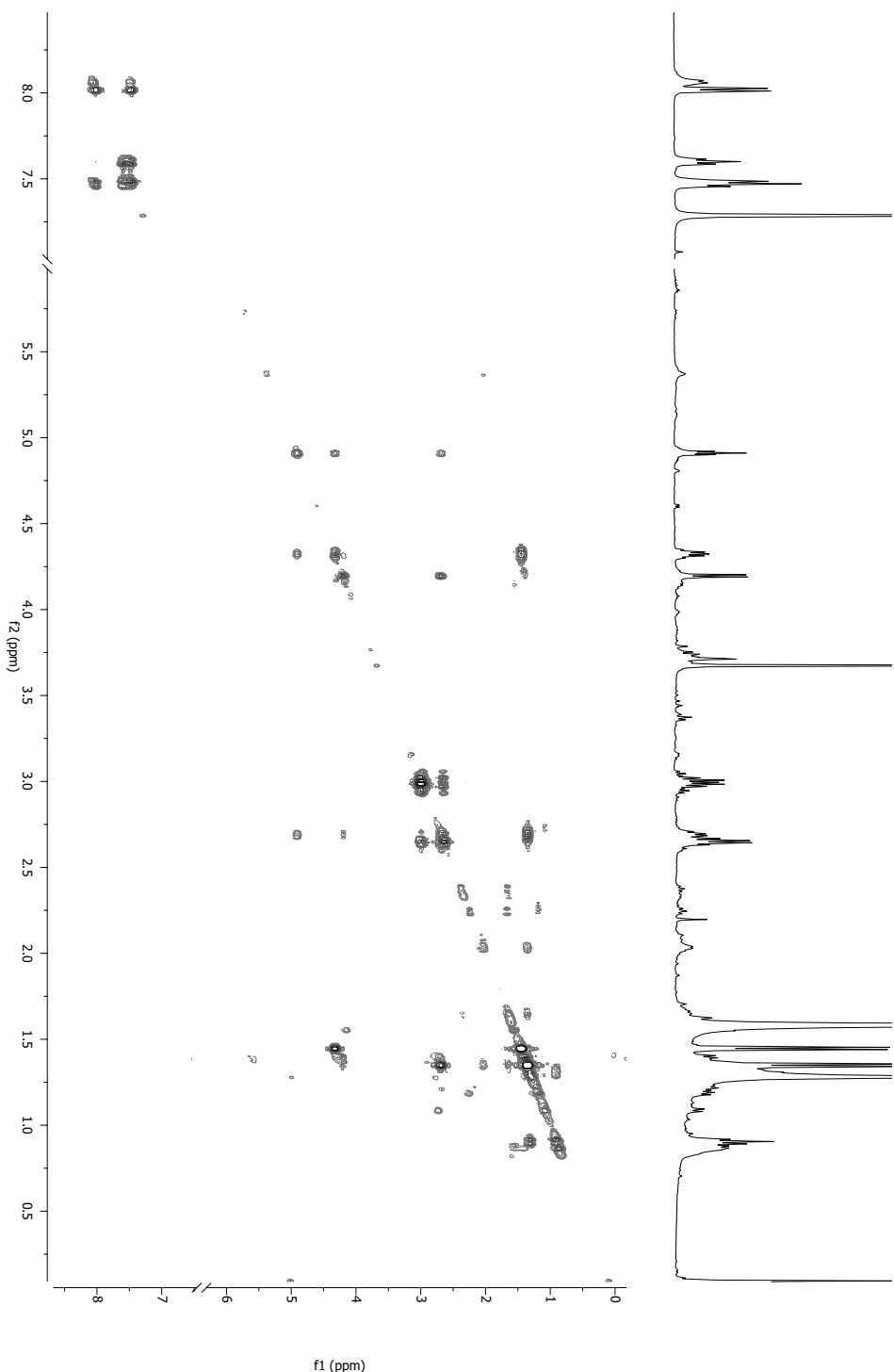


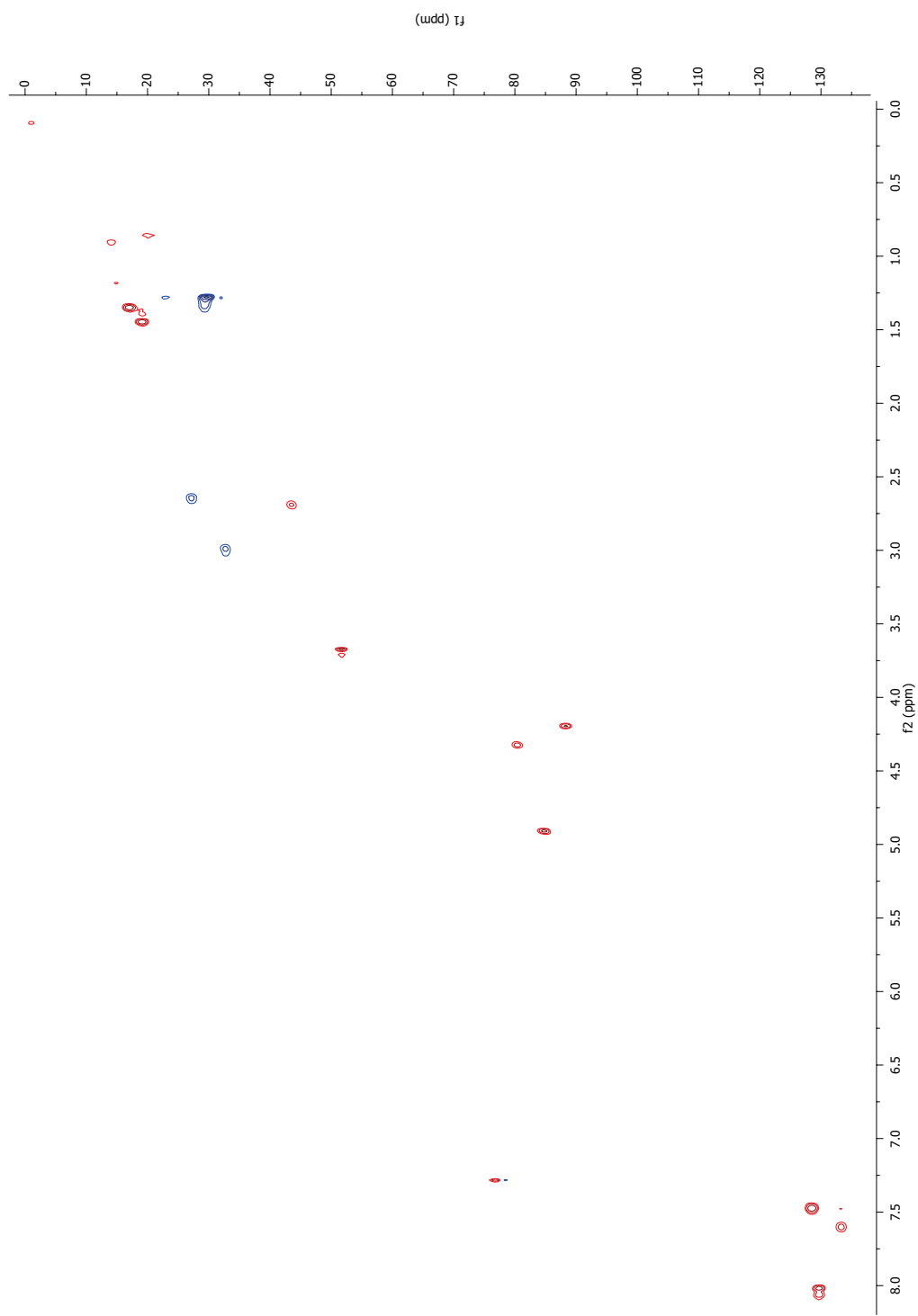


## Appendix B: Selected NMR spectra

Spectra for the unidentified product formed during the palladium catalysed carbonylative cyclisation:

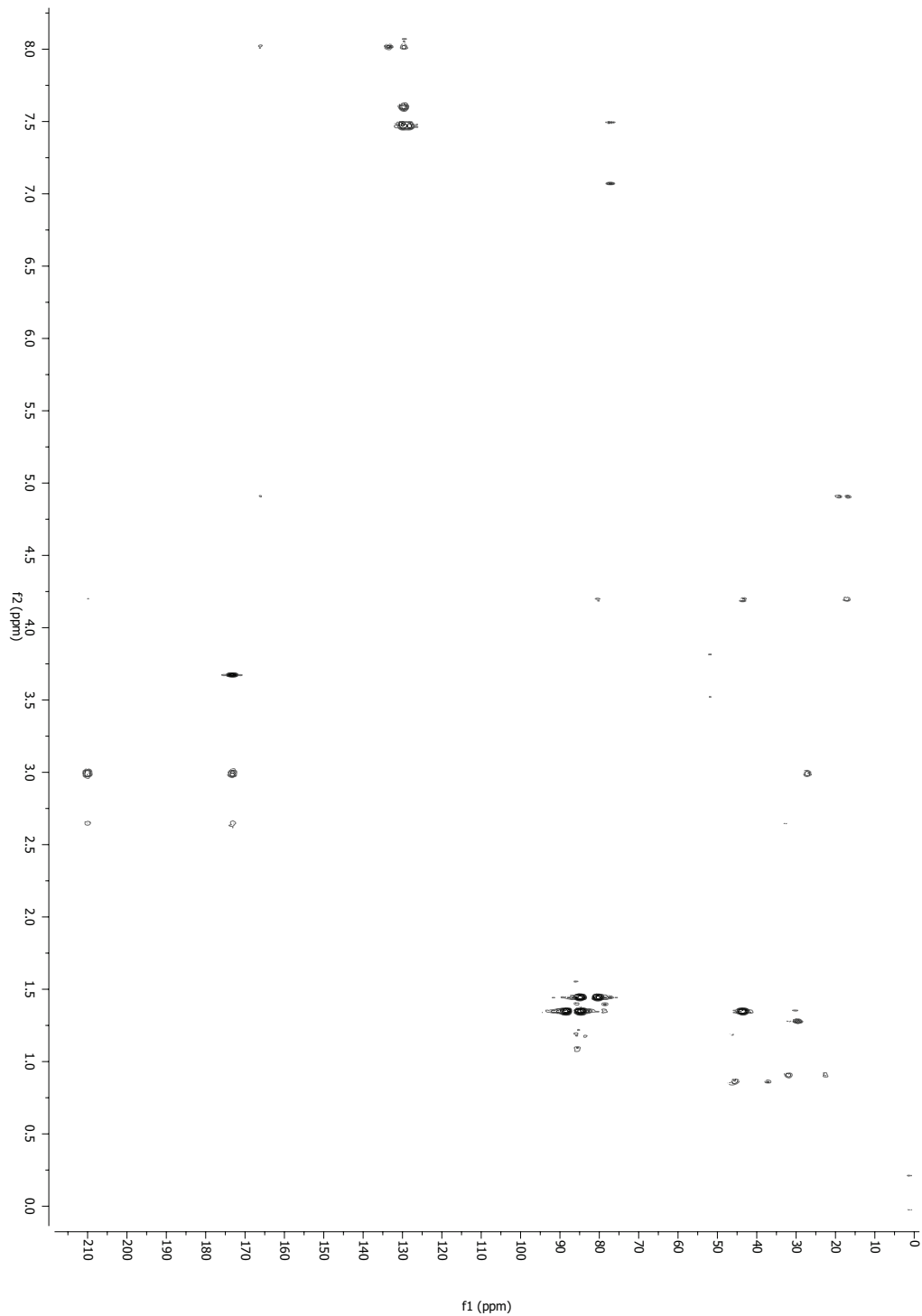
**$^1\text{H}$  NMR** (500 MHz,  $\text{CDCl}_3$ ) and **DQF-COSY**.



**HSQC-DEPT135ed**

## Appendix B: Selected NMR spectra

### HMBC



# C

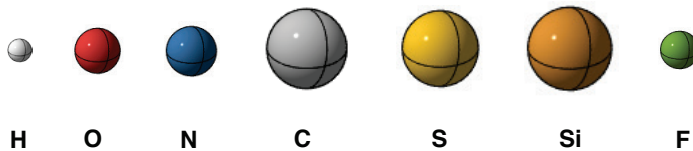
## APPENDIX C: DETAILS OF COMPUTATIONAL PROCEDURES

### GENERAL DETAILS

**Molecular mechanics:** Conformational searches were carried out using Schrodinger MacroModel using the MMFF-94 forcefield in the gas-phase (unless otherwise stated). Mixed-torsional/low-mode sampling was used to generate conformers, using 1000 steps per rotatable bond and an energy cut-off of 50 kJ/mol. Conformers were minimised using a truncated Newton conjugate gradient (TNCG) method. Following the conformational search, redundant conformer elimination was used to eliminate conformers with an RMSD cut-off of 0.5 Å.

**Density functional theory:** DFT calculations were carried out using Schrodinger Jaguar with B3LYP functional and 6-31G basis set. Polarisation and diffusion corrections were used as indicated in the text to better describe charged structures. Frequency calculations were carried out on all transition state structures to confirm the presence of a single negative frequency. Where indicated, gas-phase structures were re-optimised using the PBF solvent model, as implemented in Jaguar. Gaussian 09 was used for all IRC/MEP calculations.

**Visualisation:** Structural representations were generated using CYLView. The following scheme is used for atom colours:



**Clustering:** Clustering of conformers was carried out using SPSS. An RMSD matrix was first exported from Schrodinger Maestro, describing the pairwise similarity between each conformer. This matrix was used in a multidimensional scaling calculation in combination with the relative energy and torsional angles for each conformer. The results of the calculation were plotted using Tableau, giving rise to the clustering diagrams given within the body of the text.

**Structures:** Cartesian coordinates (in .xyz format) for key intermediates and transition states will be made available via the University of Cambridge date repository, Apollo ([repository.cam.ac.uk](http://repository.cam.ac.uk)).





# REFERENCES

- [1] Borchardt, J. K. *Drug News Perspect.* **2002**, *15*, 187.
- [2] Hensen, B. *Drug Discov. Today* **2005**, *10*, 459.
- [3] Ramirez-Llodra, E.; Brandt, A.; Danovaro, R.; De Mol, B.; Escobar, E.; German, C. R.; Levin, L. A.; Arbizu, P. M. *Biogeosciences* **2010**, *7*, 2851.
- [4] Blunt, J.; Munro, M. H. G. *Dictionary of Marine Natural Products*; Taylor & Francis, 2008.
- [5] Munro, M. H.; Blunt, J. W.; Dumdei, E. J.; Hickford, S. J.; Lill, R. E.; Li, S.; Battershill, C. N.; Duckworth, A. R. *J. Biotechnol.* **1999**, *70*, 15.
- [6] Altmann, K.-H. *Chim. Int. J. Chem.* **2017**, *71*, 646.
- [7] Cuevas, C.; Francesch, A. *Nat. Prod. Rep.* **2009**, *26*, 322.
- [8] Tao, L.; Zhu, F.; Qin, C.; Zhang, C.; Chen, S.; Zhang, P.; Zhang, C.; Tan, C.; Gao, C.; Chen, Z.; et al. *Sci. Rep.* **2015**, *5*, 9325.
- [9] Lachance, H.; Wetzel, S.; Kumar, K.; Waldmann, H. *J. Med. Chem.* **2012**, *55*, 5989.
- [10] Mickel, S. J.; Niederer, D.; Daeffler, R.; Osmani, A.; Kuesters, E.; Schmid, E.; Schaer, K.; Gamboni, R.; Chen, W.; Loeser, E.; et al. *Org. Process Res. Dev.* **2004**, *8*, 122.
- [11] Mickel, S. J.; Sedelmeier, G. H.; Niederer, D.; Schuerch, F.; Seger, M.; Schreiner, K.; Daeffler, R.; Osmani, A.; Bixel, D.; Loiseleur, O.; et al. *Org. Process Res. Dev.* **2004**, *8*, 113.
- [12] Mickel, S. J.; Sedelmeier, G. H.; Niederer, D.; Schuerch, F.; Koch, G.; Kuesters, E.; Daeffler, R.; Osmani, A.; Seeger-Weibel, M.; Schmid, E.; et al. *Org. Process Res. Dev.* **2004**, *8*, 107.
- [13] Mickel, S. J.; Sedelmeier, G. H.; Niederer, D.; Schuerch, F.; Grimler, D.; Koch, G.; Daeffler, R.; Osmani, A.; Hirni, A.; Schaer, K.; et al. *Org. Process Res. Dev.* **2004**, *8*, 101.
- [14] Mickel, S. J.; Sedelmeier, G. H.; Niederer, D.; Daeffler, R.; Osmani, A.; Schreiner, K.; Seeger-Weibel, M.; Bérod, B.; Schaer, K.; Gamboni, R.; et al. *Org. Process Res. Dev.* **2004**, *8*, 92.
- [15] Yu, M. J.; Zheng, W.; Seletsky, B. M. *Nat. Prod. Rep.* **2013**, *30*, 1158.
- [16] Naito, H. Halaven FDA Approval Press Conference Statement  
<https://www.eisai.com/ir/library/presentations/pdf/material20101116e1.pdf>  
(accessed Jul 1, 2018).
- [17] Cuevas, C.; Pérez, M.; Martín, M. J.; Chicharro, J. L.; Fernández-Rivas, C.; Flores, M.; Francesch, A.; Gallego, P.; Zarzuelo, M.; De La Calle, F.; et al. *Org. Lett.* **2000**, *2*, 2545.
- [18] Dalisay, D. S.; Molinski, T. F. *Org. Lett.* **2009**, *11*, 1967.
- [19] Woodward, R. B.; Logusch, E.; Nambiar, K. P.; Sakan, K.; Ward, D. E.; Au-Yeung, B. W.; Balaram, P.; Browne, L. J.; Card, P. J.; Chen, C. H. *J. Am. Chem. Soc.* **1981**, *103*, 3215.
- [20] Smith, A. B.; Hogan, A.-M. L.; Liu, Z.; Razler, T. M.; Meis, R. M.; Morinaka, B. I.; Molinski, T. F. *Tetrahedron* **2011**, *67*, 5069.
- [21] Nicolaou, K. C.; Snyder, S. A. *Angew. Chem. Int. Ed.* **2005**, *44*, 1012.

## References

- [22] Suyama, T. L.; Gerwick, W. H.; Mcphail, K. L. *Bioorg. Med. Chem.* **2011**, *19*, 6675.
- [23] Paterson, I.; Dalby, S. M.; Roberts, J. C.; Naylor, G. J.; Guzmán, E. A.; Isbrucker, R.; Pitts, T. P.; Linley, P.; Divlianska, D.; Reed, J. K.; et al. *Angew. Chem. Int. Ed.* **2011**, *50*, 3219.
- [24] Trost, B. M.; Harrington, P. E. *J. Am. Chem. Soc.* **2004**, *126*, 5028.
- [25] Tripathi, A.; Schofield, M. M.; Chlipala, G. E.; Schultz, P. J.; Yim, I.; Newmister, S. A.; Nusca, T. D.; Scaglione, J. B.; Hanna, P. C.; Tamayo-Castillo, G.; et al. *J. Am. Chem. Soc.* **2014**, *136*, 1579.
- [26] Matsumori, N.; Kaneno, D.; Murata, M.; Nakamura, H.; Tachibana, K. *J. Org. Chem.* **1999**, *64*, 866.
- [27] Wu, J.; Lorenzo, P.; Zhong, S.; Ali, M.; Butts, C. P.; Myers, E. L.; Aggarwal, V. K. *Nature* **2017**, *547*, 436.
- [28] Sandler, J. S.; Colin, P. L.; Kelly, M.; Fenical, W. *J. Org. Chem.* **2006**, *71*, 7245.
- [29] Wright, A. E.; Roberts, J. C.; Guzmán, E. A.; Pitts, T. P.; Pomponi, S. A.; Reed, J. K. *J. Nat. Prod.* **2017**, *80*, 735.
- [30] Paterson, I.; Ng, K. K.-H.; Williams, S.; Millican, D. C.; Dalby, S. M. *Angew. Chem. Int. Ed.* **2014**, *53*, 2692.
- [31] Larivée, A.; Unger, J. B.; Thomas, M.; Wirtz, C.; Dubost, C.; Handa, S.; Fürstner, A. *Angew. Chem. Int. Ed.* **2011**, *50*, 304.
- [32] Ren, R.-G.; Li, M.; Si, C.-M.; Mao, Z.-Y.; Wei, B.-G. *Tetrahedron Lett.* **2014**, *55*, 6903.
- [33] Chellat, M. F.; Proust, N.; Lauer, M. G.; Stambuli, J. P. *Org. Lett.* **2011**, *13*, 3246.
- [34] Claridge, T. D. W. *High-Resolution NMR Techniques in Organic Chemistry*; Elsevier, 2016.
- [35] Schauer, R. *Chemistry, Metabolism, and Biological Functions of Sialic Acids*; Academic Press, 1982; Vol. 40.
- [36] Smith, S. G.; Goodman, J. M. *J. Am. Chem. Soc.* **2010**, *132*, 12946.
- [37] Naylor, G. University of Cambridge, 2010.
- [38] Ermanis, K.; Parkes, K. E. B.; Agback, T.; Goodman, J. M. *Org. Biomol. Chem.* **2017**, *15*, 8998.
- [39] Grimblat, N.; Zanardi, M. M.; Sarotti, A. M. *J. Org. Chem.* **2015**, *80*, 12526.
- [40] Winder, P. *Therapeutic Potential, Mechanism of Action, and Ecology of Novel Marine Natural Products*; 2009.
- [41] Deer, E. L.; González-Hernández, J.; Coursen, J. D.; Shea, J. E.; Ngatia, J.; Scaife, C. L.; Firpo, M. A.; Mulvihill, S. J. *Pancreas* **2010**, *39*, 425.
- [42] Zhang, H.; Zhao, Z.; Wang, H. *Mar. Drugs* **2017**, *15*, 68.
- [43] Sanglard, D. In *Candida albicans: Cellular and Molecular Biology*; Springer International Publishing: Cham, 2017; pp 287–311.
- [44] Sikorska, J.; Hau, A. M.; Anklin, C.; Parker-Nance, S.; Davies-Coleman, M. T.; Ishmael, J. E.; McPhail, K. L. *J. Org. Chem.* **2012**, *77*, 6066.
- [45] Willwacher, J.; Fürstner, A. *Angew. Chem. Int. Ed.* **2014**, *53*, 4217.
- [46] Lei, H.; Yan, J.; Yu, J.; Liu, Y.; Wang, Z.; Xu, Z.; Ye, T. *Angew. Chem. Int. Ed.* **2014**, *53*, 6533.
- [47] Willwacher, J. Technischen Universität Dortmund, 2015.
- [48] Willwacher, J.; Heggen, B.; Wirtz, C.; Thiel, W.; Fürstner, A. *Chem. Eur. J.* **2015**, *21*, 10416.

- [49] Nazari, M.; Serrill, J. D.; Wan, X.; Nguyen, M. H.; Anklin, C.; Gallegos, D. A.; Smith, A. B.; Ishmael, J. E.; McPhail, K. L. *J. Med. Chem.* **2017**, *60*, 7850.
- [50] Lopera, J.; Miller, I. J.; McPhail, K. L.; Kwan, J. C. *mSystems* **2017**, *2*, e00096.
- [51] Weinberg, R. A. *The Biology of Cancer*, 2nd ed.; Garland Science, 2014.
- [52] Jackson, P. A.; Widen, J. C.; Harki, D. A.; Brummond, K. M. *J. Med. Chem.* **2017**, *60*, 839.
- [53] Paterson, I.; Haslett, G. W. *Org. Lett.* **2013**, *15*, 1338.
- [54] Watanabe, K.; Li, J.; Veerasamy, N.; Ghosh, A.; Carter, R. G. *Org. Lett.* **2016**, *18*, 1744.
- [55] Hwang, S.; Baek, I.; Lee, C. *Org. Lett.* **2016**, *18*, 2154.
- [56] Haslett, G. W. University of Cambridge, 2015.
- [57] Paterson, I.; Goodman, J. M.; Anne Lister, M.; Schumann, R. C.; McClure, C. K.; Norcross, R. D. *Tetrahedron* **1990**, *46*, 4663.
- [58] Reddy, K. M.; Yamini, V.; Singarapu, K. K.; Ghosh, S. *Org. Lett.* **2014**, *16*, 2658.
- [59] Paterson, I.; Arnott, E. A. *Tetrahedron Lett.* **1998**, *39*, 7185.
- [60] Danishefsky, S. J.; Pearson, W. H.; Harvey, D. F.; Maring, C. J.; Springer, J. P. *J. Am. Chem. Soc.* **1985**, *107*, 1256.
- [61] Fearnley, S. P. *Unpublished Work*; 2012.
- [62] Veerasamy, N.; Ghosh, A.; Li, J.; Watanabe, K.; Serrill, J. D.; Ishmael, J. E.; McPhail, K. L.; Carter, R. G. *J. Am. Chem. Soc.* **2016**, *138*, 770.
- [63] Huang, Z.; Negishi, E. I. *Org. Lett.* **2006**, *8*, 3675.
- [64] Mahapatra, S.; Carter, R. G. *J. Am. Chem. Soc.* **2013**, *135*, 10792.
- [65] Kim, H.; Lee, C. *Angew. Chem. Int. Ed.* **2012**, *51*, 12303.
- [66] Abiko, A.; Liu, J.-F.; Masamune, S. *J. Am. Chem. Soc.* **1997**, *119*, 2586.
- [67] Hartwig, J. F. *Organotransition Metal Chemistry: From Bonding to Catalysis*; University Science Books, 2010.
- [68] Ziegler, F. E.; Chakraborty, U. R.; Weisenfeld, R. B. *Tetrahedron* **1981**, *3*, 4035.
- [69] Nguyen, M. H.; Imanishi, M.; Kurogi, T.; Smith, A. B. *J. Am. Chem. Soc.* **2016**, *138*, 3675.
- [70] Kim, H.; Hong, J. *Org. Lett.* **2010**, *12*, 2880.
- [71] Dias, L. C.; de Lucca, E. C. *Org. Lett.* **2015**, *17*, 6278.
- [72] Storer, R. I.; Takemoto, T.; Jackson, P. S.; Brown, D. S.; Baxendale, I. R.; Ley, S. V. *Chem. Eur. J.* **2004**, *10*, 2529.
- [73] Laurent Ferrié; Sébastien Reymond; Patrice Capdevielle, and; Cossy\*, J. **2007**.
- [74] Paton, R. S. University of Cambridge, 2008.
- [75] Goodman, J. M.; Paterson, I. *Tetrahedron Lett.* **1992**, *33*, 7223.
- [76] Goodman, J. M.; Paton, R. S. *Chem. Commun.* **2007**, No. 21, 2124.
- [77] Hoye, T. R.; Jeffrey, C. S.; Shao, F. **2007**.
- [78] José Manuel Seco; Emilio Quiñoá, and; Riguera\*, R. **2004**.
- [79] Rychnovsky, S. D.; Rogers, B.; Yang, G. *J. Org. Chem.* **1993**, *58*, 3511.
- [80] Evans, D. A.; Rieger, D. L.; Gage, J. R. *Tetrahedron Lett.* **1990**, *31*, 7099.
- [81] Ando, K. *J. Org. Chem.* **1999**, *64*, 6815.

## References

- [82] Perry, M. A.; Rychnovsky, S. D.; Sizemore, N. In *Topics in Heterocyclic Chemistry Volume 35: Synthesis of Saturated Oxygenated Heterocycles I*; 2014; pp 43–95.
- [83] Nasir, N. M.; Ermanis, K.; Clarke, P. A. *Org. Biomol. Chem.* **2014**, *12*, 3323.
- [84] Hu, J.; Bian, M.; Ding, H. *Tetrahedron Lett.* **2016**, *57*, 5519.
- [85] Fuwa, H.; Ichinokawa, N.; Noto, K.; Sasaki, M. *J. Org. Chem.* **2012**, *77*, 2588.
- [86] Fuwa, H.; Ichinokawa, N.; Noto, K.; Sasaki, M. .
- [87] Clarke, P. A.; Ermanis, K. *Org. Lett.* **2012**, *14*, 5550.
- [88] Pellicena, M.; Krämer, K.; Romea, P.; Urpí, F. *Org. Lett.* **2011**, *13*, 5350.
- [89] Ermanis, K. *Personal Communications*; Cambridge, 2017.
- [90] Anslyn, E. V; Dougherty, D. A. *Modern Physical Organic Chemistry*; University Science Books, 2006.
- [91] Halgren, T. A. *J. Comput. Chem.* **1996**, *17*, 490.
- [92] Stephens, P. J.; Devlin, F. J.; Chabalowski, C. F.; Frisch, M. J. *J. Phys. Chem.* **1994**, *98*, 11623.
- [93] Hehre, W. J.; Ditchfield, K.; Pople, J. A. *J. Chem. Phys.* **1972**, *56*, 2257.
- [94] Ditchfield, R.; Hehre, W. J.; Pople, J. A. *J. Chem. Phys.* **1971**, *54*, 724.
- [95] Jensen, F. *Introduction to Computational Chemistry*, 3rd ed.; Wiley, 2007.
- [96] Kirschning, A.; Jesberger, M.; Schöning, K.-U. *Synthesis* **2001**, No. 4, 507.
- [97] Kirschning, A.; Bechthold, A. F.-W.; Rohr, J. Springer, Berlin, Heidelberg, 1997; Vol. 188, pp 1–84.
- [98] Gildersleeve, J.; Smith, A.; Sakurai, K.; Raghavan, S.; Kahne, D. *J. Am. Chem. Soc.* **1999**, *121*, 6176.
- [99] Suzuki, K.; Sulikowski, G. A.; Friesen, R. W.; Danishefsky, S. J. *J. Am. Chem. Soc.* **1990**, *112*, 8895.
- [100] Raghavan, S.; Kahne, D. *J. Am. Chem. Soc.* **1993**, *115*, 1580.
- [101] Schmidt, B.; Hauke, S. *Beilstein J. Org. Chem.* **2014**, *10*, 1023.
- [102] Li, M.; Scott, J.; O'Doherty, G. A. *Tetrahedron Lett.* **2004**, *45*, 1005.
- [103] Haack, K.-J.; Hashiguchi, S.; Fujii, A.; Ikariya, T.; Noyori, R. *Angew. Chem. Int. Ed.* **1997**, *36*, 285.
- [104] Fujii, A.; Hashiguchi, S.; Uematsu, N.; Ikariya, T.; Noyori, R. *J. Am. Chem. Soc.* **1996**, *118*, 2521.
- [105] Achmatowicz, O.; Bukowski, P.; Szechner, B.; Zwierzchowska, Z.; Zamojski, A. *Tetrahedron* **1971**, *27*, 1973.
- [106] Mahoney, W. S.; Brestensky, D. M.; Stryker, J. M. *J. Am. Chem. Soc.* **1988**, *110*, 291.
- [107] Lipshutz, B. H. In *Modern Organocupper Chemistry*; Krause, N., Ed.; Wiley-VCH Verlag GmbH: Weinheim, FRG, 2002; pp 167–187.
- [108] Koenig, T. M.; Daeuble, J. F.; Brestensky, D. M.; Stryker, J. M. *Tetrahedron Lett.* **1990**, *31*, 3237.
- [109] Baker, B. A.; Bošković, Ž. V.; Lipshutz, B. H. *Org. Lett.* **2008**, *10*, 289.
- [110] Lipshutz, B. H.; Keith, J.; Papa, P.; Vivian, R. *Tetrahedron Lett.* **1998**, *39*, 4627.
- [111] Lee, D. W.; Yun, J. *Tetrahedron Lett.* **2005**, *46*, 2037.
- [112] Lee, D. W.; Yun, J. *Tetrahedron Lett.* **2004**, *45*, 5415.

- [113] Rendler, S.; Oestreich, M. *Angewandte Chemie - International Edition*. 2007, pp 498–504.
- [114] Paterson, I.; Collett, L. A. *Tetrahedron Lett.* **2001**, *42*, 1187.
- [115] Still, W. C.; Barrish, J. C. *J. Am. Chem. Soc.* **1983**, *105*, 2487.
- [116] Thompson, J. *Unpublished Work*; 2015.
- [117] Broeker, J. L.; Hoffmann, R. W.; Houk, K. N. *J. Am. Chem. Soc.* **1991**, *113*, 5006.
- [118] Yadav, V. K. *Steric and Stereoelectronic Effects in Organic Chemistry*; Springer Singapore: Singapore, 2016.
- [119] Houk, K. N.; Rondan, N. G.; Wu, Y.-D.; Metz, J. T.; Paddon-Row, M. N. *Tetrahedron* **1984**, *40*, 2257.
- [120] Evans, D. A.; Fu, G. C.; Hoveyda, A. H. *J. Am. Chem. Soc.* **1988**, *110*, 6917.
- [121] Nicolaou, K. C.; Bulger, P. G.; Sarlah, D. *Angew. Chem. Int. Ed.* **2005**, *44*, 4442.
- [122] Chemler, S. R.; Trauner, D.; Danishefsky, S. J. *Angew. Chem. Int. Ed.* **2001**, *40*, 4544.
- [123] Lee, J. C. H.; Hall, D. G. In *Metal-Catalyzed Cross-Coupling Reactions and More*; Meijere, A. de, Bräse, S., Oestreich, M., Eds.; Wiley-VCH Verlag GmbH & Co. KGaA: Weinheim, Germany, 2013; pp 65–132.
- [124] Martin, V. S.; Woodard, S. S.; Katsuki, T.; Yamada, Y.; Ikeda, M.; Sharpless, K. B. *J. Am. Chem. Soc.* **1981**, *103*, 6237.
- [125] Ghosh, A. K.; Gong, G. *Chem. Asian J.* **2008**, *3*, 1811.
- [126] Corey, E. J.; Helal, C. *J. Angew. Chem. Int. Ed.* **1998**, *37*, 1986.
- [127] Haack, K.-J.; Hashiguchi, S.; Fujii, A.; Ikariya, T.; Noyori, R. *Angew. Chem. Int. Ed.* **1997**, *36*, 285.
- [128] Noyori, R.; Yamakawa, M.; Hashiguchi, S. *J. Org. Chem.* **2001**, *66*, 7931.
- [129] Yamakawa, M.; Ito, H.; Noyori, R. *J. Am. Chem. Soc.* **2000**, *122*, 1466.
- [130] Haack, K.-J.; Hashiguchi, S.; Fujii, A.; Ikariya, T.; Noyori, R. *Angew. Chem. Int. Ed.* **1997**, *36*, 285.
- [131] *Synthesis of Saturated Oxygenated Heterocycles I*; Cossy, J., Ed.; Topics in Heterocyclic Chemistry; Springer Berlin Heidelberg: Berlin, Heidelberg, 2014; Vol. 35.
- [132] Larrosa, I.; Romea, P.; Urpí, F. *Tetrahedron* **2008**, *64*, 2683.
- [133] *Handbook of Metathesis, Volume 2: Applications in Organic Synthesis*, 2nd ed.; Grubbs, R. H., O’Leary, D. J., Eds.; Wiley, 2015.
- [134] Paterson, I.; Wallace, D. J.; Velázquez, S. M. *Tetrahedron Lett.* **1994**, *35*, 9083.
- [135] Cheng, B.; Trauner, D. *J. Am. Chem. Soc.* **2015**, *11*, 41.
- [136] Anketell, M. J. *Unpublished Work*; 2017.
- [137] Hayashi, M.; Yoshiga, T.; Nakatani, K.; Ono, K.; Oguni, N. *Tetrahedron* **1994**, *50*, 2821.
- [138] Gaul, C.; Njardarson, J. T.; Shan, D.; Dorn, D. C.; Wu, K.-D.; Tong, W. P.; Huang, X.-Y.; Moore, M. A. S.; Danishefsky, S. J. *J. Am. Chem. Soc.* **2004**, *126*, 11326.
- [139] Knochel, P. In *Comprehensive Organic Synthesis*; Elsevier, 1991; pp 211–229.
- [140] Wuts, P. G. M.; Greene, T. W. *Greene’s Protective Groups in Organic Synthesis*, 4th ed.; Wiley, 2007.
- [141] Tronchet, J. M. J.; Zosimo-Landolfo, G.; Villedon-Denaide, F.; Balkadjian, M.; Cabrini, D.; Barbalat-Rey, F. *J. Carbohydr. Chem.* **1990**, *9*, 823.

## References

- [142] Kim, K. S.; Song, Y. H.; Lee, B. H.; Hahn, C. S. *J. Org. Chem.* **1986**, *51*, 404.
- [143] Chari, M.; Syamasundar, K. *Synthesis* **2005**, *2005*, 708.
- [144] Yadav, J. S.; Satyanarayana, M.; Raghavendra, S.; Balanarsaiah, E. *Tetrahedron Lett.* **2005**, *46*, 8745.
- [145] Gil, A.; Albericio, F.; Álvarez, M. *Chemical Reviews*. American Chemical Society June 28, 2017, pp 8420–8446.
- [146] Evans, D. A.; Chapman, K. T.; Carreira, E. M. *J. Am. Chem. Soc.* **1988**, *110*, 3560.
- [147] Saksena, A. K.; Mangiaracina, P. *Tetrahedron Lett.* **1983**, *24*, 273.
- [148] Evans, D. A.; Hoveyda, A. H. *J. Am. Chem. Soc.* **1990**, *112*, 6447.
- [149] Nicolaou, K. C.; Chakraborty, T. K.; Piscopio, A. D.; Minowa, N.; Bertinato, P. *J. Am. Chem. Soc.* **1993**, *115*, 4419.
- [150] Mohapatra, D. K.; Reddy, D. S.; Mallampudi, N. A.; Gaddam, J.; Polepalli, S.; Jain, N.; Yadav, J. S. *Org. Biomol. Chem.* **2014**, *12*, 9683.
- [151] Saccamano, N. A. In *Comprehensive Organic Synthesis. Volume I*; Fleming, I., Trost, B. M., Eds.; Elsevier, 1991; pp 173–209.
- [152] Jin, H.; Uenishi, J.; Christ, W. J.; Kishi, Y. *J. Am. Chem. Soc.* **1986**, *108*, 5644.
- [153] Okude, Y.; Hirano, S.; Hiyama, T.; Nozaki, H. *J. Am. Chem. Soc.* **1977**, *99*, 3179.
- [154] Takai, K. In *Comprehensive Organic Synthesis II. Volume I*; Knochel, P., Molander, G. A., Eds.; Elsevier, 2014; pp 159–203.
- [155] Takai, K.; Tagashira, M.; Kuroda, T.; Oshima, K.; Utimoto, K.; Nozaki, H. *J. Am. Chem. Soc.* **1986**, *108*, 6048.
- [156] Ermanis, K.; Hsiao, Y.-T.; Kaya, U.; Jeuken, A.; Clarke, P. A. *Chem. Sci.* **2017**, *8*, 482.
- [157] Kraus, H.; Français, A.; O'Brien, M.; Frost, J.; Diéguez-Vázquez, A.; Polara, A.; Baricordi, N.; Horan, R.; Hsu, D.-S.; Tsunoda, T.; et al. *Chem. Sci.* **2013**, *4*, 1989.
- [158] Kraus, H.; Français, A.; O'Brien, M.; Frost, J.; Diéguez-Vázquez, A.; Polara, A.; Baricordi, N.; Horan, R.; Hsu, D.-S.; Tsunoda, T.; et al. *Chem. Sci.* **2013**, *4*, 1989.
- [159] Liesener, F.; Jannsen, U.; Kalesse, M. *Synthesis* **2006**, *2006*, 2590.
- [160] White, J. D.; Kuntiyong, P.; Lee, T. H. *Org. Lett.* **2006**, *8*, 6039.
- [161] Ketley, A. D.; Fisher, L. P. *J. Organomet. Chem.* **1968**, *13*, 243.
- [162] Lloyd, W. G.; Luberooff, B. *J. J. Org. Chem.* **1969**, *34*, 3949.
- [163] Boiteau, J.-G.; Van de Weghe, P.; Eustache, J. *Org. Lett.* **2001**, *3*, 2737.
- [164] Anzicek, N. University of Cambridge, 2017.
- [165] Boger, D. L.; Ichikawa, S.; Zhong, W. *J. Am. Chem. Soc.* **2001**, *123*, 4161.
- [166] Gottlieb, H. E.; Kotlyar, V.; Nudelman, A. *J. Org. Chem.* **1997**, *62*, 7512.
- [167] Armarego, W. L. F.; Chai, C. L. L. *Purification of Laboratory Chemicals*, 6th ed.; Elsevier/Butterworth-Heinemann, 2009.
- [168] Chevalley, A.; Prunet, J.; Mauduit, M.; Férézou, J.-P. *Eur. J. Org. Chem.* **2013**, *2013*, 8265.
- [169] Bennett, M. A.; Huang, T.-N.; Matheson, T. W.; Smith, A. K.; Ittel, S.; Nickerson, W. *Inorg. Synth.* **2007**, *21*, 74.
- [170] Mlynarski, S. N.; Schuster, C. H.; Morken, J. P. *Nature* **2014**, *505*, 386.
- [171] Gaul, C.; Njardarson, J. T.; Danishefsky, S. J. *J Am Chem Soc* **2003**, *125*, 6042.

- [172] Koukal, P.; Ulč, J.; Nečas, D.; Kotora, M. *Eur. J. Org. Chem.* **2016**, *2016*, 2110.
- [173] Clancy, C. J.; Yu, V. L.; Morris, A. J.; Snydman, D. R.; Nguyen, M. H. *Antimicrob. Agents Chemother.* **2005**, *49*, 3171.



*We learn wisdom from failure much more than from success.*

*We often discover what will do, by finding out what will not do;  
and probably he who never made a mistake never made a discovery.*